FINAL REPORT ON

APPLICATION AND EXTENSION OF AN ANALYTICAL MODEL OF THE CONFINED ACOUSTIC BEAM GENERATED BY A TRANSDUCER

1990

SPONSORED BY

THE OFFICE OF NAVAL RESEARCH

ENVIRONMENTAL SCIENCES DIRECTORATE - CODE 425 UA

GEOPHYSICAL SCIENCES DIVISION

CONTRACT NO. N00014-85-K-0872

PRINCIPAL INVESTIGATOR:

JERRY H. GINSBERG

PROFESSOR OF MECHANICAL ENGINEERING

GEORGIA INSTITUTE OF TECHNOLOGY

ATLANTA, GEORGIA 30332

DISCLAIMER NOTICE

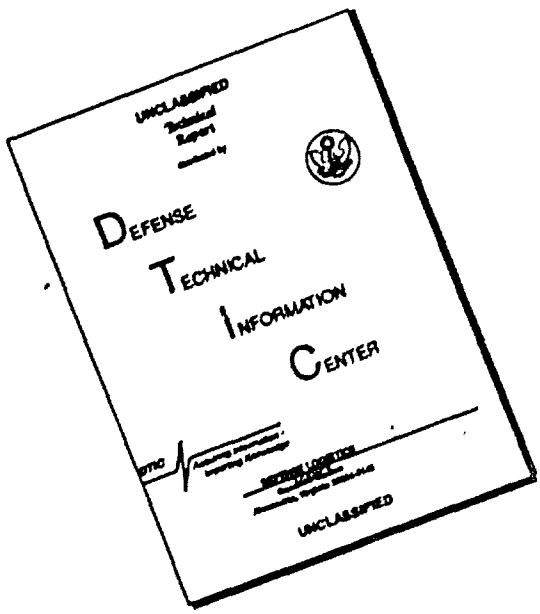

THIS DOCUMENT IS BEST QUALITY AVAILABLE. THE COPY FURNISHED TO DTIC CONTAINED A SIGNIFICANT NUMBER OF PAGES WHICH DO NOT REPRODUCE LEGIBLY.

FINAL REPORT ON

APPLICATION AND EXTENSION OF AN ANALYTICAL MODEL OF THE CONFINED ACOUSTIC BEAM GENERATED BY A TRANSDUCER

SPONSORED BY

THE OFFICE OF NAVAL RESEARCH

ENVIRONMENTAL SCIENCES DIRECTORATE - CODE 425 UA

GEOPHYSICAL SCIENCES DIVISION

CONTRACT NO. N00014-85-K-0872

PRINCIPAL INVESTIGATOR:

JERRY H. GINSBERG

PROFESSOR OF MECHANICAL ENGINEERING

GEORGIA INSTITUTE OF TECHNOLOGY

ATLANTA, GEORGIA 30332

TABLE OF CONTENTS

I. BACKGROUND

Numerous evaluations of the acoustic field radiating from a baffled transducer have appeared in the published literature. An important feature is that these theories are applicable for a wide range of parameters. Approximations, such as those describing an axisymmetric sound beam in the far field (Fraunhofer zone) can substantially reduce computational cost, but they are not necessary. Linear theory is valid when the source level is sufficiently low. Even then, diffraction effects in the near field, which lead to localized cancellations and reinforcements, complicate the task of correlating near field measurements to far field propagation properties.

The situation becomes more complicated when one tries to increase the propagation range by raising the source level. It is logical to try to overcome effects such as dissipation and scattering by generating higher level signals. Such attempts inevitably lead to a greater role for nonlinear effects. One of the effects of nonlinearity is to divert energy from the fundamental signal to higher harmonics, which is equivalent to lowering the efficiency of the transducer. In the face of these concurrent effects it is apparent that developing a unified theory for nonlinear effects in sound beams is a challenging matter. However, such a theory is necessary if understanding of the distortion phenomena is to be enhanced. A prime example of the earlier lack of insight is the observed differences between the distortion of the compression and rarefaction phases of a signal, which had no analog in simpler types of acoustic waves.

A variety of approaches have been employed to study the effects of nonlinearity in this system. One approach has relied on a conventional perturbation solution of an approximate nonlinear wave equation. Such an analysis seems to give very good results near the transducer face. However, it quickly breaks down with increasing range due to assumptions that are made in the perturbation steps.

An investigation of properties in the far field was developed based on an approximation as a quasi-spherical wave. Such a formulation assumes that the wave arrives at the transition to the far field (e.g. the Rayleigh distance) without substantial prior distortion. Hence, the spherical wave description is inherently limited to cases where the transducer excitation is comparitively low level. This type of analysis also leads to certain anomalies, such as the fact that the level of distortion is dependent on the choice for the spherical transition distance, which may be arbitrarily chosen beyond the Rayleigh distance.

Another approach that has been widely employed is founded on a version of Burgers' equation that has been modified to account for spreading and diffraction -- this is commonly referred to as the Zabolotskaya-Khokhlov equation. After its original exposition in the Soviet literature, the first solutions of the equation for harmonic excitation of the projector were obtained by finite differencing the position and time variables. Those results were difficult to obtain due to the inefficiency of the approach, so an alternative was developed by the Tjøttas and Hamilton based on the fact that a harmonic input must result in a signal that is temporally periodic. Consequently, the signal in this case may be expanded in a Fourier series whose coefficients are position dependent. Using the method of harmonic balance to make the solution satisfy the Z-K equation leads to coupled sets of ordinary differential equations for the Fourier coefficients. Although the solution could be obtained more efficiently in this manner, the basic approach is limited by the restricted nature of its input. Extending the procedure to treat multi-harmonic inputs would require a substantial increase in the number of harmonics that would need to be retained, and the method is completely invalid for predicting the signal generated by a transient input. Furthermore, the degree to which the Z-K equation is suitable for predictions of the highly diffractive field near the projector had not been explored.

II. RESEARCH TECHNIQUE

The primary goal of this project was to develop an overall description of transducer radiation in which finite amplitude effects diffraction, and spherical spreading are treated consistently, without limitation to a specific spatial domain or a specific type of input to the projector. Initially, the mathematical tools for this work were those used to develop the nonlinear King integral for nonlinear effects arising in the sound beam generated by a harmonic input [J. H. Ginsberg, Journal of the Acoustical Society of America, 76, No. 4 (1984) 1201-1214]. These techniques combined singular perturbation theory and asymptotic analysis of the behavior in specific domains.

The general approach uses the King integral in linear theory, which is a Fourier-Bessel integral transform, to develop the second order source terms that generate nonlinearities in the response. There are two kinds of nonlinear effects that arise at the second order. Some produce terms that remain bounded as the signal propagates. (One such effect is associated with the fact that the input from the transducer originates from a moving boundary, rather than the much simpler description, $z = 0$.) The smallness

of the acoustic Mach number leads to the conclusion that these fixed magnitude effects cannot account for measured levels of distortion. The other group of nonlinear effects arise from resonance-like phenomena. These terms lead to distortion that grows with increasing distance. Shocks ultimately form from this effect, unless dissipation is adequate to overcome the nonlinear distortion process. It is this cumulative growth effect that needs to be evaluated.

The growth effects in the second order terms are evaluated by using asymptotic integration techniques to identify the portion of the second order terms that grow most rapidly with increasing range. The aforementioned breakdown of conventional (i.e. regular) perturbation solutions is avoided by introducing coordinate transformations that essentially are based on the recognition that cumulative growth is a singularity. The transformation is selected such that replacing the physical position coordinates by the new variables cancels the singular terms.

The singular perturbation scheme had earlier been successful in deriving solutions for sound beams generated by a variety of sources. The first studies considered the case of harmonic input. The cumbersome evaluation of coordinate transformations was replaced by a harmonic series representation, for which the effort to evaluate each harmonic is equivalent to that required to solve the linear case [Hsu-Chiang Miao, Ph.D. thesis, Georgia Institute of Technology, Sept. 1985]. Results derived in this manner were shown to be accurate in comparison to experimental data from a region several piston radii from the projector out to the Rayleigh distance and beyond, which generally marks the onset of farfield behavior.

Subsequent work extended the basic nonlinear King integral to non-axisymmetric sound beams, such as those arising when the normal velocity on the surface of the projector resembles an azimuthal harmonic. Another extension of the analytical technique demonstrated the suitability of the method to treat situations where the projector is driven by two inputs at arbitrary frequency; the parametric array, in which the frequencies are relatively close, is included in that general case. In order to further generalize these works a major effort involved evaluation of the sound beam radiating from a baffled projector whose input is an arbitrary periodic function. This capability would be employed to explore the implications of an "anti-nonlinearity" concept. In it, the projector is manipulated to generate a signal that is phase-inverted from the waveform that would be obtained at the shock formation distance from a conventional input. (This concept will be discussed in greater detail later.)

Although the foregoing study was generally successful, it became apparent that further work, involving transient inputs to a projector, would be too cumbersome for the perturbation approach. It therefore was decided to develop a time-domain numerical simulation of finite amplitude sound beams. The physical assumptions used by Kuperman and McDonald to develop the NPE (Nonlinear Progressive wave Equation) computer code were judged to be suitable for sound beams, but the coordinate systems used in their formulation were not suitable. Therefore, attention was devoted to modifying NPE to treat wave propagation in a cylindrical geometry in which the primary propagation is axial. After the modifications were implemented, the primary question was what is the proper way in which NPE should be initialized? In brief, NPE requires as initial conditions a waveform occupying a specific spatial region, which forms a window. It then uses a time marching procedure that propagates this window at the overall sound speed, while the waveform disperses within the window. Additional questions pertained to whether one could introduce nonreflective outer boundaries for the window, which would have permitted usage of a smaller window, and whether a new coordinate system could be introduced, in order to allow account for the spherical spreading of the beam without employing an excessively fine numerical mesh transverse to the propagation direction. The general method by which any of the developments were validated was to consider three cases where results are reasonably well known: linear theory for steady-state harmonic waveforms, linear theory for transient waveforms, and nonlinear theory for harmonic input waveforms at moderate excitation levels.

A new line of research evolved out of two aspects of the analyses discussed above. The Fourier series representation of the nonlinear King integral grew out of a decomposition into an angular spectrum representation, in which each transverse wavenumber was represented by two wavelets. Far from the axis of symmetry, these wavelets have the appearance of conical wavefronts that propagate inward and outward relative to the axis of symmetry. (Near the axis of the sound beam, the wavefronts both appear to be locally planar and perpendicular to the axis.) In order to understand the interaction between wavelets, it was decided to return to waveguides. Development of a ray description of the propagation and interaction of finite amplitude waves would substantially assist understanding of the distortion mechanisms in sound beams.

The development of a ray description was further motivated by the work on phase-inverted nonlinear inputs. A few earlier experiments had use reflection from a free surface to invert the projector waveform. However, the theories used to support those experiments were highly approximate because little was known analytically regarding the reflection of finite amplitude waves. It seemed logical to follow the successful study of ray

propagation in waveguides, which had considered oblique reflection from rigid surfaces, with a study of oblique reflection and transmission from planar interfaces between two media. Although it had initally been anticipated that work in this question would be confined to fluid media, it soon became apparent that the derived theory could be applied with equal ease to elastic solids. The derivation of the theory, one of whose aspects is a modification of Snell's law to account for the dependence of propagation speed on particle velocity, was achieved by using perturbation techniques to identify the dominant nonlinear effects, and then using the method of characteristics to study those effects.

PROJECT ACHIEVEMENTS

A. Extended Analytical Descriptions of Sound Beams

The present project began by completing the studies of nonaxisymmetric [1] and two-frequency excitations [17]. With the completion of those works, several questions remained to be answered. The nature of the perturbation analysis limited the range at which the respective solutions could be applied, because shocks play an increasingly prominant role with increasing range, especially in the absence of dissipation. Furthermore, the King integral has limited usefulness for far field evaluations, even in the linear case. This is so because diffraction effects appear as an oscillatory integrand whose fluctuations become increasingly severe with increasing distance, which correspondingly requires increasingly fine resolution in any numerical integration scheme. Thus one need was to extend the analytical to farther ranges and/or higher input levels.

Parallel to this thrust was the desire to investigate a concept by which a projector could be driven at higher input levels than that currently taken as the saturation limit, which is the level at which strong shocks form near the projector. Since shocks are rich in higher harmonics, which do not propagate well, saturation serves as an absolute limit on the level to which a projector may usefully be driven. The enhancement concept was suggested by a well-known "reciprocity" feature of finite amplitude planar waves. Suppose the signal generated by a harmonic input is allowed to propagate (and distort) through a certain distance. Next consider the case where the source generates a signal whose waveform is opposite in phase from the received waveform in the first case. If dissipation is insignificant, the waveform received in the second case will be identical to the harmonic signal generated by the projector in the first case.

The significant aspect of this phenomenon for sound beams emerges when one considers the combination of this reciprocal behavior with the far field tendency to undergo spherical divergence. For a specified signal level, the rate at which distortion grows in spherical waves is significantly lower than it is for planar waves. Thus if the tendency of an oppositely distorted wave to undistort could be used to push the zone in which shocks would form out beyond the Rayleigh distance, it was reasoned that the result would be a substantial retardation in the the onset of significant nonlinear distortion. This was the concept, but no prior study had addressed the problem of determining the finite amplitude signal generated by an arbitrary periodic input to a projector, which is the type of excitation associated with a phase-inverted distorted signal resulting from a sinusoidal input.

The project expended a major effort to extend the nonlinear King integral to treat arbitrary time-periodic projector inputs [7,10]. It used those results to assess the feasibility of using phase-inverted inputs to extend the range of a saturation limited projector. The analysis for this case was found to be extremely unwieldy, due to the complications inherent to the strong interactions of harmonics in the presence of strong diffractive effects. This necessitated considering a variety of phase shifts for the higher harmonics relative to the fundamental, rather than the simple phase inversion that is suggested by the theory for planar waves. Theoretical estimates of the net gain to be derived by this concept range from 2 to 5 dB for the signal level received at the farfield, when realistic limitations are imposed on the projector. The uncertainty in the gain stems from a total absence of experimental data for sound beams resulting from a multi-harmonic input to a projector. (In the terminology of a parametric array, the downshift ratio is two.) The lack of experimental data was a serious handicap, because the theory that has been developed seems to fail in some respects in the limiting case of a parametric array, due to a singularty that arises when two primary frequencies approach a common value.

B. Numerical Modeling of Sound Beams

As a result of the complications encountered in continued extension of the analytical procedures, the next effort was devoted to developing an accurate scheme for developing a general time domain numerical prediction of distortion phenomena in sound beams resulting from arbitrary inputs. Such a description could also be used for transient excitations, and it presumably would be easier to incorporate dissipation and shock formation in a numerical prediction. This effort involved modifying the NPE computer program to treat the axisymmetric geometry of a sound beam, and then developing a method by which NPE could be driven. Numerical evaluations began with

studies of linear propagation for steady-state harmonic waves [21], as well as for transient excitation in the form of a single sine pulse [26].

The results showed that NPE can be used at much closer distances to the source than other researchers using parabolic equations had previously believed. The key aspect of this disclosure was that the quality of the near field computations is highly dependent on the manner in which the moving window is initialized. The earlier analytical and numerical studies of the modified Burgers' equation for sound beams had relied on a fundamental plane wave assumption that the pressure particle velocity at the face of the projector is proportional to the axial particle velocity. This assuption was compared in the project studies to the result obtained when a linear theory, either the Rayleigh or King integral, is used to initialize the moving window extending outward from the projector face for a few wavelengths. The waveform predicted for various locations according to each method of initialization was then compared to the integral equation prediction. The results obtained by initializing the NPE window were found to be accurate (the values were within 0.1% of those obtained from numerical evaluation of the integral equation) for distances as small as one tenth of the Rayleigh distance, while the plane wave assumption produced results that agreed with analysis only outward from the Rayleigh length.

Work nearing completion and soon to be reported [27,28] has already shown that the quality of NPE is equally good for nonlinear effects. The results have been compared to precise experimental measurements at a variety of ranges, and transverse positions. Comparisons of its predictions with the nonlinear King integral are equally good.

Early in the project NPE was reduced to run on desktop computers, but the number of computations involved in running it from the projector face out to several multiples of the Rayleigh distance is quite substantial. Work required to complete the Ph.D. thesis of the graduate assistant developing NPE involves using the nonlinear King integral to initialize the moving window, and thereby increase the efficiency of NPE for far field predictions. Another efficiency already implemented as a project task into NPE addresses the requirement that the transverse width of the window be sufficiently large to consider the pressure at the edge to be zero. The idea here is to rezone the mesh divisions of the window to extend beyond the main lobe whenever the signal at the edges is sensed to be a significant fraction of the overall signal. These efficiencies are especially appropriate to performing studies of multiharmonic inputs to the projector, because such studies require much finer divisions within the window.

C. Analyses of Reflection and Refraction of Nonlinear Waves

As the analyses aimed at generalizing the nonlinear King integral progressed, it became apparent that one of its primary features is that it treats the signal as a combination of wavelets propagating in various directions extending over an angular spectrum of transverse wave numbers. Desire to understand such wave interactions led to a question whether the perturbation techniques could be employed to study waveforms reflected from surfaces, which was believed to be a better understood process.

The first study of reflection effects [12,18] developed a ray description of the propagation of waves in a waveguide whose walls are rigid. It was shown that large amplitude excitation of a nonplanar mode could be modeled by using the method of images to follow the rays forming that mode. The distortion of the signal along each ray was shown to be determined by the total propagation distance from the original source, and the results were proven to be identical to those obtained from a modal solution previously derived in the project [1].

The ability to describe finite amplitude signals in terms of rays was further extended by a sequence of studies which were initially intended to study oblique reflection of a finite amplitude acoustic wave from a free surface. This question was motivated by the observation that several previous experiments devoted to the "anti-nonlinearity" concept had reflected the signal obliquely from a free surface in order to invert the waveforms. It was found eventually that new techniques using the method of characteristics are necessary to solve this problem. What emerged from that analysis [19,22,24] was the recognition of a nonlinear Snell's law, which was associated with new types of waveform distortion.

The procedure whereby this result was obtained, which is equally applicable for reflection and transmission at planar interfaces between media, is innovative. The analysis began with a conventional perturbation analysis based on the smallness of the particle velocity relative to the phase speed of a planar wave. This revealed that the first order signal is the linear approximation. For waves in fluids, the process involves reflection and transmission of planar acoustic waves, while stress waves in elastic solids feature dilatational and shear waves, in what is known as mode conversion. The propagation angles of these waves is dictated by the linear Snell's law, which is obtained by matching the linear (constant) trace velocities along the interface. The second order analysis revealed that the dominant nonlinear effect is the tendency of a planar acoustic and/or dilatational wave to form second harmonics, whereas shear waves and nonlinear interaction between incident and planar waves give rise to nonlinear effects that are much

weaker [8,13,15]. However, further analysis of the second order signal led to an apparent dilemma, in that no solution constructed in this manner could satisfy the boundary condition. This difficulty was traced to an assumption made at the start of the perturbation analysis, where it was implicitly assumed that the directions of the nonlinear rays are the same as those of the linearized solution.

Rather than patching the solution in an awkward procedure the knowledge of the dominant nonlinear effects was used to formulate a new solution using the method of characteristics. This involved recognizing that the characteristics of planar waves in a two-dimensional system lie on the surface of a cone in space-time coordinates. The apex angle of this cone must change with time, according to the particle speed associated with the that cone. The specific ray associated with the signal emanating from the boundary at any instant represents the projection of a characteristic onto the plane of spatial coordinates in the characteristic space. The orientation of this ray must be chosen such that the combination of signals emanating from the boundary satisfy in total the boundary conditions.

The solution obtained in this manner consists of a generalization of the results for reflection and transmission of linear waves. The nonlinear Snell's law is similar to the linear one, except that the phase speeds are the instantaneous values of the waves arriving and departing from the interface. Consequently, the transmission and reflection angles fluctuate. Similarly the reflection and transmission coefficents are like those of linear theory, except that they depend on the nonlinear transmission and reflection angles. Away from the interface, the each wave (acoustic, dilatational, or shear) propagates according to nonlinear theory for planar waves, with the distortion of the first two depending on the distance of propagation measured along the ray. Evaluating the waveform received at a specific field point in this situation is complicated, because the waves arriving at the point can originate from a region on the interface, and because the reflection and transmission coefficients have values that depend on these angles, with the angles being dependent on the instantaneous phase speeds. The latter, in turn, depend on the unknown particle velocities.

The complications described above were resolved by an iterative procedure, in which the phase of each type of wave is treated as the independent variable. Then the value of time corresponding to arrival of this phase at the selected field point is determined after a convergent value for the particle velocity is obtained. This technique was used first to describe reflection of a nonlinear dilatational wave at a stress free boundary. The results showed that the reflection process lessens the severity of the nonlinear distortion processes. Several factors influence this reduction,

primarily these are (1) a decrease in the amplitude of the dilatational wave due to mode conversion, and (2) phase inversion, which corresponds to the "anti-nonlinearity" concept.

At this time, work is underway to evaluate the case of critical incidence [20]. Qualitative consideration of the theory indicates that a wave will have a dual personality, in which the portion of the phase in which the particle velocity is negative will be reflected as a propagating planar wave (sub-critical incidence), while the phase of positive particle velocity will evanesce perpendicular to the interface. If this result is confirmed by the analysis, one can envision numerous interesting experiments that might lead to potentially useful tools for detecting spatial heterogeneities in material properties, as well as for detecting interfacial cracks in solid media.

IV. CHRONOLOGICAL LISTING OF PROJECT PUBLICATIONS AND PRESENTATIONS

1 H. C. Miao and J. H. Ginsberg, "Finite Amplitude Distortion and Dispersion of a Nonplanar Mode in a Waveguide," J. Acoust. Soc. Am., 80, No. 3, (1986) 911-920.

2 H. C. Miao and J. H. Ginsberg, "Nonsymmetric Effect in Finite Amplitude Sound Beams Radiating from a Baffled Circular Transducer," 111th Meeting of the Acoustical Society of America, Cleveland, OH, May 12-16, 1986.

3 M. A. Foda and J. H. Ginsberg, "Relationship Between Near and Farfield Effects in Second Harmonic Generation in the Piston Beam," 111th Meeting of the Acoustical Society of America, Cleveland, OH, May 12-16, 1986.

4 J. H. Ginsberg, "Theoretical and Computational Aspects of Finite Amplitude Sound Beams," First IMACS Symposium on Computational Acoustics, Yale University, New Haven, Ct, August 6-8, 1986.

5 J. H. Ginsberg, H. C. Miao, and M. A. Foda, "Diffraction and Nonlinear Distortion in Sound Beams as Interacting Wave Phenomena," 113th Meeting of the Acoustical Society of America, Indianapolis, IN, May 11-15, 1987.

6 J. H. Ginsberg, "An Analytical Model for Finite Amplitude Effects in Sound Beams," Invited Seminar, Purdue University, May 14, 1987.

7 J. B. Edgerton, Jr. and Jerry H. Ginsberg, "Finite Amplitude Acoustic Waves Generated by a Baffled, Multi-Harmonic Transducer," 113th Meeting of the Acoustical Society of America, Indianapolis, IN, May 11-15, 1987.

8 K. T. Shu and Jerry H. Ginsberg, "Third-Order Effects in the Propagation of Finite Amplitude Stress Waves," 113th Meeting of the Acoustical Society of America, Indianapolis, IN, May 11-15, 1987.

9 J. H. Ginsberg, "Theoretical and Computational Aspects of Finite Amplitude Sound Beams," Computational Acoustics, vol. 2, Algorithms and Applications, D. Lee, R. L. Steinberg, and M. H. Schultz, eds., North-Holland, Amsterdam (1988) 403-418.

10 J. B. Edgerton, Jr., "Finite Amplitude Acoustic Waves Generated by a Baffled, Multi-Harmonic Transducer," Ph.D. thesis, Georgia Institute of Technology, February 1988.

11 J. H. Ginsberg, "Similarity of a Fourier Transform Generalization of the Earnshaw Solution for Planar Waves to an Interacting Wave Model for Finite Amplitude Effects in Sound Beams," 115th Meeting of the Acoustical Society of America, Seattle, WA, May 16-20, 1988.

12 K. T. Shu and J. H. Ginsberg, "Ray Solution for Finite Amplitude Two-Dimensional Waves in a Hard-Walled Rectangular Waveguide", 115th Meeting of the Acoustical Society of America, Seattle, WA, May 16-20, 1988.

13 K. T. Shu and J. H. Ginsberg, "Oblique Reflection and Mode Conversion of Nonlinear Dilatational Waves at a Planar Boundary," Proceedings of Noise-Con 88, Purdue University, Indiana, June 20-22, 1988, 205-210.

14 J. H. Ginsberg, "Analytical and Numerical Techniques for Nonlinear Distortion in Sound Beams," Proceedings of Noise-Con 88, Purdue University, Indiana, June 20-22, 1988, 187-192.

15 K. T. Shu and J. H. Ginsberg, "Oblique Reflection of a Finite Amplitude Dilatational Wave in an Elastic Half-Space," 115th Meeting of the Acoustical Society of America, Honolulu, Nov. 14-18, 1988.

16 J. H. Ginsberg, P. H. Rogers, and A. L. VanBuren, "Comments on Radiation from a Concave Piston Source," J. Acoust. Soc. Am., 84 (1988), 442.

17 M. A. Foda and J. H. Ginsberg, "Finite Amplitude Effects in Dual Frequency Acoustic Beam." J. Acoust. Soc. Am., 85, 1857-1871 (1989).

18 K. T. Shu and J. H. Ginsberg, "Ray Theory Solution for Finite Amplitude Effects in a Two-Dimensional Waveguide," J. Acoust. Soc. Am., 86, 771-776 (1989).

19 K. T. Shu and J. H. Ginsberg, "Reflection and Refraction of an Obliquely Incident Finite Amplitude Plane P Wave at a Plane Solid-Solid Interface," 117th Meeting of the Acoustical Society of America, Syracuse, NY, May 22-26, 1989.

20 K. T. Shu and J. H. Ginsberg, "On Supercritical Incidence of a Finite Amplitude Plane Dilatational Wave in an Elastic Solid," 118th Meeting of the Acoustical Society of America, St. Louis, MO, November 27-December 1, 1989.

21 G. P. Too and J. H. Ginsberg, "Modification of the NPE Computer Code to Describe the Propagation of Axisymmetric Sound Beams in Infinite Media," 118th Meeting of the Acoustical Society of America, St. Louis, MO, November 27-December 1, 1989.

22 K. T. Shu and J. H. Ginsberg, "Oblique Reflection of a Nonlinear P Wave from the Boundary of an Elastic Half-Space," (1990, submitted).

23 J. H. Ginsberg and K. T. Shu, "Reflection and Refraction of Nonlinear Dilatational and Shear Waves at a Planar Interface," invited paper at AAPT/APS Joint Winter Meeting, Atlanta, GA, Jan. 22-25, 1990.

24 Kun-Tien Shu, "Multidimensional Reflection and Refraction of Finite Amplitude Stress Waves in Elastic Solids," Ph.D. thesis, Georgia Institute of Technology, April 1990.

25 J. H. Ginsberg, "Reflection and Refraction of Nonlinear Dilatational and Shear Waves at a Planar Interface," Invited Seminar, Wayne State University, April 11, 1990.

26 G. P. James Too and J. H. Ginsberg, "Evaluation of Transient Responses of Sound Beams Using a Modified Version of the NPE," 119th Meeting of the Acoustical Society of America, Pennsylvania State University, May 21-25, 1990.

27 G. P. James Too and J. H. Ginsberg, "Evaluation of a Finite Amplitude Sound Beam in the Time Domain Using the NPE Computer Code," 12th International Symposium on Nonlinear Acoustics, University of Texas at Austin, August 27-31, 1990.

28 Gee-Pinn Too, "Unification of Analytical, Computational, and Experimental Predicitions for High-Intensity Sound Beams," expected completion date: August 1990.

Finite amplitude distortion and dispersion of a nonplanar mode in a waveguide

J. H. Ginsberg and H. C. Miao[a)]
School of Mechanical Engineering, Georgia Institute of Technology, Atlanta, Georgia 30332

(Received 1 May 1985; accepted for publication 22 April 1986)

The perturbation method of renormalization is used to study the effect of nonlinearity on a hard-walled rectangular waveguide. The excitation would induce only the fundamental nonplanar symmetric mode if the system were linear. The analysis develops a solution that satisfies a nonlinear wave equation for the velocity potential, as well as all boundary conditions. The response consists of a pair of oblique planar waves that interact through second-order excitation of the true planar mode. The investigation discloses that in the high-frequency limit the signal has a quasiplanar behavior. In contrast, for very low frequencies exceeding the cutoff value, the oblique waves are essentially independent. The distortion is then a result of self-refraction, in which the particle motion shifts the wave fronts and rays. The transition between the low- and high-frequency limits is marked by the appearance of nonlinear frequency dispersion, which produces asymmetrical distortion of the waveform.

PACS numbers: 43.25.Cb, 43.20.Mv

INTRODUCTION

Finite amplitude effects in a waveguide feature multidimensional phenomena involving interacting waves. In linear theory, a mode in a hard-walled waveguide may be constructed from pairs of oblique planar waves that are reflected from the walls. The present study will employ the same type of decomposition to show that distortion resulting from nonlinearity displays a phenomenological change as the excitation frequency is increased. This transition is associated with an anomaly contained in previous studies, which only considered the low-frequency case.

Initial explorations of finite amplitude nonplanar modes in waveguides employed the perturbation method of multiple scales in a rudimentary fashion that considered selected aspects of wave interaction.[1-3] A different method of investigation was developed to study waves radiating from a flat plate.[4-9] To a certain extent, the latter studies were academic in nature. The system they treated featured a periodically supported plate of infinite extent. They assumed periodicity of the signal parallel to the plate, which meant that energy was propagating inward from infinite boundaries. This apparent violation of the uniqueness condition, nevertheless, proved to be instructive, because the system could be studied by a variety of analytical techniques. The perturbation methods of multiple scales and of renormalization, and the method of characteristics, mutually agreed for the case of a spatially sinusoidal excitation. One significant aspect of their result was the prediction of self-refraction, in which the wave fronts and rays of constant phase are distorted by the particle velocity.

Although the plate problem did not treat a physically realizable system, the relevance of these investigations to waveguides was recognized in a subsequent investigation.[10] The basis of that work was that there are nodal lines in the plate system along which the velocity component parallel to the surface of the plate vanishes. Such lines are perpendicular to the plate, as they are in linear theory. This observation led to the conclusion that the infinite plate analyses had actually derived a single mode in a waveguide.

The treatment of general excitation in a waveguide performed in Ref. 10, which was a straightforward extension of the method of renormalization, disclosed a type of superposition principle. Modes having identical phase speed were found to form distinct groups, whose distortion in self-refraction was a consequence of only the particle velocity arising from that group. The overall response consisted of a linear combination of the response in each group.

A similar analysis had been used to study waves radiating from cylinders.[11-14] One of those studies[12] identified a paradox associated with very long axial wavelengths. One would expect that if the wavelength along the axis of a cylinder is large, so that the rate of variation in that direction is very gradual, then the response would approach that for the case of a two-dimensional system, in which the axial wavelength is actually infinite. This was found to be the case, except that the distortion phenomena in the limit were found to be too weak by a factor of one-half. This dilemma was resolved by noting that distinct modes in the case of axial variation coalesce only when the wavelength is actually infinite.

These observations also apply to the investigation of waveguides.[10] For example, as the width of a waveguide is increased, the earlier analysis predicts that the distortion of the planar mode will be twice as strong as that of the fundamental symmetric (2,0) mode. Although the explanation of coalescing effects for infinite transverse wavelength (i.e., the planar mode) is plausible, it nevertheless is unsettling from a physical viewpoint. Distortion arises from higher harmonic souces that are generated by nonlinearity in the entire acous-

[a)] Present address: General Motors Research Laboratories, Warren, MI 48090-9055.

 0001-4966/86/090911-10$00.80

tic field. Could it be that minor discrepancies between the long and infinite wavelength cases accumulate to create the discrepancy? Lack of experimental data prevented an earlier response to this question, but discussions with researchers currently involved in such activity[15] sparked the present authors' interest in exploring these concerns.

The analysis presented herein treats an excitation of only the (2,0) mode in a hard-walled waveguide. This limitation is imposed primarily to reduce the analytical complications inherent to a more general study of multimode propagation. It also facilitates isolation of physical phenomena, such as the manner in which the nonplanar and planar modes interact nonlinearly. It will be shown that the (2,0) mode excites the planar mode in an insignificant fashion, unless $\omega L/c_0 \gg 2\pi$, where L is the transverse width of the waveguide, ω is the (circular) frequency, and c_0 is the linear speed of sound. The phase speed of the (2,0) mode, then, differs slightly from that of the planar mode. This near-coincidence sets up a mode interaction that is reminiscent of the beating response exhibited by an undamped, one-degree-of-freedom oscillator that is subjected to harmonic excitation close to, but not at, the natural frequency.

The modal interaction leads to a smooth transition to the planar mode response with increasing frequency, in the manner one would expect. The analysis will confirm the earlier theory for waveguides when $\omega L/c_0$ is not large. It will also show that the transition from the earlier theory to the high-frequency case is marked by frequency dispersion, in which the waveforms are remarkably similar to those observed in the nearfield of intense beams of sound.[16]

I. FORMULATION

A pressure excitation of the fundamental, symmetric, two-dimensional mode in a hard-walled waveguide may be written as

$$p|_{z=0} = \epsilon\rho_0 c_0^2 \sin(\omega t)\cos(k_x x), \quad \epsilon \ll 1, \quad -L/2 \le x \le L/2, \tag{1}$$

where ρ_0 is the ambient pressure, c_0 is the speed of sound at ambient conditions, and the transverse wavenumber k_x is related to the duct width L by

$$k_x = 2\pi/L. \tag{2}$$

The question to be addressed here is the effect of nonlinearity associated with the finiteness of ϵ on the waves that propagate in the positive z direction as a result of this excitation.

The equations of continuity, momentum, and state may be combined to form a single nonlinear wave equation governing the velocity potential[17] under isentropic conditions,

$$c_0^2\nabla^2\phi - \frac{\partial^2\phi}{\partial t^2} = \frac{\partial}{\partial t}\left[\frac{1}{c_0^2}(\beta_0 - 1)\left(\frac{\partial\phi}{\partial t}\right)^2 + \nabla\phi\cdot\nabla\phi\right] + O(\phi^3), \tag{3}$$

where the nonlinearity coefficient β_0 is the constant associated with the second-order term in a polynomial expansion of the pressure perturbation p as a function of the density perturbation ρ at fixed entropy,

$$p/(\rho_0 c_0^2) = \rho/\rho_0 + (\beta_0 - 1)(\rho/\rho_0^2) + \cdots. \tag{4}$$

Because the analysis shall only address the role of quadratic nonlinearities, Eq. (4) may also be applied to liquids by letting $\beta_0 = 1 + B/2A$.

The pressure is related to the potential by

$$\int_0^p \frac{dp}{(\rho_0+\rho)} + \frac{\partial\phi}{\partial t} + \frac{1}{2}\nabla\phi\cdot\nabla\phi = 0. \tag{5}$$

From Eqs. (4) and (5) p, ρ, and ϕ have the same order of magnitude, so elimination of ρ from these relations yields

$$p = -\rho_0\left[\frac{\partial\phi}{\partial t} + \frac{1}{2}\nabla\phi\cdot\nabla\phi - \frac{1}{2c_0^2}\left(\frac{\partial\phi}{\partial t}\right)^2\right] + O(\phi^3). \tag{6}$$

The boundary conditions for ϕ are obtained by making the particle velocity normal to the walls vanish,

$$\frac{\partial\phi}{\partial x} = 0 \quad \text{at } x = \pm\frac{L}{2}, \tag{7}$$

as well as by matching Eq. (6) at $z = 0$ to Eq. (1). Also, for uniqueness, it is required that the signal consist of a wave propagating in the positive z direction.

The initial stage of the solution technique employs a regular perturbation expansion of the potential in terms of the small parameter ϵ,

$$\phi = \epsilon\phi_1 + \epsilon^2\phi_2 + \cdots. \tag{8}$$

Matching like powers of ϵ in the differential equation and boundary conditions leads to a sequence of equations in the usual manner. The order ϵ terms are

$$c_0^2\nabla^2\phi_1 - \frac{\partial^2\phi_1}{\partial t^2} = 0, \tag{9a}$$

$$\left.\frac{\partial\phi_1}{\partial x}\right|_{x=\pm L/2} = 0, \tag{9b}$$

$$\left.\frac{\partial\phi_1}{\partial t}\right|_{z=0} = i\frac{c_0^2}{4}\{\exp[i(\omega t - k_x x)] + \exp[i(\omega t + k_x x)]\} + \text{c.c.}, \tag{9c}$$

where c.c., in general, shall denote the complex conjugate of all preceding terms. The order ϵ^2 perturbation equations are

$$c_0^2\nabla^2\phi_2 - \frac{\partial^2\phi_2}{\partial t^2} = \frac{\partial}{\partial t}\left[\frac{1}{c_0^2}(\beta_0 - 1)\left(\frac{\partial\phi_1}{\partial t}\right)^2 + \nabla\phi_1\cdot\nabla\phi_1\right], \tag{10a}$$

$$\left.\frac{\partial\phi_2}{\partial x}\right|_{x=\pm L/2} = 0, \tag{10b}$$

$$\left.\frac{\partial\phi_2}{\partial t}\right|_{z=0} = \left.\left[\frac{1}{c_0^2}\left(\frac{\partial\phi_1}{\partial t}\right)^2 - \frac{1}{2}\nabla\phi_1\cdot\nabla\phi_1\right]\right|_{z=0}. \tag{10c}$$

II. EVALUATION OF THE POTENTIAL

It is a straightforward matter to solve Eqs. (9) by separation of variables, with the result that

$$\phi_1 = (c_0^2/4\omega)\{\exp[i(\omega t - k_x x - k_z z)] + \exp[i(\omega t + k_x x - k_z z)]\} + \text{c.c.}, \tag{11}$$

where

$$k = \omega/c_0\,, \quad \theta = \sin^{-1}(k_x/k)\,,$$
$$k_z = k\cos\theta \equiv (k^2 - k_x^2)^{1/2}\,. \tag{12}$$

Only the case of propagating, rather than evanescent, waves is of interest, which means that $k_x < k$. This condition is obtained whenever ω exceeds the cutoff frequency for the fundamental mode, $\omega > 2\pi c_0/L$.

Equation (11) represents the first-order solution as two trains of planar waves propagating symmetrically relative to the centerline $x = 0$. These waves are depicted in Fig. 1, where e_1 and e_2 are the individual directions. The angle θ measures the direction in which these waves propagate, relative to the centerline. Each wave represents the reflection of the other from the rigid walls. Increasing either the frequency ω or the width L decreases θ. In the limit $\theta \to 0$, the combination of the two trains of waves has the same phase speed as the planar mode, and the transverse variation is much more gradual than it is in the axial direction. Hence, the (2,0) mode at high frequencies seems to be locally planar.

The first step in deriving ϕ_2 is to use Eq. (11) to form the inhomogeneous terms in Eq. (10a). This yields

$$\begin{aligned} c_0^2\nabla^2\phi_2 - \frac{\partial^2\phi_2}{\partial t^2} &= -(i/8)c_0^2\omega\beta_0\{\exp[2i(\omega t - k_x x - k_z z)] \\ &\quad + \exp[2i(\omega t + k_x x - k_z z)]\} \\ &\quad - (i/4)c_0^2\omega[\beta_0 - 2(k_x^2/k^2)]\exp[2i(\omega t - k_z z)] \\ &\quad + \text{c.c.} \end{aligned} \tag{13}$$

The first two exponentials in Eq. (13) excite second harmonics. Such signals propagate parallel to the two waves forming ϕ_1, which are homogeneous solutions of the linearized wave equation. The corresponding particular solution may be obtained by the method of variation of parameters, in which the amplitude of the homogeneous solution is considered to be an unknown function. The last inhomogeneous term is a planar second harmonic. Such an excitation matches the planar mode for the waveguide when $k_z = k$. Hence, decreasing k_x brings the planar part of the excitation into close coincidence with the planar mode for that frequency, which means that this excitation is nearly resonant at small k_x. The method of variation of parameters will also yield the solution associated with this term. Thus let

$$\begin{aligned} \phi_2 &= u(x,z)\exp(2i\omega t) + \text{c.c.}\,, \\ u &= C(z)\{\exp[-2i(k_z z + k_x x)] \\ &\quad + \exp[-2i(k_z z - k_x x)]\} \\ &\quad + D(z)\exp(-2ik_z z)\,. \end{aligned} \tag{14}$$

It should be noted that the unknown functions C and D depend on the axial distance only. The periodic nature of the excitation eliminates dependence of these functions on t. Similarly, the rigid wall conditions, Eq. (10b), imposed along $x = \pm\pi/k_x$, could not be satisfied if C or D were functions of x.

The result of requiring that Eqs. (14) satisfy Eq. (13) is a set of uncoupled differential equations for the amplitude functions. After Eq. (12) for k_z is applied, these equations are found to be

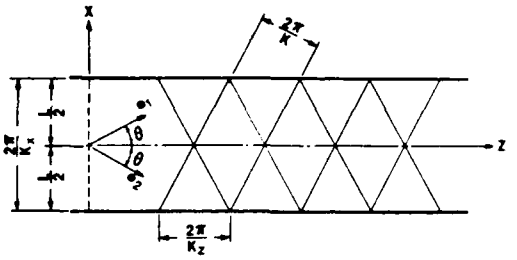

FIG. 1. Geometry of the oblique waves.

$$\begin{aligned} C'' - 4ik_z C' &= -\tfrac{1}{8}i\beta_0\omega\,, \\ D'' - 4ik_z D' + 4K_x^2 D &= -\tfrac{1}{4}i\omega(\beta_0 - 2k_x^2/k^2)\,, \end{aligned} \tag{15}$$

where a prime denotes differentiation with respect to z.

The particular solutions of Eqs. (15) are readily found to be

$$\begin{aligned} C_p &= (\beta_0\omega/32k_z)z\,, \\ D_p &= -\frac{i\omega}{16}\left(\frac{\beta_0}{k_x^2} - \frac{2}{k^2}\right). \end{aligned} \tag{16}$$

It is convenient to let the constant coefficients of C_p and D_p appear explicitly in the corresponding complementary solutions, which are therefore written as

$$\begin{aligned} C_c &= (\beta_0\omega/32k_z)[C_1 + C_2\exp(4ik_z z)]\,, \\ D_c &= -\frac{i\omega}{16}\left(\frac{\beta_0}{k_x^2} - \frac{2}{k^2}\right)[D_1\exp(\lambda_1 z) + D_2\exp(\lambda_2 z)], \end{aligned} \tag{17}$$

where λ_1 and λ_2 are roots of the characteristic equation

$$\lambda_{1,2}^2 - 4ik_z\lambda_{1,2} + 4k_x^2 = 0\,. \tag{18a}$$

The roots are found, with the aid of Eqs. (12), to be

$$\lambda_1 = 2i(k_z - k)\,, \quad \lambda_2 = 2i(k_z + k)\,. \tag{18b}$$

The expressions for ϕ_2, obtained by substituting Eqs. (16) and (17) into Eqs. (14), must satisfy the radiation condition. In order for ϕ_2 to represent an outgoing wave in the z direction, it must only contain negative imaginary exponentials in the z variable. Satisfaction of this condition requires that $C_2 = D_2 = 0$. The remaining terms yield

$$\begin{aligned} u &= \frac{\beta_0\omega}{32k_z}(z + C_1)\{\exp[-2i(k_z z + k_x x)] \\ &\quad + \exp[-2i(k_z z - k_x x)]\} - \frac{i\omega}{16}\left(\frac{\beta_0}{k_x^2} - \frac{2}{k^2}\right) \\ &\quad \times [\exp(-2ik_z z) + D_1\exp(-2ikz)]\,. \end{aligned} \tag{19}$$

Note that C_1 describes complementary solutions of the wave equation associated with second harmonics of the oblique waves, whereas D_1 is the planar eigenmode at the second harmonic frequency.

The case $k_x \equiv 0$ corresponds to a true planar mode, which is governed by the Earnshaw solution for a nonlinear planar wave. However, letting $k_x \to 0$ in Eq. (19) results in a singularity in the coefficient of the last terms.

Such behavior resembles the case of resonance in a one-degree-of-freedom oscillator, whose equation of motion is

$$\ddot{x} + \omega^2 x = F \sin \Omega t \,. \tag{20}$$

When $\Omega \to \omega$, the amplitude of the particular solution for $\Omega \neq \omega$ increases, as does the portion of the complementary solution that cancels the initial value of the particular solution. The combination of these two solutions is a temporal beating response that rises from zero at the initial time. As the difference between Ω and ω decreases further, the period of each beat increases, until ultimately at $\Omega = \omega$, only the rising portion remains. The corresponding resonant response is a harmonic, at frequency ω, whose amplitude increases linearly with time.

In the same manner, the singularity of Eq. (19) at $k_x \to 0$ may be removed by an appropriate selection of the coefficient of the homogeneous solutions. The coefficient C_1 is not used for this purpose because the singularity is associated with the planar mode.

In order to study $k_x \to 0$, the troublesome terms in Eq. (19) are expanded in a Taylor series about k_x/k,

$$\begin{aligned} k_z &\equiv (k^2 - k_x^2)^{1/2} = k - \tfrac{1}{2}(k_x^2/k) + \cdots, \\ \exp(-ik_z z) &= \exp[-i(k - \tfrac{1}{2}k_x^2/k)z + \cdots] \\ &= [1 + (ik_x^2/2k)z + \cdots] \exp(-ikz) \,. \end{aligned} \tag{21}$$

The corresponding asymptotic form of the planar terms in Eq. (19) is

$$\begin{aligned} &-\frac{i\omega}{16}\left(\frac{\beta_0}{k_x^2} - \frac{2}{k^2}\right)[\exp(-2ik_z z) + D_1 \exp(-2ikz)] \\ &\quad = -\frac{i\omega}{16}\left(\frac{\beta_0}{k_x^2} - \frac{2}{k^2}\right)\left(1 + \frac{ik_x^2 z}{2k} + D_1\right) \\ &\qquad \times \exp_1(-2ikz) \,. \end{aligned} \tag{22}$$

The singularity for $k_x \to 0$ is canceled if the leading term in $D_1 = -1$. Thus let

$$D_1 = -1 + D^* \,, \tag{23a}$$

where the coefficient D^* may depend on k_x in any manner that satisfies the condition

$$\lim_{k_x \to 0} \frac{D^*}{k_x^2} = \delta \,, \tag{23b}$$

where δ is a bounded number. Similarly, the coefficient C_1 is restricted to depend on k_x in any manner that is not singular as $k_x \to 0$.

The second-order potential is now found from Eqs. (14) and (19) to be

$$\begin{aligned} \phi_2 = &\frac{\beta_0 \omega}{32 k_z}(z + C_1)\exp(2i\omega t) \\ &\times [\exp(-2i\psi_1) + \exp(-2i\psi_2)] \\ &- \frac{i\omega}{16}\left(\frac{\beta_0}{k_x^2} - \frac{2}{k^2}\right)\exp(2i\omega t)\{\exp[-i(\psi_1 + \psi_2)] \\ &+ (-1 + D^*)\exp[-i(\psi_1 + \psi_2)k/k_z]\} + \text{c.c.} \,, \end{aligned} \tag{24}$$

where

$$\psi_1 = k_z z + k_x x \,, \quad \psi_2 = k_z z - k_x x \,. \tag{25}$$

The foregoing expression for ϕ_2 satisfies the wall conditions, Eq. (10b). At this juncture, ϕ_2 does not satisfy the boundary condition, Eq. (10c), which specifies that there should be no second-order contribution to the pressure at $z = 0$. This condition could be satisfied by appropriate selection of the coefficients C_1 and D^*. However, both of these describe homogeneous solutions for ϕ_2, and they are not singular as $k_x \to 0$. Thus they represent effects that are $O(\epsilon^2)$ at all locations. In contrast, observable distortion phenomena are associated with second-order terms that grow with increasing distance. The bounded $O(\epsilon^2)$ effects might be significant, in comparison to the cumulative growth effects near the excitation, but both are small in that region. The bounded effects are overwhelmed by the growth effects with increasing distance. Therefore, setting

$$C_1 = D^* = 0 \tag{26}$$

leads to insignificant errors at locations where nonlinear effects are substantial. The corresponding potential function obtained from Eqs. (8), (11), and (24) is

$$\begin{aligned} \phi = &\epsilon \frac{c_0^2}{4\omega}\exp(i\omega t)[\exp(-i\psi_1) + \exp(-i\psi_2)] + \epsilon^2 \frac{\beta_0 \omega}{32 k_z} z \exp(2i\omega t)[\exp(-2i\psi_1) + \exp(-2i\psi_2)] \\ &- \epsilon^2 \frac{i\omega}{16}\left(\frac{\beta_0}{k_x^2} - \frac{2}{k^2}\right)\exp(2i\omega t)\{\exp[-i(\psi_1 + \psi_2)] - \exp[-i(\psi_1 + \psi_2)k/k_z]\} + \text{c.c.} + O(\epsilon^2) \,, \end{aligned} \tag{27}$$

where $O(\epsilon^2)$ refers to terms having that order of magnitude at all locations.

III. EVALUATION OF THE PRESSURE

Prior formulations of nonlinear propagation using the velocity potential have generated the potential in the form of a separation of variables solution. Specifically, the expression was a product of functions of each space variable and time. In that situation, it was necessary to consider individually the state variables of particle velocity and pressure.

The present case is different because the potential is now represented as two planar waves, each of which is described by a single propagation distance parameter. In general, proper behavior of the expression for pressure in a simple planar wave ensures comparable results for the other state variables. The pressure is related to the potential function by Eq. (6). Omission of the quadratic products in that relation ignores terms that are uniformly $O(\epsilon^2)$, which is comparable to the error in Eq. (27) for ϕ. Thus

$$\frac{p}{\rho_0 c_0^2} = -\frac{1}{c_0^2}\frac{\partial \phi}{\partial t} + O(\epsilon^2) = -\frac{1}{4}\epsilon i \exp(i\omega t)[\exp(-i\psi_1) + \exp(-i\psi_2)] - \frac{1}{16}\epsilon^2 i\beta_0 \frac{k^2}{k_z} z \exp(2i\omega t)$$
$$\times[\exp(-2i\psi_1) + \exp(-2i\psi_2)] - \frac{1}{8}\epsilon^2\left(\beta_0 \frac{k^2}{k_x^2} - 2\right)\exp(2i\omega t)$$
$$\times\{\exp[-i(\psi_1+\psi_2)] - \exp[-i(\psi_1+\psi_2)k/k_z]\} + \text{c.c.} + O(\epsilon^2)\,. \tag{28}$$

The first set of $O(\epsilon^2)$ terms grows with increasing z in all cases, and the second set grows when k_x/k is very small. Such functional behavior is a result of using z and x as position variables, neither of which consistently matches the spatial scaling of the nonlinear processes. In order to ascertain the correct spatial dependence, a near-identity transformation in the form of a coordinate straining is employed. A different transformation is introduced for each wave variable ψ_1 and ψ_2.

The presence of $O(\epsilon^2)$ terms in Eq. (28) that depend on $\psi_1 + \psi_2$ indicates that the waves interact. Further examination of the form of Eq. (28) suggests the trial transformations

$$\psi_j = \alpha_j + \epsilon[F_j(\alpha_1,\alpha_2)\exp(i\omega t) + \bar{F}_j(\alpha_1,\alpha_2)\exp(-i\omega t)] + \cdots;\quad j = 1,2\,, \tag{29}$$

where the complex conjugate term, denoted by an overbar, is introduced in order to ensure that the transformation is real. Substitution for ψ_1 and ψ_2 into Eq. (28), followed by expansion in Taylor series in powers of ϵ, yields

$$p/\rho_0 c_0^2 = -\tfrac{1}{4}\epsilon i \exp(i\omega t)[\exp(-i\alpha_1) + \exp(-i\alpha_2)] - \tfrac{1}{4}\epsilon^2[F_1\exp(2i\omega t - i\alpha_1) + \bar{F}_1\exp(-i\alpha_1)$$
$$+ F_2\exp(2i\omega t - i\alpha_2) + \bar{F}_2\exp(-i\alpha_2)] - \tfrac{1}{16}\epsilon^2 i\beta_0(k^2/k_z)z\exp(2i\omega t)[\exp(-2i\alpha_1) + \exp(-2i\alpha_2)]$$
$$- \tfrac{1}{8}\epsilon^2[\beta_0(k^2/k_x^2) - 2]\exp(2i\omega t)\{\exp[-i(\alpha_1+\alpha_2)] - \exp[-i(\alpha_1+\alpha_2)k/k_z]\} + \text{c.c.} + O(\epsilon^2)\,. \tag{30}$$

The task now is to determine the functions F_1 and F_2 that cancel all $O(\epsilon^2)$ second harmonic terms which grow with increasing z. For this, the terms that depend on $\alpha_1 + \alpha_2$ are apportioned equally between F_1 and F_2. The appropriate choice is found to be

$$F_1 = -\frac{i\beta_0 k^2}{4k_z} z\exp(-i\alpha_1) - \frac{1}{4}\left(\beta_0\frac{k^2}{k_x^2} - 2\right)$$
$$\times\left\{\exp(-i\alpha_2) - \exp\left[-i\alpha_1\left(\frac{k}{k_z} - 1\right) - i\alpha_2\frac{k}{k_z}\right]\right\},$$
$$F_2 = -\frac{i\beta_0 k^2}{4k_z} z\exp(-i\alpha_2) - \frac{1}{4}\left(\beta_0\frac{k^2}{k_x^2} - 2\right) \tag{31}$$
$$\times\left\{\exp(-i\alpha_1) - \exp\left[-i\alpha_2\left(\frac{k}{k_z} - 1\right) - i\alpha_1\frac{k}{k_z}\right]\right\}.$$

These straining functions do not cancel all $O(\epsilon^2)$ terms in the pressure. The remaining terms, which are created by the complex conjugates of F_1 and F_2, contain combinations of the α_1 and α_2 variables. Their presence is not a problem, because they are independent of t. Their role is to cancel a mean value of the pressure that is created by the coordinate transformation.

It is convenient at this juncture to write the coordinate transformations and pressure resulting from Eqs. (28)–(30) in real functional form. The pressure is governed by

$$\frac{p}{\rho_0 c_0^2} = \frac{\epsilon}{2}[\sin(\omega t - \alpha_1) + \sin(\omega t - \alpha_2)]$$
$$+ \frac{1}{8}\epsilon^2\left(\beta_0\frac{k^2}{k_x^2} - 2\right)$$
$$\times\{2\cos(\alpha_1 - \alpha_2) - \cos[2\alpha_1 - (k/k_z)(\alpha_1+\alpha_2)]$$
$$- \cos[2\alpha_2 - (k/k_z)(\alpha_1+\alpha_2)]\}\,, \tag{32}$$

where

$$\psi_1 \equiv k_z z + k_x x$$
$$= \alpha_1 + \tfrac{1}{2}\epsilon\beta_0(k^2/k_z)z\sin(\omega t - \alpha_1)$$
$$- \tfrac{1}{2}\epsilon[\beta_0(k^2/k_x^2) - 2]\{\cos(\omega t - \alpha_2)$$
$$- \cos[\omega t - \alpha_2 - (k/k_z - 1)(\alpha_1+\alpha_2)]\}\,, \tag{33a}$$

$$\psi_2 \equiv k_z z - k_x x$$
$$= \alpha_2 + \tfrac{1}{2}\epsilon\beta_0(k^2/k_z)z\sin(\omega t - \alpha_2)$$
$$- \tfrac{1}{2}\epsilon[\beta_0(k^2/k_x^2) - 2]\{\cos(\omega t - \alpha_1)$$
$$- \cos[\omega t - \alpha_1 - (k/k_z - 1)(\alpha_1+\alpha_2)]\}\,. \tag{33b}$$

The foregoing relations fully define the pressure. The value of p at specified x, z, and t may be determined by solving Eqs. (33) simultaneously for the values of α_1 and α_2, and then using those values to compute p. It should be noted that the terms in Eqs. (33) that couple α_1 and α_2 do not explicitly grow with z. However, as $k_x/k \to 0$, their magnitude increases and their axial wavenumbers approach k for planar waves. This sets up a beating interaction that has the appearance of growth (see Sec. V).

IV. ASYMPTOTIC TRENDS

Equations (32) and (33) are generally valid, but examination of the behavior at limiting values of k_x/k provides important insights. For $k_x/k \ll 1 (\omega L/c_0 \gg 2\pi)$, the coordinate transformation may be expanded in a power series in k_x/k. First, apply the identity for the cosine of a sum to the last term in Eq. (33a).

$$\psi_1 = \alpha_1 + \frac{1}{2}\epsilon\beta_0\frac{k^2}{k_z} z\sin(\omega t - \alpha_1) + \epsilon\left(\beta_0\frac{k^2}{k_x^2} - 2\right)$$
$$\times\sin\left[\omega t - \alpha_2 - \frac{1}{2}\left(\frac{k}{k_z} - 1\right)(\alpha_1+\alpha_2)\right]$$
$$\times\sin\left[\frac{1}{2}\left(\frac{k}{k_z} - 1\right)(\alpha_1+\alpha_2)\right]. \tag{34}$$

Since $k/k_z \to 1 + k_x^2/2k^2 + \cdots$, the leading terms in a Taylor series expansion of Eqs. (33) are

$$\psi_1 \sim \alpha_1 + \tfrac{1}{2}\epsilon\beta_0 kz \sin(\omega t - \alpha_1) + \tfrac{1}{4}\epsilon\beta_0(\alpha_1 + \alpha_2)\sin(\omega t - \alpha_2) . \quad (35a)$$

When the same operations are performed on Eq. (33b), the result is

$$\psi_2 \sim \alpha_2 + \tfrac{1}{2}\epsilon\beta_0 kz \sin(\omega t - \alpha_2) + \tfrac{1}{4}\epsilon\beta_0(\alpha_1 + \alpha_2)\sin(\omega t - \alpha_1) . \quad (35b)$$

According to these relations, the values of α_1 and α_2 may be estimated as $\alpha_i = \psi_i + O(\epsilon kz)$. Hence, the factor $\epsilon(\alpha_1 + \alpha_2)$ may be replaced by $\epsilon(\psi_1 + \psi_2) \equiv 2\epsilon k_z z$, which is approximately $2\epsilon kz$ because of the smallness of k_x/k. Thus the coordinate transformations have the common limiting form

$$\psi_i \sim \alpha_i + \tfrac{1}{2}\epsilon\beta_0 kz[\sin(\omega t - \alpha_1) + \sin(\omega t - \alpha_2)] \equiv \alpha_i + \epsilon\beta_0 kz \sin\left(\omega t - \frac{\alpha_1 + \alpha_2}{2}\right)\cos\left(\frac{\alpha_1 - \alpha_2}{2}\right), \quad (36)$$

from which it follows that

$$\begin{aligned} &\psi_1 - \psi_2 \equiv 2k_x x \sim \alpha_1 - \alpha_2 , \\ &\psi_1 + \psi_2 \equiv 2k_z z \sim \alpha_1 + \alpha_2 + 2\epsilon\beta_0 kz \times \sin\left(\omega t - \frac{\alpha_1 + \alpha_2}{2}\right)\cos\left(\frac{\alpha_1 - \alpha_2}{2}\right) . \end{aligned} \quad (37)$$

The same analysis is now applied to Eq. (32). Series expansion in powers of k_x/k yields

$$\begin{aligned} \frac{p}{\rho_0 c_0^2} = {} & \frac{\epsilon}{2}[\sin(\omega t - \alpha_1) + \sin(\omega t - \alpha_2)] + \frac{1}{8}\epsilon^2\left(\beta_0 \frac{k^2}{k_x^2} - 2\right) \\ & \times \{2\cos(\alpha_1 - \alpha_2) - \cos[(\alpha_1 - \alpha_2) - (k_x^2/2k^2)(\alpha_1 + \alpha_2)] - \cos[(\alpha_1 - \alpha_2) - (k_x^2/2k^2)(\alpha_1 - \alpha_2)]\} \\ & \sim \epsilon \sin\left(\omega t - \frac{\alpha_1 + \alpha_2}{2}\right)\cos\left(\frac{\alpha_1 - \alpha_2}{2}\right) . \end{aligned} \quad (38)$$

The next step is to substitute the first of Eqs. (37) into the foregoing, and to use the resulting expression for p to eliminate $\alpha_1 + \alpha_2$ between the second of Eqs. (37) and Eq. (38). The pressure expression that is derived in this manner is

$$\frac{p}{\rho_0 c_0^2} \sim \epsilon \sin\left(\omega t - k_z z + \beta kz \frac{p}{\rho_0 c_0^2}\right)\cos(k_x x) . \quad (39)$$

If $k_x \equiv 0$, this expression reduces to the well-known solution for a planar finite amplitude wave at moderate amplitudes.[18] For very small k_x/k, the signal described by Eq. (39) is a quasiplanar wave. The distortion is meassured by the value of $\beta_0 kzp$, the change in the axial phase variable from its value $\omega t - k_z z$ in linear theory. The wave is not truly planar because the amplitude varies with transverse position as $\cos(k_x x)$. Comparable phenomena are encountered in the farfield of cylindrical and spherical waves, whose amplitude is not uniform in the transverse direction.[11,19]

Suppose that the limits of Eqs. (32) and (33) for small k_x/k had been derived without considering the interaction terms (those containing both α_1 and α_2). The result would have been the same, except that β_0 in such an expression would have been replaced by $\frac{1}{2}\beta_0$. In other words, half the nonlinear effect when $k_x \ll k$ is due to interaction between the oblique waves.

The situation for comparatively low frequencies (exceeding cutoff) can also be examined asymptotically. Suppose that $k_x/k = O(1)$ (recall that $k_x < k$ for propagating modes). In that case the interactive terms in Eqs. (32) and (33) are not asssociated with beating interactions, so they remain $O(\epsilon^2)$ at all locations. Such effects may be ignored. The remaining terms may be written as

$$p = p_1 + p_2, \quad p_j/\rho_0 c_0^2 = \tfrac{1}{2}\epsilon \sin(\omega t - \alpha_j); \quad j = 1,2 , \quad (40a)$$

where

$$\psi_j = \alpha_j + \beta_0(k^2/k_z)z(p_j/\rho_0 c_0^2) . \quad (40b)$$

The coordinate straining for each wave p_j is reminiscent of that for a planar wave, with an important exception. The nonlinear effect is measured by the difference between the nonlinear and linear spatial phases, $\alpha_j - \psi_j$. In an isolated planar wave, this difference is proportional to the propagation distance, which would be $(k_z z \pm k_x x)/k$ for waves propagating in the direction of either oblique wave. Instead, the distance parameter for each wave in Eq. (40b) is $z\ k/k_z$. It follows that although Eqs. (39) specify a superposition of the oblique waves, the presence of one affects the other by altering the spatial dependence for the distortion phenomena.

Another viewpoint for the low-frequency (long axial wavelength) case may be obtained from a different resolution. Define new strained coordinates η, ξ such that

$$\alpha_1 = \xi + \eta , \quad \alpha_2 = \xi - \eta . \quad (41)$$

Return now to Eqs. (32) and delete the second $O(\epsilon)$ term in each, because those terms are not growth effects when $k_x/k = O(1)$. The variables α_1 and α_2 are removed from the functional dependence by forming the sum and difference of those equations after substitution of Eqs. (41). This yields

$$\begin{aligned} k_z z &= \xi + \tfrac{1}{2}\epsilon\beta_0(k^2/k_z)z \sin(\omega t - \xi)\cos(\eta) , \\ k_x x &= \eta - \tfrac{1}{2}\epsilon\beta_0(k^2/k_z)z \cos(\omega t - \xi)\sin(\eta) . \end{aligned} \quad (42)$$

The corresponding expression for pressure obtained from Eq. (32) is

$$p/\rho_0 c_0^2 = \epsilon \sin(\omega t - \xi)\cos(\eta) + O(\epsilon^2) . \quad (43)$$

The significance of this representation of the signal becomes apparent when the particle velocity is evaluated. For this, the oblique planar wave decomposition is useful. The

approximation $v = p/\rho c_0$ is applicable to weakly nonlinear, as well as linear, planar waves. The propagation directions $\bar{e}_1$ and $\bar{e}_2$ in Fig. 1 may be used in conjunction with Eqs. (32) and (41) to represent the individual contributions. Thus

$$\mathbf{v} = \tfrac{1}{2}c_0\epsilon[\mathbf{e}_1 \sin(\omega t - \xi - \eta) + \mathbf{e}_2 \sin(\omega t - \xi + \eta)] + O(\epsilon^2). \tag{44a}$$

The components of particle velocity are, therefore,

$$v_z = \mathbf{v}\cdot\boldsymbol{\epsilon}_z = c_0\epsilon(k_z/k)\sin(\omega t - \xi)\cos(\eta),$$
$$v_x = \mathbf{v}\cdot\mathbf{e}_x = -c_0\epsilon(k_x/k)\cos(\omega t - \xi)\sin(\eta). \tag{44b}$$

These expressions may be substituted into Eqs. (41), with the result that the new strained coordinates are found to be governed by

$$k_z z = \xi + \frac{1}{2}\beta_0\frac{k^3}{k_z^2} z\frac{v_z}{c_0},$$
$$k_x x = \eta + \frac{1}{2}\beta_0\frac{k^3}{k_x k_z} z\frac{v_x}{c_0}. \tag{45}$$

This form was derived in the earlier analysis that assumed noninteracting modes.[10] Constant values of ξ and η are wave fronts and rays, respectively, for the phase of the wave in Eq. (43). The velocity components transverse to these lines are v_z and v_x, respectively. Hence, the dependence of the wave fronts on v_z, and of the rays on v_x, was ascribed to self-refraction in the earlier work.

V. EXAMPLE

The trends identified in Sec. IV indicate that, at low frequencies $[k_x = O(k)]$, the distortion process involves only the harmonics of the fundamental mode for the waveguide. In contrast, at high frequencies ($k_x \ll k$), the tendency is to form a quasiplanar wave that propagates like the true planar mode. Identification of these trends leaves the questions of when the transitions to each situation occur, and what happens in the intermediate regime?

These matters may be addressed by numerical examples. Quantitative results, in general, are obtained by solving the coupled transcendental equations (33) for the strained coordinates α_1 and α_2, corresponding to specified values of x, z, and t. These values then yield the pressure according to Eq. (32). If desired, a waveform may be generated by incrementing ωt through an interval 2π, and that result may be Fourier analyzed to determine the frequency response. One simplification in performing a numerical evaluation is that, for specified properties of the fluid, the value of $p/\rho_0 c_0^2$ obtained from Eqs. (32) and (33) depends only on the independent variables kx, kz, and ωt and on the value of kL (because $k_x/k \equiv 2\pi/kL$). For the discussion that follows, the fluid is air ($\rho_0 = 1.2\ \mathrm{kg/m^3}$, $c_0 = 343\ \mathrm{m/s}$, $\beta_0 = 1.2$) and $F = 10\ \mathrm{kHz}$.

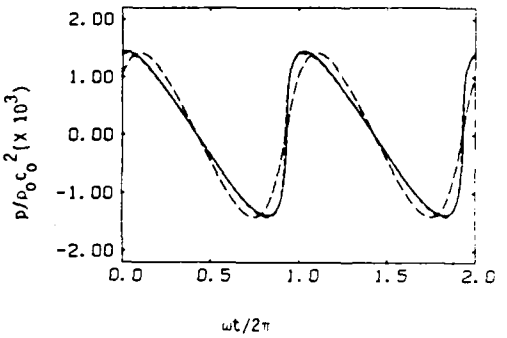

FIG. 3. Waveform on-axis at $z = 3.05$ m for 140 dB at the origin, $L = 2.0$ m, $f = 10$ kHz. —: interacting waves; – – –: noninteractive theory; - - -: quasiplanar wave.

A case of comparatively low frequency is illustrated in Fig. 2, for which $L = 0.20$ m and $\epsilon = 0.0014166$, corresponding to an excitation of 140 dB *re*: 20 μPa at the origin. For comparison, the noninteractive theory, Eqs. (40), and the quasiplanar limit, Eq. (39), are also shown in Fig. 2. The unimportance of the mixing between the oblique waves is apparent, as is the fact that the distortion associated with the planar theory is stronger.

Altering the frequency for the next example would change the overall degree of nonlinearity. For example, the distance for shock formation in the planar wave is

$$\sigma = 1/(\epsilon\beta_0 k). \tag{46}$$

Since the degree to which wave interaction is significant depends (nondimensionally) only on the value of kL, the var-

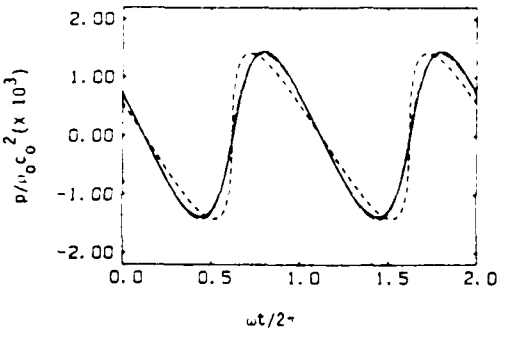

FIG. 2. Waveform on-axis at $z = 3.05$ m for 140 dB at the origin, $L = 0.2$ m, $f = 10$ kHz. —: interacting waves; – – –: noninteractive theory; - - -: quasiplanar wave.

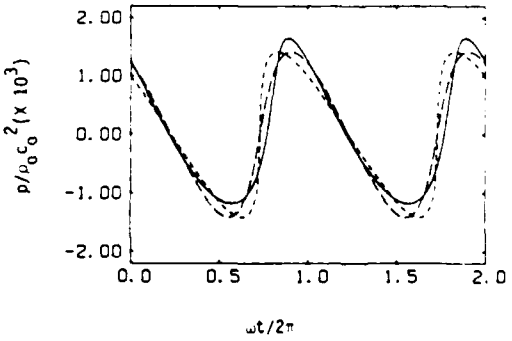

FIG. 4. Waveform on-axis at $z = 3.05$ m for 140 dB at the origin, $L = 0.5$ m, $f = 10$ kHz. —: interacting waves; – – –: noninteractive theory; - - -: quasiplanar wave.

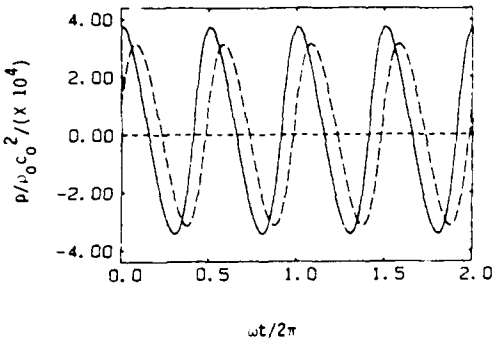

FIG. 5. Waveform at $x = 0.125$ m, $z = 3.05$ m for 140 dB at the origin, $L = 0.5$ m, $f = 10$ kHz. — : interacting waves; - - - : noninteractive theory; · · · : quasiplanar wave.

ious phenomena shall be explored by changing L. Thus the next case, illustrated in Fig. 3, is for $L = 2$ m, with the other parameters unchanged. The quasiplanar approximation is now very close to the new theory.

The situation for a transitional case is shown in Fig. 4, which corresponds to $L = 0.5$ m. Neither approximation is accurate here. The difference between the axial-phase speeds of the planar harmonic created by nonlinearity and the true planar mode is relatively small. This leads to frequency dispersion in combination with the usual amplitude dispersion that is associated with a sawtooth waveform. The effect is asymmetrical between compression and rarefaction; it is remarkably similar to the nearfield distortion observed for baffled transducers.[16]

The relatively drastic transition from one approximate theory to another, resulting from increasing kL by a factor of 10, has a direct explanation. The frequency dispersion phenomenon is attributable to spatial beating described by the last terms in the coordinate transformations, Eqs. (33). The trigonometric identity for the difference of cosines applied to these terms shows that

$$\cos(\omega t - \alpha_i) - \cos[\omega t - \alpha_i - (k/k_z - 1)(\alpha_i + \alpha_j)] = -2\sin[(\alpha_j + \alpha_i)(k/k_z - 1)]\sin[\omega t + \tfrac{1}{2}(\alpha_j - \alpha_i) - \tfrac{1}{2}(\alpha_j + \alpha_i)(k/k_z)]; \quad i,j = 1,2, \quad i \neq j. \tag{47}$$

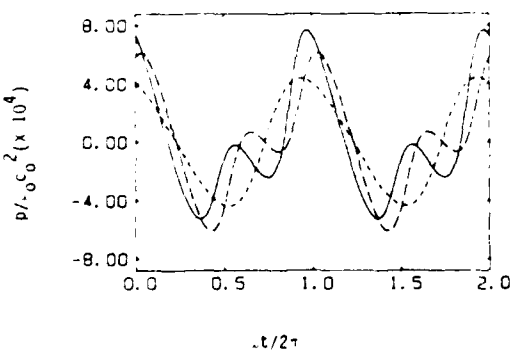

FIG. 6. Waveform at $x = 0.1$ m, $z = 3.05$ m for 140 dB at the origin, $L = 0.5$ m, $f = 10$ kHz. — : interacting waves; - - - : noninteractive theory; · · · : quasiplanar wave.

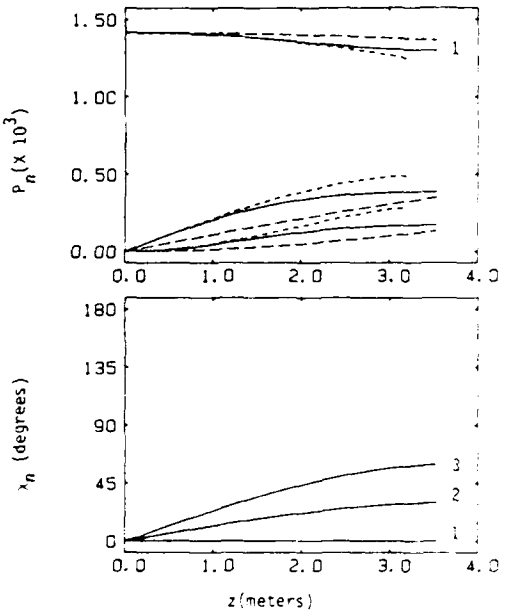

FIG. 7. Axial dependence of frequency response along $x = 0$ for 140 dB at the origin, $L = 0.5$ m, $f = 10$ kHz. — : interacting waves; - - - : noninteractive theory; · · · : quasiplanar wave.

The first sinusoidal factor is independent of time; it governs the wavelength of the beats. When the argument of that sine term is very small, compared to π, the factor is well approximately by $(\alpha_j + \alpha_i)(k/k_z - 1)$. Since α_1 and α_2 may be approximated by $k_z z$, small values of the aforementioned argument correspond to cumulative growth of the frequency dispersion effect.

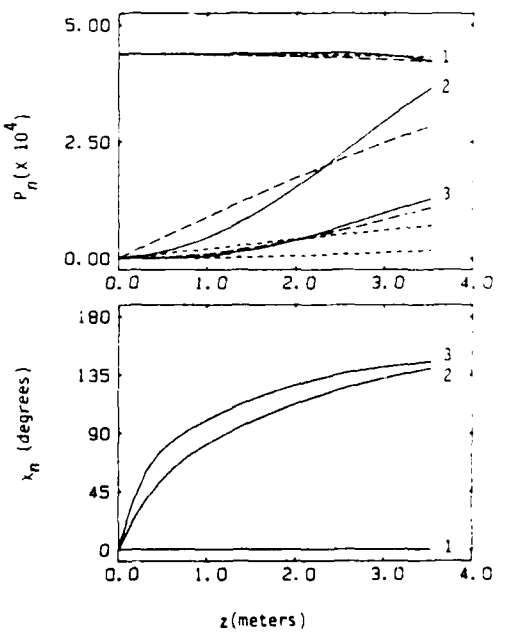

FIG. 8. Axial dependence of frequency response along $x = 0.1$ m for 140 dB at the origin, $L = 0.5$ m, $f = 10$ kHz. — interacting waves, - - - noninteractive theory; · · · : quasiplanar wave.

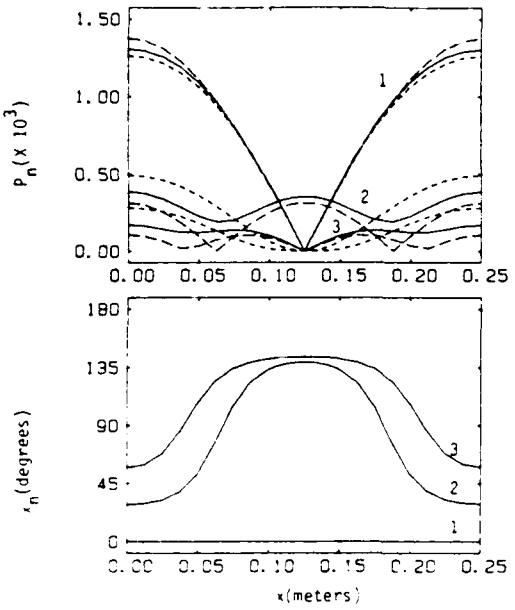

FIG. 9. Transverse dependence of frequency response along $z = 3.05$ m for 140 dB at the origin. $L = 0.5$ m, $f = 10$ kHz. — interacting waves; - - - noninteractive theory; · · · quasiplanar wave.

It follows that the prominence of frequency dispersion is indicated by $\pi/[2k_z z(k/k_z - 1)]$. In contrast, the significance of the sawtooth distortion effect is measured by the ratio of the axial distance z to the planar shock distance σ. A comparison of the two nondimensional factors indicates whether frequency dispersion will be noticeable in the presence of sawtooth distortion. Thus, define a beating parameter B according to

$$B = \frac{z/\sigma}{\pi/[2kz(k/k_z - 1)]} = \frac{2}{\pi}\epsilon\beta_0(kz)^2\left(\frac{1-(1-k_x^2/k^2)^{1/2}}{(1-k_x^2/k^2)^{1/2}}\right). \quad (48)$$

This parameter is 5.08, 0.05, and 0.798 for Figs. 2–4, respectively. Cases where B is substantially greater than unity can be anticipated to be well described by the earlier noninteractive theory for duct modes, whereas values that are much less than unity will closely fit the planar wave approximation.

Another aspect of the distortion process is displayed in Figs. 5 and 6, which are waveforms at off-axis locations. The line $x/L = \frac{1}{4}$ is a node according to linear theory, as well as the quasiplanar-nonlinear approximation. However, Fig. 5, which corresponds to such a location, shows that only the odd harmonics are nulled in the oblique wave theories. Hence, the fundamental frequency of the signal at the "nodes" is twice the excitation frequency. Note that both oblique wave theories indicate that the tendency to form a sawtooth profile is still present.

The nulling of the odd harmonics was explained in the earlier analysis of the plate problem as being a result of self-refraction.[4,6] The rays in the noninteractive theory were shown to be distorted in the direction of the transverse velocity component. This caused the nodal ray to cross the axial line of zero-linearized pressure twice per axial wavelength thereby setting up the second harmonic signal. It is apparent from Fig. 5 that this effect also occurs in the presence of frequency dispersion resulting from interaction of the oblique waves.

A waveform for a general location appears in Fig. 6. The even harmonics are more prominent than they were in Fig. 4 because the odd harmonics are lessened by the proximity to the nodal line. This effect is accompanied by amplitude dispersion, as evidenced by the tendency to a sawtooth profile, and by frequency dispersion, as indicated by the asymmetry between compression and rarefaction.

A different perspective is offered by the amplitude and phase distribution curves in Figs. 7–9. These curves were obtained by Fourier series decomposition of the computer waveforms into

$$\frac{p}{\rho_0 c_0^2} = \sum_n p_n \sin[n\omega(t - t_0) - \chi_n]; \quad \chi_1 = 0, \quad (49)$$

where t_0 is the arrival time of the fundamental in the interacting-oblique wave theory. The amplitudes p_n are displayed for the three nonlinear theories. However, the phase lags χ_n are displayed only for the latest theory—they vanish in the other descriptions in which the waveform distorts symmetrically.

Although only three harmonics are displayed in Figs. 7–9, their trends are also indicative of higher harmonics. The earlier observation of the increased relative contribution of the even harmonics in the vicinity of the "nodal" line $x = L/4$ is evident in Figs. 8 and 9. In addition, Fig. 7 shows that the phase of each harmonic tends to lag behind that of its predecessor by a uniform amount that increases as the signal propagates. This effect was also predicted for sound beams,[20] whose waveform in the nearfield is much like Fig. 4.

VI. CONCLUSION

The excitation of the true planar mode, which provides a mechanism for the interaction of the oblique waves forming the fundamental symmetric mode, has been shown to be significant for large values of kL. In the limit, multidimensionality is only manifested as sinusoidal variation in the transverse direction, much like the directivity factor for nonuniform spherical waves in the farfield.[19]

In the earlier (small kL) theory, the modes are formed from obliquely propagating waves whose interaction is only manifested by a change in the distance parameter governing the distortion. If each wave were truly independent, that parameter would have been the distance over which the wave had propagated. Instead, the distortion of the oblique waves depends on the axial distance. That theory has been shown here to be valid when the underlying assumption of distinct phase speeds is valid. In that case, kL is moderately larger than 2π, so that the scales with which the signal varies in the transverse and axial directions are comparable. The transition from small to large kL is predicted by the present theory to exhibit frequency dispersion that is responsible for distortion of the waveform that is not symmetrical between compression and rarefaction.

A planar second harmonic always results from quadratic nonlinearity acting on a mode at any nonzero-transverse wavenumber. Hence, the phenomena identified here may be expected to occur when modes other than (2,0) are excited. Also, it is reasonable to expect a similar coupling mechanism to arise between nonplanar modes in some situations. For example, suppose two such modes are excited. If they have disparate phase speeds, they superpose according to the noninteractive theory.[10] If the two modes have identical phase speeds, they combine to form a nondispersive group, for which the earlier theory is also valid. In the transitional situation, the modes interact because their phase speeds are nearly equal, but the degree of interaction varies spatially because the speeds are not identical. The interaction in this case may be expected to lead to frequency dispersion. Analytical steps paralleling those employed here should be suitable for treating nonplanar mode interactions.

ACKNOWLEDGMENT

This work was supported by the Office of Naval Research, Code 425-UA.

[1]A. H. Nayfeh and M. S. Tsai, "Nonlinear acoustic propagation in two-dimensional ducts," J. Acoust. Soc. Am. 55, 1166–1172 (1976).
[2]A. H. Nayfeh, "Nonlinear propagation of a wave packet in a hard-walled circular duct," J. Acoust. Soc. Am. 57, 803–809 (1975).
[3]P. G. Vaidya and K. S. Wang, "Non-linear propagation of complex sound fields in rectangular ducts. Part I. The self-excitation phenomenon," J. Sound Vib. 50, 29–42 (1977).
[4]J. H. Ginsberg, "Multi-dimensional non-linear acoustic wave propagation, Part II: The non-linear interaction of an acoustic fluid and plate under harmonic excitation," J. Sound Vib. 40, 359–379 (1975).
[5]A. H. Nayfeh and S. G. Kelly, "Nonlinear interactions of acoustic fields with plates under harmonic excitations," J. Sound Vib. 60, 371–377 (1978).
[6]J. H. Ginsberg, "A re-examination of the non-linear interaction between an acoustic fluid and a flat plate undergoing harmonic excitation," J. Sound Vib. 60, 449–458 (1978).
[7]J. H. Ginsberg, "A new view point for the two-dimensional non-linear acoustic wave radiating from a harmonically vibrating flat plate," J. Sound Vib. 63, 151–154 (1979).
[8]J. H. Ginsberg, "Two-dimensional finite amplitude acoustic waves radiating from a flat plate in arbitrary periodic vibration," J. Phys. (Paris) C8, 35–38 (1979).
[9]A. Kluwick, "On the non-linear distortion of waves generated by flat plates under harmonic excitations," J. Sound Vib. 74, 601–605 (1980).
[10]J. H. Ginsberg, "Finite amplitude two-dimensional waves in a rectangular duct induced by arbitrary periodic excitation," J. Acoust. Soc. Am. 65, 1127–1133 (1979).
[11]J. H. Ginsberg, "Propagation of nonlinear acoustic waves induced by a vibrating cylinder. I. The two-dimensional case," J. Acoust. Soc. Am. 64, 1671–1678 (1978).
[12]J. H. Ginsberg, "Propagation of nonlinear acoustic waves induced by a vibrating cylinder. II. The three-dimensional case," J. Acoust. Soc. Am. 64, 1671–1687 (1978).
[13]A. H. Nayfeh and S. G. Kelly, "Nonlinear propagation of waves induced by an infinite vibrating cylinder," J. Phys. (Paris) 40, 8–13 (1979).
[14]S. G. Kelly and A. H. Nayfeh, "Nonlinear propagation of directional cylindrical waves," J. Sound Vib. 79, 415–428 (1981).
[15]M. F. Hamilton and J. A. TenCate (private communication, 1984).
[16]D. G. Browning and R. H. Mellen, "Finite-amplitude distortion of 150-kHz acoustic waves in water," J. Acoust. Soc. Am. 44, 644–646 (1968).
[17]S. Goldstein, *Lectures in Fluid Mechanics* (Interscience, London, 1957), Vol. II, Chap. 4.
[18]A. D. Pierce, *Acoustics* (McGraw-Hill, New York, 1981), Chap. II.
[19]J. C. Lockwood, "Two problems in high-intensity sound," ARL, University of Texas at Austin, TX, Rept. No. ARL-TR-71-28 (1971).
[20]J. H. Ginsberg, "Nonlinear King integral for arbitrary axisymmetric sound beams at finite amplitudes—II. Derivation of uniformly accurate expression," J. Acoust. Soc. Am. 76, 1208–1214 (1984).

PROGRAM OF

The 111th Meeting of the Acoustical Society of America

Bond Court Hotel • Cleveland, Ohio • 12–16 May 1986

Session P. Physical Acoustics IV: Nonlinear Acoustics and Acousto-Optics

P2. Relationship between near and farfield effects in second harmonic generation in the piston beam. M. A. Foda and J. H. Ginsberg (School of Mechanical Engineering, Georgia Institute of Technology, Atlanta, GA 30332)

An earlier analysis [J. H. Ginsberg, J. Acoust. Soc. Am. 76, 1201–1214 (1984)] of the infinite baffle problem for an axisymmetric harmonic excitation derived a nonlinear King integral describing signal distortion in sound beams. That analysis, which considered only the contribution to the cumulative distortion process associated with secular source terms, agreed with experiments at high frequencies at ranges beyond approximately one quarter the Rayleigh length. However, there was significant discrepancy with measurements very close the transducer face. Such differences will be shown to result from neglecting nonsecular second-order terms that do not carry into the farfield. In the present work, the nonsecular contribution to the second harmonic is evaluated as a numerical inversion of a multiple integral transform for the second-order potential. The composite effects of secular distortion, which is calculated using the renormalized King integral, and the nonsecular contribution are calculated. The results obtained from the analytical model compare favorably with previous nearfield measurements. [Work supported by ONR, Code 425-UA.]

RELATIONSHIP BETWEEN NEAR AND FAR FIELD EFFECTS IN SECOND HARMONIC GENERATION IN THE PISTON BEAM

M. A. FODA & J. H. GINSBERG

GEORGIA INSTITUTE OF TECHNOLOGY

WORK SUPPORTED BY O.N.R. - CODE 425-UA

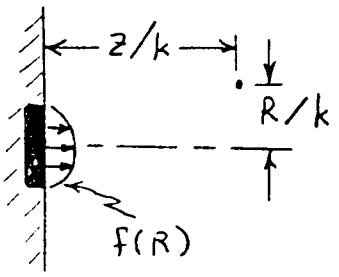

Cylindrical coords (z/k, r/k)

Time t/ω

Boundary condition:

$$v_z = \frac{\varepsilon}{2i} c_0 f(R) \exp(it) + C.C.$$

where ε = acoustic Mach number at the projector face

$f(R)$ is arbitrary

ANALYTICAL TECHNIQUES

1. Cylindrical spreading and Kutznetzov equation.

   Not suitable for near field.

2. Rayleigh integral - Ingenito & Williams (1968),

   Rogers (1970). Limited to ka = 100 & near field.

   Solution not uniformly accurate as z increases.

3. King integral: Ginsberg 1984; Miao & Ginsberg 1985.

   Asymptotic analysis to identify growth effects.

   Cumulative distortion phenomena carried from projector out to far field.

   Solution does not agree with measurements near the projector.

4. Present method - numerical analysis using King integral - goal is to identify cause of breakdown in asymptotic analysis.

Nonlinear wave equation for velocity potential.

Perturbation expansion : $\phi = \varepsilon\, \phi_1 + \varepsilon\, \phi_2 + \cdots$

Hankel transform ==> Helmholtz equation in z, t &

transverse wavenumber n

$$\phi_1 = \int_0^\infty \frac{n\, V_n}{\mu_n} \exp(it - \mu_n z)\, J_0(nR)\, dn + C.C.$$

$$\mu_n = (n^2 - 1)^{1/2}\ , \quad V_n = \frac{1}{2i} \int_0^\infty R\, f(R)\, J_0(nR)\, dn$$

Propagating spectrum : $n < 1$

Evanescent spectrum : $n > 1$

SECOND ORDER SOURCE TERMS

$$\frac{\partial}{\partial t}\left[(\beta_0-1)\left(\frac{\partial \phi_1}{\partial t}\right)^2 + \nabla\phi_1 \cdot \nabla\phi_1\right]$$

Form second order terms from linear King integral.

$$\nabla^2\phi_2 - \frac{\partial^2\phi_2}{\partial t^2} = \iint_0^\infty \{J_0(mR)\ J_0(nR),\ J_1(mR)\ J_1(nR)\}$$
$$\times \exp[2it - (\mu_m + \mu_n)z]\ dm\ dn$$

Form ϕ_2 as a double integral over m & n.

Linear combinations of products of Bessel functions.

MATCHED ASYMPTOTIC EXPANSION

$$J_0'(nR) = -J_1(nR) \; ; \quad J_1'(nR) = J_0(nR) - \frac{1}{nR} J_1(nR)$$

Near axis (small nR) ==> drop products containing higher order functions.

Off axis (large nR) ==> drop 1/nR terms.

Result: Off-axis solution for small nR identically equals near-axis solution.

OFF-AXIS EXPANSION DESCRIBES NEAR-AXIS REGION ALSO!

SECOND ORDER SOLUTION

Dual wavenumber spectrum ==> multiple Hankel transform.

$$\phi_2 = \int_0^\infty \int_0^\infty \{A_1(z)\,[J_0(mR)\,J_0(nR) - J_1(mR)\,J_1(nR)] + A_2(z)\,[J_0(mR)\,J_0(nR) + J_1(mR)\,J_1(nR)]\} \times \exp[2it - (\mu_m + \mu_n)z]\,dm\,dn$$

Substitute into wave equation.

Off-axis ==> ignore 1/nR terms.

Ordinary differential equations for A_1 and A_2.

General form:

$$d^2A_j/dz^2 - 2(\mu_m+\mu_n)\, dA_j/dz + \beta_j(m, n)\, A_j = \Gamma_j(m, n)$$

Solve for arbitrary m & n.

a) Complementary solution:

$$A_j = a_{j1}e^{\sigma_1 z} + a_{j2}e^{\sigma_2 z} \; ; \quad \sigma^2 - 2(\mu_m + \mu_n)\sigma + \beta = 0$$

Find Re $\sigma_2 > (\mu_m + \mu_n)$ ==> violates radiation cond.

Set $a_{j2} = 0$

b) Particular solution = Γ_j/β_j.

c) Total solution must satisfy b.c. at $z = 0$:

$$\frac{\partial \phi_2}{\partial z} = 0 \text{ at } z = 0$$

This yields a_{j1}.

Dual integral transform solution:

$$\phi_z = \iint_0^\infty \{\Gamma_1 \frac{N_1}{D_1} [J_0(mR)\, J_0(nR) - J_1(mR)\, J_1(nR)] + \Gamma_2 \frac{N_2}{D_2} [J_0(mR)\, J_0(nR) + J_1(mR)\, J_1(nR)]\} \times \exp[2it - (\mu_m + \mu_n)z]\, dm\, dn + C.C.$$

$$N_j = 1 - \exp\{[\mu_n + \mu_m - (m^2 \pm 2mn + n^2 - 4)^{1/2}]z\}$$

$$D_j = (\mu_n + \mu_m)^2 - (m \pm n)^2 + 4$$

$$\Gamma_j = -2i \frac{V_n V_m}{\mu_n \mu_m} (\beta_0 - 1 - \mu_n \mu_m \pm nm)$$

EVALUATION OF PRESSURE

Integrate numerically to find second harmonic:

$$P_2/\rho c^2 = - \varepsilon \frac{\partial \phi_2}{\partial t} \Longrightarrow \text{cancel } \exp(2it) \text{ factor}$$

Singularity at $m = n$: Γ_1 & $D_1 \rightarrow 0$.

a) Prior developments evaluated this part (only) by asymptotic integration for large z.

b) Singularity is finite: $\Gamma_1/D_1 \sim z$ as $m \rightarrow n$.

c) Avoid $m = n$ ==> integrate over $0 \leq m, n < \infty$ by segmenting domain and using interior points in a segment.

d) Use series expansions of Γ_1 & D_1 around $m = n$ in order to avoid loss of precision.

Symmetry of integrand ==> integration domain is:

$$0 \leq n < \infty, \quad 0 \leq m \leq n$$

Three regions: m & n in propagating or evanescent range.

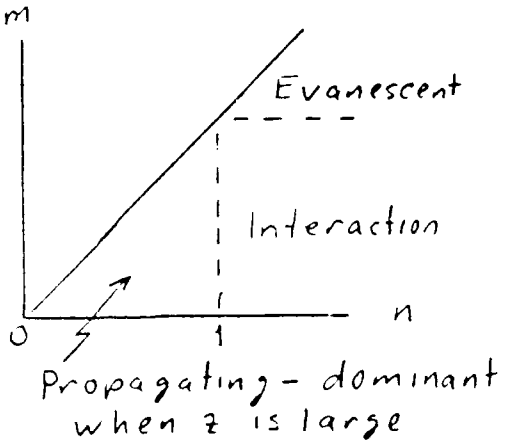

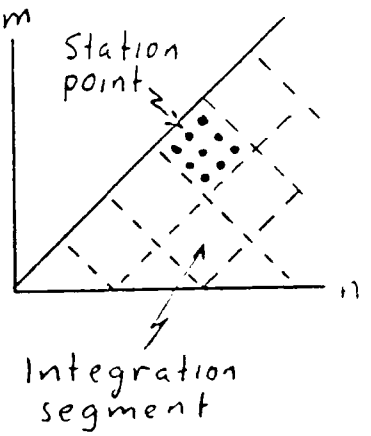

AXIAL PLOT

2.58 MHz, ka = 114.5, peak axial SPL = 234 dB

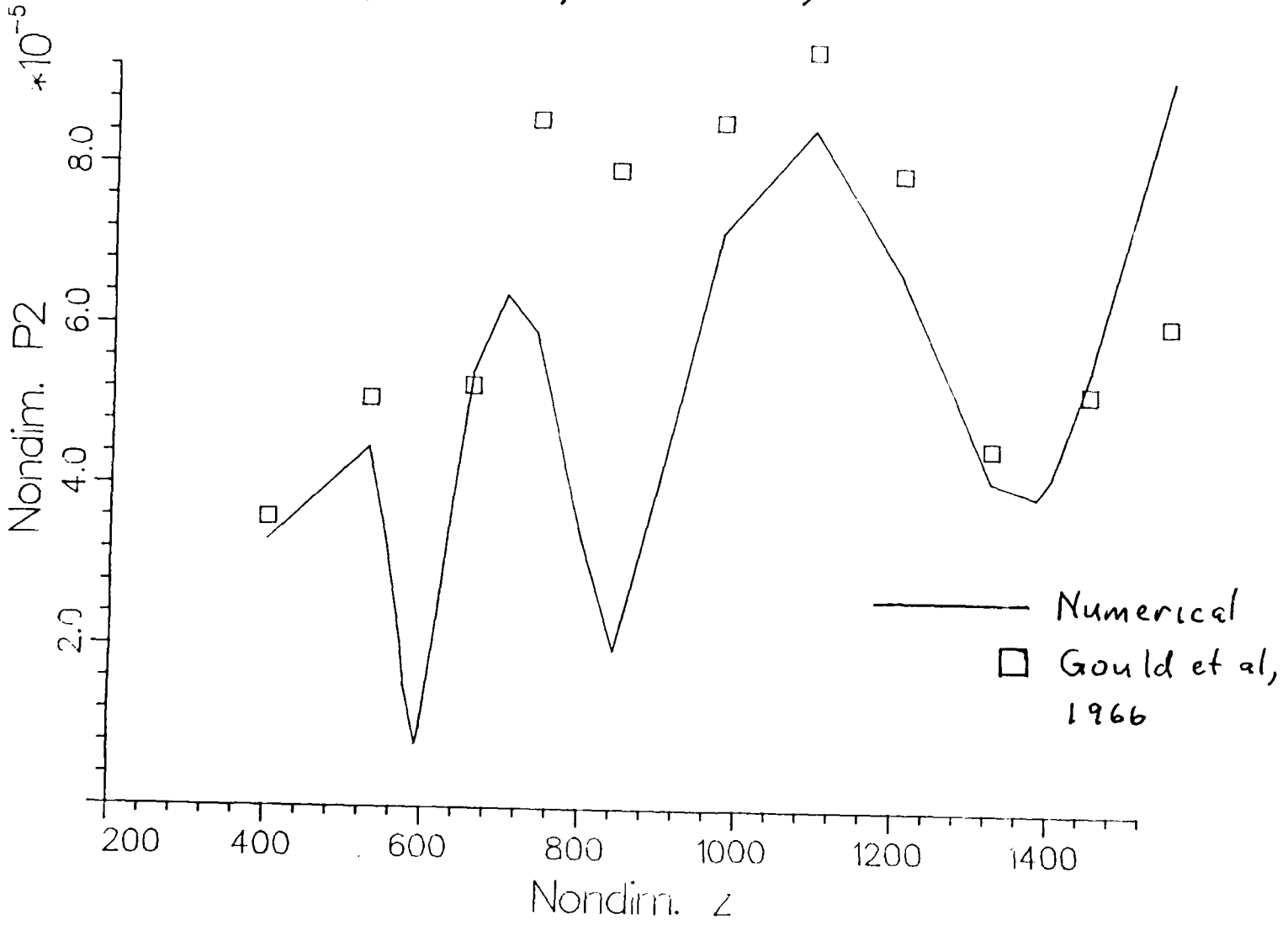

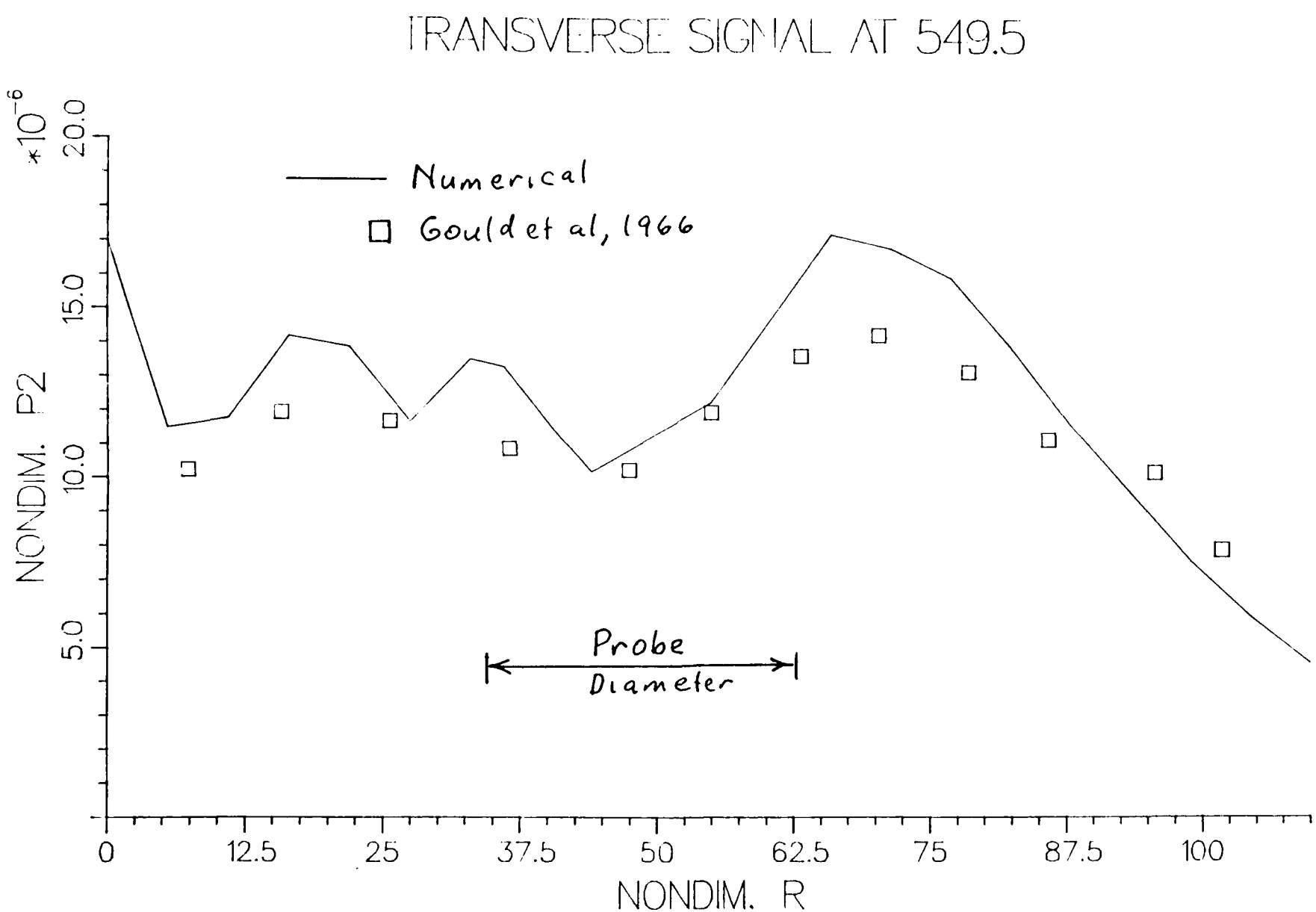
TRANSVERSE SIGNAL AT 549.5
Numerical
Gould et al, 1966
NONDIM. P2
*10^-6
20.0
15.0
10.0
5.0
Probe
Diameter
0
12.5
25
37.5
50
62.5
75
87.5
100
NONDIM. R

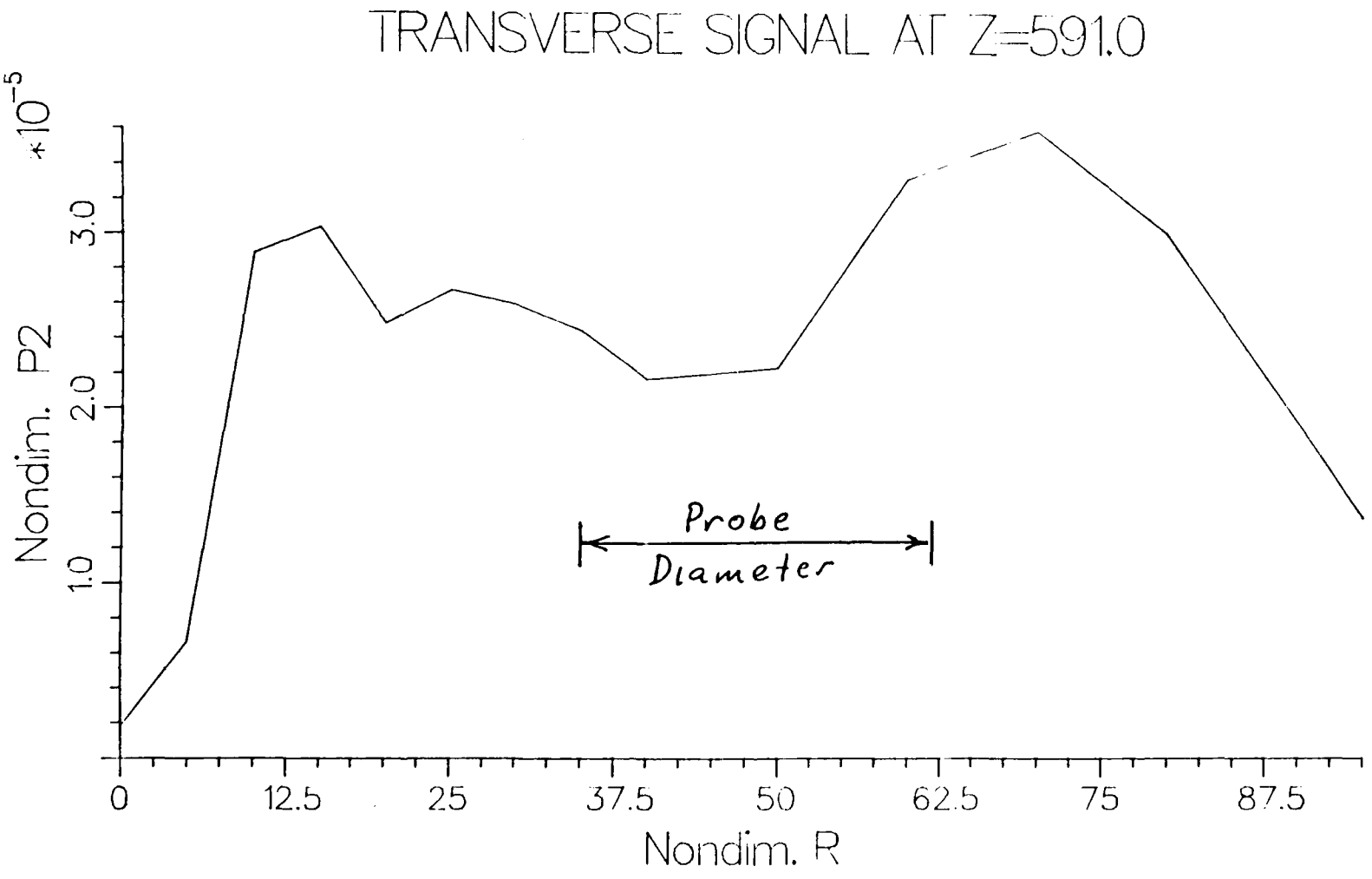
TRANSVERSE SIGNAL AT Z=591.0
Nondim. P2
*10^-5
1.0
2.0
3.0
Probe
Diameter
0
12.5
25
37.5
50
62.5
75
87.5
Nondim. R

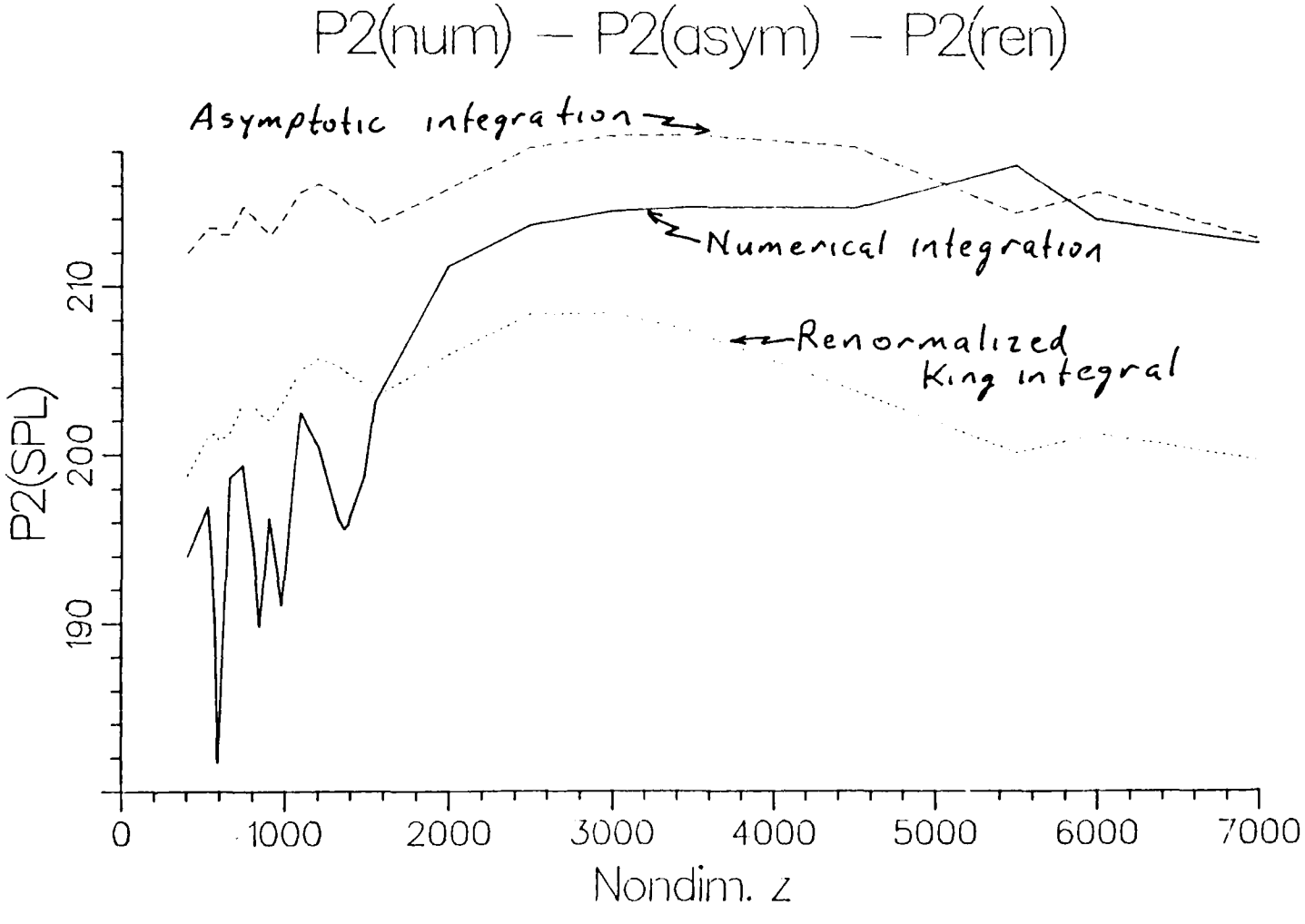
P2(num) – P2(asym) – P2(ren)
Asymptotic integration
Numerical integration
Renormalized
King integral
P2(SPL)
190
200
210
0
1000
2000
3000
4000
5000
6000
7000
Nondim. z

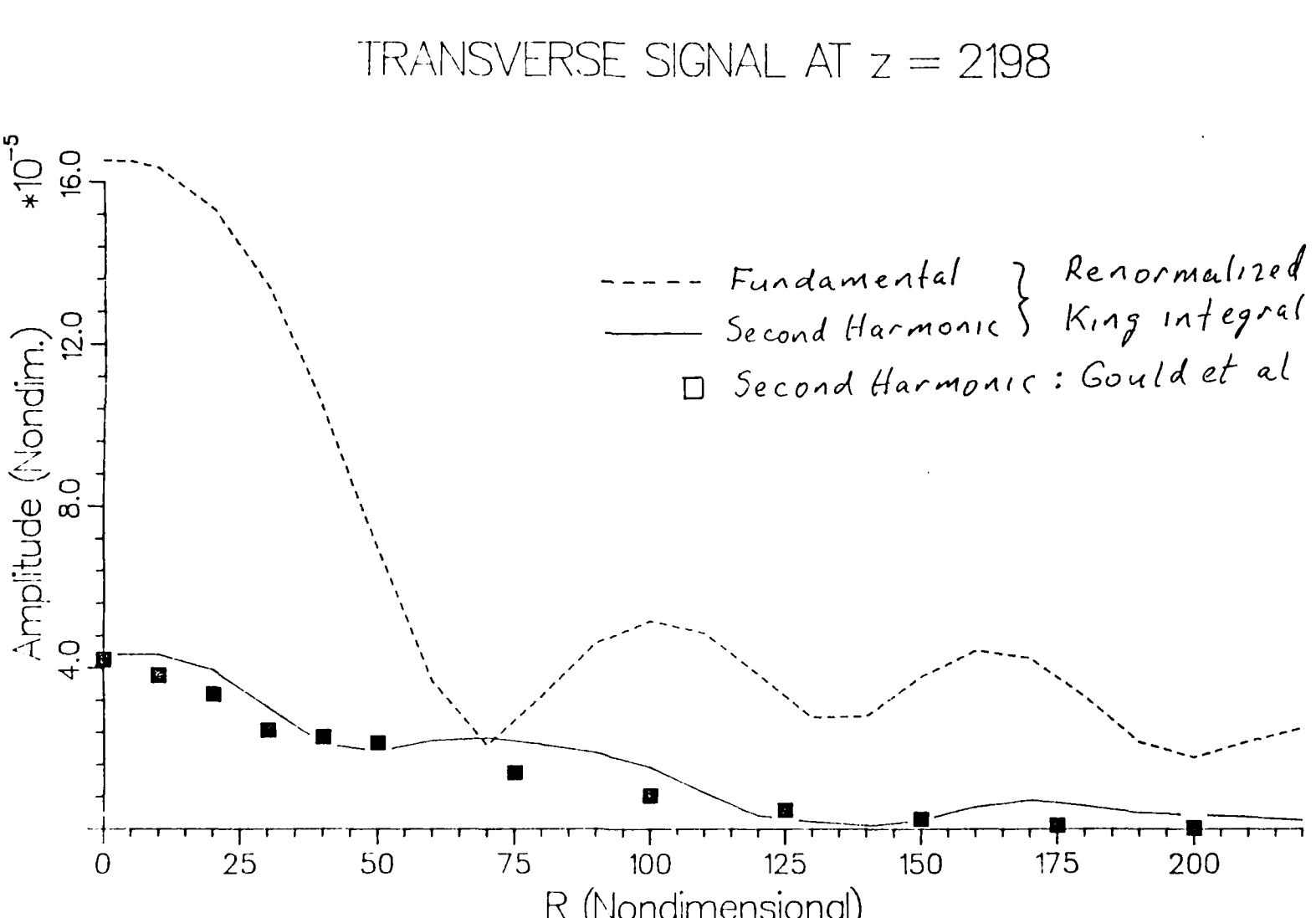
TRANSVERSE SIGNAL AT z = 2198
Amplitude (Nondim.)
*10^-5
16.0
12.0
8.0
4.0
0
25
50
75
100
125
150
175
200
R (Nondimensional)
Fundamental
Second Harmonic
Renormalized King integral
Second Harmonic : Gould et al

CONCLUSIONS

1. Nonsecular second order terms (region away from singularity at m = n) are significant in near field.
2. Reasonable agreement between numerical integration and experiment for axial propagation properties near the transducer, except for ? predicted additional nulls ?
3. Asymptotic integration describes dominant effect outward from the farthest anti-node.

4. Transverse pattern agrees with experiment -

   a) Numerical integration near the transducer.

   b) Asymptotic analysis in transition zone.

5. Numerical integration is VERY INTENSIVE.

PROGRAM OF

The 111th Meeting of the Acoustical Society of America

Bond Court Hotel • Cleveland, Ohio • 12–16 May 1986

Session P. Physical Acoustics IV: Nonlinear Acoustics and Acousto-Optics

P1. Nonsymmetric effect in finite amplitude sound beams radiating from a baffled circular transducer. H. C. Miao (General Motors Research Laboratories, Warren, MI 48090-9055) and J. H. Ginsberg (School of Mechanical Engineering, Georgia Institute of Technology, Atlanta, GA 30338)

Prior investigations of nonlinear effects in sound beams have treated cases where the transducer oscillates axisymmetrically. Here, an analysis of a situation where the harmonic spatial vibration of the transducer has a $\cos\theta$ dependence on the azimuth angle, as would be the case for a piston that rocks about its diameter, shall be presented. The method of investigation parallels that employed earlier [H. C. Miao and J. H. Ginsberg, J. Acoust. Soc. Am. Suppl. 1 **78**, S39 (1985)], which used the King integral to generate nonlinear source terms. A dual asymptotic description based on assumptions appropriate to the regions very close to, and far from, the beam axis is obtained, and then reconciled to obtain a uniformly accurate description. An intermediate form of the solution featuring coordinate straining transformations is converted to a Fourier time series. The linearized signal shows nodal lines in the azimuthal direction that match those of the transducer vibration, and it shall be shown that the higher harmonics exhibit similar behavior. [Work supported by ONR, Code 425-UA.]

NONSYMMETRIC EFFECT IN FINITE AMPLITUDE SOUND BEAMS

H. C. MIAO - GENERAL MOTORS RESEARCH LABS

J. H. GINSBERG - GEORGIA TECH

WORK SUPPORTED BY O.N.R. - CODE 425-UA

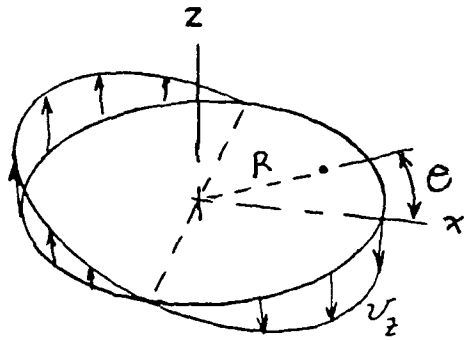

$v_z \sim x\, e^{i\omega t}$, $k = \omega/c_o$

$x = R \cos\theta$

$\omega t \Longrightarrow t$

$kz,\ kR \Longrightarrow z,\ R$

Consider $v_z = \epsilon\, c_o\, f(R) \cos\theta \exp it + C.C.$

LINEAR SOLUTION

Hankel transform

transverse distance R <==> transverse wavenumber n

One dimensional wave equation for axial direction.

$$\phi_{lin} = \int_0^\infty \frac{n\, V_n}{\mu_n} \exp(it - \mu_n z)\, J_1(nR) \cos\theta \, dn + C.C.$$

$$\mu_n = (n^2 - 1)^{1/2} , \quad V_n = \int_0^\infty R\, f(R)\, J_1(nR)\, dn$$

NONLINEAR FORMULATION

Nonlinear wave equation - exact - define E.O.S.

Perturbation series for velocity potential

$$\phi = \varepsilon \phi_1 + \varepsilon \phi_2 + \cdots$$

Form second order terms from linear term, ϕ_1:

$$\nabla^2 \phi_2 - \frac{\partial^2 \phi_2}{\partial t^2} = \iint_0^\infty \{J_1(nR)\, J_1(nR),\ J_1'(nR)\, J_1'(nR)\} \times \exp[2it - (\mu_m + \mu_n)z] \begin{Bmatrix} 1 \\ \cos 2\theta \end{Bmatrix} dm\, dn$$

MATCHED ASYMPTOTIC EXPANSION

$$J_1'(nR) = \frac{1}{nR} J_1(nR) - J_2(nR)$$

Near axis (small nR) ==> $J_{\nu+1}(nR) << J_\nu(nR)$

Off axis (large nR) ==> $J_1'(nR) \approx - J_2(nR)$

Solve for $p(z,R,\theta,t)$ in each region, then match.

OFF AXIS

Dual wavenumber spectrum ==> multiple Hankel transform.

$$\phi_2 = \int_0^\infty \int_0^\infty \{A_1(z)\,[J_1(mR)\,J_1(nR) - J_2(mR)\,J_2(nR)] + A_2(z)\,[J_1(mR)\,J_1(nR) + J_2(mR)\,J_2(nR)]\} \times \exp[2it - (\mu_m + \mu_n)z]\,\cos^2\theta\,dm\,dn$$

Substitute into wave equation & ignore 1/nR terms ==>

ordinary differential equations for A_1 and A_2.

NEAR AXIS

Form solution from two parts - R.H.S. + dual transform.

$$\phi_2 = \int_0^{\infty}\int \frac{imF_nF_m}{\mu_n\mu_m} \cos^2\theta \; J_1(mR) \; J_1(nR) \; \exp[2it - (\mu_m + \mu_n)z] \; dm \; dn + \int_0^{\infty}\int \Psi_2 \; dm \; dn$$

Substitute into wave equation ==> identities yield:

$$\nabla^2\Psi - \frac{\partial^2\Psi}{\partial t^2} \sim J_1(mR) \; J_1(nR) \; \exp[2it - (\mu_m + \mu_n)z] \cos^2\theta$$

NOTE: First integral is bounded as z increases.

Introduce $nR \ll 1$ ==> Neumann-Lommel Addition Formula

$$\frac{1}{2}\left[J_2(x+y) - J_0(x-y)\right]$$
$$= J_1(x)\,J_1(y) - J_1(x)\,J_3(y) - J_1(x)\,J_3(y) + \cdots$$

Thus

$$J_1(mR)\,J_1(nR) \approx \frac{1}{2}\left[J_2(mR+nR) - J_2(mR-nR)\right]$$

For large z and small nR:

$$\phi_2 \sim \int_0^\infty \left[\begin{matrix} F_1(z) \\ F_3(z) \end{matrix} J_2(mR+nR) - \begin{matrix} F_2(z) \\ F_4(z) \end{matrix} J_2(mR-nR) \right] \times \exp[2it - (\mu_m + \mu_n)z] \begin{matrix} \cos\theta \\ 1 \end{matrix} \, dm\, dn$$

Differential equations for $F_j(z)$ by substitution.

ASYMPTOTIC INTEGRATION - LAPLACE

The differential equations for A_1 & A_2 off axis,

or F_1 & F_2 near the axis, are similar in form:

$$d^2U/dz^2 - 2(\mu_m + \mu_n)\, dU/dz + \beta(m, n)\, U = \Gamma(m, n)$$

Case (a) $\beta \neq 0$ ==> $U = \Gamma/\beta$ ==> no growth effect.

General situation, except for A_1 & F_1 when $m = n$.

Case (b) $\beta \to 0$ ==> $U \to z\, \Gamma/2(\mu_m + \mu_n)$ ==> growth.

Case for A_1 & F_1 when $m = n$ <==> eigensolutions.

1. Expand around singularity: $m = n - q$, $|q| \ll 1$
2. Expand d.e. in terms of q.
3. Find general solution (complemetary & particular)
   for $q \neq 0$.
4. Find particular solution when $q \sim 0$.
5. Match #3 & #4 ==> coeffs of complementary solution.
6. Integrate over m spectrum: $\delta \ll 1$

$$\int_0^{\infty} dm = \int_0^{n-\delta} dm + \int_{-\delta}^{\delta} dq + \int_{n-\delta}^{\infty} dm$$

(a) First & third integrals give bounded solution.

(b) Portion of second integral away from $q = 0$ becomes less important as z increases.

(c) Letting $\delta \to \infty$ simplifies integration & affects subdominant terms only.

After integration, dominant part of ϕ consists of a single spectrum. For $z \gg 1$ & $nR \ll 1$ or $nR \gg 1$:

$$\phi = \int_0^\infty (\varepsilon \, \Phi_1 + \varepsilon^2 \Phi_2) \, dn$$

EVALUATION OF PRESSURE

$$\frac{p}{\rho c^2} = -\frac{\partial \phi}{\partial t} = \int_0^\infty [\varepsilon P_1 + \varepsilon^2 P_2]\, dn$$

OFF AXIS

Here $P_1 \sim \cos\theta$ and $P_2 \sim \cos^2\theta$

$$J_\nu(nR) \sim \left(\frac{1}{2\pi nR}\right)^{1/2} \{\exp[i(nR - \frac{2\nu + 1}{4}\pi/4)] + \exp[-i(nR - \frac{2\nu + 1}{4}\pi)]\}$$

Hence $P = P\{R^{-1/2}, it - \mu_n z \pm (nR - 3\pi/4), \cos\theta\}$

"+" ==> axial & inward cylindrical wave ==> $P_j^{(1)}$

"-" ==> axial & outward cylindrical wave ==> $P_j^{(2)}$

NEAR AXIS

Here $P_1 \sim J_1(nR) \cos \theta$ and $P_2 \sim J_1(nR)^2 \cos 2\theta$

but

$$\cos \theta = (e^{i\theta} + e^{-i\theta})/2$$

Hence $P = P\{J_1(nR), \exp(it - \mu z \pm i\theta)\}$

Two waves - both axial, opposing circumferentially.

RENORMALIZATION

In either region:

$\frac{P_2^{(j)}}{P_1^{(j)}}$ grows without bound as z increases.

Solution is not uniformly accurate!

Introduce a change of variables to correct dependence.

OFF AXIS - different variable for 1 and 2 waves.

$$P^{(j)} = \varepsilon \frac{inF_n}{\mu_n} \frac{1}{2\pi nR}^{1/2} \exp[it - \alpha_j \mp (inR - i\tfrac{3}{4}\pi)] \cos\theta$$

$$\mu_n z = \alpha_j + D(n, z) \frac{1}{2\pi nR}^{1/2} \{\exp[it - \alpha_j \mp (inR - i\tfrac{3}{4}\pi)] + C.C.\} \cos\theta$$

NEAR AXIS - different variables for each

circumferential wave.

$$P^{(j)} = \varepsilon \frac{inF_n}{2\mu_n} J_1(nR) \exp(it \pm \zeta_j \pm i\theta)$$

$$\mu_n z = \zeta_j + E(n, z) J_1(nR) \{\exp(it \pm \zeta_j \pm i\theta) + C.C.\}$$

MATCH INNER & OUTER EXPANSIONS

NEAR AXIS:

Combine & simplify using $\zeta_1 - \zeta_2 << \zeta_1 + \zeta_2$ ==> define

$$\zeta = \frac{1}{2}(\zeta_1 + \zeta_2) \Longrightarrow P = P(it - \zeta, \cos\theta)$$

OFF AXIS:

When $nR >> 1$ ==> $\frac{1}{\sqrt{2\pi nR}}^{1/2} \exp(inR - i\frac{3}{4}\pi)$

$$- J_1(nR) + i\, J_2(nR)$$

Replace R dependence, then compare with near axis expressions.

(a) Dependence of pressure alike in both regions.

(b) The $O(\varepsilon)$ coefficient in coordinate transformation is larger by a factor of 2 near the axis.

NOTE:

$$nR \gg 1 \Longrightarrow \frac{J_2(nR)}{nR} \sim 0$$

$$nR \ll 1 \Longrightarrow \frac{J_2(nR)}{nR} \sim \frac{1}{4} J_1(nR)$$

Near axis: Replace $J_1(nR)$ by $\frac{1}{2} J_1(nR) + \frac{2 J_2(nR)}{nR}$

Off axis: Replace $J_1(nR)$ by $J_1(nR) + \frac{4 J_2(nR)}{nR}$

RESULT

Convert to real form for $n \ll 1$:

$$p/\rho c^2 = \int_0^1 \frac{\varepsilon n F_n}{\lambda}\{[\cos(t - \lambda\alpha_1) + \cos(t - \lambda\alpha_2)]\, J_1(nR) + [\sin(t - \lambda\alpha_1) - \sin(t - \lambda\alpha_2)]\, J_2(nR)\}\, dn \times \cos\theta + \text{linear evanescent term}$$

$$\lambda z = \alpha_j - 2\varepsilon n F_n (\pi z/\lambda)^{1/2} \{\sin(t - \lambda\alpha_j + \pi/4) \times [J_1(nR) + 4\, J_2(nR)/nR] \pm \cos(t - \lambda\alpha_j + \pi/4) \times J_1(nR)\} \cos\theta$$

COMPUTATIONS

Direct evaluation is very complicated.

Strained coordinate α_1 and α_2 are uncoupled:

quasi-one-dimensional ==> Fourier-Fubini series.

EXAMPLE

Parameters by Gould et al (1965) - was axisymmetric.

2.58 MHz , a = 10.1 mm , c_0 = 1475 m/s , ka = 114

GT
Acoustics & Dynamics
Research Laboratory

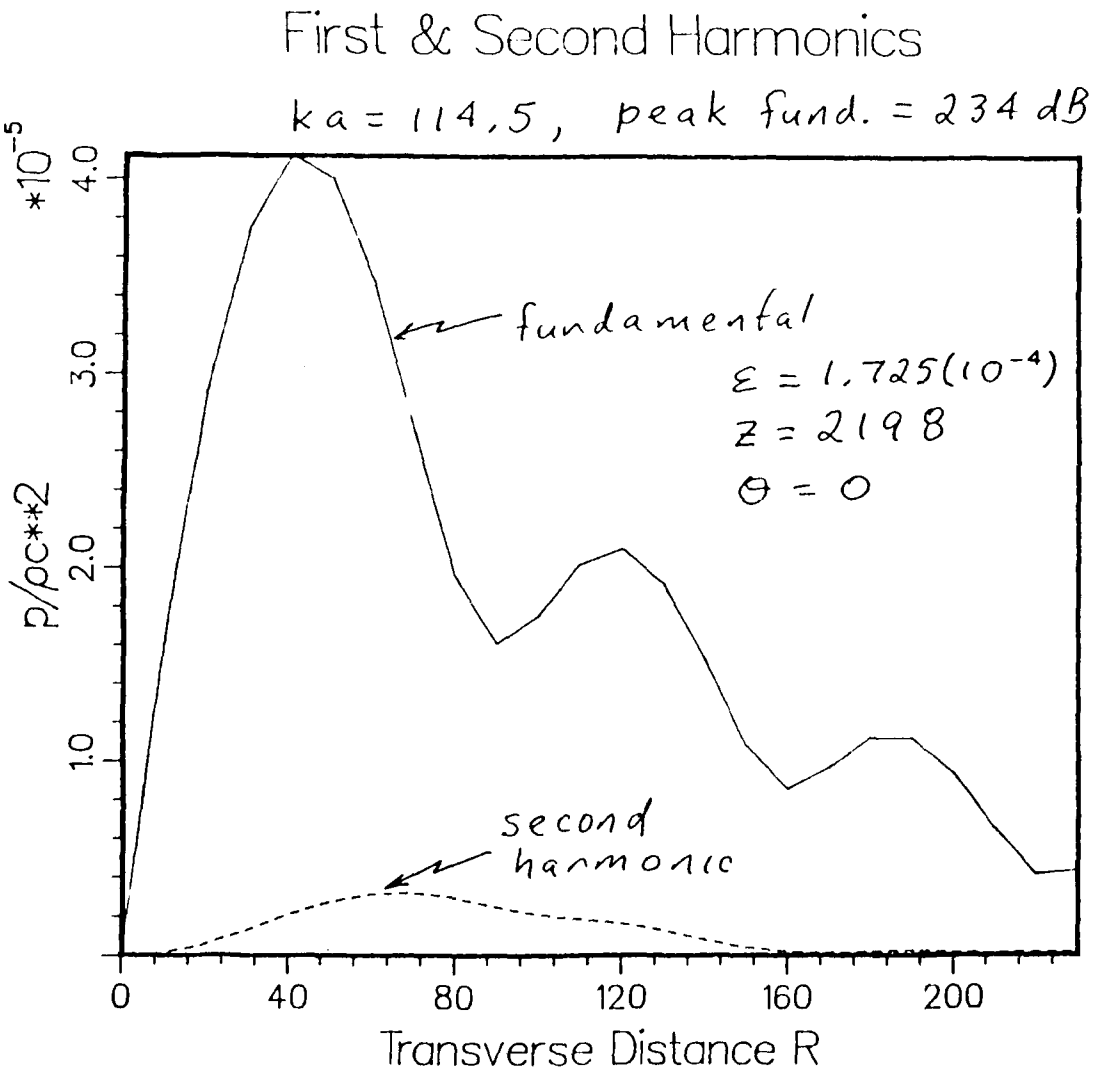

GT

Acoustics & Dynamics
Research Laboratory

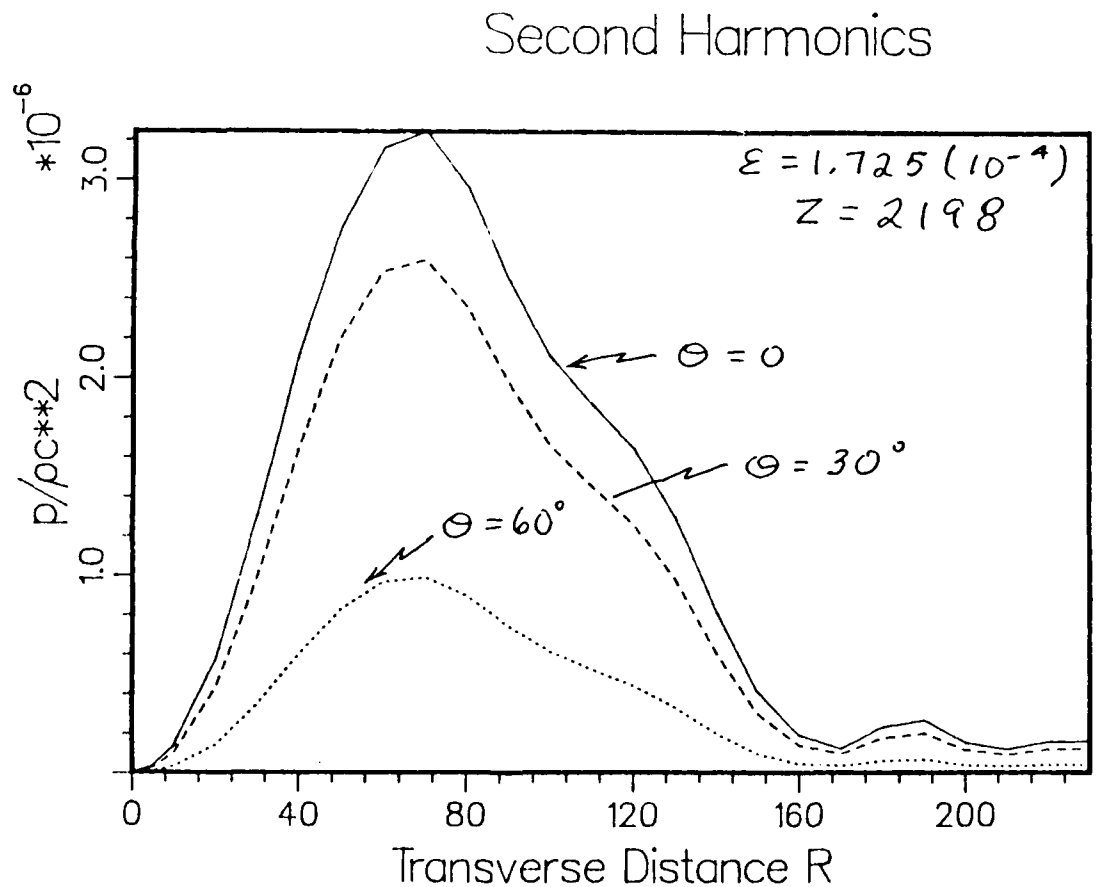

GT

Acoustics & Dynamics
Research Laboratory

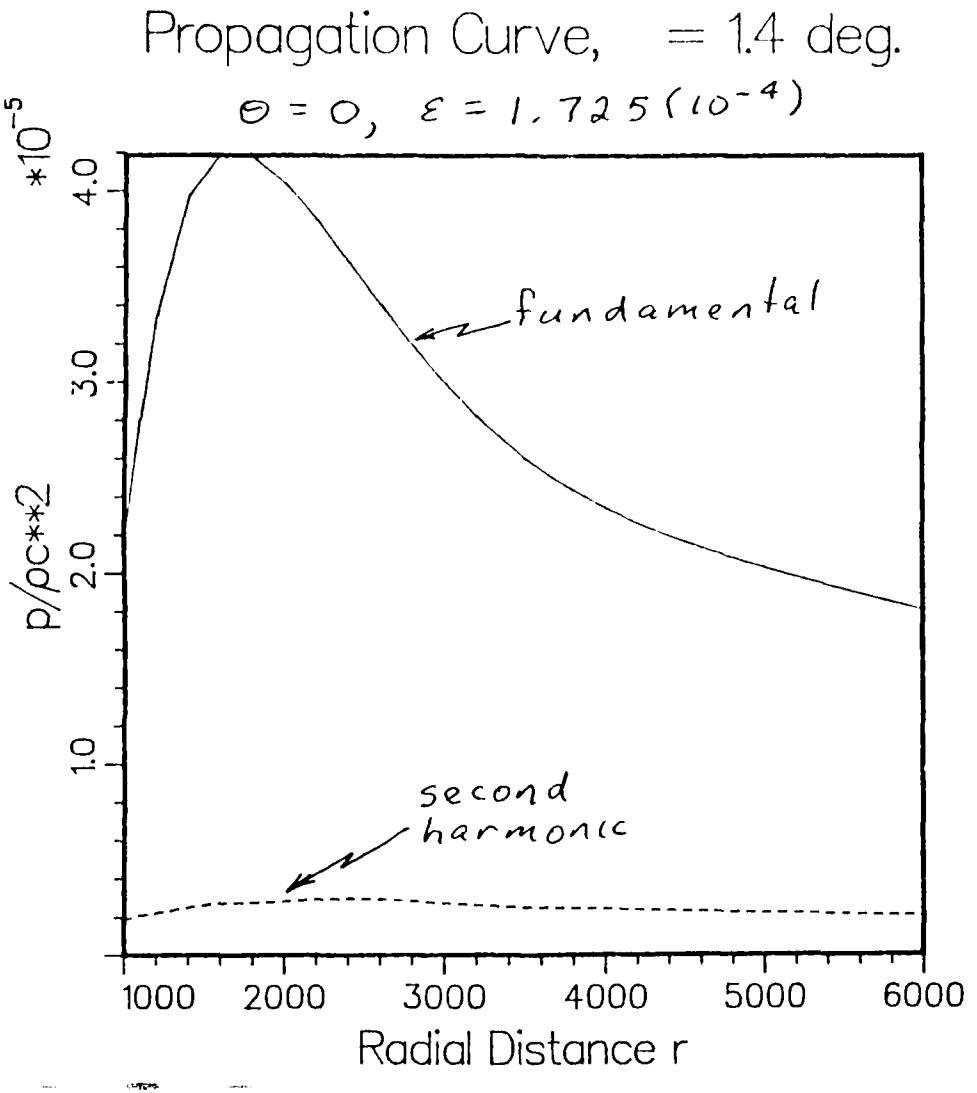

GT
Acoustics & Dynamics
Research Laboratory

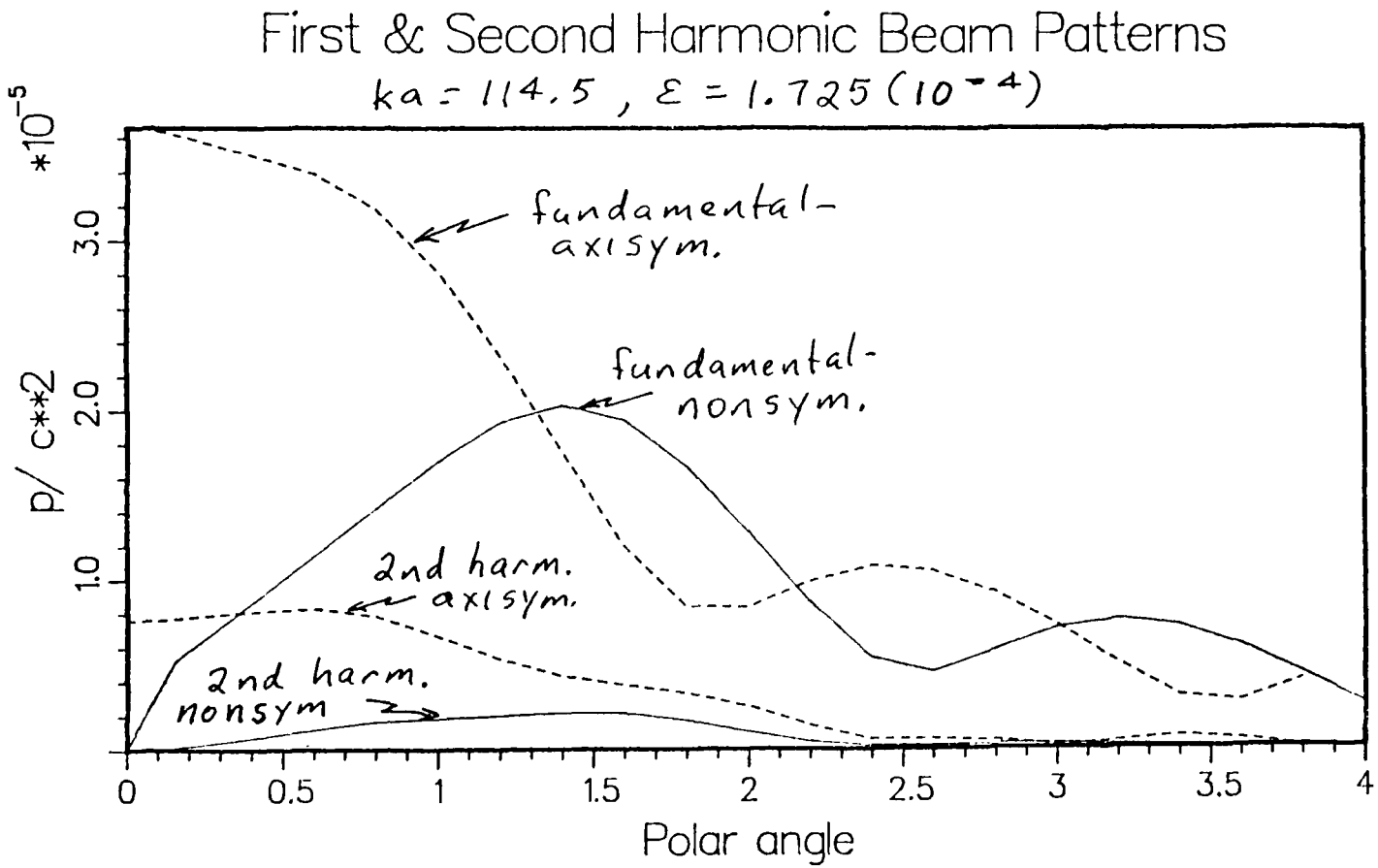

Diffraction and Nonlinear Distortion in Sound Beams as Interacting Wave Phenomena

J. H. Ginsberg, H. C. Miao[†], and M. A. Foda[*]

Acoustics and Dynamics Research Laboratory

School of Mechanical Engineering

Georgia Institute of Technology

Atlanta, Georgia 30332

Discrepancies between experiment and the nonlinear King integral [15] for a finite amplitude sound beam, which are encountered in the inner portion of the Fresnel region, are addressed by a new integral transform solution that accounts for all contributions to second harmonic formation in the nearfield. Although the result agrees well with experiments, it is limited in its region of validity. A more general solution covering the entire domain is obtained by the introduction of a coordinate straining transformation. Crucial to that step is a new decomposition of the nonlinear, as well as linear, signal at all locations into groups of quasi-conical waves that converge and diverge from the axis as they propagate away from the projector. Nonlinear distortion in the nearfield arises from interaction of different transverse wavenumber modes in each group, and also from interaction between the groups. The latter effect ceases to be significant in the farfield, whereas the self-distortion arising in either

---

[†] Present address: Power Systems Research Dept., General Motors Research Laboratories, Warren, Michigan 48090-9057.

[*] Present address: Department of Mechanical and Industrial Engineering, El-Mansoura University, El-Mansoura, Egypt.

group grows. The earlier nonlinear King integral, which is derived as the limiting form for long ranges of the present result, is suitable within the Fresnel zone, provided that the distance is substantially larger than the piston radius. Fourier series analysis of the long range limit leads to a sequence of King-type integrals for each harmonic.

LIST OF SYMBOLS

A,B	modal amplitudes forming the second harmonic
a	radius of the projector
a_j, b_j	Fourier coefficients for the long range approximation
c_0	speed of sound according to linear theory
C.C.	denotes the complex conjugate of all preceding terms
D_n	parametric combination for the Fourier series
F_n	Hankel transform of f(R)
$f(R)$	shading function for the projector displacement
G_n	Hankel transform of the pressure at the projector
$H(z,n)$	correction function for behavior near the cutoff frequency of a mode
$J_\ell(x)$	Bessel function of order ℓ
k	dimensional axial wave number for a planar wave, $=\omega/c_0$
N_j	coefficients affecting A and B (j=1,2,3)
n,m	transverse wave numbers
P_j	amplitude of the j th harmonic according to the long range approximation
p	acoustic pressure

p_j	pressure of the quasi-conical waves at a specified wave number (j=I,II)
Q_n	amplitude of $J_0(nR) + i\ J_1(nR)$
R	nondimensional distance transverse to the beam axis
T_j	mean value residuals introduced by the coordinate straining transformations (j=I,II)
t	nondimesional time
U_j, W_j	undetermined fuctions for the coordinate transformations (j=I,II)
V_n	modulus of F_n
w	normal displacement of the projector face
z	nondimensional distance along the beam axis
I, II	denotes inward and outward propagating groups of quasi-conical waves, respectively
α_n, β_n	strained coordinates for the I and II wave groups, respectively
β_0	coefficient of nonlinearity in the pressure-density relation
Γ_j	complex amplitude of the j th harmonic according to the nearfield theory
Δ_n	phase of $J_0(nR) + i\ J_1(nR)$
δ_j	modal phase lag at harmonic j
ε	acoustic Mach number at the projector
ζ,θ	change of variables for transverse wave numbers
η,ξ	phase variables for group I and group II nonlinear waves
θ_n	phase of F_n
λ_n	axial wave number for the propagating spectrum
μ_n	complex axial wave number
ν_j	phase lag of harmonic j according to the long range approximation
ρ_0	density at ambient conditions

σ_{Aj}, σ_{Bj}	characteristic roots for the modal amplitudes
Φ_{21}	second order potential due to field effects
Φ_{22}	second order potential due to nonlinear conditions at the projector interface
ϕ	nondimensional velocity potential
ϕ_j	perturbation potentials (j = 1,2)
Ψ_I, Ψ_{II}	phase variables for group I and group II linear waves
ω	frequency (rad/sec) of the projector

INTRODUCTION

The prediction of the signal generated by a transducer in an infinite baffle is a challenging task in the linear domain. Good approximations are available for the Fraunhofer (farfield) region, but analytical treatments of the nearfield, whose outer limit is characterized by the Fresnel theory of diffraction [1], become progressively less accurate with decreasing range. Comparable predictions for nonlinear effects that arise with increasing signal levels are inherently more complicated than their linear analogs. A variety of approaches have been developed, based on restrictions to specific domains. A theory for second harmonic generation in the Fresnel region was developed by Ingenito and Williams [2], and extended by Rogers [3]. The technique there was to use the free space Green's function to superpose the source radiation associated with nonlinearities in the field equations. Aside from being restricted to the Fresnel domain and high frequencies ($ka>100$), the primary limitation of this formulation is that it does not address higher harmonics and depletion in the fundamental. Consequently, it does not provide sufficient information to predict waveforms.

A different approach was employed by Lockwood, Muir, and Blackstock [4] to predict farfield distortion. That analysis, which was based on Lockwood's treatment of spherical waves [5], is limited to situations where the level at the source is not excessively high. Under such a restriction, it is reasonable to assume that the signal is undistorted at some transition distance in the farfield. However, the resulting theory features some anomolies, such as an apparent dependence of the predicted signal on the (assumed) transition distance. Also, the absence of nearfield distortion

leads to a waveform whose shape is distorted in the same manner in the rarefaction and compression phases. Observations of high intensity sound beams, such as the measurements by Browning and Mellen [6], indicate that the rarefaction phase tends to broaden and decrease in amplitude, while the compression phase tends to narrow and gain amplitude.

Numerous analyses of finite amplitude effects have been based on a Burgers-type equation that was derived by Zabolotskaya and Khokhlov [7] for the nondissipative case, then modified by Kuznetsov [8] to account for dissipation. A variety of techniques have been employed to solve this equation for a CW transducer. A direct numerical simulation using finite differences has been employed in several studies by Bakvalov and colleagues, exemplified by References [9 & 10]. Recent works by Hamilton, J. N. Tjótta, S. Tjótta and colleagues [11,12] have developed more efficient algorithms based on temporal Fourier series whose amplitudes are position dependent. The resulting differential equations have, for the most part, been solved numerically, although an analytical quasilinear approximation has also been discussed [13].

Several approximations must be made to derive the aforementioned modified Burgers' equation. Most significant are the assumption that the relationship between particle velocity and pressure is like that for a one-dimensional wave, and that the transverse variation is intermediate in scale to the wavelength and the Rayleigh length. It is generally recognized that the equation is only suitable in the vicinity of the axis of the sound beam, so that the governing equation is often referred to as the paraxial parabolic equation. However, even within that limitation, there is a

troublesome aspect. In the lossless case, the nondimensional equation for pressure depends only on the ratio of the Rayleigh length to the planar shock formation distance. In terms of the variables to be employed here, this ratio reduces to $\varepsilon\beta_0(ka)^2$, where ε is the acoustic Mach number at the source and β_0 is the coefficient of nonlinearity for the fluid. In order to obtain the nondimensional form, pressure is scaled by a factor ε. Hence, the implication of this theory is that the (dimensional) pressure field will merely be changed by a factor if the value of ε is increased, while $\varepsilon(ka)^2$ is held constant. In other words, two transducers whose radii satisfy $a_2/a_1 = (\varepsilon_1/\varepsilon_2)^{1/2}$ operating at the same frequency are predicted to radiate signals in proportion to their respective Mach numbers. This clearly cannot be the case. For example, the number of on-axis nulls predicted by linear theory (very small values of ε) is strongly dependent on the ka value [1]. This implies that the paraxial equation, in addition to being limited to the vicinity of the axis, should not be employed within the Fresnel diffraction region.

The present analysis is descended from Ginsberg's treatment [14,15] of a consistent nonlinear wave equation for the velocity potential. He used the King integral [16] to generate the second order source terms appearing in the field equations. The hierarchy of equations were solved by asymptotic integration and coordinate straining transformations, based on an assumption that the only second order effects significant to the distortion process are those that grow with increasing distance from the transducer. Such an assumption is fundamental to most analyses of one-dimensional waves. Ginsberg's nonlinear King integral was analytical, in that it had quadrature

form. However, the complicated nature of the integrands necessitated numerical evaluations of the pressure.

Discrepancies between Ginsberg's theory and experiments by Gould et al [17] were disclosed by Miao [18]. The measurements were carried out for a high ka case (ka=114) very close to the transducer. A subsequent analysis by Foda and Ginsberg [19] suggested the present analysis. It disclosed that it is not appropriate in the Fresnel region to assume that all distortion is associated with an effect that grows with increasing distance. In the present paper we shall develop an analysis that is descriptive of the entire field. Its predictions for the second harmonic will be seen to be in close agreement with Gould's measurements. In addition, the investigation will demonstrate that differences between the behavior in the Fresnel and Fraunhoffer regions are a consequence of a variety of interacting wave phenomena that occur everywhere in the acoustic field. An ancillary benefit of the analysis will be a new interpretation of the King integral for linear theory. Ginsberg's earlier results will be shown to be the long range (that is, many wavelengths) limit of the more general theory. The present viewpoint will lead to a Fourier series decomposition of this long range form. That representation permits evaluations in the farther portion of the Fresnel region, and beyond, with the same efficiency as the King integral for the fundamental in linear theory.

I. BASIC EQUATIONS

The foundation for the formulation is the nonlinear wave equation for the velocity potential [20], whose nondimensional form is

$$\nabla^2\phi - \frac{\partial^2\phi}{\partial t^2} = \frac{\partial}{\partial t}\left[(\beta_0 - 1)\left(\frac{\partial\phi}{\partial t}\right)^2 + \nabla\phi\cdot\nabla\phi\right] + O(\phi^3) \qquad (1)$$

where the nondimensional cylindrical coordinates z and R represent, respectively, the axial and transverse distances relative to the center of the transducer, multiplied by the wavenumber k, and t is dimensional time multiplied by ω.

We desire to address the effect of nonlinearities at the projector-fluid interface, as well as in the field equations. Let $w(R,t)$ denote the normal displacement of the projector face. As shown in Figure 1, continuity of the particle velocity at the interface must be imposed at the displaced location of the projector in the direction normal to the deformed surface. Thus,

$$c_0\left(\cos\gamma\,\frac{\partial\phi}{\partial z} - \sin\gamma\,\frac{\partial\phi}{\partial R}\right)\Bigg|_{z/k=w} = \dot{w}\cos\gamma\,, \quad \gamma = \tan^{-1}\left(k\,\frac{\partial w}{\partial R}\right) \qquad (2)$$

We let $f(R)$ be an amplitude shading function, possibly complex. A general representation of monochromatic oscillation at (dimensional) frequency ω and (small) acoustic Mach number ε is

$$\dot{w} = \frac{1}{2i}\,\varepsilon\,c_0\,f(R)\exp(it) + C.C.$$

$$w = -\frac{1}{2k}\,\varepsilon\,f(R)\exp(it) + C.C. \qquad (3)$$

Because w is $O(\varepsilon)$, the surface rotation γ may be replaced by its tangent. For the same reason, Taylor series expansion allows the derivatives in Eq.

(3) to be evaluated at the undeformed location of the projector face, z = 0, according to

$$c_0 \left(\frac{\partial \phi}{\partial z} + k\, w\, \frac{\partial^2 \phi}{\partial z^2} - k\, \frac{\partial w}{\partial R}\, \frac{\partial \phi}{\partial z}\right)\Bigg|_{z=0} = \dot{w} + O(\epsilon^3) \qquad (4)$$

Earlier investigations expanded ϕ in a straightforward perturbation series. A slight modification of such an expansion leads to a sequence of equations that more prominantly displays the role of β_0 in the formation of nonlinear distortion. Specifically, we let

$$\phi = \epsilon \phi_1 + \epsilon^2 \left[\frac{1}{2} \frac{\partial}{\partial t}(\phi_1^2) + \phi_2\right] + O(\epsilon^3) \qquad (5)$$

The corresponding first and second order portions of the wave equation (1) are

$$\nabla^2 \phi_1 - \frac{\partial^2}{\partial t^2} \phi_1 = 0 \qquad (6a)$$

$$\nabla^2 \phi_2 - \frac{\partial^2}{\partial t^2} \phi_2 = \beta_0 \frac{\partial}{\partial t} \left(\frac{\partial \phi_1}{\partial t}\right)^2 \qquad (6b)$$

Satisfying the boundary condition in Eq. (4) at each perturbation step leads to

$$\epsilon \frac{\partial \phi_1}{\partial z}\Bigg|_{z=0} = \dot{w}/c_0 \qquad (7a)$$

$$\varepsilon^2 \left.\frac{\partial \phi_2}{\partial z}\right|_{z=0} = \left[-\varepsilon^2 \frac{\partial^2}{\partial z\, \partial t}(\phi_1)^2 - \varepsilon\, k\, w \frac{\partial^2 \phi_1}{\partial z^2} + \varepsilon\, k \frac{\partial w}{\partial R} \frac{\partial \phi_1}{\partial z} \right]_{z=0} \qquad (7b)$$

Note that Eqs. (6a) and (7a) are the governing equations for linear theory, so ϕ_1 is a bounded function. Consequently, any cumulative growth effects that appear in Eq. (5) must be asssociated with ϕ_2. Since the nonlinearities appear in Eq. (6b) as source terms that are proportional to β_0, it follows that cumulative growth effects will be proportional to β_0. This feature is well-documented for one-dimensional waves. The generality of the perturbation treatment thus far permits us to extend this conclusion to any nonlinear acoustic wave, not just the present one, provided that the acoustic Mach number is a small fraction.

The first order equations (6a) and (7a), supplemented by the Sommerfeld radiation condition, are the linear equations for an arbitrary bafffled projector. The King integral provides the solution for this signal in a form that is useful for forming the source terms in Eq. (6b). The Hankel transform of the amplitude shading function is

$$F_n = \int_0^\infty R\, f(R)\, J_0(nR)\, dR \qquad (8)$$

The King integral is an inverse Hankel transform given by

$$\phi_1 = \frac{i}{2} \int_0^\infty G_n \exp(i\omega t - \mu_n z)\, J_0(nR)\, dn \qquad (9)$$

where

$$\mu_n = \begin{cases} i\,(1 - n^2)^{1/2} & ; \quad n < 1 \\ (n^2 - 1)^{1/2} & ; \quad n > 1 \end{cases} \tag{10}$$

$$G_n = n\,F_n/\mu_n \tag{11}$$

Note that transverse wave numbers $n < 1$ corrrespond to modes that are above the cutoff frequency, and therefore propagate. In contrast, modes for $n > 1$ are evanescent.

Substitution of Eq. (9) into Eqs. (6b) and (7b) leads to an inhomogeneous differential equation and an inhomogeneous boundary condition. In accord with standard procedures, we split ϕ_2 into two parts by defining

$$\phi_2 = \Phi_{21} + \Phi_{22} \tag{12}$$

where

$$\nabla^2\Phi_{21} - \frac{\partial^2}{\partial t^2}\Phi_{21} = \beta_0 \frac{\partial}{\partial t}\left(\frac{\partial \phi_1}{\partial t}\right)^2$$

$$\left.\frac{\partial \Phi_{21}}{\partial z}\right|_{z=0} = 0 \tag{13}$$

and

$$\nabla^2\Phi_{22} - \frac{\partial^2}{\partial t^2}\Phi_{22} = 0$$

$$\left.\frac{\partial\Phi_{22}}{\partial z}\right|_{z=0} = \left[-\frac{\partial^2}{\partial z\,\partial t}(\phi_1)^2 - \frac{k}{\epsilon} w \frac{\partial^2\phi_1}{\partial z^2} + \frac{k}{\epsilon}\frac{\partial w}{\partial R}\frac{\partial\phi_1}{\partial z}\right)\Bigg|_{z=0} \tag{14}$$

Aside from the different form of the inhomogeneous term in the boundary condition, Eqs. (14) are essentially the same as Eqs. (6a) and (7a). It follows that the task of determining Φ_{22} is quite similar to that required to obtain ϕ_1. The difficulty in the present case is the more complicated form of the boundary condition, owing to Eq. (3) for w and Eq. (9) for ϕ_1. Furthermore, it can be argued that the precise nature of the function f(R) is not known. For example, the model of a piston transducer considers f(R) to be a step function, but high-frequency projectors of large diameter are usually composed of numerous small piezoelectric elements that do not respond identically. It is inappropriate to attempt to form a precise solution satisfying an imprecise boundary condition. Accordingly, we shall set

$$\Phi_{22} = 0 \tag{15}$$

Another justification for this choice comes from the recognition that because Eqs. (14) are those for linear radiation, Φ_{22} represents an effect that is $O(\epsilon^2)$ at all locations. Other effects having this order of magnitude, which we will evaluate later, will be seen to have negligible importance.

II. SECOND ORDER NEARFIELD SIGNAL

Our objective here is to derive an expression for Φ_{21} and the corresponding pressure, without regard for breakdown of the perturbation hierarchy resulting from cumulative growth effects. Such a representation, which is analogous to the one derived by Ingenito and Williams [2], may be expected to be suitable in regions reasonably close to the projector. We begin by substituting Eq. (9) into Eq. (6b), which leads to

$$\nabla^2\Phi_{21} - \frac{\partial^2}{\partial t^2}\Phi_{21} = i\beta_0 \int_0^\infty \int_0^n G_n G_m \exp[2it - (\mu_n + \mu_m)z] \times J_0(nR)\, J_0(mR)\, dm\, dn + C.C. \tag{16}$$

Note that we have used the symmetry of the integrand with respect to m and n to reduce the inner integral to the finite domain $0 \le m \le n$.

It does not seem possible to solve Eq. (16) in exact form, because of the presence of a product of Bessel functions. We therefore shall develop a matched asysmptotic expansion that compares the form of Φ_{21} in the off-axis region (large R) to one in the paraxial region (small R). We begin with the off-axis analysis, for which the asymptotic representations of the Bessel functions lead to

$$\left(\frac{d^2}{dR^2} + \frac{1}{R}\frac{d}{dR}\right) J_0(nR)\, J_0(nR) = -(n^2 + m^2)\, J_0(nR)\, J_0(nR) + 2nm\, J_1(nR)\, J_1(nR)$$

$$\left(\frac{d^2}{dR^2} + \frac{1}{R}\frac{d}{dR}\right) J_1(nR)\, J_1(nR) = 2nm\, J_0(nR)\, J_0(nR) - (n^2 + m^2)\, J_1(nR)\, J_1(nR) + O(1/R^2) \qquad (17)$$

Because the source term in Eq. (16) contains only $J_0(nR)\, J_0(mR)$, we form the trial solution using sums and differences of the above products of Bessel functions. Specifically, we try

$$\Phi_{21} = \int_0^\infty \int_0^n G_n G_m \{A(z, n, m)[J_0(nR)\, J_0(mR) - J_1(nR)\, J_1(mR)] + B(z, n, m)[J_0(nR)\, J_0(mR) + J_1(nR)\, J_1(mR)]\} \exp[2it - (\mu_n + \mu_m)z]\, dm\, dn + O(1/R^2) \qquad (18)$$

where A and B are undetermined functions. Note that these functions are not considered to depend on R because cumulative growth is generally anticipated to occur with increasing distance from the boundary. Also, dependence of these functions on R would conflict with the need to satisfy the boundary condition (13) for arbitrary values of R.

We find that Eq. (18) satisfies Eq. (16) for all R (assuming R is large), provided that

$$A'' - 2N_1 A' + (N_1^2 - N_2^2)A = i\beta_0/2 \qquad (19a)$$

$$B'' - 2N_1 B' + (N_1^2 - N_3^2)B = i\beta_0/2 \qquad (19b)$$

where a prime denotes differentiation with respect to z, and the coefficients N_j are functions of n and m, given by

$$N_1 = \mu_n + \mu_m \ , \quad N_2 = [(n + m)^2 - 4]^{1/2}$$

$$N_3 = [(n - m)^2 - 4]^{1/2} \tag{20}$$

We obtain the boundary conditions for A and B by requiring that Eq. (18) satisfy the boundary condition (13), which leads to

$$A' - N_1 A = 0 \ , \quad B' - N_1 B = 0 \quad \text{for } z = 0 \tag{21}$$

In addition to the foregoing, the functions A and B must be chosen such that Φ_{21} does not represent a signal coming from the farfield toward the projector.

Before we address the solution of Eqs. (19) subject to Eqs. (21), we shall consider the paraxial approximation. We wish to derive a solution for Φ_{21}, valid for small R, that may be compared to the off-axis form in Eq. (18). The usual power series expansions of Bessel functions for small argument is unsuitable, since our objective is to identify the functional form of Φ_{21}. Instead, we develop a representation that is derived from the Neumann addition theorem [21],

$$J_j(nR + mR) = \sum_{k=-\infty}^{\infty} J_{j-k}(nR)\, J_k(mR)$$

$$J_j(nR - mR) = \sum_{k=-\infty}^{\infty} J_{j+k}(nR)\, J_k(mR) \tag{22}$$

In the region where R is small, $J_j(nR)$ decreases very rapidly for increasing j and fixed nR. Furthermore, $J_{-j}(nR) = (-1)^j J_j(nR)$. As a result, we find that in the paraxial region,

$$J_0(nR)\, J_0(mR) = \frac{1}{2}\left[J_0(nR + mR) + J_0(nR - mR)\right] + O(R^4) \tag{23}$$

We employ Eq. (23) to represent the source term in Eq. (16). A suitable trial solution for Φ_{21} in the paraxial region depends on R in the same manner. Hence, we set

$$\Phi_{21} = \int_0^{\infty} \int_0^{n} G_n G_m \left[C(z, n, m)\, J_0(nR + mR) + D(z, n, m)\, J_0(nR + mR)\right] \times \exp[2it - (\mu_n + \mu_m)z]\, dm\, dn \tag{24}$$

Substitution of Eq. (24) into the paraxial approximation of Eq. (16), and into the boundary condition (13), leads to an important observation -- the equations governing C and D are identical to Eqs. (19) for A and B, respectively.

Let us compare the two forms of Φ_{21}, Eqs. (18) and (24), under the condition that C = A and D = B. Since the exponential factors in each equation are the same, the two representations are identical in their dependence on t and z. For the transverse direction, we note that when nR and mR are small, the first two terms in a Taylor series expansions of the coefficient of C in Eq. (24) and of the coefficient of A in Eq. (18) are

identical. The same statement applies to the coefficients of B and D. In contrast, when nR and mR are large, the asymptotic expansions of these corresponding coefficients are not alike.

The conclusion that we derive from these considerations is that the paraxial representation, Eq. (24), in its range of validity gives the same solution as that which would be obtained if the off-axis solution, Eq. (18), were applied in the paraxial region. In other words, the off-axis form is actually correct for the entire field. This confirms Ginsberg's hypothesis [14] that the physical processes causing nonlinear interactions are not dependent on the transverse position.

Now that we have identified the dependence of Φ_{21} on t and R, we return to the evaluation of the amplitude factors A and B, which are functions of z. Ginsberg [14] and Miao [18] performed this analysis by using asymptotic methods to solve the differential equations (19), based on a limitation to comparitively long ranges (large z). We shall develop a more general solution here. Adding the complementary and particular solutions of Eqs. (19) leads to

$$A = \frac{i\beta_0}{2(N_1^2 - N_2^2)} + A_1 \exp(\sigma_{A1} z) + A_2 \exp(\sigma_{A2} z)$$

$$B = \frac{i\beta_0}{2(N_1^2 - N_3^2)} + B_1 \exp(\sigma_{B1} z) + A_2 \exp(\sigma_{B2} z) \qquad (25)$$

where the coefficients σ_{Aj} and σ_{Bj} are the roc s of the respective characteristic equations. These values are readily found to be

$$\sigma_{A1} = N_1 - N_2 , \quad \sigma_{A2} = N_1 + N_2$$

$$\sigma_{B1} = N_1 - N_3 , \quad \sigma_{B2} = N_1 + N_3 \tag{26}$$

We evaluate the constants A_j and B_j by satisfying the boundary conditions, Eq. (21), as well as the radiation condition for Φ_{21}. The dependence on t and z appearing in Eq. (18) is A(z) exp(it - N_1z) and B(z) exp(it - N_1z). In view of Eqs. (25), this means that Φ_{21} contains terms having the appearance of exp[it - (N_1 - σ_{Aj}) z] and exp[it - (N_1 - σ_{Bj}) z]. Any term in which either the real or imaginary part of N_1 - σ_{Aj} or N_1 - σ_{Bj} is positive will violate the condition that the signal is either an outgoing wave, or an exponentially decaying wave. Since N_3 is positive as either a real or imaginary number, we require that

$$A_2 = B_2 = 0 \tag{27a}$$

The constants A_1 and B_1 obtained by satisfying Eq. (21) are

$$A_1 = - \frac{i\beta_0 N_1}{2(N_1^2 - N_2^2)N_2} , \quad B_1 = - \frac{i\beta_0 N_1}{2(N_1^2 - N_3^2)N_3} \tag{27b}$$

which, when substituted into Eqs. (25) yield

$$A = \frac{i\beta_0}{2(N_1^2 - N_2^2)N_2} \{N_2 - N_1 \exp[(N_1 - N_2)z]\} \tag{28a}$$

$$B = \frac{i\beta_0}{2(N_1^2 - N_3^2)N_3} \{N_3 - N_1 \exp[(N_1 - N_3)z]\} \tag{28b}$$

We form Φ_{21} by substituting these expressions into Eq. (18). Once ϕ_1 and Φ_{21} are known, it is a simple matter to describe the corresponding pressure signal. The pressure relation obtained from Kelvin's equation [20], specialized to the case of an $O(\varepsilon)$ signal, is

$$p/\rho_0 c_0^2 = -\frac{\partial\phi}{\partial t} - \frac{1}{2}\left[\nabla\phi\cdot\nabla\phi - \left(\frac{\partial\phi}{\partial t}\right)^2\right] + O(\varepsilon^3) \tag{29}$$

Recall that we have set $\Phi_{22} = 0$, so $\phi_2 = \Phi_{21}$. Therefore, the perturbation expansion, Eq. (5), and some simple manipulations lead to

$$p/\rho_0 c_0^2 = -\varepsilon\frac{\partial\phi_1}{\partial t} - \varepsilon^2\frac{\partial\Phi_{21}}{\partial t} - \frac{1}{2}\left[\left(\frac{\partial\phi_1}{\partial t}\right)^2 + 2\,\phi_1\frac{\partial^2\phi_1}{\partial t^2} + \nabla\phi_1\cdot\nabla\phi_1\right] + O(\varepsilon^3) \tag{30}$$

We now recall Eq. (9) for ϕ_1 and Eq. (18) for Φ_{21}. Their substitution into the above yields an expression for the pressure in the form of a single integral for the $O(\varepsilon)$ term and two double integrals for the $O(\varepsilon^2)$ terms. The result may be written as

$$p/\rho_0 c_0^2 = \left[\frac{1}{2}\Gamma_1(z, R)\exp(it) + \frac{1}{2}\Gamma_2(z, R)\exp(2it)\right] + C.C. + \Gamma_0 \tag{31}$$

where Γ_1 and Γ_2 are the complex amplitudes of the fundamental and second harmonic, respectively, and Γ_0 is the mean value radiation pressure. When Eq. (10) is used to replace G_n, these quantities are given by

$$\Gamma_1 = \epsilon \int_0^\infty \frac{nF_n}{\mu_n} \exp(-\mu_n z)\, J_0(nR)\, dn \tag{32a}$$

$$\Gamma_2 = -\frac{1}{2}\epsilon^2 \int_0^\infty \int_0^n \frac{nmF_nF_m}{\mu_n\mu_m} \{[8i(A+B) + 3 - \mu_n\mu_m]\, J_0(nR)\, J_0(mR) - [8i(A-B) + nm]\, J_1(nR)\, J_1(mR)]\} \exp[-(\mu_n + \mu_m)z]\, dm\, dn \tag{32b}$$

$$\Gamma_0 = -\frac{1}{2}\epsilon^2 \int_0^\infty \int_0^n \frac{nmV_nV_m}{\mu_n\mu_m^*} \{[-1 + \mu_n\mu_m^*]\, J_0(nR)\, J_0(mR) + nm\, J_1(nR)\, J_1(mR)]\} \exp[-(\mu_n + \mu_m^*)z]\, dm\, dn + C.C. \tag{32c}$$

The fundamental amplitude is the linear King integral, which cannot been evaluated in closed form. Analytical integration of Γ_2 and Γ_0 therefore does not seem to be feasible. However, it is possible to evaluate the coefficients by numerical methods. An important aspect of such an evaluation is the presence of three types of singularities.

In terms of its implications for later developments, the most important singularity contained in Eqs. (32) occurs in the coefficient A when $m = n$. In this situation, N_1 and N_2 both equal $2\mu_n$, which causes the denominator in Eq. (28a) to vanish. A similar situation arises for the function B when $m = n = 0$, in which case N_1 and N_3 both equal $2i$. Neither situation is a

serious complication for a numerical integration, because both A and B have finite limits as $m \to n$. In the case of A, Taylor series expansion in powers of $N_1 - N_2$ gives

$$A = -\frac{i\beta_0}{2(N_1 + N_2)N_2}\left\{1 + N_1 z\left[1 + \frac{1}{2}(N_1 - N_2)z + \frac{1}{6}(N_1 - N_2)^2 z^2 + \cdots\right]\right\} \tag{33}$$

The expansion for B near $n = m = 0$ is the same as the foregoing, except that N_3 replaces N_2. As $m \to n$, we find that

$$\lim_{m\to n} A = -\frac{i\beta_0}{16\mu_n^2}(1 + 2\mu_n z + \cdots), \quad \lim_{\substack{m\to 0\\ n\to 0}} B = -\frac{i\beta_0}{16}(1 + 2iz + \cdots) \tag{34}$$

The coefficients A and B contain additional singularities, associated with $N_2 = 0$ or $N_3 = 0$. Reference to Eqs. (20) shows that these occur in the integration domain along $m = 2 - n$ and $m = n - 2$, respectively. The roots σ_{A1} and σ_{A2}, or σ_{B1} and σ_{B2}, in Eqs. (26) are equal along the respective lines. The second homogeneous solution, which is obtained in this case by multiplying the first solution by z, is needed to satisfy the boundary condition. Thus, this is a finite singularity.

The third singularity that occurs in the complex coefficients Γ_j is associated with the axial wave number μ_n. Its definition in Eq. (10) shows that $\mu_n \to 0$ as $n \to 1$, which leads to a singularity due to the presence of this parameter in the denominators of both of Eqs. (32). The singularity

may be removed by a simple change of variables. We write Eqs. (32) in the generic forms

$$\Gamma_1 = \int_0^\infty \Lambda_1(n,z,R)\,\frac{dn}{\mu_n} + C.C.$$

$$\Gamma_j = \int_0^\infty \int_0^n \Lambda_j(n,m,z,R)\,\frac{dm}{\mu_m}\,\frac{dn}{\mu_n} + C.C.\ , \quad j = 0,2 \tag{35}$$

where the Λ_j are functions that have finite limits as $n \to 1$ and $m \to 1$. We replace the wave numbers n and m by new variables ζ and ξ, such that

$$n = \cos\zeta\ , \quad \mu_n = i \sin\zeta\ ; \quad n < 1$$

$$n = \cosh\zeta\ , \quad \mu_n = \sinh\zeta\ ; \quad n > 1 \tag{36}$$

which converts Eqs. (35) to

$$\Gamma_1 = -\,i \int_0^{\pi/2} \Lambda_1(\cos\zeta,z,R,t)\,d\zeta + \int_0^\infty \Lambda_1(\cosh\zeta,z,R,t)\,d\zeta + C.C.$$

$$\Gamma_j = -\int_0^{\pi/2}\int_0^{\pi/2} \Lambda_j(\cos\zeta,\cos\theta,z,R,t)\,d\theta\,d\zeta - i\int_0^\infty\int_0^{\pi/2} \Lambda_j(\cosh\zeta,\cos\theta,z,R,t)\,d\theta\,d\zeta + \int_0^\infty\int_0^\infty \Lambda_j(\cosh\zeta,\cosh\theta,z,R,t)\,d\theta\,d\zeta + C.C.\ , \quad j = 0,2 \tag{37}$$

The first integrals for Γ_0 and Γ_2 represents the second order effects associated with interactions between propagating modes. Similarly, the third integrals arise from interactions between evanescent modes, while interaction between propagating and evanescent modes gives rise to the second integrals. The integration scheme we employed for each of these double integrals is based on a nine point integration scheme for a square segment [21], while linear interpolation was effective for the single integral.

Well-documented experimental data describing nonlinear effects in the nearfield is quite sparse. Gould et al [17] measured the field generated by a piston vibrating at 2.58 MHz when c_0 = 1475 m/s, which corresponds to k = 10.99 mm^{-1}. The geometrical radius was 10.1 mm, but subsequent analysis of the primary frequency field caused Ingenito and Williams [2] to suggest that a = 10.42 mm is more appropriate. The results were presented in Gould's paper as selected traces of the amplitudes of the fundamental and second harmonic, either along or transverse to the axis of the beam. Such traces were obtained by photographing an oscilloscope screen, so they are difficult to read accurately. However, traveling microscope readings of the axial distribution of the second harmonic were reported by Ingenito and Williams [2], while Rogers [3] gave comparable data for transverse distribution at selected locations.

Figure 2 compares the measured axial distribution of the second harmonic with our prediction. The projector in this case was driven at a source pressure of 5 atmospheres, which corresponds to $\varepsilon = 2.49(10^{-4})$ because the source pressure equals $\varepsilon\rho_0 c_0^2$. The sound pressure level at an

axial antinode would have been 237 dB//1μPa if the projector were an ideal piston and nonlinearity had no effect. The overall agreement between theory and experiment is quite good. It should be noted that our prediction for the farthest dip, near the nondimensional distance z = 1400, is somewhat less deep than that predicted by Ingenito and Williams, while the dip near z = 600 is comparable to their prediction and the one near z = 800 is substantially deeper. Our computations indicate that many more such dips occur with decreasing distance from the projector, but no more occur beyond the region described by Figure 2.

No physical explanation for such dips has been offered in the past. We cannot say for certain what the mechanism is, because the second harmonic is a field effect resulting from a three-dimensional distribution of sources. A plausible explanation is that the antinodes of the fundamental field, which occupy small regions, generate the largest contribution to the nonlinear sources. It seems logical to consider the peaks and valleys of the second harmonic axial distribution to arise from constructive and destructive interference of the radiation from these local "hotspots".

Figure 3 describes the transverse distribution of the second harmonic at 50 mm from the projector for the same parameters as Figure 2; the measurements are taken from Rogers description of the experiment. The dotted line for the King integral prediction of the fundamental is provided as a reference. (The dashed curve describing the farfield approximation concerns with developments.) The agreement between theory and experiment for the second harmonic amplitude is quite good. The fact that the overall level of the predicted result is somewhat lower than the measurements might

be attributable to the aforementioned uncertainty regarding the appropriate value of ka. A small change in this quantity can significantly shift the location of the maxima and minima. Another uncertainty regarding the comparison between our prediction and the measured data is the possibility that the projector did not act as a true piston, which is indicated by the aforementioned correction for the active radius. We also should note that the wire probe used for the measurements had a diameter of 28.6 nondimensional units. This limits the ability to resolve fine scale features, due to spatial averaging of the amplitudes. This limitation, which was noted by Gould et al, is exemplified by the transverse distribution in Figure 4, where the axial distance z = 589 is selected to match the axial minimum in Figure 2. As may be seen in this figure, the probe diameter is comparable to the extent of the depressed region surrounding the axis.

Although the theoretical development thus far is consistent with experiment, the result is not sufficient. We shall next employ the description as the foundation for an extension to larger distances from the projector. In addition to enhancing the domain of validity, the extended theory will be descriptive of a waveform.

III. RENORMALIZATION ANALYSIS

An important aspect of Figure 2 is the overall rise in the level of the second harmonic with increasing axial distance. In general, such behavior

arises in nondispersive media because nonlinearity provides a self-interaction mechanism for the linearized signal. The basic concern when growth is encountered in a regular perturbation series, such as Eq. (5), is that the second order term might exceed the estimate of its magnitude. Such behavior is known as nonuniform validity. In this section, we will derive an expression for the pressure that behaves properly at all locations.

First, we shall introduce a simplification that results from inspection of the quantitative results. In all situations of interest, ε is extremely small, for example, $\varepsilon \approx 0.0002$ for a signal whose maximum on-axis amplitude is 240 dB//1 μPa. Also, recall that cumulative growth of the $O(\varepsilon^2)$ signal can only arise in Φ_{21}. In the present context, this is manifested by an increase in the magnitude of the functions A and B with increasing z, as exhibited in Eqs. (34). The terms appearing in Eqs. (32b and 32c) that do not depend on A or B arise either from the quadratic term that was inserted into the perturbation series, Eq. (5), or from nonlinearities in Kelvin's equation (29). Both effects remain bounded for all z. It is reasonable therefore that any term in either Γ_2 and Γ_0 that does not originate from the second order perturbation Φ_{21} will be smaller than the fundamental signal by a factor ε.

When we ignore the constant magnitude $O(\varepsilon^2)$ effects, the expression for pressure obtained from Eqs. (31) and (32) under this simplification is

$$p/\rho_0 c_0^2 = \frac{1}{2}\,\varepsilon \int_0^\infty G_n \exp(it - \mu_n z)\, J_0(nR)\, dn$$

$$- 2i\varepsilon^2 \int_0^{\infty} \int_0^{n} G_n G_m \{A [J_0(nR)\, J_0(mR) - J_1(nR)\, J_1(mR)]$$
$$+ B [J_0(nR)\, J_0(mR) + J_1(nR)\, J_1(mR)]\}$$
$$\times \exp[2it - (\mu_n + \mu_m)z]\, dm\, dn + C.C. \qquad (38)$$

Note that we have returned to the use of G_n as the transform of the transducer shading function solely as a convenience.

The first step in correcting the growth of the $O(\varepsilon^2)$ terms is to write the pressure in the form of waves in the transverse, as well, as axial direction. Such a representation is suggested by the asymptotic expansions of Bessel functions for large arguments [21], which leads to

$$J_0(nR) \sim (1/2\pi nmR)^{1/2} \exp[i(nR - \pi/4)] + C.C.$$

$$J_0(nR)\, J_0(mR) - J_1(nR)\, J_1(mR)$$
$$\sim (1/\pi^2 nmR^2)^{1/2} \exp\{i[(n + m)R - \pi/2]\} + C.C. \qquad (39)$$

The part listed in each function above, when combined with the exponential terms already appearing in Eq. (38), represents a wave in the off-axis region that seems to propagate in the direction of decreasing R and increasing z. Similarly, the complex conjugate part corresponds in that region to waves that propagate in the direction of increasing R and z.

In order to highlight this wave-like feature for an arbitrary transverse location, we rewrite $J_0(nR)$ identically as

$$J_0(nR) = \frac{1}{2}\left[J_0(nR) + iJ_1(nR)\right] + C.C. = \frac{1}{2} Q_n \exp(i\Delta_n) + C.C. \qquad (40a)$$

where

$$Q_n \cos \Delta_n = J_0(nR) \ , \quad Q_n \sin \Delta_n = J_1(nR) \qquad (40b)$$

Note that Q_n and Δ_n are functions of R, as well as n, but such dependence is not indicated in the notation as a matter of convenience. The second function in Eqs. (39) may also be expressed in terms of Q_n and Δ_n, according to

$$\begin{aligned} &J_0(nR)\, J_0(mR) - J_1(nR)\, J_1(mR) \\ &\quad = \frac{1}{2}\left[J_0(nR) + iJ_1(nR)\right]\left[J_0(mR) + iJ_1(mR)\right] + C.C. \\ &\quad = \frac{1}{2} Q_n Q_m \exp[i(\Delta_n + \Delta_m)] + C.C. \end{aligned} \qquad (40c)$$

When we substitute Eqs. (40) into Eqs. (38), we decompose the signal into two parts, such that

$$p/\rho_0 c_0^{\,2} = \int_0^\infty (p_I + p_{II})\, dn \qquad (41)$$

where

$$\begin{aligned} p_I = \frac{1}{4} \varepsilon G_n Q_n \exp(it - \mu_n z + i\Delta_n) \{1 - 4i\varepsilon \int_0^n G_m Q_m [A \exp(it \\ - \mu_n z + i\Delta_m) + B \exp(it - \mu_n z - i\Delta_m)]\, dm\} + C.C. \end{aligned} \qquad (42a)$$

$$p_{II} = \frac{1}{4}\varepsilon G_n Q_n \exp(it - \mu_n z - i\Delta_n)\left\{1 - 4i\varepsilon \int_0^n G_m Q_m \left[A \exp(it - \mu_n z - i\Delta_m) + B \exp(it - \mu_n z + i\Delta_m)\right] dm\right\} + C.C. \qquad (42b)$$

It is important to recognize that no new approximations are contained in the foregoing expressions; they are identical to Eq. (38).

Wavefronts of constant phase for the I and II waves consist of surfaces along which the phase functions

$$\Psi_j(z, R) = t - (\mu_n/i)z \pm \Delta_n \ , \quad j = I, II \qquad (43)$$

are constant. A few such surfaces for n = 0.10 and n = 0.20 are depicted in Figure 5. The wavefronts for the two families of waves seem to be nearly linear in z vs. R in each case, corresponding to nearly conical surfaces. This property becomes evident when we take the gradient of the phase functions in order to identify the rays for each wave.

$$\nabla\Psi_j = -\frac{\mu_n}{i}\underline{k} \pm \frac{\partial\Delta_n}{\partial R}\underline{e}_R \qquad (44)$$

The value of Δ_n is approximately $\frac{1}{2}nR$ for $nR < 0.2$, while it is well approximated as $nR - \pi/4$ for $nR > 5$. Hence, the above gradient is nearly constant in each region. As evidenced by Figure 5, the gradient changes slowly in the transition region of intermediate nR. It is interesting to note that the apex angles of these surfaces increase monotonically with increasing n, until for $n > 1$, the wavefronts are parallel to the z axis, and the waves evanesce in that direction. It is also worth noting that this

interpretation of the signal as the superposition of two families of conical waves is equally valid for the linear King integral.

We have seen that the $O(\epsilon^2)$ terms in both waves tend to grow at large distances from the transducer, ultimately leading to nonuniform validity. Furthermore, the growth in the second harmonic has not yet led to depletion of the fundamental from its value in linear theory. Both features result from using as the independent variables, position coordinates that do not correctly match the spatial scale of the nonlinear processes. To a first order (linear) approximation, the appropriate nonlinear variables match the physical coordinates. However, the gradual nature of the nonlinearity causes the two sets of variables to diverge over many axial wavelengths. This leads to the concept of a coordinate straining transformation. The process of deriving this transformation from the requirement that the proper forms not display unbounded growth is renormalization [22].

Let α_n be a real variable for the I wave that reduces to the axial distance z when $\epsilon \to 0$, and let β_n be the corresponding variable for the II wave. Equations (42) indicate that each wave at a specified wave number n is affected by a spectrum of wavenumbers $m < n$ associated with each wave. This suggests that the discrepancies between the linear and nonlinear position variables also depend on such a spectrum. Therefore, we seek a coordinate transformation whose form is

$$z = \alpha_n + \epsilon \int_0^n \left[U_I(z, n, m)\, Q_n \exp(it - \mu_m \alpha_m + \Delta_m) \right.$$
$$\left. + W_I(z, n, m)\, Q_n \exp(it - \mu_m \beta_m - \Delta_m) + C.C. \right] dm \qquad (45a)$$

$$z = \beta_n + \varepsilon \int_0^n [W_{II}(z, n, m)\, Q_n \exp(it - \mu_m\alpha_m + \Delta_m) + U_{II}(z, n, m)\, Q_n \exp(it - \mu_m\beta_m - \Delta_m) + C.C.]\, dm \qquad (45b)$$

where the U_j and W_j are undetermined at this juncture.

The task of identifying the undetermined functions is simplified by the dependence of the I and II waves at $O(\varepsilon)$ on a single phase variable. Consequently, the axial and transverse particle velocity components and the pressure in each wave are proportional, which means that uniform validity of the particle velocity will be assured when p_I and p_{II} behave properly. We use Eq. (45a) to replace z in any term in Eqs. (42) whose phase is $(t - \mu_n z/i + \Delta_n)$, while Eq. (45b) is used when the phase is $(t - \mu_n z/i - \Delta_n)$. The result of expanding the substituted form of p_I in Taylor series in ε is

$$p_I = \tfrac{1}{4}\varepsilon G_n Q_n \exp(it - \mu_n\alpha_n + i\Delta_n)\{1 - \varepsilon\mu_n \int_0^n [U_I \exp(it - \mu_m\alpha_m + i\Delta_m) + W_I \exp(it - \mu_m\beta_m - i\Delta_m) + U_I^* \exp(-it - \mu_m^*\alpha_m - i\Delta_m) + W_I^* \exp(-it - \mu_m^*\beta_m + i\Delta_m)]\, dm - 4i\varepsilon \int_0^n G_m Q_m [A \exp(it - \mu_m\alpha_m + i\Delta_m) + B \exp(it - \mu_m\beta_m - i\Delta_m)]\, dm\} + C.C. \qquad (46)$$

The terms containing U_I and W_I correspond to second harmonics, whereas U_I^* and W_I^* lead to terms that are independent of time. We select U_I and W_I to individually cancel the second harmonics in the last integral, which gives

$$U_I = -(4iG_m Q_m/\mu_n)\, A\ , \quad W_I = -(4iG_m Q_m/\mu_n)\, B \qquad (47)$$

The p_I signal, which consists of the terms remaining in Eq. (42a) when Eqs. (45) apply, is

$$p_I = \frac{1}{4}\,\varepsilon G_n Q_n \exp(it - \mu_n\alpha_n + i\Delta_n) + C.C. + T_I \tag{48}$$

where T_I is a mean value correction required to cancel a residual that arises from the coordinate straining.

$$T_I = -i\varepsilon^2 \frac{\mu_n}{\mu_n^*} \int_0^n G_n G_m^* Q_n Q_m \left[A^* \exp[-(\mu_n\alpha_n + \mu_m^*\alpha_m) + i(\Delta_n - \Delta_m)\right.$$
$$\left. + B^* \exp[-(\mu_n\alpha_n + \mu_m^*\beta_m) + i(\Delta_n + \Delta_m)]\right] dm + C.C. \tag{49}$$

The corresponding coordinate transformation, Eq. (45a), becomes

$$z = \alpha_n - 4\varepsilon \left\{\int_0^n (iG_m Q_m/\mu_n) \left[A \exp(it - \mu_m\alpha_m + i\Delta_m)\right.\right.$$
$$\left.\left. + B \exp(it - \mu_m\beta_m - i\Delta_m)\right] dm + C.C.\right\} \tag{50}$$

The same analysis yields the renormalized version of p_{II}. The results are essentially the same, aside from an interchange of β_m and α_m and changes in the signs preceding Δ_n and Δ_m.

$$p_{II} = \frac{1}{4}\,\varepsilon G_n Q_n \exp(it - \mu_n\beta_n - i\Delta_n) + C.C. + T_{II} \tag{51}$$

where the mean value correction for this wave is

$$T_{ii} = -i\varepsilon^2 \frac{\mu_n}{\mu_n^*} \int_0^n G_n G_m^* Q_n Q_m \{A^* \exp[-(\mu_n \beta_n + \mu_m^* \alpha_m) - i(\Delta_n - \Delta_m)]$$

$$+ B^* \exp[-(\mu_n \beta_n + \mu_m^* \alpha_m) - i(\Delta_n + \Delta_m)]\} \, dm + C.C. \qquad (52)$$

and the coordinate transformation is

$$z = \beta_n - 4\varepsilon \{\int_0^n (iG_m Q_m/\mu_n) [A \exp(it - \mu_m \beta_m + i\Delta_m)$$

$$+ B \exp(it - \mu_m \alpha_m - i\Delta_m)] \, dm + C.C.\} \qquad (53)$$

Evaluation of the pressure requires integration of Eqs. (48) and (51), whose integrands can only be evaluated when Eqs. (50) and (53) have been solved for the strained coordinates. Since these coordinate transformations are themselves integral transforms, and they are coupled, we are unaware of analytical procedures by which α_n and β_n may be determined as functions of n. Hence, it does not seem possible to solve analytically for the pressure. Indeed, the formidable nature of these equations makes even a numerical evaluation of the expressions prohibitive. Nevertheless, if such an evaluation were forthcoming, the result would be a uniformly valid description of the signal in the entire domain.

IV. LONG RANGE APPROXIMATION

It is possible to derive simplified versions of Eqs. (48)-(53), subject to the restriction that z is large. Such expressions will permit numerical evaluations of the signal at large distances from the transducer. The first

simplication stems from the earlier observation that in the vicinity of $m = n$, the function A grows with increasing z. In contrast, the function B displays such behavior only around $m = n = 0$. At sufficiently large z, the contribution of B to the integrals becomes negligible.

The different roles of these functions has a physical basis, for which we refer to Figure 5. According to the coordinate transformation, A governs the degree to which a I or II wave at wave number n interacts with a wave of the same type at wave number m. In the same viewpoint, B describes the degree to which there is cross-interaction between I and II waves at arbitrary m and n. It is logical that waves of the same type, which propagate in generally the same sense, interact more strongly than do waves whose propagation paths intersect obliquely in most of the field.

Another simplication results from the change of the axial wave number μ_m from imaginary to real with increasing n, corresponding to the transition from the propagating to evanescent spectrum at $n = 1$. Equations (48), (50), (51), and (53) feature integrals that are either oscillatory or exponential functions of m, depending on whether $m < 1$ or $m > 1$. If z is large (for example, distances that are multiples of the piston radius), then the evanescent spectrum is a negligible effect.

Let us examine the behavior of A as given by Eq. (28), based on $m < n < 1$ with n fixed and z large. Then μ_n and μ_m are imaginary, as are the coefficients N_j, which are defined in Eqs. (20). When considered as a function of m, A has a maximum at the upper limit $m = n$ and it oscillates with increasing frequency as m is decreased. These are the conditions for

which the integrals may be evaluated asymptotically by a straightforward modification of Laplace's method [23].

The integrals in the coordinate transformation, Eqs. (50) and (53), may be written as

$$I = \int_0^n A(n, m)\, F(n, m)\, dm \tag{54}$$

We isolate the region around the maximum as

$$I = \int_0^{n-\Delta} A(n, m)\, F(n, m)\, dm + \int_0^{\Delta} A(n, n - q)\, F(n, n - q)\, dv$$

$$\approx F(n, n) \int_0^{\Delta} \hat{A}(n, n - q)\, dq + \int_0^{n-\Delta} A(n, m)\, F(n, m)\, dm \tag{55}$$

It is important to the development that in the vicinity of $m = n$, the function F varies much more slowly than does A. This allowed us to factor F out of the integral containing $m = n$. Also, the original function A in this region has been replaced by $\hat{A}$, which denotes an asymptotic approximation of A for large z and small $q = n - m$.

When the value of z is increased with Δ fixed, the first integral in Eq. (55) eventually dominates the second. In addition, the first integral will converge to a value that is independent of Δ, provided that Δ has been chosen sufficiently large to include the entire contribution of A around its

maximum. Letting $\Delta \to \infty$ will not significantly alter that value. Hence, we find that

$$I = F(n, n) \int_0^\infty \hat{A}(n, n - q)\, dq + S.D.T. \tag{56}$$

where S.D.T. represents subdominant terms, which become unimportant at large z.

The limiting form of A in Eq. (33) is not adequate for $\hat{A}$, because an increasing number of terms is required as the value of z increases. In order to obtain a suitable representation we rewrite Eq. (28a) as

$$A = \frac{\beta_0 N_1 \{1 - \exp[(N_1 - N_2)z]\}}{2iN_2 (N_1^2 - N_2^2)} - \frac{\beta_0}{2i(N_1 + N_2)N_2} \tag{57}$$

We may replace the coefficients N_j, which are defined in Eqs. (20), by their Taylor series expansions in $q = n - m$. For this, we let λ_n be the modulus of the axial wave number parameter, such that

$$\lambda_n = \mu_n / i = (1 - n^2)^{1/2} \tag{58}$$

The expansions of the N_j are then found to be

$$N_1/i = \lambda_n + [1 - (n - q)^2]^{1/2} = 2\lambda_n + nq/\lambda_n - q^2/2\lambda_n^3 + O(q^3)$$

$$N_2/i = [4 - (2n - q)^2]^{1/2} = 2\lambda_n + nq/\lambda_n - q^2/4\lambda_n^3 + O(q^3) \tag{59}$$

When these expressions are substituted into Eq. (57), we find that the magnitude of the first term is $O(1/q^2)$. In contrast, the second term is $O(1)$, which means that it is a subdominant effect. Consequently, we have

$$\hat{A} = \frac{\beta_0}{2i} \lambda_n^2 q^{-2}[1 - \exp(-iq^2 z/4\lambda_n^3)] + \text{S.D.T.} \tag{60}$$

With the aid of this approximation, the integral in Eq. (56) may be evaluated in closed form, with the result that

$$I = F(n,n) \frac{\beta_0}{4i} (\pi\lambda_n z)^{1/2} \exp(i\pi/4) + \text{S.D.T.} \tag{61}$$

This formula may be applied directly to Eqs. (50) and (53), from which we obtain the following long range representation of the coordinate transformations.

$$\lambda_n z = \lambda_n \alpha_n + \varepsilon\beta_0\{(nF_n Q_n/i)(\pi z/\lambda_n)^{1/2} \exp[i(t - \lambda_n\alpha_n + \Delta_n)] + \text{C.C.}\}$$

$$\lambda_n z = \lambda_n \beta_n + \varepsilon\beta_0\{(nF_n Q_n/i)(\pi z/\lambda_n)^{1/2} \exp[i(t - \lambda_n\beta_n - \Delta_n)] + \text{C.C.}\} \tag{62}$$

The asymptotic integration formula also yields a simpler representation for the mean value residuals T_I and T_{II}, given in Eqs. (49) and (52). Applying Eq. (61) yields

$$T_I = T_{II} = -\frac{\sqrt{2}}{4} \beta_0 \varepsilon^2 G_n G_n^* Q_n^2 (\pi\lambda_n z)^{1/2} \tag{63}$$

A subtle feature of the asymptotic integration is associated with the appearance of λ_n in the denominator of the the coordinate transformations in Eqs. (62). Any solution technique would encounter difficulty around $n = 1$, where $\lambda_n = 0$. It also represents an anomoly, in the sense that it indicates that the strength of the nonlinearity is greatest at $n = 1$, where the propagating spectrum disappears. The resolution of this difficulty lies in the recognition that our asymptotic representation of $\hat{A}$ is not valid near $n = 1$, because we assumed that λ_n is not small in order to develop the expansions in Eqs. (59). We therefore reason that the combination $(\pi z/\lambda_n)^{1/2}$ is the representation for finite λ_n and large z of a function H(z, n) that is finite as $n \to 1$. In other words,

$$H(z,n) \sim \left(\frac{\pi z}{\lambda_n}\right)^{1/2} \quad \text{for large } \lambda_n z$$

$$\lim_{n \to 0} \lambda_n H(z,n) = 0 \tag{64}$$

Such reasoning led Ginsberg [14] to use the complementary error function to represent H. A different form, consisting of powers of Bessel functions, was employed by Miao [18] because of greater computational ease.

$$H(z,n) = (\pi^2/2\sigma)^{1/2} z^{\nu} \left[J_0(\lambda_n z^{2\nu-1}/\sigma)^2 + J_1(\lambda_n z^{2\nu-1}/\sigma)^2\right]^{1/2} \tag{65a}$$

where σ and ν are empirical parameters. (Miao found $\sigma = 1500$ and $\nu = 0.75$ to give good agreement with earlier measurements.)

A simpler choice is

$$H(z,n) = z\,[\pi/(\lambda_n z + \sigma' k^2 a^2)]^{1/2} \tag{65b}$$

where σ' again is a numerical parameter. This function is appealing from a physical viewpoint. According to Eqs. (62), the differences $\lambda_n(z - {}_n\alpha_n)$ and $\lambda_n(z - \beta_n)$ are proportional to H, so the magnitude of H represents the overall degree to which the nonlinear pressure differs from the prediction of linear theory. In the case of Eq. (65b), H is proportional to z for $\lambda_n z \ll \sigma' k^2 a^2$, which is the growth characteristic of a planar wave. In contrast, if $z \gg \sigma' k^2 a^2$, then the nonlinear effect is proportional to $z^{1/2}$. Note that $z = ka$ at a single transducer radius from the boundary, while the Rayleigh distance, nondimensionalized by the scale factor k, is $k^2a^2/2$. Hence, σ' provides a parameter that may be adjusted to match the transition from planar to diverging waves. We found $\sigma' = 1/2$ to give results that are consistent with Miao's work, as well as with measurements discussed later.

V. FOURIER SERIES REPRESENTATION

A primary benefit of the present two wave representation at long ranges is that it leads to a Fourier series representation; such a form eliminates the need to solve coordinate straining transformations. The derivation is much like the Fubini-Ghiron solution [24] for a planar wave. First, in order to avoid ambiguities, let us convert the transform F_n to polar,

$$F_n = V_n \exp(i\theta_n) \tag{66}$$

If the transducer vibration is such that all points on its surface are in phase, then the amplitude shading function f(R) and its transform F_n are real. In that case, $\theta_n = 0$ if $F_n > 0$ and $\theta_n = \pi$ if $F_n < 0$. It is also convenient to collect several parameters in a single coefficient D_n, according to

$$D_n = 2\beta_0 \epsilon n V_n Q_n H(z,n) \tag{67}$$

Next, we define real variables ξ and η to represent the phase of each omplex exponential term in the coordinate coordinate transformations, Eqs. (62). Thus,

$$\xi = t + \theta_n - \lambda_n \alpha_n + \Delta_n - \pi/4$$

$$\eta = t + \theta_n - \lambda_n \beta_n - \Delta_n + \pi/4 \tag{68}$$

It is useful to redefine the phase variables Ψ_I and Ψ_{II} for the linearized p_I and p_{II} waves to have in a similar form.

$$\Psi_I = t + \theta_n - \lambda_n z + \Delta_n - \pi/4$$

$$\Psi_{II} = t + \theta_n - \lambda_n z_n - \Delta_n + \pi/4 \tag{69}$$

When we substitute Eqs. (66-68) into the coordinate transformations and convert the results to real form, we obtain

$$\Psi_I = \xi - D_n \sin \xi \ , \quad \Psi_{II} = \eta - D_n \sin \eta \tag{70}$$

while Eqs. (48) and (51) for the pressures reduce to

$$p_I = \frac{\sqrt{2}}{4} \epsilon \frac{nV_n}{\lambda_n} Q_n [\sin \xi + \cos \xi] + T_I$$

$$p_{II} = \frac{\sqrt{2}}{4} \epsilon \frac{nV_n}{\lambda_n} Q_n [\sin n + \cos n] + T_{II} \tag{71}$$

It is possible to develop Fourier series for each of the trigonometric terms appearing above. Because of the similarity of the expressions for p_I and p_{II}, we shall only describe the analysis for p_I. It is not difficult to demonstrate that sin ξ and cos ξ have period 2π when considered as functions of Ψ_I. Furthermore, sin ξ is an odd function of that parameter, while cos ξ is an even function. It follows that the appppropriate Fourier series are

$$\sin \xi = \sum_{j=1}^{\infty} a_j \sin(j\Psi_I) \ , \quad \cos \xi = b_0 + \sum_{j=1}^{\infty} b_j \cos(j\Psi_I) \tag{72}$$

where

$$a_j = \frac{2}{\pi} \int_0^{\pi} \sin \xi \sin(j\Psi_I) \, d\Psi_I \tag{73a}$$

$$b_0 = \frac{1}{\pi} \int_0^{\pi} \cos \xi \, d\Psi_I \tag{73b}$$

$$b_j = \frac{2}{\pi} \int_0^{\pi} \cos \xi \cos(j\Psi_I) \, d\Psi_I \tag{73c}$$

We evaluate Eq. (73a) by integrating by parts, and then substituting Eq. (70) for Ψ_I. The trigonometric identity for the product of cosines then leads to

$$a_j = \frac{1}{\pi j} \int_0^{\pi} \{\cos [(j-1)\xi - D_n \sin \xi] + \cos [(j+1)\xi - D_n \sin \xi]\, d\xi$$
$$= \frac{1}{j} [J_{j-1}(jD_n) + J_{j+1}(jD_n)] \tag{74a}$$

The same analysis applied to Eq. (73c) yields

$$b_j = \frac{1}{j} [J_{j-1}(jD_n) - J_{j+1}(jD_n)] , \quad j > 0 \tag{74b}$$

An integration by parts is not required to evaluate b_0 in Eq. (73b). The result is

$$b_0 = -\frac{1}{2} D_n \tag{74c}$$

When we use Eqs. (72) and (73) to form the first of Eqs. (71), we find that b_0 cancels the mean value residual T_I. The remaining terms are

$$p_I = \frac{\sqrt{2}}{4} \epsilon \frac{nV_n}{\lambda_n} Q_n \sum_{j=1}^{\infty} \frac{1}{j} \{[J_{j-1}(jD_n) + J_{j+1}(jD_n)] \sin(j\Psi_I) + [J_{j-1}(jD_n) - J_{j+1}(jD_n)] \cos(j\Psi_I)\} \tag{75}$$

A comparable series expansion of p_{II} leads to the same result as Eq. (75), except that Ψ_{II} replaces Ψ_I.

The Fourier series analysis is not in its final form, because we seek a representation that explicitly displays the time dependence. We therefore substitute Eqs. (69) for the phase variables into Eq. (75) and the corresponding expression for p_{II}. When we employ identities to manipulate the sum of sines and cosines, we find that

$$p_I + p_{II} = \epsilon \frac{nV_n}{\lambda_n} Q_n \sum_{j=1}^{\infty} \frac{1}{j} \cos(j\Delta_n) \left[J_{j-1}(jD_n) \sin(jt - \delta_j) - J_{j+1}(jD_n) \cos(jt - \delta_j)\right] \tag{76}$$

where δ_j is a position dependent phase lag given by

$$\delta_j = j\left(\lambda_n z - \theta_n + \frac{\pi}{4}\right) - \frac{\pi}{4} \tag{77}$$

We now recall Eq. (41), subject to the restriction that only the propagating spectrum, $n < 1$, need be retained. When we write the result in the form of amplitude and phase lag for each harmonic, we obtain

$$p/\rho_0 c_0^2 = \sum_{j=1}^{\infty} P_j \sin(jt - \nu_j) \tag{78a}$$

where

$$P_j \cos \nu_j = \epsilon \int_0^1 \frac{nV_n}{j\lambda_n} Q_n \cos(j\Delta_n) \left[J_{j-1}(jD_n) \cos \delta_j - J_{j+1}(jD_n) \sin \delta_j\right] dn$$

$$P_j \sin \nu_j = \epsilon \int_0^1 \frac{nV_n}{j\lambda_n} Q_n \cos(j\Delta_n) \left[J_{j-1}(jD_n) \sin \delta_j\right.$$

$$+ J_{j+1}(jD_n) \cos \delta_j] \, dn \tag{78b}$$

According to Eq. (78a), the phase lags ν_j describe the signal relative to a pure sine for each harmonic. A more significant parameter is a relative lag, based on a time scale in which the fundamental looks like a sine term. We obtain such quantities by shifting the time scale, such that

$$t' = t - \nu_1 \tag{79a}$$

which converts the Fourier series to

$$p/\rho_0 c_0^2 = \sum_{j=1}^{\infty} P_j \sin (jt' - \nu_j') \, , \quad \nu_j' = \nu_j - j \, \nu_1 \tag{79b}$$

As a closure to the derivation, we note that the linear signal may be readily recovered from these expressions by taking the limit as $\varepsilon \to 0$. Correspondingly setting $D_n = 0$ leaves only the fundamental harmonic, since only the zero order Bessel function is nonzero when its argument vanishes. The result obtained in this manner is merely the linear King integral for the pressure expressed in terms of amplitude and phase lag. Of course, the present result is simplified by limiting the integration to the propagating spectrum.

A significant aspect of the similarity of Eqs. (78) to the Fubini-Ghiron solution [26] for a planar wave is recognition of the way in which shocks form. When the parameter D_n associated with wave number n attains a critical value, then the corresponding mode becomes shocked. (In the case

of a planar wave, $D_n = 1$ for a shock.) Since D_n is a function of position, as well as n, modes at various wave numbers will not attain the critical condition simultaneously. This explains why experiments, such as those performed by Gallego-Juarez and Gaete-Gareton [25] failed to identify a specific location at which a discontinuity occurs.

We at first endeavored to compare our predictions to Gould's measurements [17] of transverse distribution of the second harmonic for a 5 atm source level at a range of 175 mm. (The Rayleigh length for the experiment is 597 mm, so the location is well inside the farfield.) However, we found that the aforementioned shock formation condition occurred in a significant segment of the wave number spectrum, which caused our computations to display several anomolies. We therefore display in Figure 6 the transverse distribution 200 mm from the projector for a source level of 2.5 atm. The agreement between theory and experiment is excellent. No measurement of the fundamental at this distance appears in Gould's paper, but the prediction for the fundamental is consistent in shape with the measurement at 175 mm in the 5 atm case.

For comparison, Figure 6 also shows the prediction for the second harmonic obtained from the nearfield theory in Section II. The degree to which the lack of uniform validity in that theory causes over-prediction of the amplitude is obvious, although the shape of the distribution predicted by the nearfield theory is consistent with the actual result. In contrast, the second harmonic distribution obtained from the long range approximation is erroneous in both shape and magnitude at a location in the very nearfield. As shown in Figure 3, applying the long range theory close to

the projector yields a prediction that is a nearfield projection of the farfield behavior.

For further confirmation of the long range approximation, we compared its predictions to Moffett's measurements [26] of the fundamental and second harmonic on axis. The projector in that experiment vibrated at 450 kHz, and the diameter was 102 mm; the corresponding Rayleigh length is 2.59 m. According to linear theory, the pressure at an axial antinode in this case would be 213.1 dB//1μPa. The results obtained from the long range approximation, shown in Figure 7, compare favorably with Moffett's measurements in the domain of interest.

Waveform measurements are inherently difficult to make. The close agreement of the long range theory with a measured waveform was reported earlier [15]. Another example is shown in Figure 8, for a later experiment by Moffett [27], in which a 508 mm diameter projector was driven at 60 kHz, with c_0 = 1473 m/s. The pressure at an axial antinode corresponding to this waveform is 226.5 dB according to linear theory. Note that both the measured and predicted waveforms have been shifted in time to begin close to the origin.

The asymmetrical nature of the distortion of the waveform is intimately related to the phase shifts that the higher harmonics experience relative to the fundamental, apparently as the result of diffraction. Figure 9 shows the relative phase lags ν_j' corresponding to the amplitudes in Figure 7. It is difficult to discern a pattern in the nearfield, primarily because of sudden changes in the values resulting from limiting the phase angle to a

360° range. However, we can see that the phase lags grow in the nearfield with increasing distance almost in proportion to both range and harmonic number. Even more interesting is the indication that the phase angles eventually become nearly equal at a location close to the farthest antinode for the fundamental, and then grow outward from that location, tending toward a constant difference between successive harmonics.

VI. DISCUSSION AND CONCLUSIONS

We have developed a comprehensive analytical representation of the finite amplitude CW signal radiated by a baffled projector undergoing monocromatic excitation. The face velocity at the projector is restricted to be axisymmetric, but the radial distribution is arbitrary. We obtained three overlapping descriptions. The nearfield formulation, which is suitable for distances that are a small fraction of the Rayleigh length, was obtained by generating a dual Hankel transform that is excited by the linear King integral. This formulation, whose quantitative results must be obtained by numerical methods, is limited because it only describes the fundamental and second harmonic. Also, it does not treat depletion of the fundamental signal associated with nonlinear generation of higher harmonics.

The second description, which we refer to as the uniformly valid solution, combines a Hankel integral transforms and coordinate straining transformations. A decomposition of the King integral into two two famailies of quasi-conical waves was crucial to the derivation of this form.

Although this description is suitable at any location, it is sufficiently complicated that quantitative evaluations would require new numerical methods and extraordinary computational expenditures. The third description, which is the long range asymptotic approximation of the uniformly valid solution, is the simplest of all to evaluate. It previously had been called the nonlinear King integral, but that term is equally applicable to the uniformly valid solution.

Both the nearfield and long range formulations can only be evaluated by numerical methods. For a fixed location, computational times for the nearfield formulation, which requires a double integration in the transverse wave number spectrum, are much larger than for the long range approximation, which involves a single integral. However, the requirements for both increase with increasing distance from the projector. When either the axial or transverse distance is many multiples of a wavelength (z or $R \gg 2\pi$), the King integral becomes a rapidly oscillating function of the transverse wave number. Numerical analysis in such conditions requires a fine discretization of the continuous spectrum. One could employ the long range version to generate interface conditions that drive the solution for a finite amplitude spherical wave with directivity [5], but that approach is suspect when dealing with strong diffractive effects [14]. Alternatively, the same interface prediction could be used to drive the modified Burgers equation. The latter is a particularly attractive prospect, since it provides a method by which shock formation, and other types of dissipation, may be treated.

ACKNOWLEDGEMENT

This research was supported by the Office of Naval Research, code 1125-UA.

REFERENCES

1 A. D. Pierce, Acoustics (McGraw-Hill, New York, 1981), Chap. 5.

2 F. Ingenito and A. O. Williams, Jr., "Calculation of second-harmonic generation in a piston beam," J. Acoust. Soc. Am. 49, 319-328 (1971).

3 P. H. Rogers, "A Theoretical Study of Second-Harmonic Generation in the Acoustic Beam of a Circular Plane Piston," Ph.D. thesis, Brown University (1970).

4 J. C. Lockwood, T. G. Muir, and D. T. Blackstock, "Directive harmonic generation in the radiation field of a circular piston," J. Acoust. Soc. Am. 53, 1148-1153 (1971).

5 J. C. Lockwood, "Two problems in high-intensity sound," Univ. Texas at Austin, Appl. Res. Lab., ARL-TR-71-26 (1971).

6 D. G. Browning and R. H. Mellen, Finite-amplitude distortion of 150-kHz acoustic waves in water," J. Acoust. Soc. Am. 44, 644-646 (1968).

7 E. A. Zabolotskaya and R. V. Khokhlov, "Quasi-plane waves in the nonlinear acoustics of confined beams," Sov. Phys. Acoust. 15, 35-40 (1969).

8 V. P. Kuznetsov, "Equations of nonlinear acoustics," Sov. Phys. Acoust. 15, 467-470 (1971).

9 N. S. Bakvalov, Ya. M. Zhileikin, E. A. Zabolotskaya, and R. V. Khokhlov, "Nonlinear propagation of a sound beam in a nondissipative medium," Sov. Phys. Acoust. 22, 272-274 (1976).

10 N. S. Bakvalov, Ya. M. Zhileikin, E. A. Zabolotskaya, and R. V. Khokhlov, "Harmonic generation on sound beams," Sov. Phys. Acoust. 25, 101-106 (1978).

11 S. I. Aanonsen, T. Barkve, J. Naze Tjøtta, and S. Tjøtta, "Distortion and harmonic generation in the nearfield of a finite amplitude sound beam," J. Acoust. Soc. Am. 75, 749-768 (1984).

12 M. F. Hamilton, J. Naze Tjøtta, and S. Tjøtta, "Nonlinear effects in the farfield of a directive sound source," J. Acoust. Soc. Am. 78, 202-216 (1985).

13 J. Bernsten, J. Naze Tjøtta, and S. Tjøtta, "Nearfield of a large acoustic radiator, Part IV: Second harmonic and sum frequency radiation," J. Acoust. Soc. Am. 75, 1383-1391 (1984).

14 J. H. Ginsberg, "Nonlinear King integral for arbitrary axisymmetric sound beams at finite amplitude. I. Asymptotic evaluation of the velocity potential," J. Acoust. Soc. Am. 76, 1201-1207 (1984).

15 J. H. Ginsberg, "Nonlinear King integral for arbitrary axisymmetric sound beams at finite amplitude. II. Derivation of uniformly accurate expressions," J. Acoust. Soc. Am. 76, 1208-1214 (1984).

16 E. Skudrzyk, The Foundations of Acoustics (Springer-Verlag, New York, 1971), pp. 429-430.

17 R. K. Gould, C. W. Smith, A. O. Williams, Jr., and R. P. Ryan, "Measured structure of harmonics self-generated in an acoustic beam," J. Acoust. Soc. Am. 40, 421-427 (1966).

18 H. C. Miao, "Analysis of nonsymmetric effects in finite amplitude sound beams," Ph. D. thesis, Georgia Institute of Technology, 1985.

19 M. A. Foda and J. H. Ginsberg, "Relationship between near and farfield effects in second harmonic generation in the piston beam," J. Acoust. Soc. Am. 79, Suppl. 1 (1986)

20 S. Goldstein, Lectures in Fluid Mechanics (Interscience, London, 1957), Vol II, Ch. 4.

21 Handbook of Mathematical Functions, edited by M. Abramowitz and I. A. Stegun (Dover, New York, 1965), Chaps. 9 and 25.

22 A. H. Nayfeh, Perturbation Methods (Wiley-Interscience, New York, 1973), pp. 95-98.

23 C. M. Bender and S. A. Orszag, Advance Mathematical Methods for Scientists and Engineers (McGraw-Hill, New York, 1978), pp. 261-267.

24 D. T. Blackstock, "Propagation of plane sound waves of finite amplitude," J. Acoust. Soc. Am. 34, 9-30 (1962).

25 J. A. Gallego-Juarez and L. Gaete-Garreton, "Propagation of finite-amplitude ultrasonic waves in air — I. Spherically diverging waves in the free field," J. Acoust. Soc. Am. 73, 761-765 (1983).

26 M. B. Moffett, "Measurement of fundamental and second harmonic pressures in the field of a circular piston source," J. Acoust. Soc. Am. 65, 318-323 (1979).

27 M. B. Moffett, unpublished (1983).

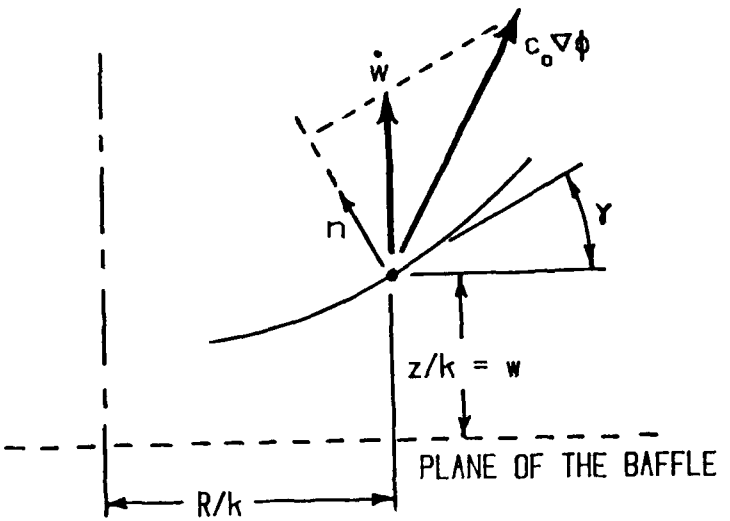

FIGURE 1

FIGURE 2

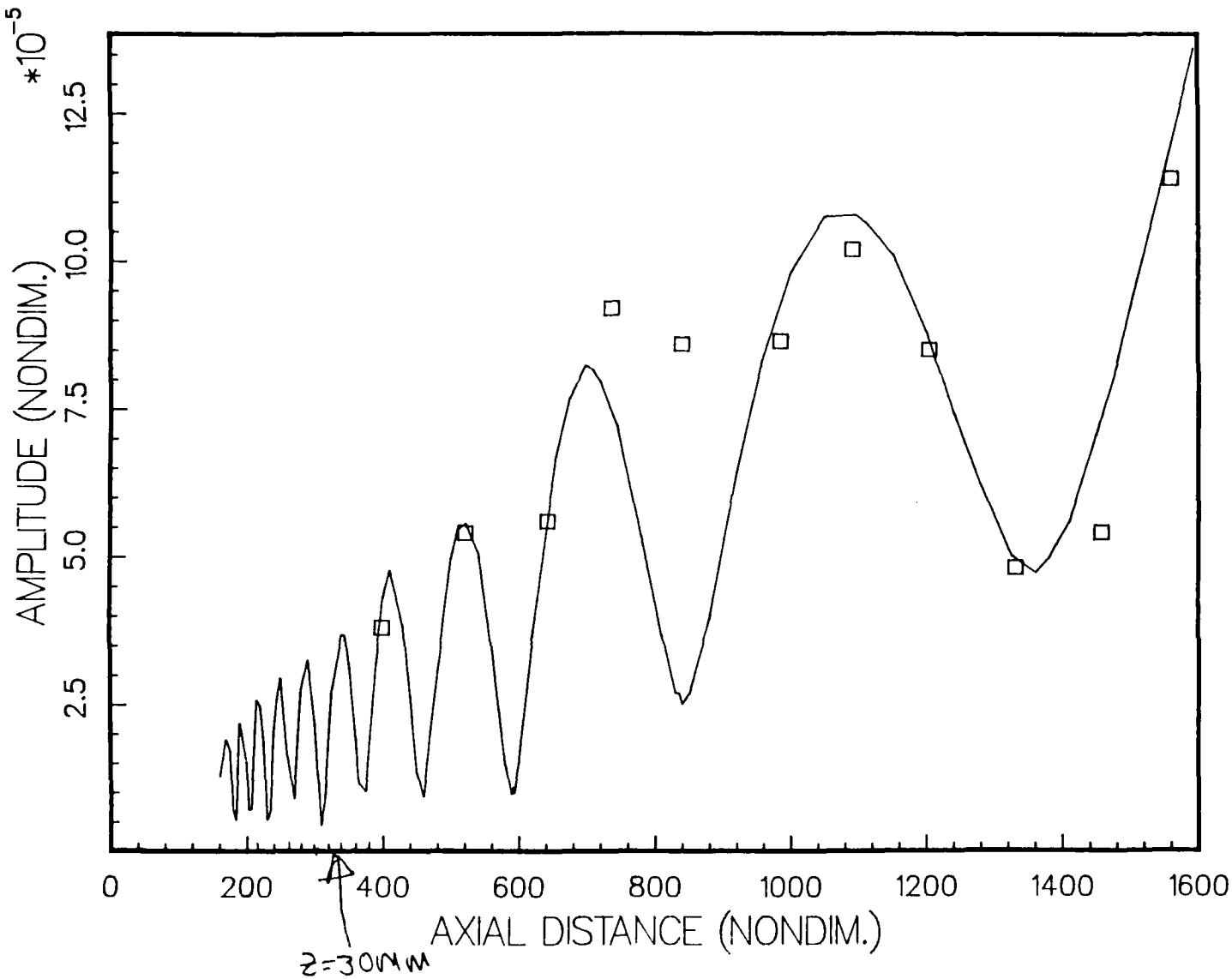
AMPLITUDE (NONDIM.)
*10^-5
2.5
5.0
7.5
10.0
12.5
0
200
400
600
800
1000
1200
1400
1600
AXIAL DISTANCE (NONDIM.)
Z=30MM

FIGURE 3

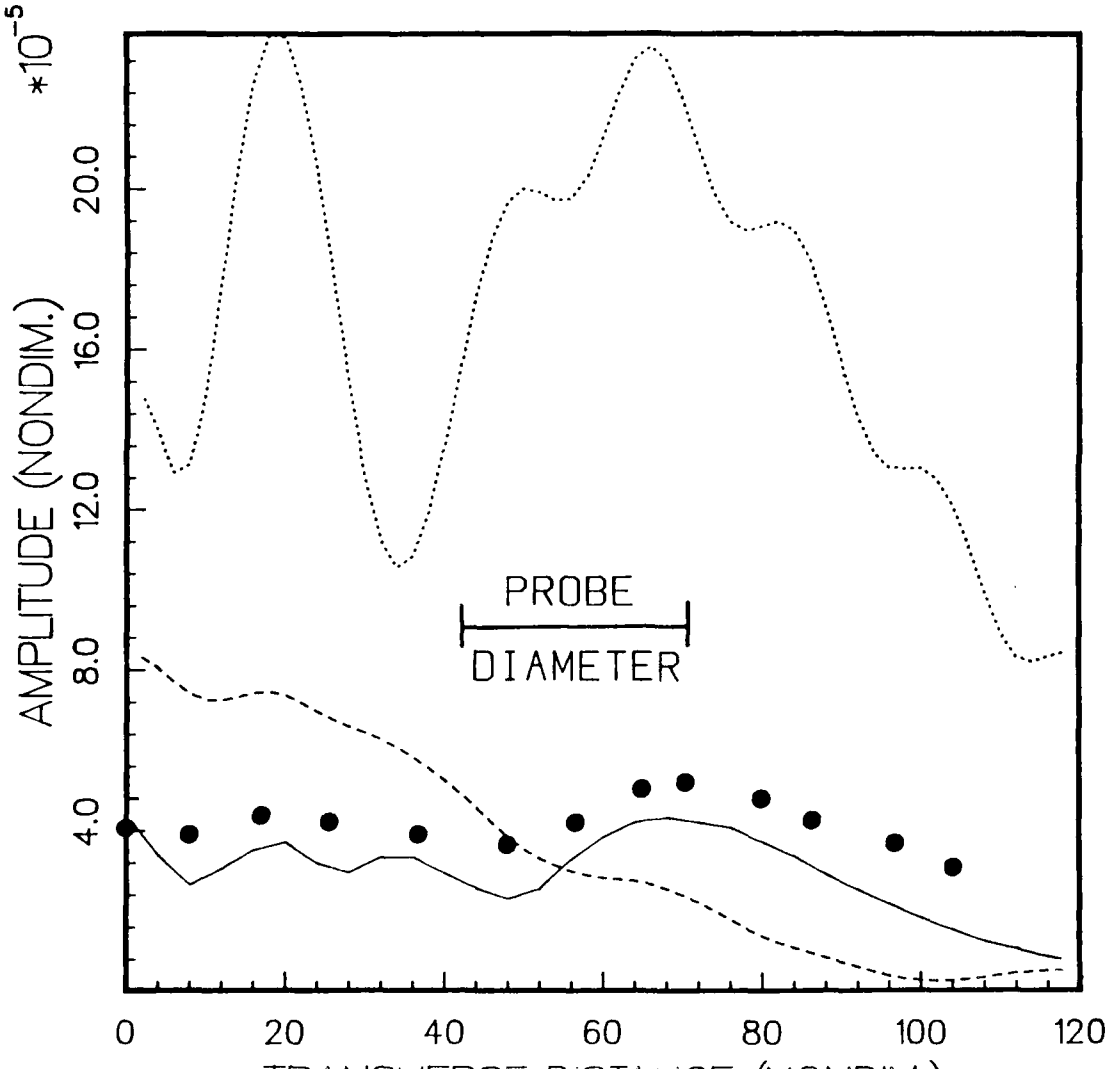
AMPLITUDE (NONDIM.)
*10^-5
4.0
8.0
12.0
16.0
20.0
PROBE
DIAMETER
0
20
40
60
80
100
120
TRANSVERSE DISTANCE (NONDIM.)

FIGURE 4

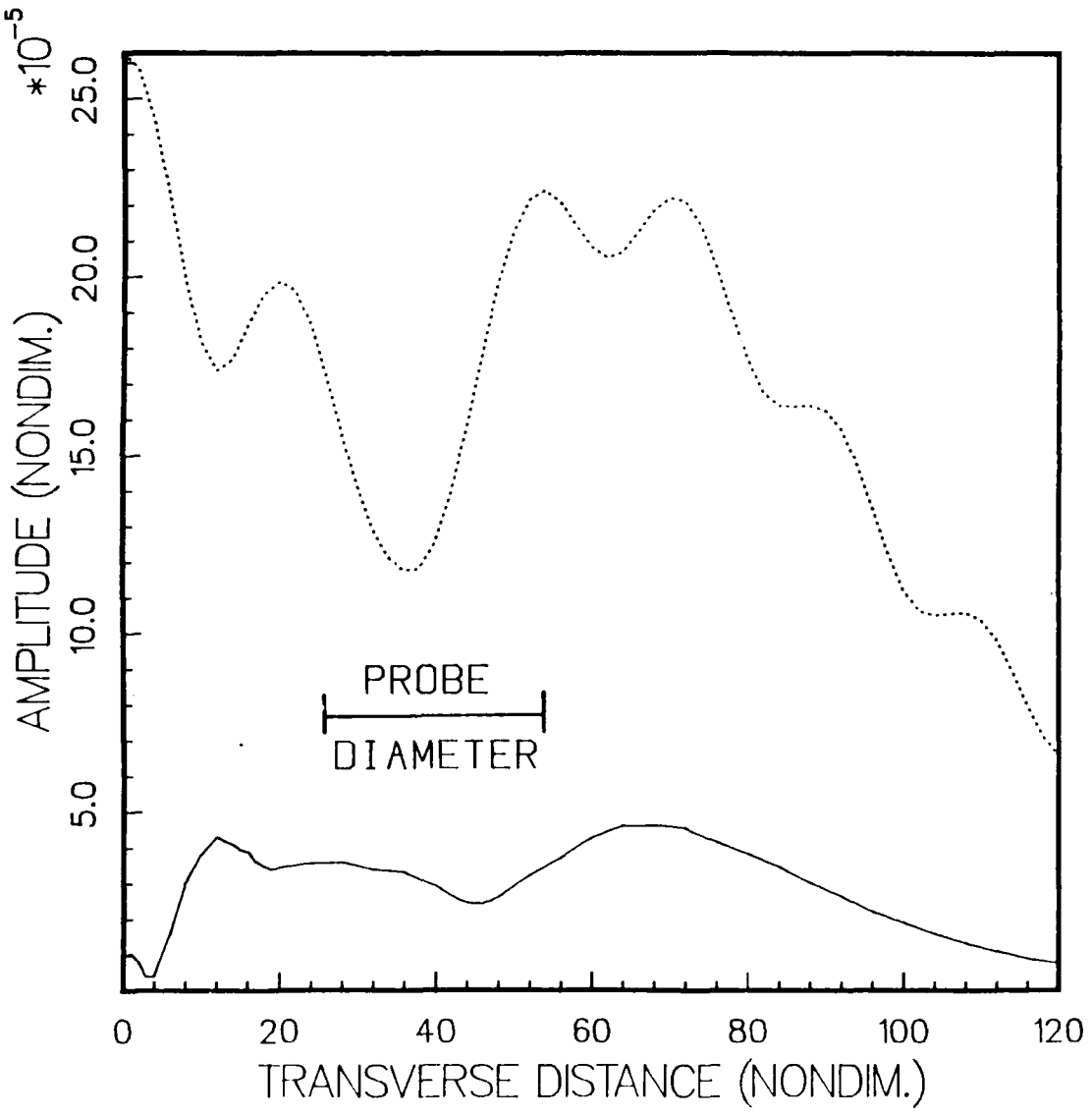
*10^-5
25.0
20.0
15.0
10.0
5.0
AMPLITUDE (NONDIM.)
PROBE
DIAMETER
0
20
40
60
80
100
120
TRANSVERSE DISTANCE (NONDIM.)

FIGURE 5.

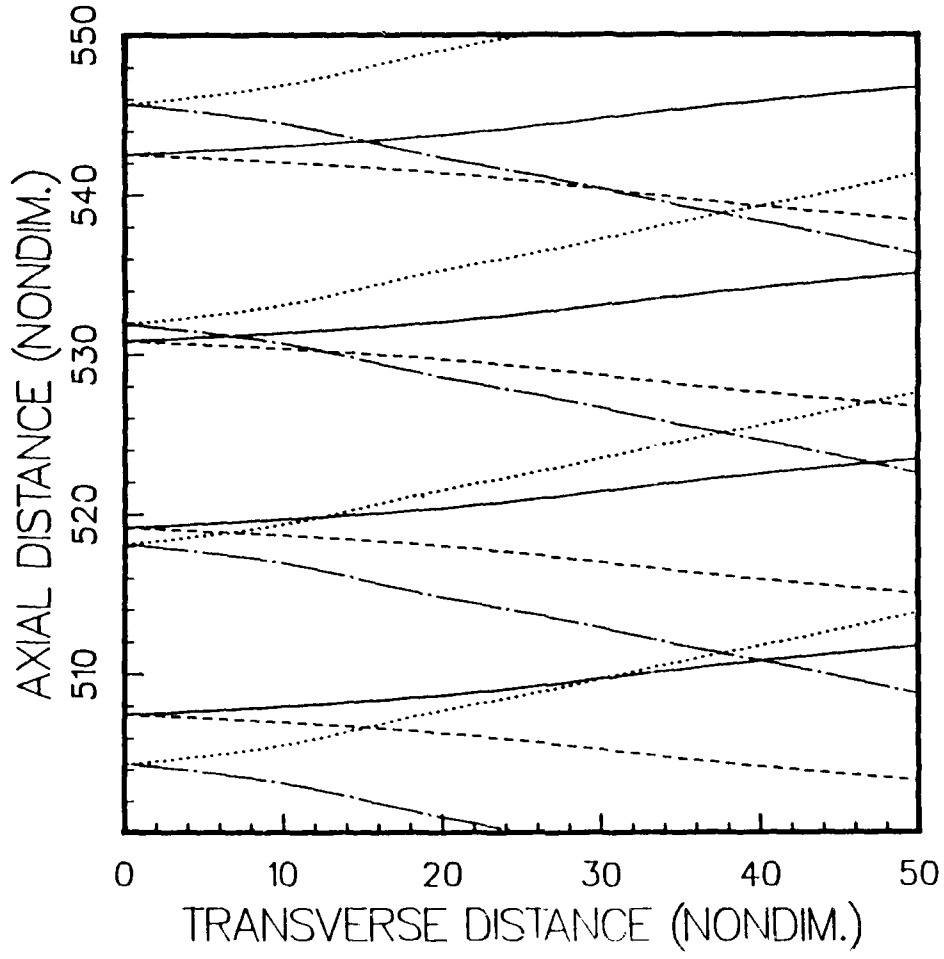
AXIAL DISTANCE (NONDIM.)
550
540
530
520
510
0
10
20
30
40
50
TRANSVERSE DISTANCE (NONDIM.)

FIGURE 6

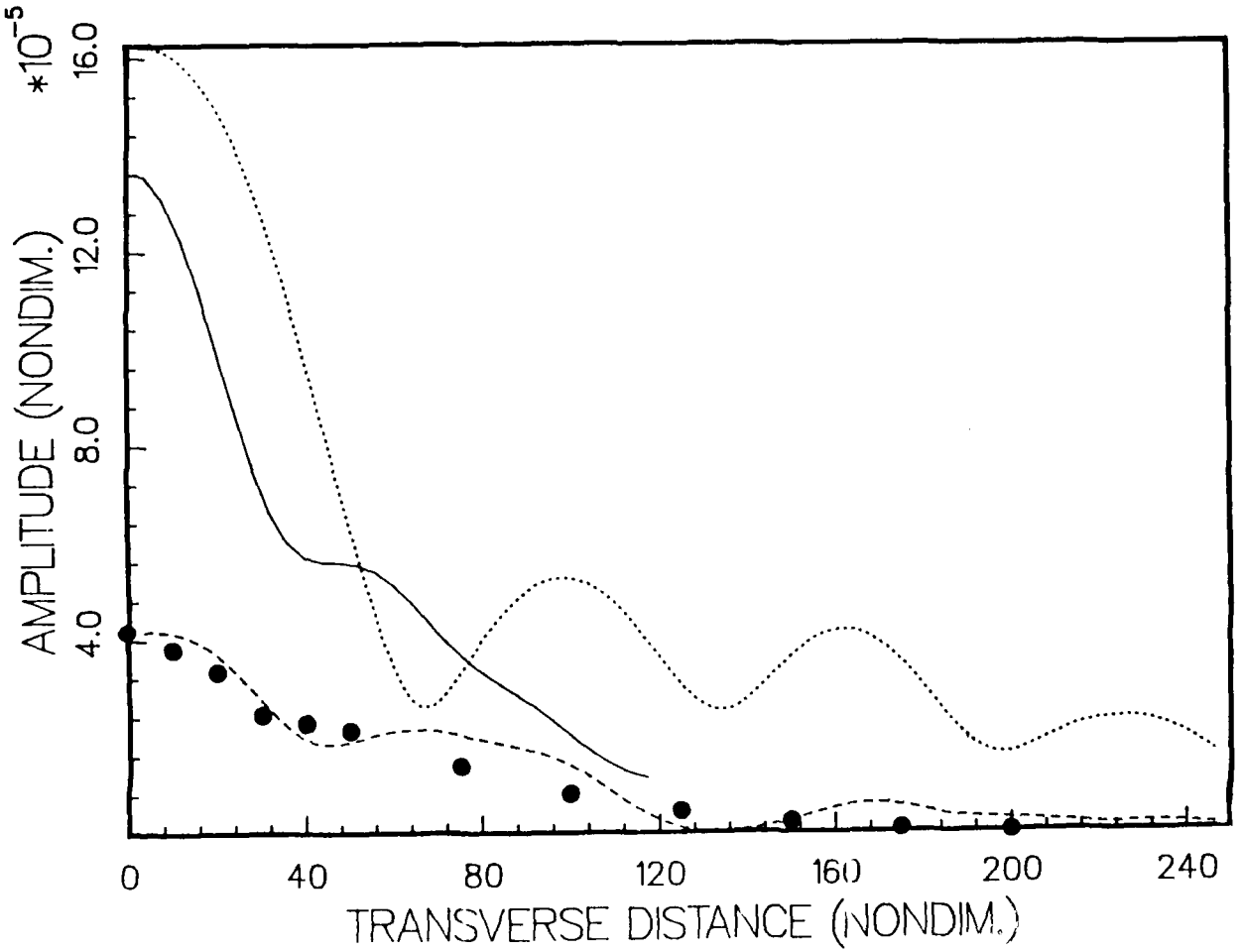
AMPLITUDE (NONDIM.)
*10^-5
16.0
12.0
8.0
4.0
0
40
80
120
160
200
240
TRANSVERSE DISTANCE (NONDIM.)

FIGURE 7

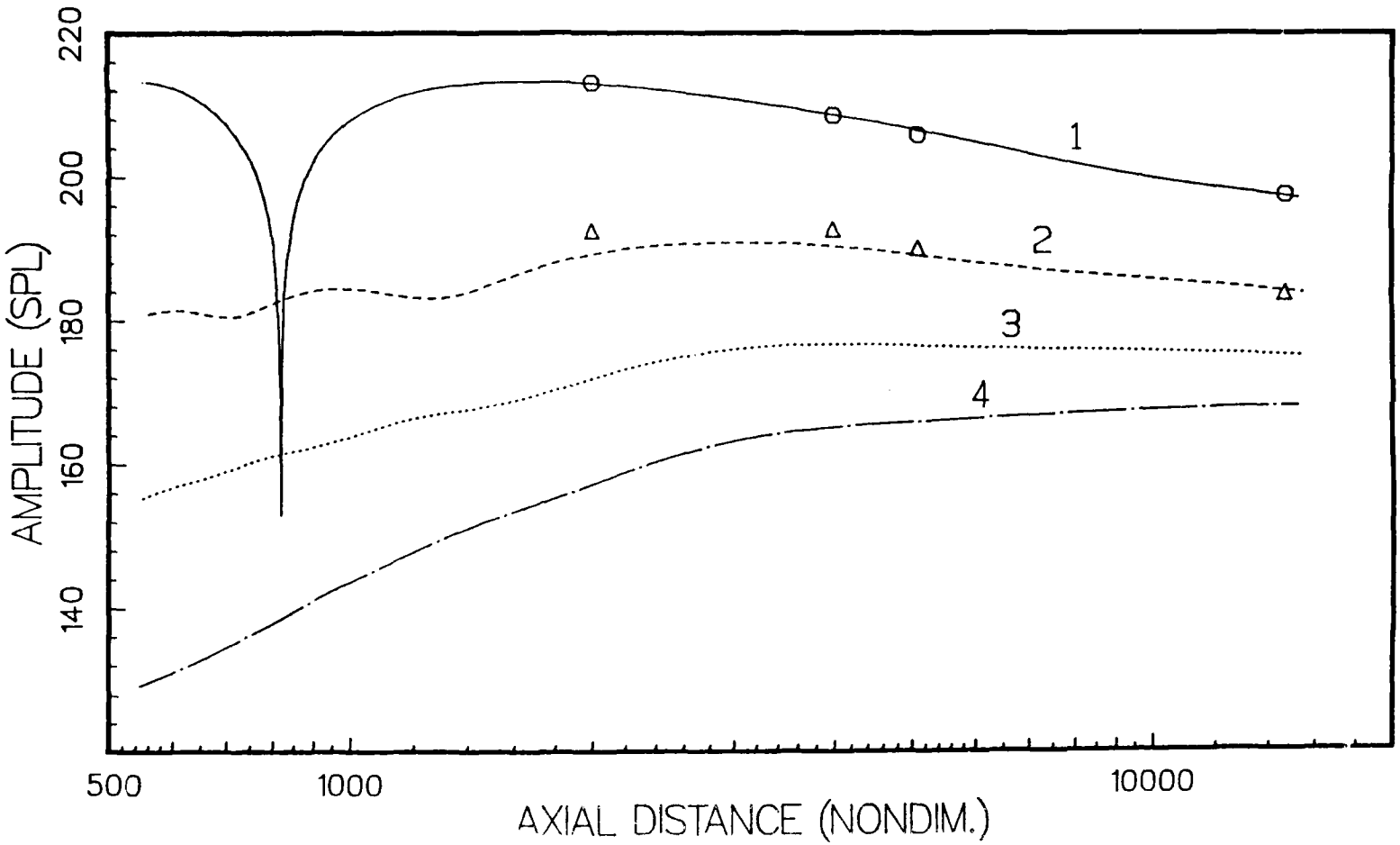
AMPLITUDE (SPL)
220
200
180
160
140
500
1000
10000
AXIAL DISTANCE (NONDIM.)
1
2
3
4

FIGURE 8

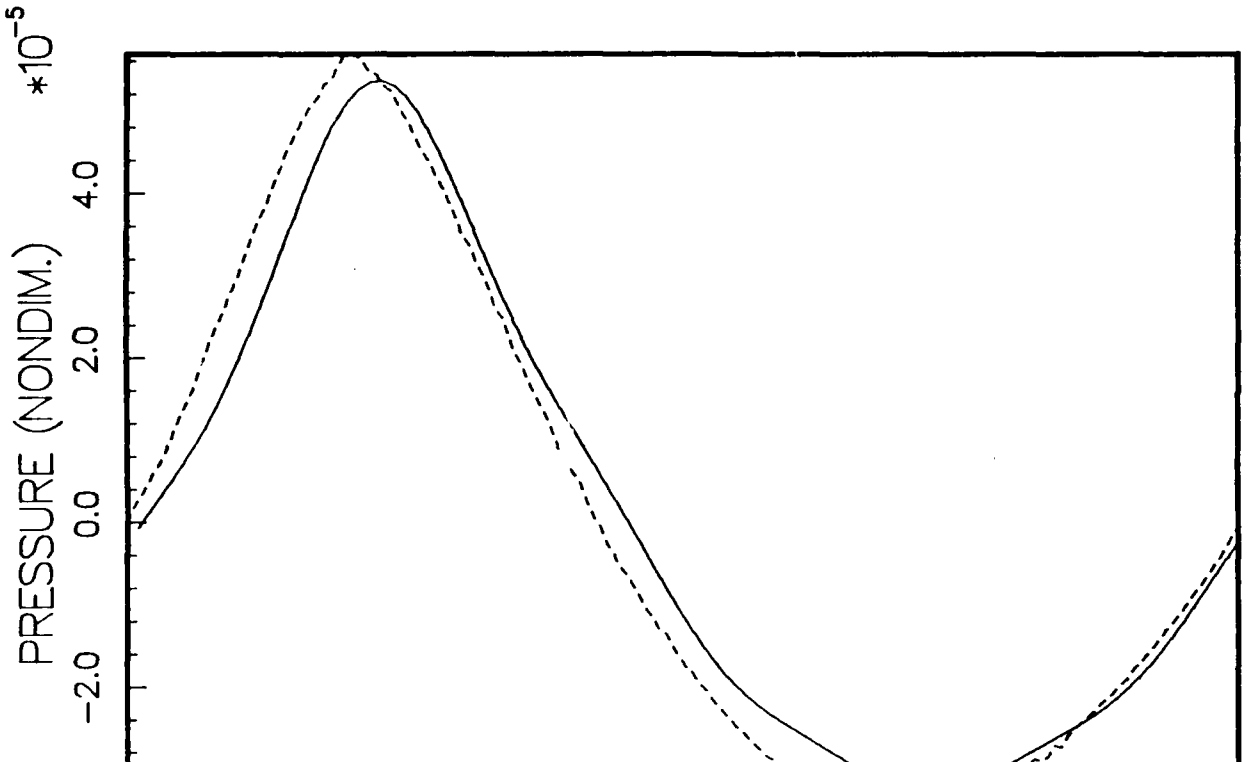

FIGURE 9

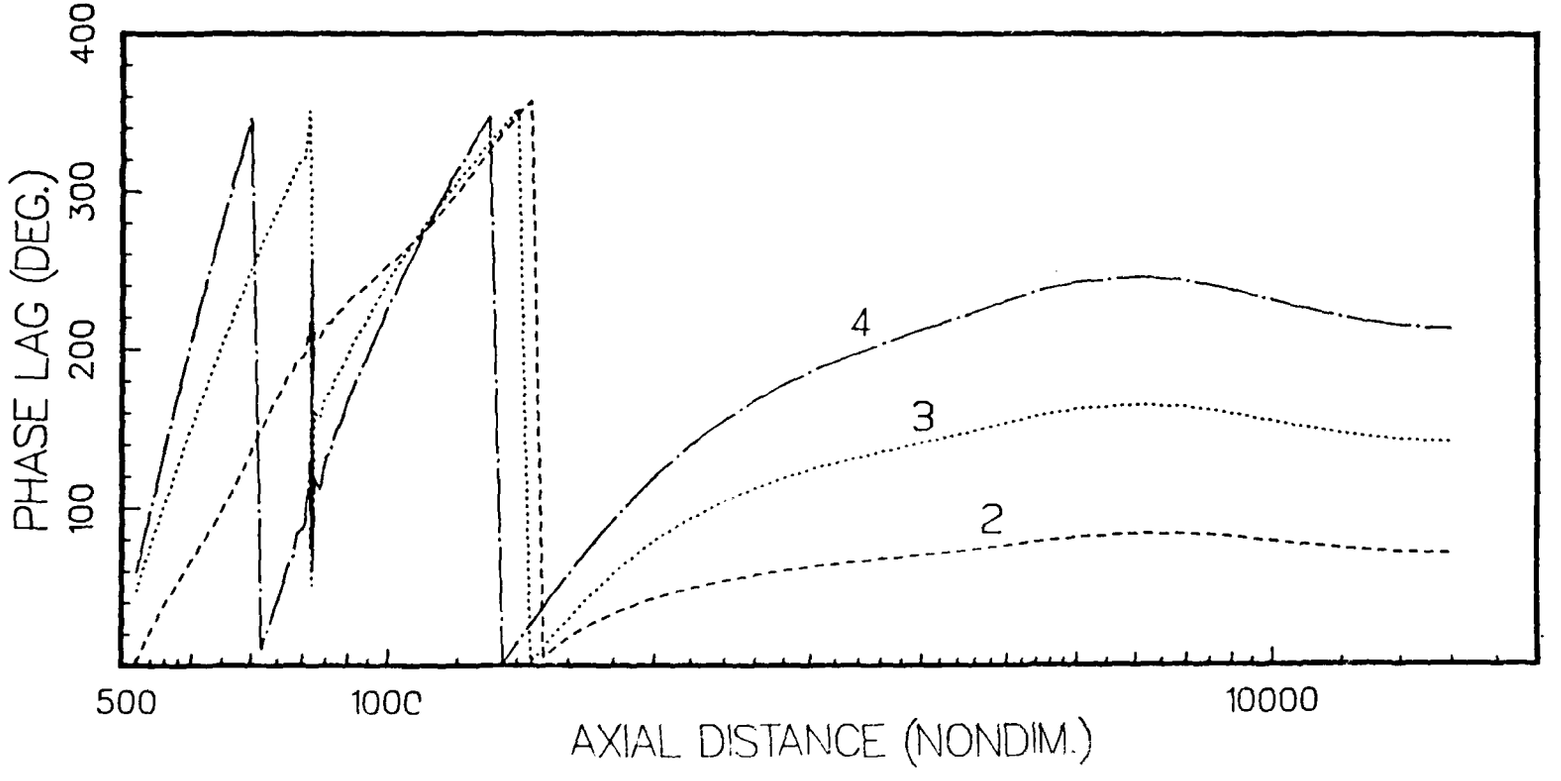
PHASE LAG (DEG.)
100
200
300
400
500
1000
10000
AXIAL DISTANCE (NONDIM.)
4
3
2

THE JOURNAL of the Acoustical Society of America

Supplement 1, Vol. 81, Spring 1987

Program of the 113th Meeting

Hyatt Regency Hotel Indianapolis, Indiana 11–15 May 1987

TUESDAY AFTERNOON, 12 MAY 1987 REGENCY BALLROOM D, 1:30 TO 4:15 P.M.

Session J. Physical Acoustics II: Nonlinear, Loss and Bubble Phenomena

J4. Finite amplitude acoustic waves generated by a baffled, multiharmonic transducer. James B. Edgerton, Jr. and Jerry H. Ginsberg (School of Mechanical Engineering, Georgia Institute of Technology, Atlanta, GA 30332)

Arbitrary periodic excitation of a baffled piston transducer leads to harmonic and intermodulation distortion when finite amplitude effects are considered. An analysis of the radiation signal in such a situation is initiated by representing the linearized signal as a sum of King integrals associated with each harmonic in the excitation. A nonuniformly accurate expression for the velocity potential is derived using a singular perturbation procedure that identifies the dominant tendency of nonlinearity to generate second-order interactions. This form is obtained from an asymptotic integration, which leads to spectral decomposition of the signal into groups of quasi-one-dimensional waves. The renormalization version of the method of strained coordinates is used to obtain a uniformly accurate expression for the acoustic pressure at all locations preceding the formation of a shock. [Work supported by the ONR, Code 1125-UA.]

FINITE AMPLITUDE ACOUSTIC WAVES GENERATED BY A BAFFLED, MULTIHARMONIC TRANSDUCER

James B. Edgerton, Jr.

Jerry H. Ginsberg

Georgia Institute of Technology

Atlanta, Georgia

INTRODUCTION

PROBLEM DEFINITION:

* FINITE AMPLITUDE SOUND BEAM
* AXISYMMETRIC, BAFFLED TRANSDUCER
* MULTIHARMONIC EXCITATION OF TRANSDUCER

SOLUTION FEATURES:

* HARMONIC AND INTERMODULATION DISTORTION

THEORY

The perturbation series,

$$\phi = \varepsilon \phi_1 + \varepsilon^2 \left[\frac{1}{2} \frac{\partial}{\partial t} (\phi_1^2) + \phi_2 \right] + \cdots$$

is introduced into the nonlinear velocity potential equation, resulting in:

FIRST ORDER D.E. (LINEAR):

$$\nabla^2 \phi_1 - \frac{\partial^2 \phi_1}{\partial t^2} = 0$$

SECOND ORDER D.E.:

$$\nabla^2 \phi_2 - \frac{\partial^2 \phi_2}{\partial t^2} = \beta_0 \frac{\partial}{\partial t} \left(\frac{\partial \phi_1}{\partial t} \right)^2$$

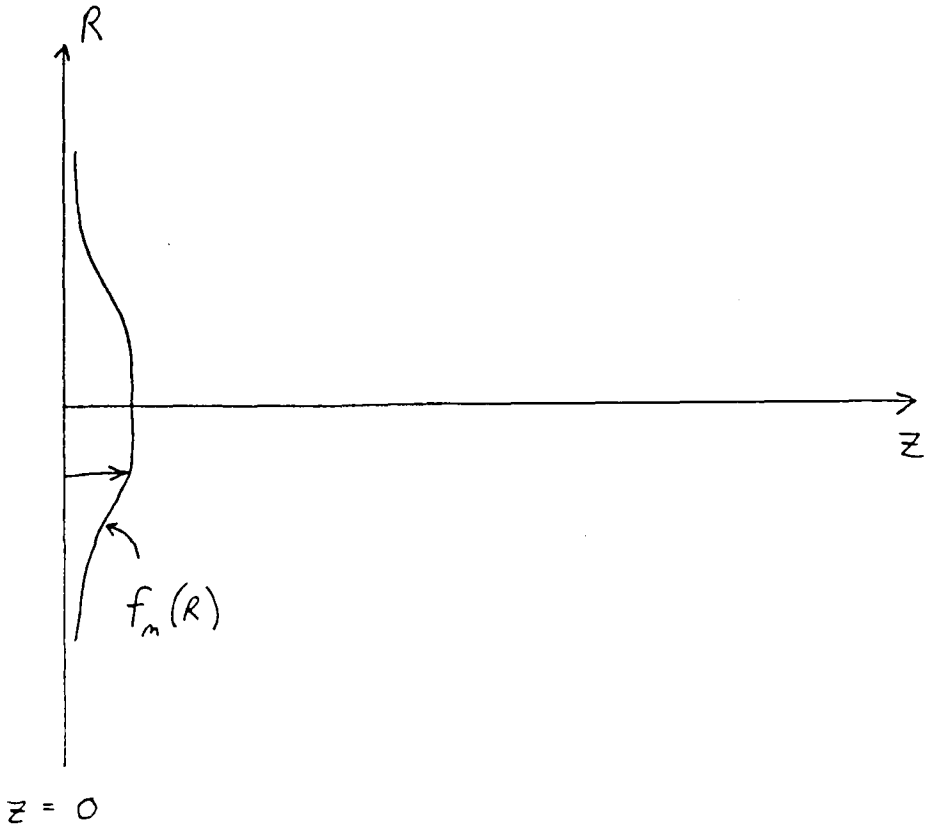

FIRST ORDER BOUNDARY CONDITION:

$$\left.\frac{\partial \phi_1}{\partial z}\right|_{z=0} = \frac{1}{2i} \sum_{m=1}^{\infty} f_m(R) e^{i\omega_m t} + \text{c.c.}$$

$f_m(R)$ is an amplitude shading function.

FIRST ORDER SOLUTION

SUM OF KING INTEGRALS:

$$\phi_1 = -\sum_{m=1}^{\infty} \int_0^{\infty} \frac{\lambda V_m(\lambda)}{\mu_\lambda} J_0(\omega_m \lambda R) \exp\left[\omega_m (i\tau - \mu_\lambda z)\right] d\lambda + c.c.$$

AXIAL WAVENUMBER:

$$\mu_\lambda = \begin{cases} i(1-\lambda^2)^{\frac{1}{2}} & 0 \le \lambda \le 1 \\ (\lambda^2 - 1)^{\frac{1}{2}} & \lambda > 1 \end{cases}$$

$V_m(\lambda)$ is a Hankel transform of $f_m(R)$

SECOND ORDER SOLUTION

INITIAL FORM:

$$\phi_2 = \beta_0 \sum_{n=1}^{\infty} \sum_{m=1}^{\infty} \int_0^{\infty} \int_0^{\infty} I_{nm}^{SUM}(\lambda, \nu, z, R, t) + I_{nm}^{DIFF}(\lambda, \nu, z, R, t)\, d\nu\, d\lambda$$

I_{nm}^{SUM} DEPENDS ON $\omega_n + \omega_m$

I_{nm}^{DIFF} DEPENDS ON $\omega_n - \omega_m$

Asymptotic integration for large z leads to

$$\phi_2 = \beta_0 \sum_{n=1}^{\infty} \sum_{m=1}^{\infty} \int_0^{\infty} I_{nm}^{SUM\,\prime}(\lambda, z, R, t) + I_{nm}^{DIFF\,\prime}(\lambda, z, R, t)\, d\lambda$$

SOLUTION IS NONUNIFORMLY VALID SINCE

$$I_{nm}^{SUM\,\prime}, I_{nm}^{DIFF\,\prime} \propto z^{\frac{1}{2}}$$

RENORMALIZATION

EXPRESSION FOR ACOUSTIC PRESSURE IS RENORMALIZED

* PRESSURE EXPRESSION IS DECOMPOSED INTO GROUPS OF QUASI-ONE-DIMENSIONAL WAVES

* EACH GROUP IS RENORMALIZED INDEPENDENTLY BY THE INTRODUCTION OF STRAINED COORDINATES

RESULT IS A UNIFORMLY ACCURATE PRESSURE EXPRESSION

ACOUSTIC PRESSURE

$$p = \rho_0 c_0^2 \int_0^1 P \, d\lambda$$

$$P = \frac{\varepsilon}{2} \sum_{m=1}^{\infty} A(\omega_m, \lambda, R) \left\{ \cos(\alpha_m^-) + \cos(\beta_m^- + \xi) + \cos(\psi_m^- + \xi \right.$$

$$\left. + \text{ADDITIONAL TERMS FROM OTHER WAVE GROUPS} \right\}$$

ψ_m^- = UNSTRAINED PHASE COORDINATE FOR FIRST GROUP

$$\alpha_m^- = \psi_m^- + 2\varepsilon\beta_0 \sum_{m=1}^{\infty} B(\omega_m, \omega_m, \lambda, R) \cos(\beta_m^- + \xi)$$

$$\beta_m^- = \psi_m^- + 2\varepsilon\beta_0 \sum_{m=1}^{\infty} B(\omega_m, \omega_m, \lambda, R) \cos(\alpha_m^-)$$

TWO HARMONIC EXCITATION

CASE 1 : CIRCULAR PLANE PISTON, KA = 50

———————— = FUNDAMENTAL ONLY, SPL = 206.99 dB

– – – – – – – – = FUNDAMENTAL SPL = 206.99 dB
2ND HARMONIC SPL = 206.99 dB
RELATIVE PHASE = 0

. . . . . = RELATIVE PHASE = 90

—— · —— · —— = RELATIVE PHASE = 180

—— – —— – —— = RELATIVE PHASE = 270

PISTON AR = 1.0 KA = 50

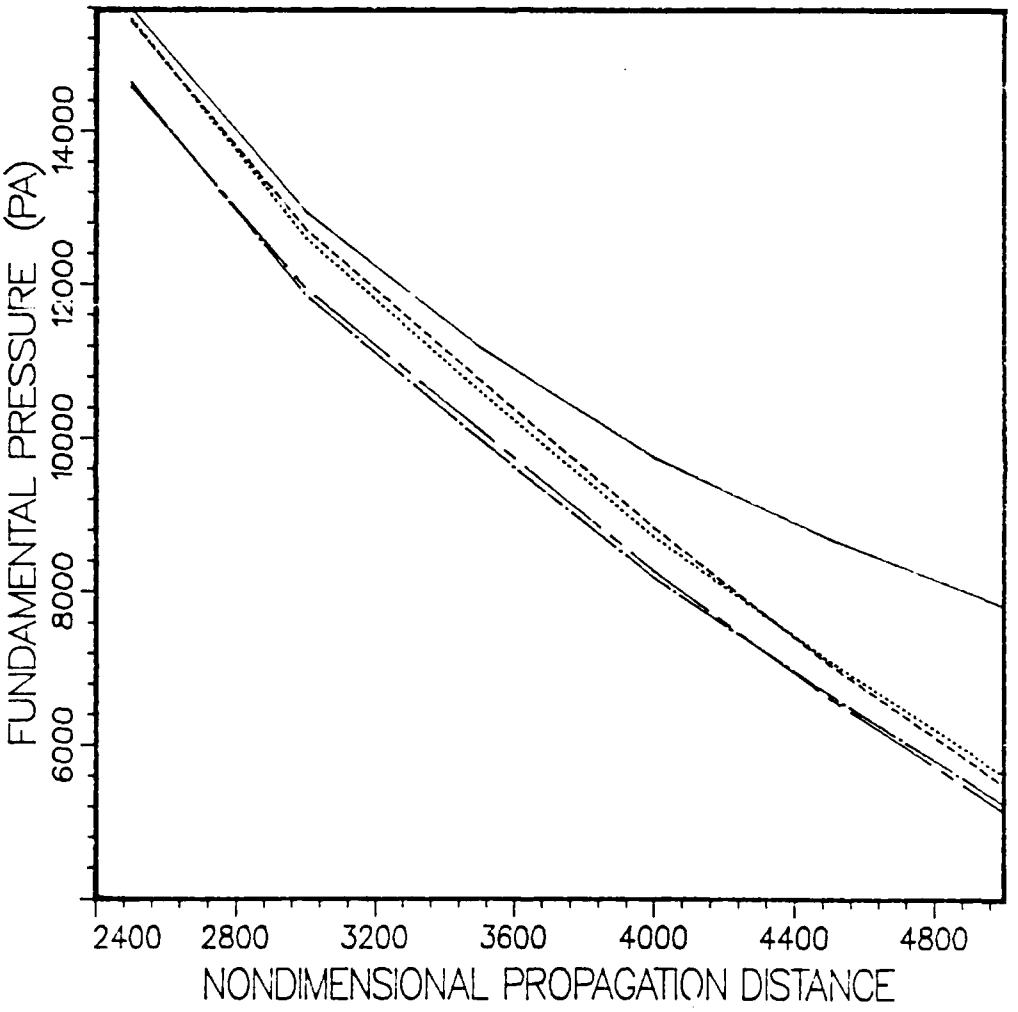

PISTON AR = 1.0 KA = 50

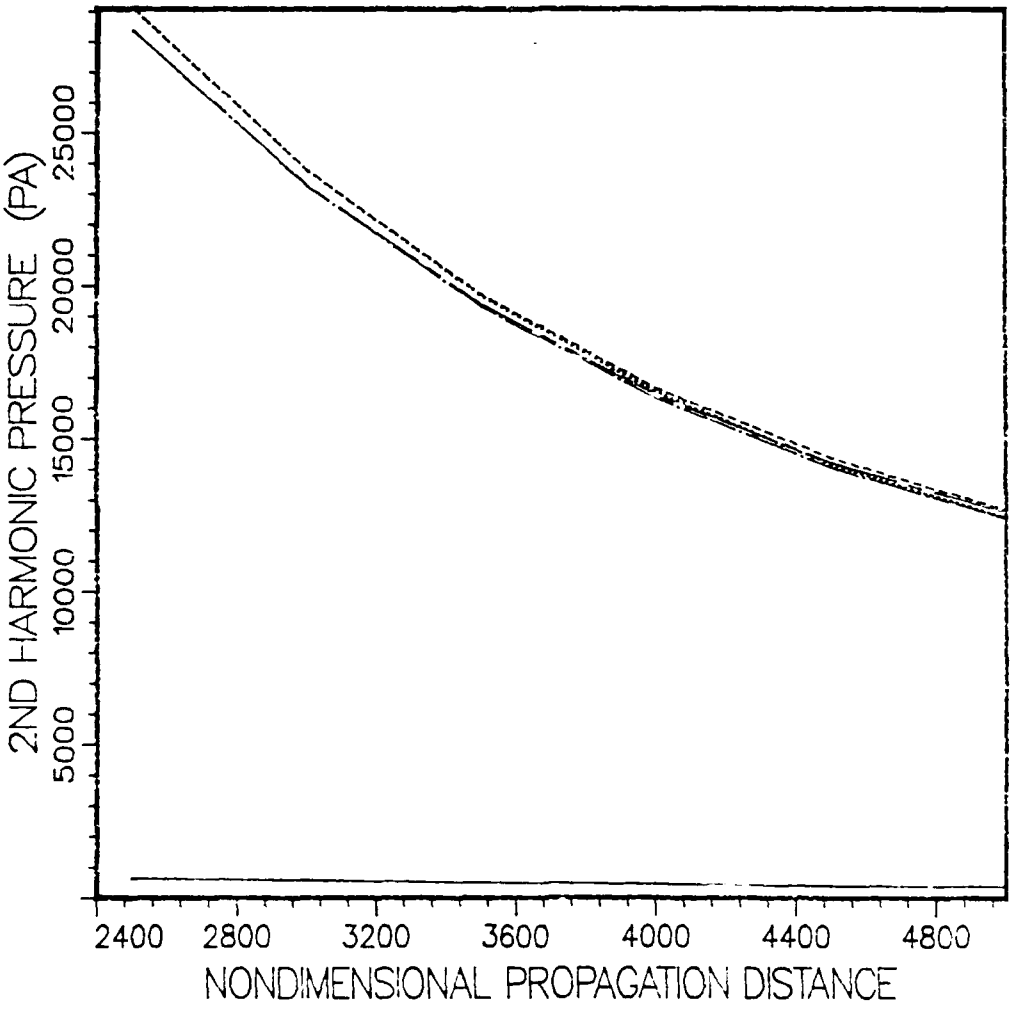

PISTON AR = 1.0 KA = 50

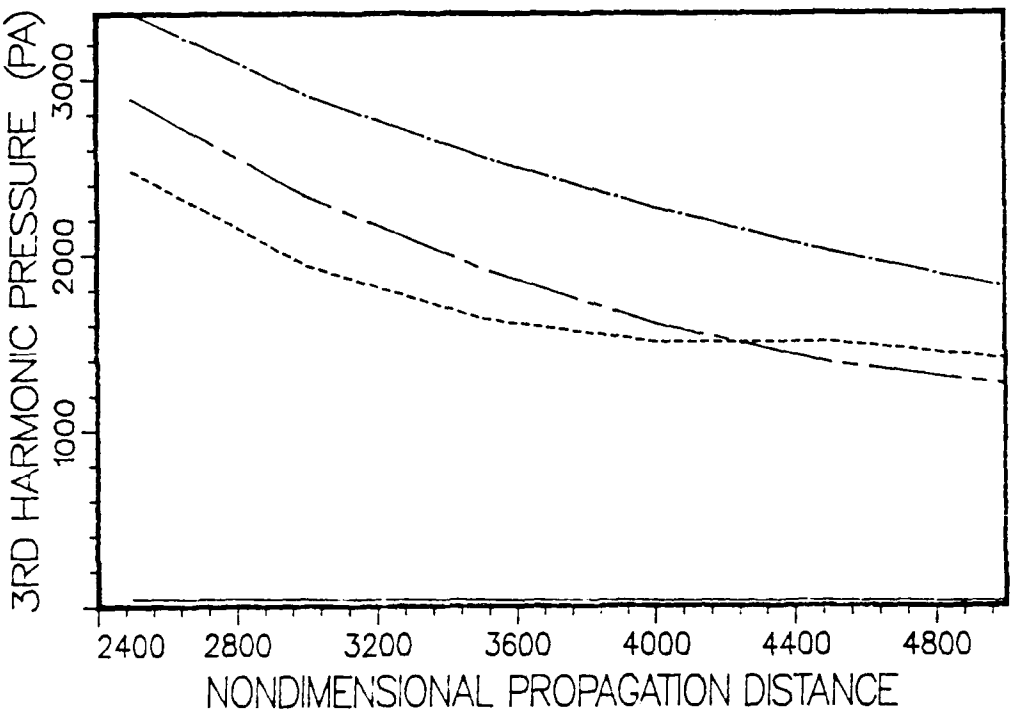

CASE 2 : GAUSSIAN TRANSDUCER, KA = 50

VELOCITY DISTRIBUTION ON BOUNDARY IS GIVEN BY :

$$f_m(R) = \exp\left[2R^2/(KA)^2\right]$$

———— = FUNDAMENTAL ONLY, SPL = 213.01 dB

– – – – – – – = FUNDAMENTAL SPL = 213.01 dB
2ND HARMONIC SPL = 213.01 dB
RELATIVE PHASE = 0

. . . . . = RELATIVE PHASE = 90

—·—·— = RELATIVE PHASE = 180

—— – —— – —— = RELATIVE PHASE = 270

GAUSSIAN AR = 1.0 KA = 50

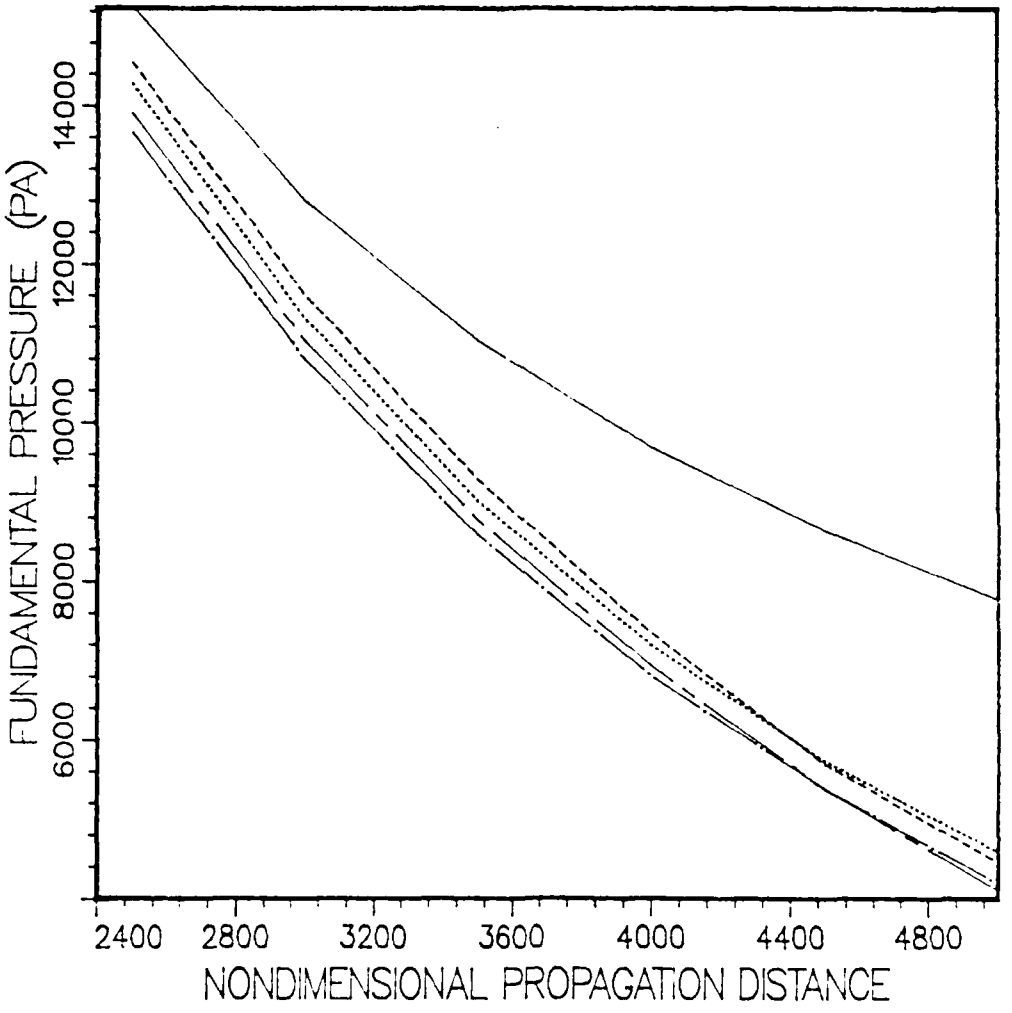

GAUSSIAN AR = 1.0 KA = 50

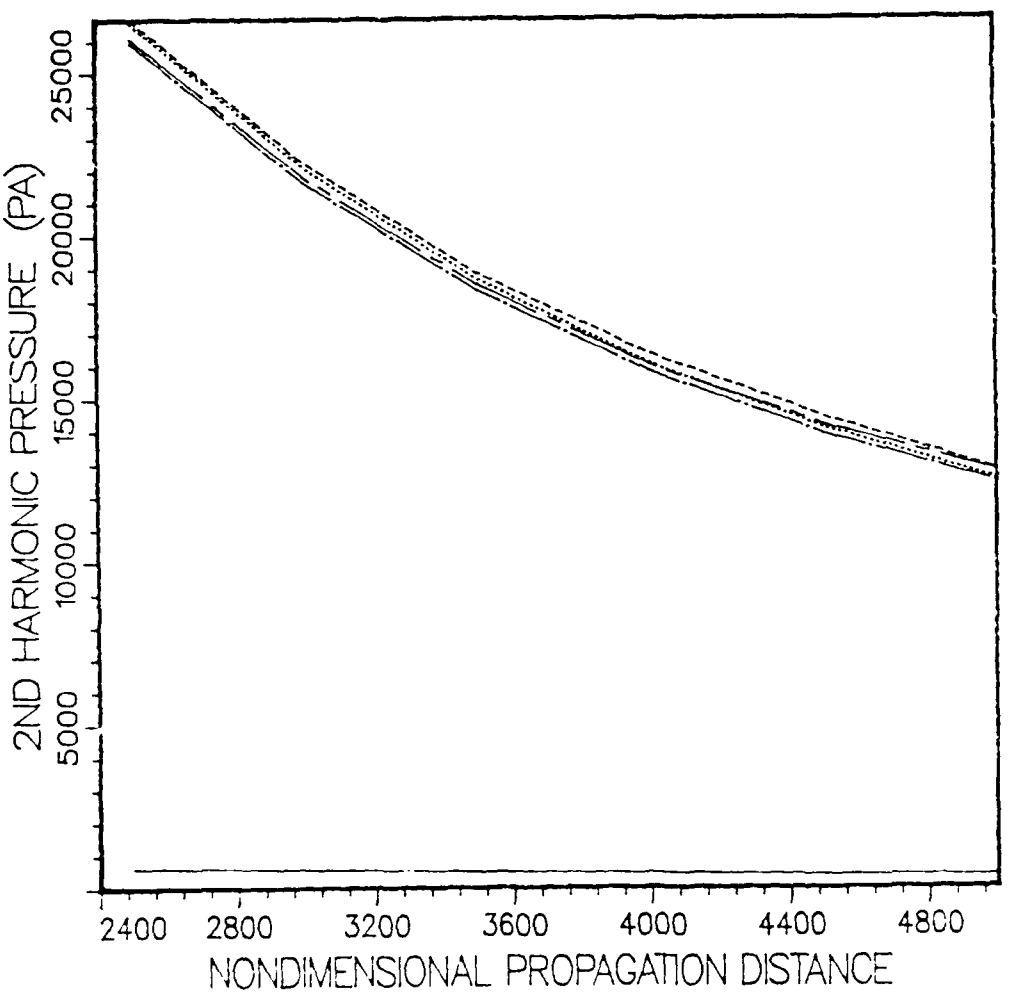

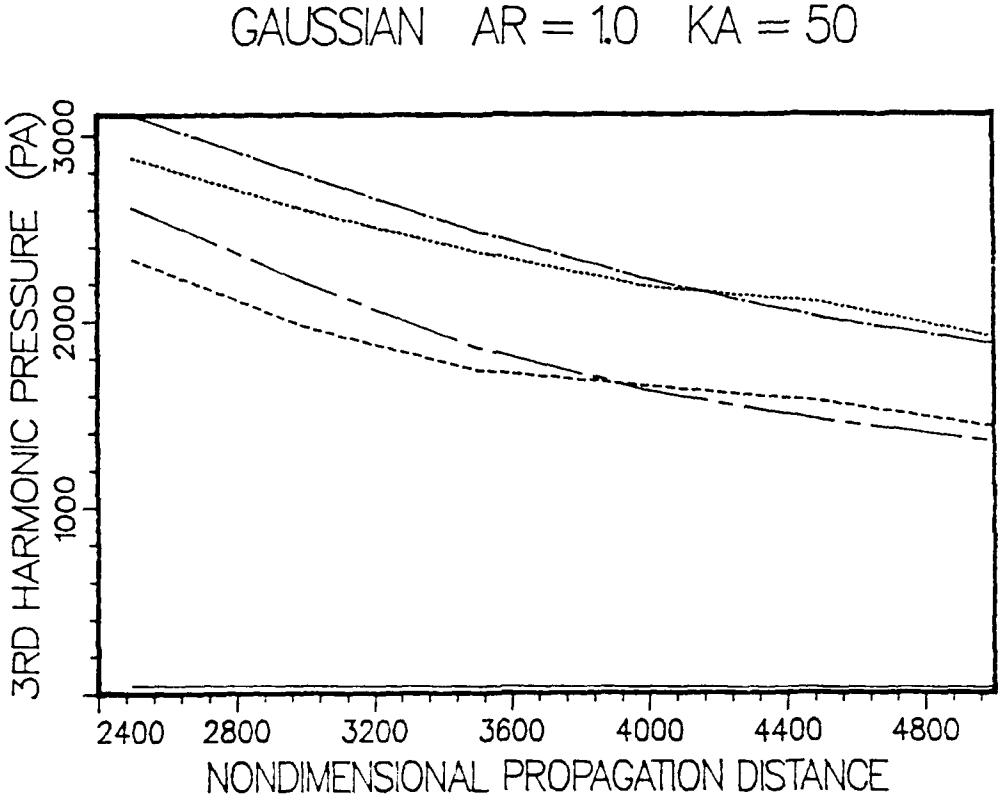
GAUSSIAN AR = 1.0 KA = 50
3RD HARMONIC PRESSURE (PA)
3000
2000
1000
2400
2800
3200
3600
4000
4400
4800
NONDIMENSIONAL PROPAGATION DISTANCE

CONCLUSIONS

* INTERACTION OF THE FUNDAMENTAL AND 2ND HARMONIC SIGNALS REDUCES THE ENERGY IN THE FUNDAMENTAL SIGNAL IN THE FARFIELD FOR THE CASES CONSIDERED.

* INTERACTION OF THE FUNDAMENTAL AND 2ND HARMONIC SIGNALS CREATES A 3RD HARMONIC SIGNAL WHICH IS SUBSTANTIALLY HIGHER THAN THAT GENERATED BY HARMONIC DISTORTION OF THE FUNDAMENTAL ALONE.

Third-order Effects in the Propagation of Finite Amplitude Stress Waves

KUN-TIEN SHU and JERRY H. GINSBERG

Acoustics and Dynamics Research Laboratory

School of Mechanical Engineering

Georgia Institute of Technology

Atlanta, Georgia

[work supported by NSF]

Presented at 113th meeting of ASA

- Finite amplitude planar waves in an elastic solid — harmonic excitation

§ BASIC EQUATIONS:

I. Momentum equation

$$L_{iK,K} + \rho_0 f_i = \rho_0 u_{i,tt}$$

L_{iK} ≡ Lagrangian stress tensor

I. Constitutive equation

$$L_{iK} = \rho_0 \frac{\partial U}{\partial u_{i,K}}$$

U ≡ Strain energy density function

II. Nonlinear geometrical strain-displacement

$$\gamma_{ij} = \tfrac{1}{2}\left(u_{i,j} + u_{j,i} + u_{k,i} u_{k,j} \right)$$

γ_{ij} ≡ Green's strain tensor

displacement :

$$U(a,t,\varepsilon) = \varepsilon U_1 + \varepsilon^2 U_2 + \varepsilon^3 U_3 + \cdots\cdots$$

$$V(a,t,\varepsilon) = \varepsilon V_1 + \varepsilon^2 V_2 + \varepsilon^3 V_3 + \cdots\cdots$$

Stress :

$$N(a,t,\varepsilon) = \varepsilon N_1 + \varepsilon^2 N_2 + \varepsilon^3 N_3 + \cdots\cdots$$

$$S(a,t,\varepsilon) = \varepsilon S_1 + \varepsilon^2 S_2 + \varepsilon^3 S_3 + \cdots\cdots$$

Strain :

$$\Sigma(a,t,\varepsilon) = \varepsilon \Sigma_1 + \varepsilon^2 \Sigma_2 + \varepsilon^3 \Sigma_3 + \cdots\cdots$$

$$\Gamma(a,t,\varepsilon) = \varepsilon^2 \Gamma_1 + \varepsilon^2 \Gamma_2 + \varepsilon^3 \Gamma_3 + \cdots\cdots$$

The strain energy density is an invariant form function of the Green's strain tensor

$$U = U(I_1^2, I_2, I_1^3, I_1 I_2, I_3, \cdots\cdots)$$

where

$$I_1 = \gamma_{ii}$$

$$I_2 = \gamma_{ij}\,\gamma_{ij}$$

$$I_3 = \gamma_{ij}\,\gamma_{jk}\,\gamma_{ki}$$

$$\left\{\begin{array}{l}\text{One-dimensional wave}\\ \text{equation in solid}\end{array}\right\}$$

$$\left[\ \frac{\partial^2 u}{\partial t^2} - c^2 \frac{\partial^2 u}{\partial a^2}\ \right]$$

$$\left\{\begin{array}{ll} = 0 & O(\varepsilon) \\ = \text{excitation due to } 1^{st} \text{ order displacements} & O(\varepsilon^2) \\ = \text{excitation due to } 1^{st} \text{ and } 2^{nd} \text{ order displacement} & O(\varepsilon^3) \end{array}\right.$$

Solutions:

$$u_1 = 0 \quad ; \quad \boxed{V_1 = -B_1 \cos\left[K_s(a - C_s t)\right]}$$

$$\boxed{u_2 = A_2 \sin\left[2K_s(a - C_s t)\right]} \quad ; \quad V_2 = 0$$

$$u_3 = 0 \quad ; \quad \boxed{\begin{aligned} V_3 = {} & B_3(K_s a)\sin\left[K_s(a - C_s t)\right] \\ & + D_3(K_s a)\sin\left[3K_s(a - C_s t)\right] \end{aligned}}$$

where

$$A_2 = \frac{1}{8}\frac{K_s M_1}{\rho_0(C_p^2 - C_s^2)}B_1^2 \quad ; \quad M_1 = \lambda + 2\mu + \beta + \tfrac{3}{2}\delta$$

$$B_3 = \frac{4B_1 A_2 K_s M_1 + B_1^3 K_s^2 M_2}{8\rho_0 C_s^2} \quad ; \quad M_2 = \tfrac{3}{2}\lambda + 3\mu + 3\beta + \tfrac{9}{2}\delta + 3\xi$$

$$D_3 = \frac{-12B_1 A_2 K_s M_1 + B_1^3 K_s^2 M_2}{24\rho_0 C_s^2}$$

Normal Strain (uniformly valid)

$$\Sigma = \epsilon^2 \left\{ \frac{1}{4} B_1^2 K_s + \left[2 K_s A_2 - \frac{1}{4} B_1^2 K_s^2 \right] \cos\left[2 K_s (a - C_s t) \right] \right\} + O(\epsilon^4)$$

Shear Strain (not uniformly valid)

$$\Gamma = \frac{1}{2} \epsilon B_1 K_s \sin\left[K_s (a - C_s t) \right]$$

$$+ \frac{1}{2} \epsilon^3 K_s \left\{ B_3 \sin\left[K_s (a - C_s t) \right] + D_3 \sin\left[3 K_s (a - C_s t) \right] \right\}$$

$$+ \frac{1}{2} \epsilon^3 K_s^2 a \left\{ B_3 \cos\left[K_s (a - C_s t) \right] + 3 D_3 \cos\left[3 K_s (a - C_s t) \right] \right\}$$

$$+ O(\epsilon^5)$$

The method of renormalization

Near identity transformation:

$$\psi = a - c_s t$$

$$= \phi + \varepsilon^2 \psi_2(a, \phi)$$

ψ_2 will be chosen so that no secular terms occur in the shear strain expansion.

Uniformly valid approximation

$$\Sigma = \varepsilon^2 \left\{ \tfrac{1}{4} B_1^2 K_s^2 + \left[2K_s A_2 - \tfrac{1}{4} B_1^2 K_s^2 \right] \cos(2K_s \phi) \right\} + O(\varepsilon^4)$$

$$\Gamma = \tfrac{1}{2} \varepsilon B_1 K_s \sin(K_s \phi)$$

$$+ \tfrac{1}{2} \varepsilon^3 K_s \left\{ B_3 \sin(K_s \phi) + D_3 \sin(3K_s \phi) \right\}$$

$$+ O(\varepsilon^5)$$

where

$$\psi = a - C_s t$$

$$= \phi + \varepsilon^2 \psi_2(a, \phi)$$

$$= \phi + \varepsilon^2 \frac{a}{B_1} \left[\underbrace{B_3 - 3D_3}_{\text{phase shift}} + \underbrace{6 D_3 \cos(2K_s \phi)}_{\text{amplitude dispersion}} \right]$$

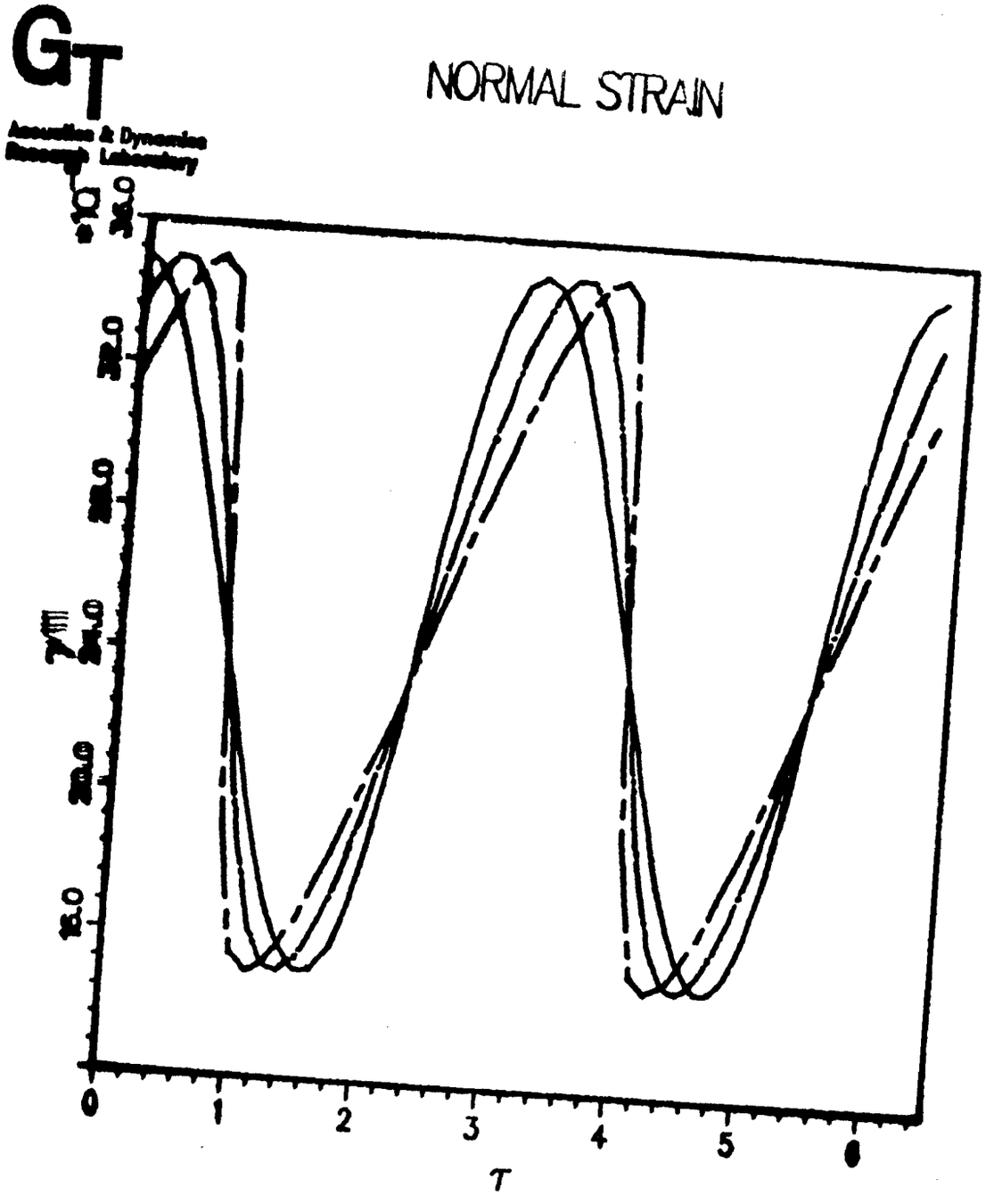
GT
NORMAL STRAIN
Aeroelastic & Dynamics Laboratory
30.0
28.0
26.0
24.0
22.0
20.0
18.0
0
1
2
3
4
5
6
T

SHEAR STRAIN

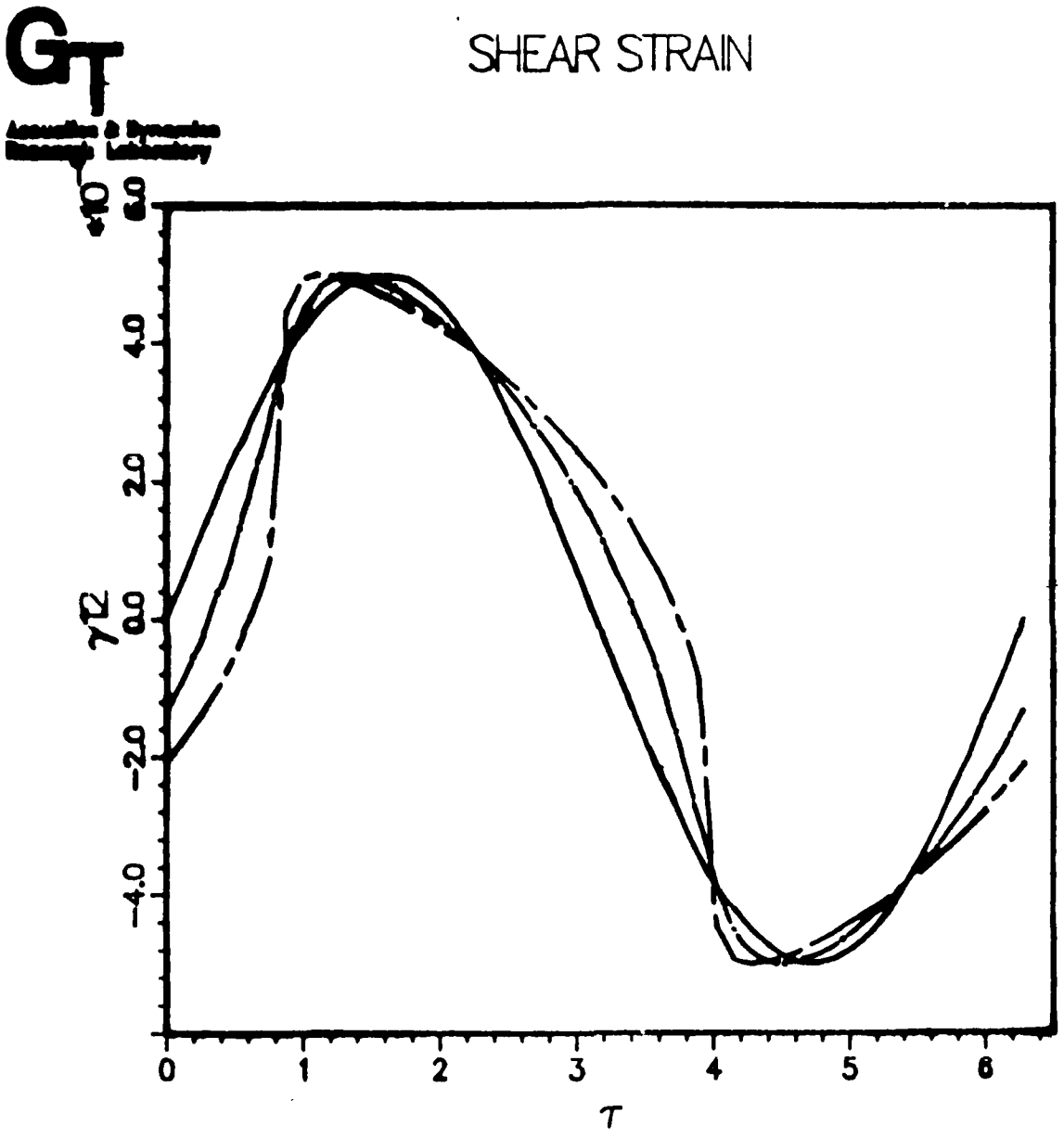

§ Conclusions

- Transmits a planar shear wave into the elastic medium:

  — 2nd order dilatational displacement.

  — 3rd order shear displacement.

- In reality, the 3rd order nonlinear effect is very small.

- Overall effect of nonlinearity:

  amplitude dispersion and small phase shift in the wave form.

COMPUTATIONAL ACOUSTICS: Algorithms and Applications
D. Lee, R.L. Sternberg, M.H. Schultz (Editors)
Elsevier Science Publishers B.V. (North-Holland)

Wiley.

oach to
3-397.

THEORETICAL AND COMPUTATIONAL ASPECTS OF FINITE AMPLITUDE SOUND BEAMS

Jerry H. Ginsberg

School of Mechanical Engineering
Georgia Institute of Technology
Atlanta, Georgia

ABSTRACT

The diffracted sound field radiating from a harmonically vibrating transducer in a baffle is known as a sound beam. In the case of linear (i.e., infinitesimal) theory, the properties of such a signal have been evaluated by algorithms derived from a variety of formulations. A comparable variety of approaches have been developed to treat the effects of nonlinearity, such as the generation of higher harmonics, which are encountered in large amplitude signals. In contrast to the linear case, earlier solutions to the nonlinear problem have been limited to certain regions, such as the near or far field, or the vicinity of the axis of the sound beam.

This paper begins with a survey of the theoretical formulations and corresponding algorithms that have been used in the past. The specific approaches consist of a quasi-planar approximation valid near the transducer face, a nonuniform spherical wave approximation appropriate to the far field, and a modified Burgers' equation based on a paraxial assumption appropriate in the vicinity of the axis and not too close to the transducer. After these methods are reviewed, a singular perturbation solution that seems to be suitable for most of the domain will be described. A key feature of the discussion is the evolution of the solution starting from a Hankel transform solution of the linear problem to its present form as a Fourier series in time; the position dependent coefficients of that series are inversions of Hankel transforms. The nature of the computational algorithms has been altered with the advances in the theory.

1. INTRODUCTION

High-intensity sound beams are generated by a transducer in a baffle, provided that the frequency is sufficiently high that the axial wavelength is much less than the radius of the transducer.

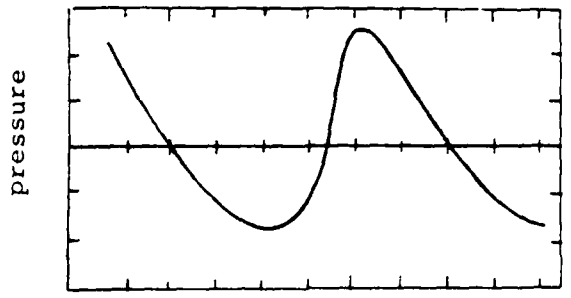

Fig. 1. Measured nonlinear waveform [1].

In conventional one-dimensional waves, nonlinear effects are associated with harmonic generation that distorts the waveform, ultimately leading to the formation of shocks. Both effects deplete the fundamental frequency, leading to decreased intensity at a specified range. Unlike the one-dimensional case, the signal radiated by a transducer displays diffractive effects, even in the linear regime. The interplay between diffraction and nonlinearity leads to distortion phenomena that are different in the compression and rarefaction phases. This phenomenon is depicted in Fig. 1, which is taken from the experiments of Browning and Mellen [1].

A wide variety of analytical techniques, both analytical and numerical, have been employed in investigations whose goals range from evaluating second harmonic amplitudes to predicting waveforms. The latter is far more demanding, because it requires accuracy in the prediction of the phase, as well as the amplitude, of the harmonics.

II. LINEAR MODELS

The low-intensity signal radiated by a harmonically vibrating transducer embedded in an infinite planar baffle has received extensive attention. Exact solutions for the signal at an arbitrary location are available in quadrature form only, but approximate formulae are available for some regions, notably the field far from the transducer. The analytical difficulties are attributable to the effects of diffraction. When the transducer vibrates as a piston, the velocity discontinuity at the edge leads to spatial fluctuations in the signal level. At a sufficiently high frequency, $ka \gg 1$, where a is the piston radius and $k = \omega/c_0$ is the

wavenumber for a (linear) planar wave at frequency ω in a medium whose speed of sound is c_0, one obtains a sound beam. The strength of such a signal is essentially confined to a region very close to the axis of symmetry. Near the transducer, the overall wave motion seems to be planar, with varying intensity along wavefronts. As the wave propagates, one encounters a transition to spherical propagation.

An exact expression is available [2] for the amplitude along the axis of symmetry of the beam radiated by a piston. If εc_0 is the peak velocity of the piston, then

$$|p| = 2\varepsilon\rho_0 c_0^2 \left|\sin\left[k\left(\sqrt{z^2 + a^2} - z\right)/2\right]\right| \qquad (1)$$

There are nodes and anti-nodes that become increasingly separated with increasing distance from the transducer. The last node occurs approximately at $r_0 = ka^2/2\pi$, where a is the piston diameter. Spherical propagation is well-established at the Rayleigh distance, $z = ka^2/2$. The near field fluctuations increase with increasing values of k, corresponding to decreasing spatial scale. The signal off-axis shows comparable behavior.

Quadrature solutions for the linearized signal of an arbitrary axisymmetric transducer have been derived from two viewpoints. One may consider the moving face of the transducer to consist of a distribution of sources, which leads to the Kirchhoff-Helmholtz integral theorem. The method of images leads to the appropriate Green's function for a semi-infinite half-space, which is then specialized to the case where sources are distributed along the plane. The result is known as the Rayleigh integral [2].

$$p(\vec{x},t) = -\frac{i\omega\rho}{2\pi}\int_S \frac{1}{r}\, v(\vec{\xi})\, \exp[i(kr - \omega t)]\, dS \qquad (2)$$

where r is the distance from a point $\vec{\xi}$ on the plane to field point $\vec{x}$. The function $v(\vec{\xi})$ represents the normal velocity distribution on the planar boundary S.

A less obvious treatment, attributable to King [3], regards the infinite half-space to be a circular waveguide of infinite diameter. The eigenvalues of such a system lie in a continuous spectrum, so the mode superposition corresponds to a Hankel integral transform. Let V_n denote the Hankel transform of the transducer velocity distribution v(R). Then, the pressure is found from the inverse transform,

$$p = \varepsilon\rho_0 c_0^2 \int_0^\infty \frac{nV_n}{\mu_n} \exp(i\omega t - \mu_n kz) J_0(nkR)\, dn \tag{3}$$

where (z,R) are cylindrical coordinates, and μ_n is the nondimensional axial wavenumber,

$$\mu_n = \begin{cases} (1 - n^2)^{1/2} & n < 1 \\ (n^2 - 1)^{1/2} & n > 1 \end{cases} \tag{4}$$

The spectrum $n > 1$ represents evanescent waves, whose contribution is negligible at a few multiples of the transducer radius.

The King integral is more efficient for numerical evaluation of the near field, because it is a single integral. However, its integrand oscillates rapidly as a function of n when either z or R is large, which raises the number of integration sub-intervals. Also, the King integral is limited to axisymmetric situations. The Rayleigh integral has proven to be more amenable to analytical approximations in restricted regions, such as near the axis of the sound beam, but the King integral representation, which uses separable wave functions, has advantages for estimating nonlinear effects.

III. NEAR FIELD PERTURBATION ANALYSIS

The field equations employed in analyses of finite amplitude effects may be formulated in terms of a velocity potential ϕ. Assuming an isentropic process in an inviscid, compressible fluid, spatial and temporal derivatives of Euler's equation, with the convective nonlinearity retained, yield an exact equation for ϕ in which $c^2 = dp/d\rho$ appears explicitly. In a linearized formulation, this derivative is evaluated at the ambient conditions, so it is the square of the conventional speed of sound. However, a nonlinear formulation requires that c be evaluated at the current pressure. For a first approximation of nonlinear effects it is permissible to expand the pressure-density relation in a power series that is accurate to the second order,

$$p = \rho_0 c_0^2 \left[\left(\frac{\rho'}{\rho_0}\right) + (\beta_0 - 1)\left(\frac{\rho'}{\rho_0}\right)^2 + \cdots \right] \tag{5}$$

where ρ' is the density perturbation. Substitution of Eq. (5) into Kelvin's equation yields an expression for the pressure as a function of velocity potential,

$$p = -\rho_0 \frac{\partial \phi}{\partial t} + \rho_0 \left[\left(\frac{\partial \phi}{\partial t} \right)^2 - \nabla\phi \cdot \nabla\phi \right] \tag{6}$$

which when combined with Euler's equation leads to

$$\nabla^2\phi - \frac{\partial^2 \phi}{\partial t^2} = 2(\beta_0 - 1) \frac{\partial \phi}{\partial t} \nabla^2\phi + \frac{\partial}{\partial t} \nabla\phi \cdot \nabla\phi \tag{7}$$

Note that the position variables in this nonlinear wave equation have been nondimensionalized by the reciprocal of the axial wave number k, and time has been scaled by the frequency.

The first consistent analysis of nonlinearity in sound beams was performed by Ingenito and Williams [4]. They simplified Eq. (7) by assuming that the one-dimensional relation between pressure and particle velocity holds, $p = \rho c v_z$. Expansion of the potential in a perturbation series,

$$\phi = \varepsilon\phi_1 + \phi^2\phi_2 \tag{8}$$

led at the first order to the equations for the linear problem. They used the Rayleigh integral for the first order term to generate a Helmholtz equation for the second harmonic, in which the quadratic nonlinearity appears as inhomogeneous terms representing a spatial distribution of sources. Ingenito and Williams identified the portion of the second order solution that predominates in the near field, provided one is not very close to the transducer and ka is very large. Their solution was obtained by using the free space Green's function, thereby ignoring the portion of the Green's function required to satisfy the boundary condition at z = 0. The solution has the form of a volume integral over the second order sources, in which rational approximations were used to simplify the Green's function contribution. Only the second harmonic along the axis of symmetry was evaluated, but Rogers [5] made comparable approximations to obtain a representation of the signal off-axis.

The results of this formulation matched well with measurements in a domain that is neither very close to the transducer, nor out where the propagation has spherical characteristics. There are other limitations to the analysis, in that it describes only very high frequency sound beams, and it ignores the energy depletion in the fundamental harmonic that accompanies the formation of higher harmonics. The latter difficulty appears in a mathematical context as a perturbation solution that loses validity at long ranges,

where the smallness assumption for the perturbation correction is violated.

IV. SPHERICAL PROPAGATION MODELS

A different approach was taken by Lockwood, Muir, and Blackwood [6] in order to develop a model that could describe the far field. They used an earlier solution for nonlinear spherical waves with directivity, which is dependence of the signal level on the polar angle. This model is limited by the assumption that the transducer drive level is sufficiently low to ignore distortion out to a radial distance r_d in the vicinity of the Rayleigh length. The signal at that location may then be described by the far field approximation,

$$p = \rho_0 c_0^2 ka D(\theta) \frac{a}{r_d} \sin(kr_d - \omega t) \tag{9}$$

where $D(\theta)$ is the directivity factor,

$$D(\theta) = \frac{2J_1(ka \sin\theta)}{ka \sin\theta} \tag{10}$$

Using the pressure at the transition distance to drive a finite amplitude spherical wave leads to an algebraic equation for the pressure beyond the transition,

$$p = \rho_0 c_0^2 ka D(\theta) \frac{r_d}{r} \sin\left[\omega t - k(r - r_d) + \beta_0 kr \left(\ln \frac{r}{r_d}\right) \frac{p}{\rho_0 c_0^2}\right] \tag{11}$$

This expression may be solved numerically by the Newton-Raphson method for the pressure at any instant and location. A closed form Fourier series expansion of Eq. (11) was obtained by exploiting its similarity to the solution for a planar wave.

The primary difficulty with this formulation is the restriction to signal levels that are sufficiently small to suppress nonlinear distortion in the near field. Many applications require consideration of substantial near field distortion. A less obvious limitation of the theory is its prediction that higher harmonics are in-phase with the primary. Thus, the assumption of spherical propagation leads to a model that cannot reproduce the asymmetrical waveform in Fig. 1.

V. MODIFIED BURGERS' EQUATION

A prototypical model combining nonlinear distortion and dissipation for planar waves is Burgers' equation. Part of its attraction is the availability of the Weiner-Hopf transformation, which leads to analytical solutions. A comparable model for sound beams, which is sometimes referred to as the paraxial parabolic equation, was developed by Zabolotskaya and Khoklov [7] for the ideal case, and then rederived by Kuznetsov [8] to include dissipation. One must make several assumptions to obtain it from the basic hydrodynamical equations. The planar wave assumption is invoked, $p = \rho c_0 v_z$, but more severe are the assumptions regarding the spatial scales. Let $\varepsilon \ll 1$ be the acoustic Mach number at the transducer. The axial wavelength defines the shortest scale, which is taken as $O(1)$. The longest scale is taken as the distance at which a planar wave would shock; that scale is $O(\varepsilon^{-1})$. Diffraction is then assumed to occur over an intermediate scale, which is considered to be $O(\varepsilon^{-1/2})$. The corresponding dependence of the pressure is $p = p(t - z/c_0, \varepsilon^{1/2}z, \varepsilon^{1/2}R, \varepsilon z)$. By collecting terms having like orders of magnitude, one obtains the modified Burgers' equation,

$$\rho_0 c_0^2 \varepsilon \left[4 \frac{\partial^2}{\partial \tau \partial \sigma} - \nabla_t^2 - 4\alpha r_0 \frac{\partial^3}{\partial \tau^3} \right] p = \frac{2 r_0}{\tau_d} \frac{\partial^2}{\partial \tau^2} (p^2) \qquad (12)$$

where $\tau = \omega t - kz$, $\sigma = z/r_0$, ∇_t^2 is the transverse Laplace operator, α is an absorbtion coefficient, and τ_d is the distance at which a uniform planar wave shocks.

Due to the assumption that the only $O(1)$ scale is $t - z/c_0$, the equation is only suitable near the beam axis. Even there, it should not be applied much closer to the transducer than the farthest antinode, because diffraction effects in the true near field occur over a very small scale. Less apparent is the planar wave assumption, which is also imposed on the boundary. Consequently, a piston transducer, for which there is a velocity discontinuity at the edge, is replaced by a discontinuous pressure distribution; diffraction from the latter excitation is significantly less than it is for an actual piston. Indeed, the fundamental frequency obtained from Eq. (12) does not match that obtained from Eq. (1) in the limit as $\alpha \to 0$, except in the far field.

The Soviet analyses for a transducer vibrating harmonically employed the finite difference simulation described by Bakhvalov et al. [9]. The domain for the difference mesh was $z \geq 0$,

$0 \leq t - z/c_0 \leq 2\pi$, $0 \leq R(1 + z/W) \leq W$, where W was selected to make the domain extend beyond the width of the linear beam. Results obtained from this formulation agreed qualitatively with measurements, in the sense that the asymmetrical features of the distortion in Fig. 1 were found. However, no evaluations were performed for the parameters of prior experiments, which led to conjecture that the finite difference program might suffer from instabilities. Also, the computational demands required to model the space-time grid seemed to be exceptional.

Another approach to solving Eq. (12) has been developed recently by Aanonsen et al. [10]. They exploited the periodicity of the signal to expand the pressure in a Fourier series whose amplitudes are position dependent. Substituting such an expansion leads to coupled partial differential equations for the amplitudes, thereby removing time from the equations to be solved. These equations could only be solved numerically; an implicit backward difference formula was used for the axial variable. The transverse variable was modeled by central differences over a closed domain that is sufficiently large to carry the main features of the linearized signal. In comparison to the earlier formulation of Eq. (12), the foregoing gained by removing the time grid, at the expense of solving coupled partial differential equations. The computer programs required to evaluate the signal placed severe demands on the available resources, but numerical instabilities seemed to be less of a problem. Results for amplitude levels seem to compare well with far field measurements, but comparisons of waveforms with experiments were not made.

VI. NONLINEAR KING INTEGRAL

Parallel to the foregoing developments, significant progress had been made toward deriving a general approach for implementing singular perturbation theory in acoustic wave propagation. The starting point for the approach is similar to Ingenito and Williams, in that one must obtain the second order potential corresponding to the wave equation (7). Because the medium is nondispersive, some of the first order harmonics, which form the source terms for the second order terms, propagate at the phase velocity of second order modes. This produces secular terms in the inhomogeneous linear wave equation governing ϕ_2, much like the situation in a nonlinear oscillator. As a result some, or all, of the terms forming ϕ_2 grow with increasing propagation distance.

By itself, such growth is not necessarily incorrect, but the physical variables derived from the perturbation potential show the same behavior. Such a perturbation solution is not uniformly accurate, in that the magnitude of the perturbation correction is dependent on the position. Indeed, at a sufficiently large distance, it would exceed the magnitude of the first order solution.

The growth effect may be explained if one considers the possibility that the independent variables chosen to represent the solution differ slightly from the physical coordinates. For example, suppose the wave depended on a spatial grid that was stretched slightly from the Cartesian coordinate system. At the beginning the two representations would appear to be alike, but the differences would grow as the distorted grid diverges from the physical grid. This concept leads to the method of strained coordinates.

The basic solution for a sound beam was derived by Ginsberg [11]. The analysis began by using the King integral to generate the second order source terms, which become integrals over a dual spectrum of transverse wavenumbers. The general form of these terms is

$$\nabla^2\Phi_2 - \frac{\partial^2\Phi_2}{\partial t^2} = \int_0^\infty\int_0^\infty \Gamma(m,n)\,\exp[2i\omega t - (\mu_n + \mu_m)z] \times \begin{matrix} J_0(\mu_n R)\ J_0(\mu_m R) \\ J_1(\mu_n R)\ J_1(\mu_m R) \end{matrix} dm\,dn \tag{13}$$

Asymptotic representations of the Bessel functions lead to expansions of the signal near the axis ($R \ll 1$) and far from the axis ($R = O(1)$). The latter was shown by Miao and Ginsberg [12] to contain the inner solution, so the discussion will focus on the off-axis region. The smallness of $1/R$ there leads to a solution for Φ_2 in the form of two dual Hankel transforms,

$$\Phi_2 = \int_0^\infty\int_0^\infty A_j(z)\,\exp[2i\omega t - (\mu_n \pm \mu_m)z][J_0(\mu_n R)\ J_0(\mu_m R) \cdot J_0(\mu_n R)\ J_0(\mu_m R)]\,dm\,dn \tag{14}$$

where the amplitude functions $A_j(z)$ must satisfy the following differential equation.

$$A_j'' - 2(\mu_n \pm \mu_m)A_j' + \beta_j(m,n)A_j = \Gamma_j(m,n) \tag{15}$$

The complementary solution for A_j contains one part that corresponds to waves propagating inward from the far field—these must be discarded in order to satisfy the radiation condition. The particular solutions for the A_j are independent of z. The solution is fully defined when the condition that there be no nonlinear radiation from the boundary is satisfied.

This seemingly simple recipe for constructing ϕ_2 overlooks the presence of a singularity at m = n, where β_1 vanishes. In contrast to the situation where m ≠ n, the particular solution for A_1 when m = n is proportional to z. As z increases (increasing distance from the transducer), the contribution of the region around m = n grows due to the interaction of a harmonic at a specified wavenumber with its neighbors. This effect is the same as the cumulative growth effect encountered in earlier studies of harmonic generation. In contrast, harmonics that correspond to substantially different transverse wave numbers destructively interfere. This process is evaluated mathematically by integrating Eq. (14) asymptotically using Laplace's method, which is a straightforward extension of the method of stationary phase.

The result of this procedure is to reduce ϕ_2 to a single integral. The evaluation of the pressure signal after ϕ_2 has been evaluated follows comparable steps to those for simple acoustic waves. Expressions for the second order pressure are not uniformly accurate, due to the growth of ϕ_2. Coordinate straining transformations are needed to regularize the expansion, with the new feature that the transformation must depend on the transverse wave number. The resulting expression was termed the nonlinear King integral, because it differed from the linear analog only by the replacement of the physical coordinates by their corresponding strained coordinate. The specific result was

$$p = \varepsilon\rho_0 c_0^2 \int_0^\infty \frac{nV_n}{\mu_n} \exp(it - \mu_n \xi)\, J_0(n\alpha)\, dn + C.C. \qquad (16)$$

where C.C. is used to denote the complex conjugate. The variables ξ and α are strained coordinates whose values are obtained by solving the following pair of coupled transcendental equations.

$$\begin{aligned} z &= \zeta + [i\varepsilon\beta_0 nV_n H(z,n) \exp(it - \mu_n \xi) + C.C.]\, J_0(n\alpha) \\ R &= \alpha - [i\varepsilon\beta_0 V_n H(z,n) \exp(it - \mu_n \xi) + C.C.]\, J_1(n\alpha) \end{aligned} \qquad (17)$$

where H(z,n) represents a function that approaches $(z/\mu_n^3)^{1/2}$ for large z, but is finite for n = 1 (μ_n = 0).

One simplification in evaluating Eq. (16) is the ability to ignore the nonlinear contribution of the spectrum n > 1, due to its evanescent nature. Nevertheless, numerical evaluations are substantially complicated by the need to solve Eqs. (17) for α and ξ in order to determine the value of the integrand at a specified wave number. This complication is compounded by the dependence of the integrand on n, which is highly oscillatory when z is large. The algorithm that was developed used a Gauss-Chebychev integration rule to remove the $1/\mu_n$ singularity. Evaluation of the coordinate transformation was achieved by using a coupled Newton-Raphson scheme based on an initial guess that equates the strained coordinates to their physical counterparts. An empirical rule for the number of integration points was found to be that the number of points should exceed the nondimensional distance from the center of the transducer. This is quite prohibitive, since the distance is quite large for most situations of interest. For example, at the Rayleigh length marking the onset of spherical propagation, the nondimensional value is $(ka)^2/2$, where ka > 40 for most situations of interest.

An important property of the nonlinear signal is its frequency content. Evaluation of such information for the nonlinear King integral was achieved by computing the signal at a selected location at many equally spaced intervals covering one period, after which a discrete Fourier transform disclosed the amplitude and phase relative to the fundamental of higher harmonics. Unfortunately, the need to evaluate Eq. (16) at a succession of instants greatly multiplied the computational time. CPU times of 2 minutes or more were not unusual on a CDC CYBER 785.

This situation greatly improved with a recent derivation performed by Miao and Ginsberg [12]. Rather than straining two physical coordinates, the analysis decomposed the wave at each wave number n into two interacting one-dimensional waves. The technique used for that step was the same as that by which a nonplanar mode in a rectangular duct may be decomposed into planar waves that bounce off the walls. The advantage of this representation was that each wave is a function of only one phase variable, so only one strained coordinate need be introduced for each wave. This new representation was

$$p = \rho_0 c_0^2 \int_0^1 \frac{nV_n}{\mu_n} \left[J_0(nR)^2 + J_1(nR)^2\right]^{1/2} \left[\cos \tau_1 + \cos \tau_2\right] dn \tag{18}$$

where the phase variable ξ_j for each wave is a strained coordinate that is related to the phase ψ_j of the linear signal by a single transformation equation. These variables depend on R only through two phase angles Δ and δ, with the transformation equations having the form

$$\psi_j = t - \mu_n z \pm \Delta = \xi_j - 2\varepsilon\beta_0\mu_n H(z,n)\cos(\xi_j \pm \delta) \qquad (19)$$

The phase of the individual waves is a periodic function of only one transformed variable. This is analogous to the situation for planar waves. The resemblance suggested a Fourier-Fubini series expansion for the contribution to the fundamental and higher harmonics corresponding to each transverse wave number n. Integrating over the spectrum of wave numbers yielded a temporal Fourier series for the amplitude and phase of each harmonic, whose coefficients are King-type integrals. In other words, the new formulation replaced a single integral, Eq. (16), whose integrand was known implicitly through a coordinate straining, Eq. (17), with several integrals whose integrands are known explicitly. The gain in computational efficiency was found to be enormous—in most cases CPU time was reduced by a factor of 30 or more.

The results of this analysis have been found to be very accurate outward from the last antinode. Figure 2 compares a waveform measured by Moffett [13] with the digitized prediction of the theory. The propagation curve in Fig. 3, which depicts theoretical harmonic dependence on-axis, compares the prediction with measurements made by Moffett [14] on a prior occasion.

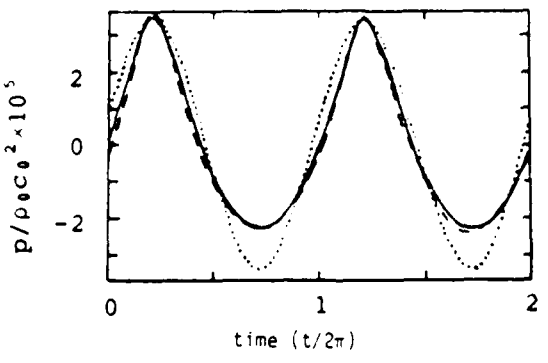

Fig. 2. Waveform on-axis at 10 meters, ka = 64.3, source level = 234 dB//1 μPa. ——, theoretical; ···· [14].

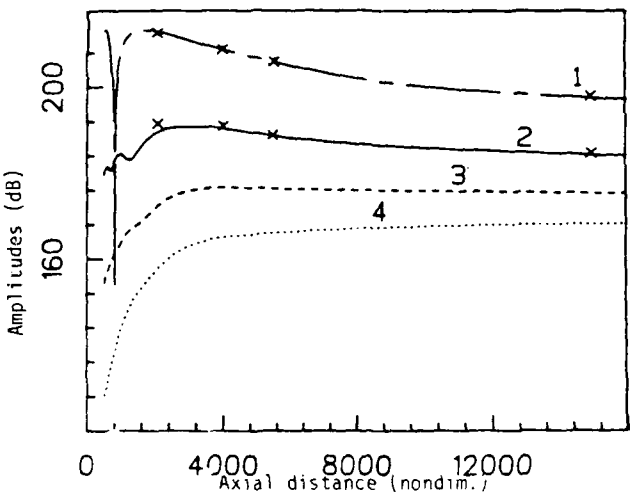

Fig. 3. Axial propagation of harmonics, ka = 101.7. ——, theoretical; x [13].

The theoretical predictions for this series of experiments shows an interesting trend in regard to the phase lag of the harmonics relative to the fundamental. (Phase measurements were not made by Moffett.) As shown in Fig. 4, each harmonic tends to lag 90° relative to the preceding one in the region outward from the farthest maximum in the fundamental amplitude. In contrast, the

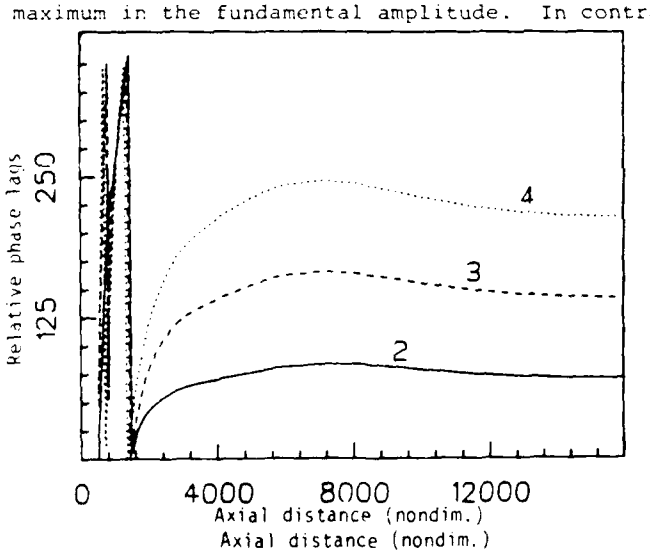

Fig. 4. Axial variation of phase of higher harmonics relative to the fundamental, same parameters as in Fig. 3.

harmonics are more or less in phase inward from that location. This seems to be a consequence of the 90° shift that a linear signal undergoes in the transition from near field to far field propagation. Another significant feature is the rapid change in the relative phase angles at the farthest null of the fundamental. This is a consequence of the 180° inversion the fundamental undergoes at a null, while the phase of the higher harmonics changes smoothly. Note that the term "null" is used loosely to describe the deep dip in the fundamental, because nonlinear effects seem to leave a residual, even though the linear signal vanishes.

Some theoretical questions still remain. In the region very close to the transducer, for example at one tenth the Rayleigh length, the cumulative growth effects associated with secularity do not yet dominate. This was disclosed in a preliminary analysis [15] that numerically evaluated the interactions of all modes in the King integral. Development of an overall theory requires that such effects be merged into the coordinate straining analysis that led to the nonlinear King integral. Another topic requiring attention is the formation of shocks. The coordinate transformations are singular when a shock forms, corresponding to a loss of uniqueness. Physically, a shock causes the compression phase of the sound beam signal to become a spike, while the rarefaction phase broadens and lessens. It is hoped that the latest representation of the sound beam, in which two quasi-planar waves interact to form a mode of main transverse wave number, will suggest how to [illegible] shock formation.

ACKNOWLEDGMENT

This work was supported by the Office of Naval Research, Code 432-SA.

REFERENCES

1. [illegible], D. T., and R. H. Mellen, Finite-amplitude distortion of 210-kHz acoustic waves in water, JOURNAL OF THE ACOUSTICAL SOCIETY OF AMERICA 44 [illegible], 944-[illegible].

2. Pierce, A. D., ACOUSTICS, McGraw-Hill, New York, 1981, Chap. [illegible].

3. Skudrzyk, E., THE FOUNDATIONS OF ACOUSTICS, Springer-Verlag, Berlin, 1971.

4. Ingenito, F., and A. O. Williams, Jr., Calculation of second-harmonic generation in a piston beam, JOURNAL OF THE ACOUSTICAL SOCIETY OF AMERICA 49 (1971), 319-328.

5. Rogers, P. H., and A. O. Williams, Jr., Second harmonic generation in plane-piston beams, JOURNAL OF THE ACOUSTICAL SOCIETY OF AMERICA 47 (1970), 82(A).

6. Lockwood, J. C., T. G. Muir, and D. T. Blackstock, Directive harmonic generation in the radiation field of a circular piston, JOURNAL OF THE ACOUSTICAL SOCIETY OF AMERICA 53 (1970), 1148-1153.

7. Zabolotskaya, E. A., and R. V. Khokhlov, Quasi-plane waves in the nonlinear acoustics of confined beams, SOVIET PHYSICS-ACOUSTICS 15 (1969), 35-40.

8. Kuznetsov, V. P., Equations of nonlinear acoustics, SOVIET PHYSICS-ACOUSTICS 16 (1971), 467-470.

9. Baknvalov, N. S., Ya. M. Zhileiken, E. A. Zabolotskaya, and R. V. Khokhlov, Nonlinear propagation of a sound beam in a nondissipative medium, SOVIET PHYSICS-ACOUSTICS 22 (1976), 272-274.

10. Aanonsen, S. I., T. Barkve, J. N. Tjøtta, and S. Tjøtta, Directive and harmonic generation in the nearfield of a finite amplitude sound beam, JOURNAL OF THE ACOUSTICAL SOCIETY OF AMERICA 75 (1984), 749-768.

11. Jinsberg, J. H., Nonlinear King integral for arbitrary axisymmetric sound beams at finite amplitudes, Parts I and II, JOURNAL OF THE ACOUSTICAL SOCIETY OF AMERICA 76 (1984), 1211-1214.

12. Miao, H. C., and J. H. Jinsberg, Fourier series representation of finite amplitude sound beams, JOURNAL OF THE ACOUSTICAL SOCIETY OF AMERICA 78 (1979), S39.

13. Moffett, M. B., Measurement of fundamental and second harmonic pressures in the field of a circular piston, JOURNAL OF THE ACOUSTICAL SOCIETY OF AMERICA 65 (1979), 318-323.

14. Moffett, M. B., and J. H. Jinsberg, Finite-amplitude waveforms produced by a circular piston projector, JOURNAL OF THE ACOUSTICAL SOCIETY OF AMERICA 72 (1982), S41.

15. Foda, M. A., and J. H. Ginsberg, Relationship between near and far field effects in second harmonic generation in the piston beam, JOURNAL OF THE ACOUSTICAL SOCIETY OF AMERICA 79 (1986), S31-S32.

FINITE AMPLITUDE ACOUSTIC WAVES GENERATED BY A BAFFLED, MULTIHARMONIC TRANSDUCER

A THESIS
Presented to
The Faculty of the Division of Graduate Studies

By

James Becton Edgerton, Jr.

In Partial Fulfillment
of the Requirements for the Degree
Doctor of Philosophy in Mechanical Engineering

Georgia Institute of Technology
February, 1988

Front matter only
Thesis already sent

TABLE OF CONTENTS

The overall signal predicted by this combined model is interfaced with a nonlinear propagation model for spherical waves with directivity. The transition between the models is performed at the Rayleigh length for the second harmonic. The results indicate that a modest gain in the level of the farfield fundamental signal is possible, depending on the limitations of the transducer.

SIMILARITY OF A FOURIER TRANSFORM GENERALIZATION OF THE EARNSHAW SOLUTION FOR PLANAR WAVES TO AN INTERACTING WAVE MODEL FOR FINITE AMPLITUDE PLANAR WAVES

JERRY H. GINSBERG

SCHOOL OF MECHANICAL ENGINEERING

GEORGIA INSTITUTE OF TECHNOLOGY

ATLANTA, GEORGIA

Presented at 115 th Meeting of ASA

WORK SUPPORTED BY ONR - CODE 1125-OA

FINITE AMPLITUDE PLANAR WAVE

PRE-SHOCK CONDITION

EARNSHAW SOLUTION (1859)

BOUNDARY EXCITATION: $v = \epsilon c_0 f(t)$ at $x = 0$

IMPLICIT FUNCTIONAL FORM:

$$v(x, t) = \epsilon c_0 f(t - x/c)$$

where

$$c = c_0\left[1 + \frac{1}{2}(\gamma - 1)\,\frac{v}{c_0}\right]^{(\gamma+1)/(\gamma-1)}$$

SMALL SIGNAL APPROXIMATION

$$\epsilon \ll 1 \;\rightarrow\; p = \rho_0 c_0 v = \epsilon \rho_0 c_0^2 f(t - x/c)$$

$$c = c_0 + \beta_0 v \quad \text{where } \beta_0 = \frac{1}{2}(\gamma + 1)$$

ALTERNATIVE IMPLICIT FORM

$$p = \epsilon \rho_0 c_0^2 f(t - \alpha/c_0)$$

COORDINATE STRAINING TRANSFORMATION

$$x = \alpha + \epsilon \beta_0 x \, f(t - \alpha/c_0)$$

SOLUTION TECHNIQUES

1. FUNCTIONAL INVERSION - for spatial waveforms:

   Fix t. Select a value of p (i.e. f). Solve for x.

   Increment p and repeat.

2. GRAPHICAL METHODS - follow characteristics

3. NUMERICAL METHODS - Newton-Raphson, etc.

4. SERIES EXPANSION - for harmonic f(t)

SOLUTION OF FUBINI-GHIRON (1935)

$$p = \epsilon \rho_0 c_0^2 \sum_{n=1}^{\infty} p_n(\sigma) \sin[n(\omega t - kx)] \; ; \quad k = \omega / c_0$$

$$p_n = \frac{2}{n\sigma} J_n(n\sigma) \; ; \quad \sigma < 1$$

where σ is the distance relative to shock formation,

$$\sigma = \epsilon \beta_0 kx$$

QUESTION

IS THERE AN ANALOG TO THE FUBINI-GHIRON SOLUTION FOR TRANSIENT EXCITATIONS THAT ARE DEFINED IN THE FREQUENCY DOMAIN?

FOURIER TRANSFORM VERSION OF

SMALL SIGNAL APPROXIMATION

INVERSION TO RECOVER THE INPUT:

$$f(t) = \frac{1}{2\pi} \int_{-\infty}^{\infty} F(\omega) \exp(-i\omega t)\, d\omega$$

REPLACE f(t) IN EARNSHAW SOLUTION

$$p = \frac{\epsilon}{2\pi} \rho_0 c_0^2 \int_{-\infty}^{\infty} F(\omega) \exp[-i\omega(t - \alpha/c_0)]\, d\omega$$

where

$$x = \alpha + \frac{\epsilon}{2\pi} \beta_0 x \int_{-\infty}^{\infty} F(\omega) \exp[-i(\omega t - k\alpha)]\, d\omega$$

PHASE VARIABLE REPRESENTATION

REPRESENT $F(\omega)$ IN POLAR FORM: $F = \frac{1}{i}V(\omega)\ \exp[i\theta(\omega)]$

DEFINE PHASE VARIABLES:

$$\psi(\omega) = \omega(t - x/c_0) - \theta(\omega)\ ;\quad \xi(\omega) = \omega(t - \alpha/c_0) - \theta(\omega)$$

COORDINATE TRANSFORMATION:

$$\psi(\omega) = \xi(\omega) - \frac{\epsilon}{2\pi i}\beta_0 kx \int_{-\infty}^{\infty} V(\lambda)\ \exp[-i\xi(\lambda)]\ d\lambda$$

$$= \xi(\omega) - \frac{\epsilon}{\pi}\beta_0 kx \int_0^{\infty} V(\lambda)\ \sin[\xi(\lambda)]\ d\lambda$$

PRESSURE INTEGRAL:

$$p = \frac{\epsilon}{\pi}\rho_0 c_0^2 \int_0^{\infty} V(\omega)\ \sin[\xi(\omega)]\ d\omega$$

BASIC PROPERTIES

If $\xi^*(\omega)$ corresponds to a specific $\psi^*(\omega)$, then

1) $\xi^*(\omega) + 2\pi$ corresponds to $\psi^*(\omega) + 2\pi$,

2) $-\xi^*(\omega)$ corresponds to $-\psi^*(\omega)$.

FOURIER SERIES

From 1) and 2), $\sin(\xi)$ may be expanded in a sine series.

$$\sin[\xi(\omega)] = \sum_{n=1}^{\infty} a_n(\omega) \sin[n\psi(\omega)]$$

where

$$\text{FORM 1: } a_n(\omega) = \frac{2}{\pi} \int_0^{\pi} \sin[\xi(\omega)] \sin(n\psi(\omega)] \, d\psi(\omega)$$

INTEGRATE BY PARTS & ELIMINATE $\psi(\omega)$

FORM 2: $$a_n(\omega) = \frac{2}{\pi}\int_0^{\pi}\cos\left[n\xi(\omega) - \frac{\epsilon}{\pi}n\beta_0 kx\int_0^{\infty} V(\lambda)\,\sin[\xi(\lambda)]\,d\lambda\right]\cos[\xi(\omega)]\,d\xi(\omega)$$

SPECIAL CASE - MONOCHROMATIC EXCITATION

$V(\omega) = V_0\,\delta(\omega - \Omega)$ ⟹ FUBINI SOLUTION

ARBITRARY FREQUENCY DISTRIBUTION

Cannot integrate over frequency domain because relation between $\xi(\omega)$ AND $\xi(\lambda)$ is not known

USE FOURIER SERIES TO ELIMINATE $\xi(\omega)$ IN FORM 1.

$$a_n(\omega) = \frac{2}{\pi}\int_0^{\pi}\left[\psi(\omega) + \frac{\epsilon}{\pi}\beta_0 kx\sum_{n=1}^{\infty} G_n[\psi(\omega)]\right] \times \sin[n\psi(\omega)]\,d\psi(\omega)$$

where

$$G_n[\psi(\omega)] = \int_0^{\infty} V(\lambda)\,a_n(\lambda)\,\sin[\psi(\lambda)]\,d\lambda\Big]$$

NOTE: $$\psi(\lambda) = \frac{\lambda}{\omega}\psi(\omega) + \frac{\lambda}{\omega}\theta(\omega) - \theta(\lambda)$$

PRESSURE

$$p = \frac{\epsilon}{\pi}\rho_0 c_0^2\sum_{n=1}^{\infty} G_n[\psi(\omega)]$$

ITERATIVE NUMERICAL ALGORITHM

1. DISCRETIZE FREQUENCY DOMAIN - INTEGRAL BECOMES A SUM.

2. DISCRETIZE PHASE VARIABLES OVER $0 < \psi < \pi$

   Converts $\psi(\omega)$ to $\psi_\ell(\omega_j)$

3. INITITIALIZE USING LINEAR THEORY: $a_n(\omega) = \delta_{1n}$

4. FOR EACH ω_j:

   (A) EVALUATE $G_n[\psi_\ell(\omega_j)]$ FOR EACH ℓ AND EACH n BY NUMERICAL INTEGRATION.

   (B) EVALUATE NEW ITERATION FOR $a_n(\omega_j)$ BY NUMERICAL INTEGRATION OVER DISCRETIZED VALUES OF $\psi(\omega)$.

5. CHECK FOR CONVERGENCE BY EXAMINING PRESSURES - RETURN TO STEP 4 TO CONTINUE ITERATION, IF NECESSARY.

****

THIS IS AN INEFFICIENT PROCEDURE.

IT IS UNNECESSARY FOR PLANAR WAVES.

GENERALIZATION FOR DISPERSIVE WAVES

FOURIER SPECTRUM OF WAVENUMBERS:

$$p = \frac{\epsilon}{2\pi}\rho_0 c_0^2 \int_{-\infty}^{\infty} F(k)\, \exp\Big[ik[\alpha(k) - c(k)t]\Big]\, dk$$

WHERE $\alpha(k)$ IS A STRAINED COORDINATE THAT VARIES WITH WAVENUMBER. FOR EXAMPLE,

$$x = \alpha(k) + \frac{\epsilon}{2\pi}\beta_0 x \int_{-\infty}^{\infty} F(k,\Lambda)\, \exp\Big[i\Lambda[\alpha(\Lambda) - c(\Lambda)t]\Big]\, d\Lambda$$

NOTE: $F(k,\Lambda)$ IS A MUTUAL INTERACTION FACTOR BETWEEN WAVELETS AT THE RESPECTIVE WAVENUMBERS.

RELEVANCE TO SOUND BEAM

LINEAR KING INTEGRAL:

$$p = \epsilon\rho_0 c_0^2 \int_0^\infty G(n)\, \exp\Big[i[\lambda(n)z - \omega t]\Big]\, J_0(nR)\, dn + c.c.$$

QUASI-CONICAL WAVES:

$$J_0(nR) = \tfrac{1}{2}[J_0(nR) + i\, J_1(nR)] + c.c.$$
$$= \tfrac{1}{2}Q(nR)\, \exp[i\Delta(nR)] + c.c.$$

TWO GROUPS

$$p = P^I + P^{II}$$

$$P^{I,II} = \tfrac{1}{2}\epsilon\rho_0 c_0^2 \int_0^\infty G(n)\, Q(nR)\, \exp\Big[i[\lambda(n)z \pm \Delta(nR) - \omega t]\Big]\, dn + c.c.$$

NONLINEAR ANALOG (GINSBERG, MIAO, & FODA, 1987)

$$P^J = \frac{1}{2}\epsilon\rho_0 c_0^2 \int_0^\infty G(n)\ \exp\Big[i[\lambda(n)\alpha^J(n) \pm \Delta(nR) - \omega t]\Big]\ dn + c.c.$$

COUPLED COORDINATE TRANSFORMATION

$$z = \alpha^I(n) - \epsilon \int_0^n \Big\{A(n,m)\ \exp\Big[i[\lambda(m)\alpha^I(m) + \Delta(mR) - \omega t]\Big] + B(n,m)\ \exp\Big[i[\lambda(m)\alpha^{II}(m) - \Delta(mR) - \omega t]\Big] + c.c.\Big\}\ dm$$

Similar form for $\alpha^{II}(n)$

NOTE: A(n,m) governs interaction WITHIN A GROUP

B(n,m) governs interaction BETWEEN GROUPS

CONCLUSIONS

1. IT IS POSSIBLE TO EVALUATE ARBITRARY PLANAR ACOUSTIC WAVES ANALOGOUSLY TO THE FUBINI SOLUTION.

2. FINITE AMPLITUDE RADIATION FROM A PROJECTOR IS AN INTERACTION PROCESS BETWEEN FINITE AMPLITUDE DISPERSIVE WAVES OF SIMPLE TYPE.

3. THE ANALOGY WITH THE FORM FOR PLANAR WAVES SUGGESTS A METHOD FOR EVALUATING THE COORDINATE TRANSFORMATIONS FOR A SOUND BEAM.

RAY SOLUTION FOR FINITE AMPLITUDE TWO DIMENSIONAL WAVES IN A HARD-WALLED RECTANGULAR WAVEGUIDE

Kun-Tien Shu
Jerry H. Ginsberg

Acoustics & Dynamics Research Laboratory
School of Mechanical Engineering
Georgia Institute of Technology
Atlanta, Georgia 30332

[Work supported by NSF and ONR]

The 115th meeting of Acoustical Society of America
Seattle, Washington
16-20 May 1988

NONDIMENSIONAL PERTURBATION WAVE EQUATIONS AND ASSOCIATED BOUNDARY CONDITIONS

$$\nabla^2\phi_1 - k^2\frac{\partial^2\phi_1}{\partial t^2} = 0$$

$$\nabla^2\phi_2 - k^2\frac{\partial^2\phi_2}{\partial t^2} = k^2\left[(\gamma-1)\frac{\partial\phi_1}{\partial t}\nabla^2\phi_1 + \frac{\partial}{\partial t}(\nabla\phi_1\cdot\nabla\phi_1)\right]$$

$$k = L\omega/c_0$$

- **Zero particle velocity transverse to the walls**
- **Excitation of the fundamental symmetric$(2,0)$mode**

$$\left.\frac{\partial\phi}{\partial z}\right|_{z=0} = -\epsilon W_{12}\sin(t)\cos(2\pi x)$$

$$\vec{v} = \nabla\phi \qquad \text{and} \qquad \epsilon = O(|\vec{v}|/c_0)$$

DECOMPOSITION OF THE LINEAR MODE SOLUTION INTO A PAIR OF OBLIQUE PLANAR WAVES

$$\phi_1 = -\frac{W_{12}}{\lambda_{12}} \cos(\lambda_{12} z - t) \cos(2\pi x) + (\phi_1)_{\text{exp}}$$

$$\lambda_{12} = \left[k^2 - (2\pi)^2\right]^{1/2} \qquad \text{for} \qquad k \geq 2\pi$$

$$\phi_1 = -A \exp[ik(-x \sin\theta + z \cos\theta - t/k)] - A \exp[ik(x \sin\theta + z \cos\theta - t/k)] + c.c.$$

where

$$A = \frac{1}{4} \frac{W_{12}}{\lambda_{12}} \qquad \text{and} \qquad \theta = \tan^{-1}\left(\frac{2\pi}{\lambda_{12}}\right)$$

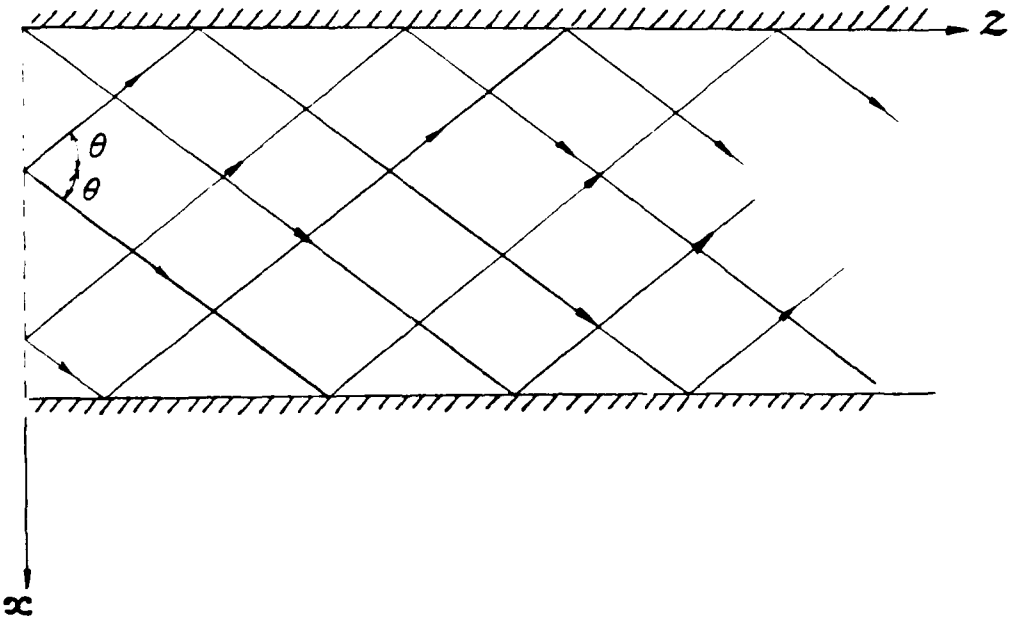

DISTORTION EFFECTS OF PLANAR WAVES REFLECTION

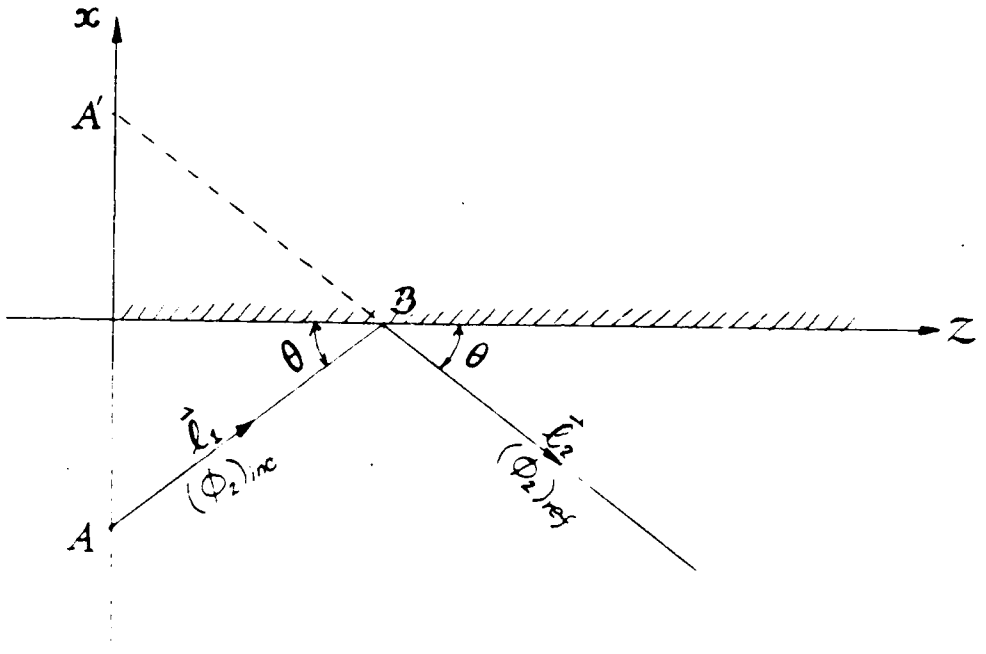

Nonlinear self-action:

$$(\phi_2)_{\text{inc}} \sim |\vec{\ell}_1 \cdot \vec{r}_{C/A}| \exp[i2k(z_1 - t/k)]$$

$$(\phi_2)_{\text{ref}} \sim |\vec{\ell}_2 \cdot \vec{r}_{C/A'}| \exp[i2k(z_2 - t/k)]$$

Nonlinear interaction:

$$\text{NSW} \sim e^{i2k(z\cos\theta - t/k)}$$

where

$$z_1 = x\sin\theta + z\cos\theta, \qquad z_2 = -x\sin\theta + z\cos\theta$$

REFLECTION PROCESS

The wave reflected at B:

$$\phi_{II} = -\epsilon A e^{ik(z_1 - t/k)} + \epsilon^2 B S_1 e^{i2k(z_1 - t/k)} + c.c.$$

The wave reflected at D:

$$\phi_{II'} = -\epsilon A e^{ik(z_2 - t/k)} + \epsilon^2 B S_2 e^{i2k(z_2 - t/k)} + c.c.$$

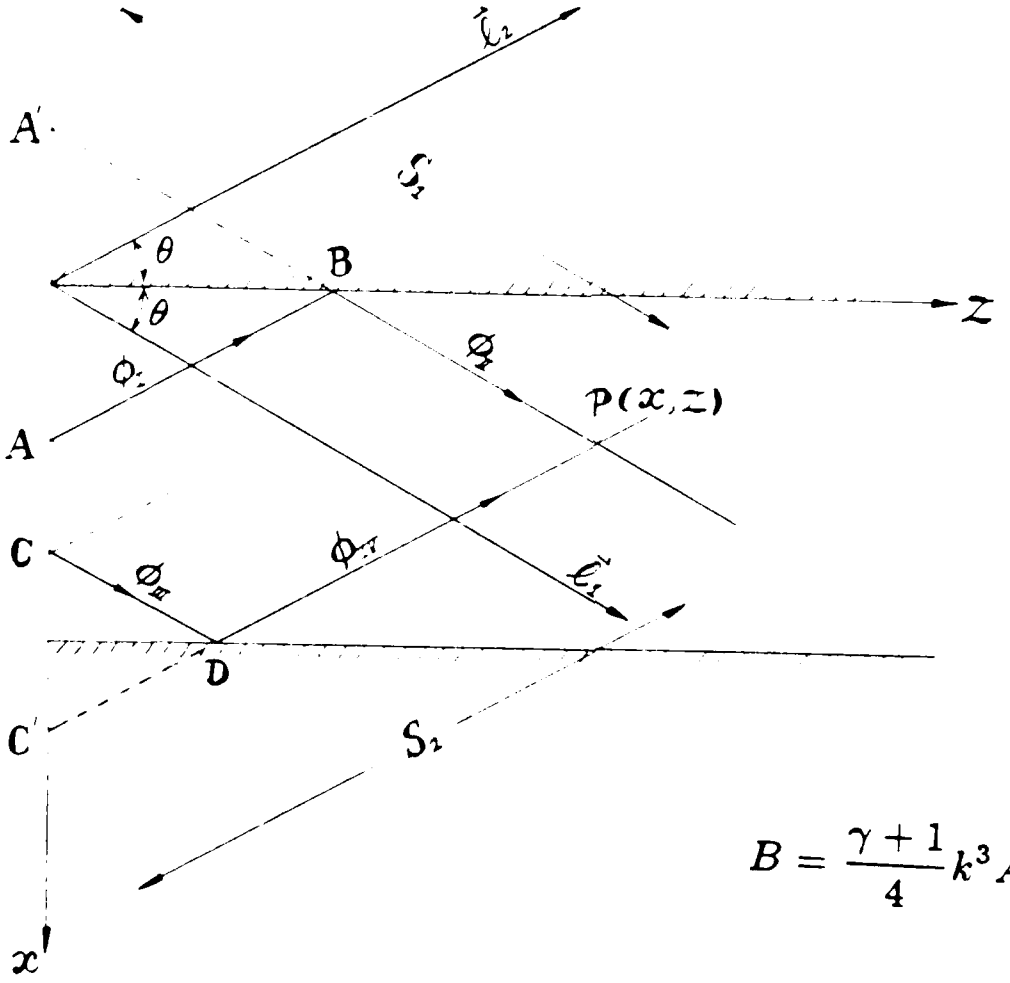

$$B = \frac{\gamma + 1}{4} k^3 A^2$$

SOLUTION BEFORE RENORMALIZATION

$$S_1 = S_2 = z \sec\theta$$

$$\begin{aligned}\phi(x,z,t) &= \phi_{II}(x,z,t) + \phi_{IV}(x,z,t) \\ &= \epsilon\phi_1(x,z,t) + \epsilon^2\phi_2(x,z,t)\end{aligned}$$

where

$$\phi_1 = -\frac{W_{12}}{\lambda_{12}} \cos(\lambda_{12} z - t) \cos(2\pi x)$$

$$\phi_2 = \frac{\gamma+1}{16} k^4 \frac{W_{12}^2}{\lambda_{12}^3} z \cos[2(\lambda_{12} z - t)] \cos(4\pi x)$$

RENORMALIZATION PROCESS

$$\vec{v}_{II} = \frac{\partial \phi_{II}}{\partial z_1}\vec{\ell}_1, \qquad \vec{v}_{IV} = \frac{\partial \phi_{IV}}{\partial z_2}\vec{\ell}_2$$

Near identity transformation

$$z_1 = \beta_1 + \epsilon S_1 Z_1(\beta_1, t), \qquad z_2 = \beta_2 + \epsilon S_2 Z_2(\beta_2, t)$$

Uniformly valid approximation

$$\vec{v}_{II} = 2\epsilon k A\vec{\ell}_1 \sin(k\beta_1 - t), \qquad \vec{v}_{IV} = 2\epsilon k A\vec{\ell}_2 \sin(k\beta_2 - t)$$

where

$$z_1 = \beta_1 + \epsilon\frac{4B}{kA} S_1 \sin(k\beta_1 - t)$$

$$z_2 = \beta_2 + \epsilon\frac{4B}{kA} S_2 \sin(k\beta_2 - t)$$

Paradox:

Individual wave distortion is scaled by travelling distance along propagation path of each wave(S_1 or S_2). But mode solution indicates that distortion only depend on axial distance along the waveguide.

COMBINATION OF TWO SET OF NORMALIZED PLANAR WAVES

$$(v_{II})_x = \vec{v}_{II} \cdot \vec{\ell}_1 \sin\theta, \qquad (v_{II})_z = \vec{v}_{II} \cdot \vec{\ell}_1 \cos\theta$$

$$(v_{IV})_x = -\vec{v}_{IV} \cdot \vec{\ell}_2 \sin\theta, \qquad (v_{IV})_z = \vec{v}_{IV} \cdot \vec{\ell}_2 \cos\theta$$

$$\begin{aligned} v_x &= (v_{II})_x + (v_{IV})_x \\ &= 2\epsilon k A \sin\theta[\sin(k\beta_1 - t) - \sin(k\beta_2 - t)] \end{aligned}$$

$$\begin{aligned} v_z &= (v_{II})_z + (v_{IV})_z \\ &= 2\epsilon k A \cos\theta[\sin(k\beta_1 - t) + \sin(k\beta_2 - t)] \end{aligned}$$

THERE IS NO PARADOX!

Near identity transformation of mode solution

$$x = \alpha + \epsilon X(\alpha, \beta, t), \qquad z = \beta + \epsilon Z(\alpha, \beta, t)$$

Coordinates transformation

$$z_1 = x \sin\theta + z \cos\theta, \qquad z_2 = -x \sin\theta + z \cos\theta$$

$$\beta_1 = \alpha \sin\theta + \beta \cos\theta, \qquad \beta_2 = -\alpha \sin\theta + \beta \cos\theta$$

$$x = (1/2 \sin\theta)(z_1 - z_2), \qquad z = (1/2 \cos\theta)(z_1 + z_2)$$

Uniformly valid particle velocity

$$v_x = \epsilon(2\pi)\frac{W_{12}}{\lambda_{12}} \cos(\lambda_{12}\beta - t) \sin(2\pi\alpha) + O(\epsilon^2)$$

$$v_z = \epsilon W_{12} \sin(\lambda_{12}\beta - t) \cos(2\pi\alpha) + O(\epsilon^2)$$

$$x = \alpha + \frac{\gamma + 1}{16\pi^2} \frac{k^4}{\lambda_{12}} z v_x$$

$$z = \beta + \frac{\gamma + 1}{4} \frac{k^4}{\lambda_{12}^3} z v_z$$

SUMMARY

- Rays behave as simple planar waves undergoing amplitude distortion

- Phases of fundamental and second harmonics depend on distance measured from the origin

- Distortion is proportional to total propagating distance from source to field point

- Amplitude along the wavefronts is not constant but phase is constant corresponding to each group of rays

- The ray solution is the same as a modal description of the wave propagation using separation of variables technique

- The total distortion process is scaled only by the axial distance along the waveguide

NOISE-CON 88
Purdue University
West Lafayette, Indiana
June 20-22, 1988

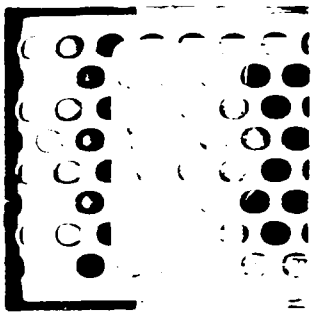

OBLIQUE REFLECTION AND MODE CONVERSION OF NONLINEAR DILATATIONAL WAVES AT A PLANAR BOUNDARY

Kun-Tien Shu and Jerry H. Ginsberg

School of Mechanical Engineering
Georgia Institute of Technology
Atlanta, Georgia 30332

I. INTRODUCTION

Because of the presence of nonlinearity in the equations of motion, the propagation of an initially sinusoidal, finite amplitude dilatational wave in a solid is accompanied by the generation of higher-order harmonics, corresponding to waveform distortion. Even under the simplification of linear theory, the reflection of planar stress waves at an interface is more complicated than the reflection of an acoustic wave in a fluid. Multiple stress and displacement conditions must be satisfied at the reflecting boundaries. Correspondingly, incidence of either dilatational waves or vertically polarized shear waves will result in mode conversion between these two types of wave. For example, P waves incident upon a stress-free boundary will reflect as SV waves, as well as P waves. Since such reflections play an important role in a variety of ultrasonic testing techniques, it is necessary to consider how nonlinearity affects mode conversion.

The problem of one-dimensional finite-amplitude elastic waves at normal incidence to a stress-free boundary was studied by Buck and Thompson[1] in 1966, based on a one-dimensional equation of motion for the Lagrangian displacement. Their analysis indicated that the amplitudes of the higher harmonics in the reflected wave should decrease due to phase reversal in the reflection, with the eventual result that they would vanish when the wave returns to its source. Van Buren and Breazeale[2,3] treated the reflection of finite-amplitude ultrasonic waves by assuming there is no coupling among the harmonics.

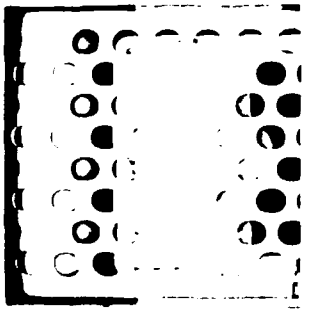

Studies of the reflection of obliquely incident finite amplitude waves have been limited for the most part to acoustic waves in fluids. The first study of a two-dimensional reflection problem was performed by Feng[4], who considered finite-amplitude sound waves upon reflection from a rigid wall at oblique incidence in the special case where the angle of incidence is 45°

Much later, Qian[5] extended Feng's work to the arbitrary, two-dimensional reflection problem. He found that nonlinear interaction of the incident and reflected waves produces a new type of constant magnitude second harmonic wave that propagates parallel to the surface, which he named the Q-wave.

In this paper, we consider all possible sources of accumulative effects in the propagation and reflection of nonlinear dilatational waves in an elastic half-space. Evaluation of nonlinear self-actions and interactions between incident and reflected waves is the main objective of this paper. In addition to nonlinear accumulative effects associated with self-action of the P waves, other types of non-growing second order effects are shown to occur, including the analogy of the Q-wave.

II. EQUATIONS OF MOTION

In the absence of body forces, the Lagrangian equations of motion for adiabatic dynamic deformation of an elastic solid are[6]

$$\rho_o u_{i,tt} - \rho_o(c_p^2 - c_s^2)u_{m,mi} - \rho_o c_s^2 u_{i,mm} = (\lambda + \mu + \frac{\beta}{4} + \frac{3}{4}\eta) \times(u_{n,m}u_{n,im} + u_{i,m}u_{n,nm}) + (\lambda + \frac{\beta}{4})u_{n,n}u_{i,mm} + (\mu + \frac{3}{4}\eta) \times(u_{n,i}u_{n,mm} + 2u_{m,n}u_{i,mn} + u_{i,n}u_{n,mm}) + \frac{1}{4}(\alpha + \beta)u_{n,n}u_{m,mi} + \frac{1}{4}(\beta + 3\eta)(u_{m,n}u_{n,im} + u_{n,i}u_{m,mn}) \quad (1)$$

where the summation convention applies. The corresponding stress-displacement equations are

$$L_{ij} = \lambda u_{m,m}\delta_{ij} + \mu(u_{i,j} + u_{j,i}) + (\frac{\lambda}{2}u_{m,n}u_{m,n} + \frac{\alpha}{8}u_{m,m}u_{n,n})\delta_{ij} + \frac{\beta}{4}u_{m,m}u_{j,i} + \frac{\beta}{8}(u_{m,n}u_{m,n} + u_{m,n}u_{n,m})\delta_{ij} + \frac{3}{4}\eta u_{j,m}u_{m,i} + (\lambda + \frac{\beta}{4})u_{m,m}u_{i,j} + (\mu + \frac{3}{4}\eta)(u_{i,m}u_{j,m} + u_{m,i}u_{m,j} + u_{i,m}u_{m,j}) \quad (2)$$

In these equations, u_i are the displacement components, λ and μ are Lamé coefficients, α, β, and η are third-order elastic constants, ρ_o is the initial density, and c_p and c_s are the propagation speeds of dilatational and shear waves, respectively. The dependent variables are expanded in perturbation series in a small parameter ϵ that scales the overall stress level.

$$u_i = \epsilon u_{i,1} + \epsilon^2 u_{i,2} + O(\epsilon^3), \quad L_{ij} = \epsilon L_{ij,1} + \epsilon^2 L_{ij,2} + O(\epsilon^3) \quad (3)$$

Substitution of Eqs. (3) into Eqs. (1) and (2), followed by matching of like powers of ϵ, converts the equations of motion and stress-displacement relations to the following form.

$$\frac{\partial^2 Q_i}{\partial t^2} - (c_p^2 - c_s^2)\frac{\partial^2 Q_m}{\partial x_m \partial x_i} - c_s^2 \frac{\partial^2 Q_i}{\partial x_m \partial x_m} = K_i \tag{4}$$

$$T_{ij} = \lambda \frac{\partial Q_m}{\partial x_m}\delta_{ij} + \mu\left(\frac{\partial Q_i}{\partial x_j} + \frac{\partial Q_j}{\partial x_i}\right) + G_{ij} \tag{5}$$

where Q_i represents either first- or second-order displacements to be determined, T_{ij} stands for either first- or second-order stresses, x_i are the Lagrangian coordinates, and the inhomogeneities K_i and G_{ij} are zero for the first order, while the second order terms are known in terms of the first order results. The analysis of aspecific system involves the solutioon of the perturbation wave equations (4) subject to a set of boundary conditions obtained from an appropriate combination of Eqs. (5) and displacement conditions.

III. REFLECTION AT A STRESS-FREE BOUNDARY

Consider finite-amplitude plane harmonic P waves propagating in the half-space $z \geq 0$. We assume a plane strain condition with the wave normal $\boldsymbol{\ell}$ in the xz-plane. If the wave arrives at the stress free surface in a weakly distorted manner as a result of nonlinearity preceding shock formation, its displacement may be written as

$$\mathbf{u} = \epsilon A_1 \boldsymbol{\ell} \exp[ik_p(\boldsymbol{\ell}\cdot\mathbf{r} - c_p t)] + \epsilon^2 A_2 \boldsymbol{\ell}(\boldsymbol{\ell}\cdot\mathbf{r})\exp[i2k_p(\boldsymbol{\ell}\cdot\mathbf{r} - c_p t)] \tag{6}$$

where k_p is the wavenumber of dilatational waves, and $\mathbf{r}$ is the position vector measured from the source. The amplitude constants are A_1 for first-order displacement and A_2 for second-order displacement, which is determined in terms of A_1 by obtaining a particular solution of second-order equations of motion. The second term on the right-hand side of Eq. (6) is an accumulative (growing) wave, which is generated by the self-action of the first-order incident wave. Let us consider a specific ray, originating from source A at (x_A, z_A), that is incident at the origin on the plane stress-free boundary.

(a) Linear Reflection The linearized reflection problem, which is governed by the first order version of Eqs. (4) subject to homogeneous boundary conditions derived from the first order form of Eqs. (5), can be solved by using the Helmholtz resolution theorem to decompose the equations of motion and boundary conditions into a pair of uncoupled problems[7]. The resulting first-order solutions for stress-free conditions at $z = 0$ are

Incident P wave: $A_1 \boldsymbol{\ell} \exp[ik_p(x \sin\theta - z\cos\theta - c_p t + \psi)]$ (7.a)

Reflected P wave: $B_1 \mathbf{m} \exp[ik_p(x \sin\theta + z\cos\theta - c_p t + \psi)]$ (7.b)

Reflected SV wave:

$$C_1(-j\times n)\exp[ik_s(x\sin\phi + z\cos\phi - c_s t + k_p\psi/k_s)] \qquad (7.c)$$

where matching trace velocities leads to Snell's law, $\sin\theta/\sin\phi = k_s/k_p = \gamma$, and the amplitudes of the first-order reflected P and SV waves satisfy

$$\frac{B_1}{A_1} = \frac{\sin 2\theta \sin 2\phi - \gamma^2\cos^2 2\phi}{\sin 2\theta \sin 2\phi + \gamma^2\cos^2 2\phi}, \quad \frac{C_1}{A_1} = \frac{-2\gamma \sin 2\theta \cos 2\phi}{\sin 2\theta \sin 2\phi + \gamma^2\cos^2 2\phi} \qquad (8)$$

In the foregoing, $\psi = z_A\cos\theta - x_A\sin\theta$, k_s is the wavenumber of the SV wave, and **m** and **n** are the normals to the wavefronts of the reflected P and SV waves, respectively.

(b) Reflection of Nonlinearly Generated Harmonics Because dilatational and shear waves are usually coupled by nonlinear terms, the Helmholtz resolution technique is not suitable for the evaluation of reflection coefficients for generated higher-order harmonics. Therefore, the second-order displacement equations is split into two parts through the substitution,

$$u_{i,2} = \sum_{\ell=1}^{2} v_{i,\ell} \qquad (9)$$

which decomposes the governing equations to

$$\frac{\partial^2 v_{i,\ell}}{\partial t^2} - (c_p^2 - c_s^2)\frac{\partial^2 v_{m,\ell}}{\partial x_m \partial x_i} - c_s^2 \frac{\partial^2 v_{i,\ell}}{\partial x_m \partial x_m} = K_{i,\ell}, \quad \ell = 1,2 \qquad (10.a)$$

$$\lambda \frac{\partial v_{m,\ell}}{\partial x_m}\delta_{ij} + \mu\left(\frac{\partial v_{i,\ell}}{\partial x_j} + \frac{\partial v_{j,\ell}}{\partial x_i}\right) = -G_{ij,\ell} \text{ on } z = 0 \qquad (10.b)$$

If terms are collected in a judicious manner, one is led to a representation in which $v_{i,1}$ is governed by inhomogeneous equations of motion ($K_{i,1} \neq 0$) and homogeneous boundary conditions. It will display cumulatively growing terms that become significant with increasing propagation distance. In contrast, the inhomogeneous boundary conditions ($G_{ij,2} \neq 0$ on $z = 0$) will be satisfied by $v_{i,2}$, whose homogeneous equations of motion cannot lead to secular terms in the second-order solutions. Although such solutions might represent new types of waves, they will always have small magnitude. It therefore is permissible to neglect $v_{i,2}$ in an analysis of the dominant nonlinear effects. Substituting the solution, Eq. (7,) into Eq. (10.a) leads to

$$\frac{\partial^2 v_{i,1}}{\partial t^2} - (c_p^2 - c_s^2)\frac{\partial^2 v_{m,1}}{\partial x_m \partial x_i} - c_s^2 \frac{\partial^2 v_{i,1}}{\partial x_m \partial x_m} = (A_2)_i \exp[i2k_p(x\sin\theta - z\cos\theta - c_p t + \psi)] + (B_2)_i \exp[i2k_p(x\sin\theta + z\cos\theta - c_p t + \psi)] + (C_2)_i \exp[i2k_s(x\sin\phi + z\cos\phi - c_s t + k_p\psi/k_s)] + (D_2)_i \exp[i2k_p(x\sin\theta - c_p t + \psi)] + (E_2)_i \exp\{i[(k_p\sin\theta + k_s\sin\phi)x + (k_s\cos\phi - k_p\cos\theta)z - 2\omega t + 2k_p\psi]\} + (F_2)_i \exp\{i[(k_p\sin\theta + k_s\sin\phi)x + (k_s\cos\phi + k_p\cos\theta)z - 2\omega t + 2k_p\psi]\} \quad (11)$$

The boundary conditions are

$$\lambda \frac{\partial v_{m,1}}{\partial x_m}\delta_{ij} + \mu\left(\frac{\partial v_{i,1}}{\partial x_j} + \frac{\partial v_{j,1}}{\partial x_i}\right) = 0 \quad \text{at } z = 0 \quad (12)$$

where $(A_2)_i, (B_2)_i, (c_2)_i, (D_2)_i, (E_2)_i$, and $(F_2)_i$ are function of ϑ. The first two terms on the right-hand side of Eq. (11) are self-products of first-order incident and reflected P waves, respectively. They are solutions of the homogeneous wave equation, so they are secular terms that generate cumulative growth in the corresponding particular solutions. In contrast, the third term in Eq. (11), which arises from nonlinear self-action of the first-order reflected SV wave, and the last three terms, which arise from products of two different first-order waves, are not solutions of the homogeneous wave equation. Hence, they do not result in accumulative waves. With these observation, it is reasonable to assume a trial solution of Eq. (11) subject to boundary conditions (12) as:

Incident P wave:

$$A_2 \ell(x\sin\theta - z\cos\theta + \psi)\exp[i2k_p(x\sin\theta - z\cos\theta - c_p t + \psi)] \quad (13.a)$$

Reflected P wave:

$$B_3 m \exp[i2k_p(x\sin\theta + z\cos\theta - c_p t + \psi)] + B_2 m(x\sin\theta + z\cos\theta + \psi)\exp[2ik_p(x\sin\theta + z\cos\theta - c_p t + \psi)] \quad (13.b)$$

Reflected SV wave:

$$C_3(-j\times n)\exp[i2k_s(x\sin\phi + z\cos\phi - c_s t + k_p\psi/k_s)] \quad (13.c)$$

Self-action of first-order SV wave:

$$C_2 \exp[i2k_s(x\sin\phi + z\cos\phi - c_s t + k_p\psi/k_s)] \quad (13.d)$$

Interaction of first-order incident and reflected P waves:

$$D_2 \exp[i2k_p(x\sin\theta - c_p t + \psi)] \quad (13.e)$$

Interaction of first-order incident P and reflected SV waves:

$$E_2 \exp\{i[(k_p \sin\theta + k_s \sin\phi)x + (k_s \cos\phi - k_p \cos\theta)z - 2\omega t + 2k_p \psi]\} \qquad (13.f)$$

Interaction between first-order reflected P and SV waves:

$$F_2 \exp\{i[(k_p \sin\theta + k_s \sin\phi)x + (k_s \cos\phi + k_p \cos\theta)z - 2\omega t + 2k_p \psi]\} \qquad (13.g)$$

The coefficients having subscript 2 are found by forming particular solutions of Eqs. (12). The coefficients of the cumulative growth terms are

$$\frac{A_2}{A_1^2} = \frac{B_2}{B_1^2} = \frac{12\lambda + 24\mu + \alpha + 6\beta + 24\eta}{16\rho_0 c_p^2} k_p^2 \qquad (14)$$

The other unknown amplitude constants B_3 and C_3 appearing in the trial solution (13) are determined by satisfying two stress-free boundary conditions. These two equations govern mode conversion among second-order incident P, reflected P and reflected SV waves. Note that secular terms arise only in the incident and reflected P waves as a continuing process of nonlinear self-action of a P waves on itself. No secular SV wave arises, which means that shearing effects will never deviate much from their linear representation. Expression (13.e) is the Q-wave, which always propagates parallel to the boundary surface.

ACKNOWLEDGEMENT

This work was supported by the National Science Foundation and the Office of Naval Research.

REFERENCES

1. Buck and D. O. Thompson, Mater. Sci. Eng., 1, 117-140 (1966).
2. A. L. Van Buren and M. A. Breazeale, J. Acoust. Soc. Am., 44, 1014-1020 (1968).
3. A. L. Van Buren and M. A. Breazeale, J. Acoust. Soc. Am., 44, 1021-1027 (1968).
4. Shao-sung Feng, Sov. Phys. Acoust., 6, pp. 488-490 (1961).
5. Zuwen Qian, Sci. Sin., 25, 492-501 (1982).
6. A. D. Fine, "Second Order Effects in the Propagation of Elastic Waves," Ph.D. Thesis, Brown University (1965).
7. L. M. Brekhovskikh, Waves in Layered Media, 2nd Ed. (Academic Press, New York, 1980).

NOISE-CON 88
Purdue University
West Lafayette, Indiana
June 20-22, 1988

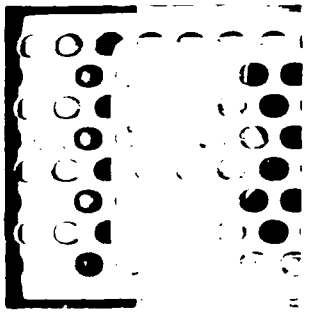

ANALYTICAL AND NUMERICAL TECHNIQUES FOR NONLINEAR DISTORTION IN SOUND BEAMS

Jerry H. Ginsberg

School of Mechanical Engineering
Georgia Institute of Technology
Atlanta, Georgia 30332

I. INTRODUCTION

Nonlinear effects in acoustic waves result in harmonic generation and depletion of the fundamental frequency level, which is manifested in the time domain by waveform distortion ultimately leading to the formation of shocks. Unlike one-dimensional waves, the signal radiated by a transducer displays diffractive effects, even in the linear regime. The interplay between diffraction and nonlinearity leads to distortion phenomena that are different in the compression and rarefaction phases [1]. A wide variety of techniques, both analytical and numerical, have been brought to bear on this problem.

II. LINEAR MODELS

Linear theories for the sound beam radiated by a harmonically vibrating transducer embedded in an infinite planar baffle are well developed, although exact solutions for the signal at an arbitrary location are available in quadrature form only. Such solutions for an arbitrary axisymmetric transducer have been derived from two viewpoints. One may consider the moving face of the transducer to consist of a distribution of sources. The Green's function for an infinite half-space is known from the method of images, from which one obtains the Rayleigh integral.

A less familiar treatment is the King integral [2], which results when one considers the fluid medium to be a circular waveguide of infinite diameter. The eigenvalues of such a system lie in a continuous spectrum, so a mode superposition corresponds to a Hankel integral transform. Let V_n denote the Hankel transform of the transducer velocity distribution $v(R)$. Then, the pressure is found from the inverse transform.

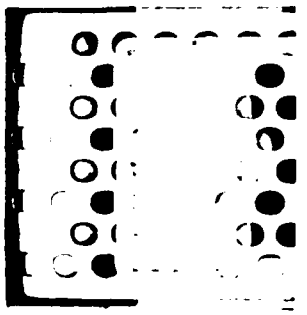

$$p = \epsilon \rho_0 c_0^2 \int_0^\infty \frac{nV_n}{i\mu_n} \exp[i(\omega t - \mu_n kz)]\, J_0(nkR)\, dn \qquad (1)$$

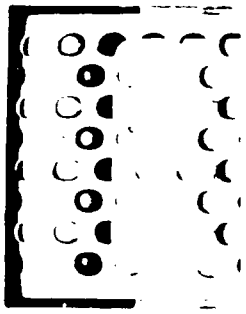

where (z,R) are cylindrical coordinates, and μ_n is the nondimensional axial wavenumber, $\mu_n^2 = 1 - n^2$. Numerical evaluation of the King integral is fairly efficient for the near field. However, its integrand oscillates rapidly as a function of n when either z or R is large, which requires a corresponding increase in the required number of integration sub-intervals.

III. NEAR FIELD PERTURBATION ANALYSIS

A nonlinear wave equation governing the potential function ϕ associated with an acoustic fluid is

$$c_0^4 \nabla^2\phi - c_0^2 \frac{\partial^2\phi}{\partial t^2} = \beta_0 \frac{\partial}{\partial t}\left(\frac{\partial\phi}{\partial t}\right)^2 , \quad p = -\rho_0 c_0^2 \frac{\partial\phi}{\partial t} \qquad (2)$$

where terms of $O(\phi^3)$ have been neglected because of their small magnitude in acoustic applications. Equations (2) were the basis of the paper by Ingenito and Williams [3], which was one of the first consistent analyses of nonlinearity in sound beams. Expansion of the potential in a perturbation series,

$$\phi = \epsilon\phi_1 + \epsilon^2\phi_2 + \cdots \qquad (3)$$

shows the first order equations to be those of the linear problem, for which the Rayleigh integral was used. This led to a Helmholtz equation for the second harmonic, in which the quadratic nonlinearity leads to inhomogeneous terms representing a spatial distribution of sources. An evaluation of the volume integral describing the combined effect of the second order source terms was carried out by using asymptotic reperesentations of several functions. A key feature of that analysis was the assumption that the signal propagates as a quasi-planar wave. The analysis is appropriate to a high frequency case, ka > 100, in a region that is neither very close to the transducer nor in the far field. Only the second harmonic along the axis of symmetry was evaluated, but Rogers [4] made comparable approximations to obtain a representation of the signal off-axis.

The results of this formulation matched well with measurements in the domain for which it was derived. However, the solution ignores the energy depletion in the fundamental harmonic that accompanies the formation of higher harmonics.

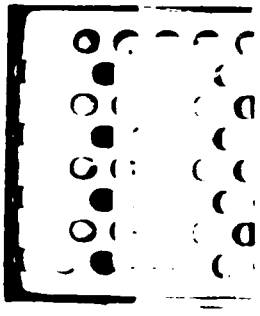

IV. SPHERICAL PROPAGATION MODELS

A different approach was taken by Lockwood, Muir, and Blackstock [5] in order to develop a far field model. It was assumed that the transducer drive level is sufficiently low to

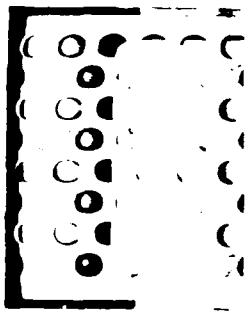

ignore distortion out to a radial distance r_d in the vicinity of the Rayleigh length $r_0 = ka^2/2$. Beyond that distance the sound beam has the appearance of a spherical wave with directivity. Matching the farfield solution for a finite amplitude spherical wave to the directivity properties for a linear sound beam at the transition distance led to the implicit representation

$$p = \epsilon\rho_0 c_0^2 kaD(\theta)\frac{r_d}{r}\sin\left[\omega t - kr + \beta_0 kr_d \ln\left(\frac{r}{r_d}\right)\frac{r}{r_d}\frac{p}{\rho_0 c_0^2}\right] \qquad (4)$$

where $D(\theta)$ is the sound beam directivity from linear theory. A variety of techniques are available for evaluating Eq. (4).

The primary difficulty with this formulation is the restriction to signal levels that are sufficiently small to suppress nonlinear distortion in the near field. Many applications require consideration of substantial near field distortion. A less obvious limitation of the theory is its prediction that higher harmonics are in-phase with the primary, which means that it cannot describe asymmetrical distortion of a waveform.

V. MODIFIED BURGERS' EQUATION

In regions not too close to the projector face, the pressure amplitude in a sound beam near its axis varies over a longer scale in the transverse direction than it does in the axial direction. In turn, that transverse scale is small compared to the distance at which nonlinear features become significant. These observations correspond to the dependency: $p = p(t - z/c_0, \sqrt{\epsilon}R, \epsilon z)$, which leads to a modified Burgers' equation [6]

$$\rho_0 c_0^2 \epsilon\left(4\frac{\partial^2}{\partial\tau\partial\sigma} - \nabla_\perp^2 - 4\alpha r_0\frac{\partial^3}{\partial\tau^3}\right) p = (2r_0/\ell_d)\frac{\partial^2}{\partial\tau^2}\left(p^2\right)$$

where $\tau = \omega t - kz$, $\sigma = z/r_0$, $\nabla_\perp^2$ is the transverse Laplace operator, α is an absorbtion coefficient, and ℓ_d is the distance at which a planar wave shocks.

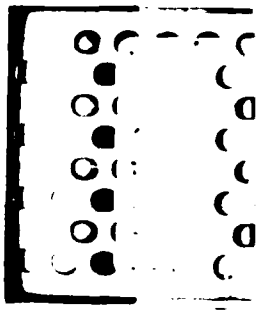

Since Eq. (5) is a parabolic differential equation, it has many advantages for numerical treatments. Other than its limitation to the paraxial region, its main restriction is that it is not valid for very short ranges. Also, cases of CW excitation of the transducer have thus far only been solved by finite difference techniques.

Soviet analyses for a transducer vibrating harmonically have employed a finite difference simulation of the three independent variables, τ, R, and σ, developed by Bakhvalov et al [7]. Their results agree qualitatively with measurements, in the sense that the asymmetrical features of waveform distortion are obtained. However, few evaluations were performed for the parameters of prior experiments, which led to conjecture that the formulation might suffer from instabilities. Also, the need to implement a

finite difference mesh for three variables imposes large computational demands.

Aanonsen et al [8] developed a different approach for solving Eq. (5). They exploited the periodicity of the signal to expand the pressure in a Fourier series, whose amplitudes are position dependent. Such an expansion leads to coupled partial differential equations for the amplitudes, thereby removing time from the equations to be solved. Although these equations still must be solved numerically, the Fourier series approach is an improvement because it does not require a finite difference grid for time. Results for amplitude levels compare well with far field measurements, but comparisons of waveforms with experiments have not been presented.

VI. NONLINEAR KING INTEGRAL

An analytical treatment aimed at an overall description has been pursued by the author, based on the the King integral representation of a sound beam. Like Ingenito and Williams' analysis, it uses the solution of the linear problem to generate the right side of Eq. (2). Due to the spectral form of the linear King integral, these source terms have the general form of an integral over two spectra of transverse wave numbers. Examination of the paraxial region and the region far off-axis leads to a dual-integral solution appropriate to both domains. That solution may be evaluated numerically to determine the second harmonic [9], but the result suffers from the same limitations as those for Ingenito and Williams' analysis.

Further examination of the first and second order terms reveals that each may be decomposed into two groups of quasi-conical wavelets. Each group exists in a spectrum of wavenumbers, with the conical angle of each wavelet depending on that number. The wavelets in the two groups are differentiated according to whether they propagate toward or away from the beam axis as they progress away from the transducer. The form of the perturbation solution at this stage of the analysis is

$$p/\rho_0 c_0^2 = \int_0^\infty \left[p^I + p^{II}\right] dn$$

$$p^J = \epsilon(nV_n Q_n/4i\mu_n)\exp(\psi_n^J)\left\{1 + \epsilon\int_0^n [g(\psi_m^J) + h(\psi_n^J)]\, dm\right\} \quad (6)$$

where J,K are either I or II. The parameters ψ_n^I and ψ_n^{II} are phase variables for the respective waves, $\psi_n^J = \omega t - \mu_n kz \pm \Delta_n$, while Q_n and Δ_n represent Bessel functions in polar form, $Q_n \cos \Delta_n = J_0(nkR)$, $Q_n \cos \Delta_n = J_1(nkR)$. The function g describes the degree of nonlinear interaction between wavelets at wave numbers m and n in the same group, while h describes the comparable interaction between wavelets in different groups.

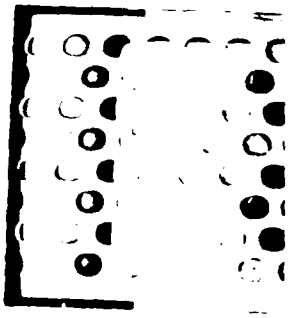

It is possible to integrate Eqs. (6) numerically. Such an evaluation reveals that the contribution of the second order effects associated with g grows with increasing distance, which means that the analysis is not uniformly valid. Such a situation is not unusual for perturbation expansions. It is generally the result of using independent variables for the formulation that do not match the physical scales, which may be corrected by a coordinate straining transformation. The transformation appropriate to Eqs. (6) was found [10] to have the form of a Fredholm integral equation. The essential features of wavelet J at transverse wave number n are given by

$$p^J = \epsilon(nV_nQ_n/4i\mu_n)\exp(i\alpha_n^J)$$

$$\psi_n^J = \alpha_n^J - 4\epsilon\int_0^n\left\{(V_mQ_m/\mu_m)\left[A\exp(i\alpha_m^J) + B\exp(i\alpha_m^K)\right] + C.C.\right\}dm \qquad (7)$$

where A and B are functions of n, m, and z. The parameters α_n^J are strained phase variables that resemble the linear phase variables only at very short ranges.

Quantitative evaluation of Eqs. (7) may be performed by a fairly simple numerical procedure. As is true for linear evaluations of the King integral, the computational effort grows with increasing distance, because of the need to increase the number of integration subintervals. For ranges comparable to the Rayleigh length the procedure becomes prohibitive. However, in that case the integrals may be evaluated analytically by asymptotic techniques, with the eventual solution taking on the form of a Fourier series whose coefficients are inverse Hankel transforms. That representation features numerical parameters whose value is irrelevant for long range predictions. However, improved agreement at shorter ranges requires comparison of theoretical predictions with experiment, which is work still in progress.

The only limitation imposed on the integral formulation is that shocks, which are analogous to the breaking of water waves as they steepen, do not occur. The results obtained from the nonlinear King integral display the steppening and asymmetrical distortion features observed in the waveforms of a finite amplitude sound beam, as shown in Fig. 1. Its predictions for levels of the fundamental and second harmonic are in close agreement with measurements, as shown by Fig. 2 for the experiment performed by Gould et al [11]. Data for comparison of waveforms is sparse because generating distorted low frequency waveforms requires a large and powerful low frequency projector, while accurate measurement of ultrasonic waveforms requires hydrophones having a small size (preferably, the diameter should be comparable to a wavelength) and wide bandwidth; such work is now underway by the author.

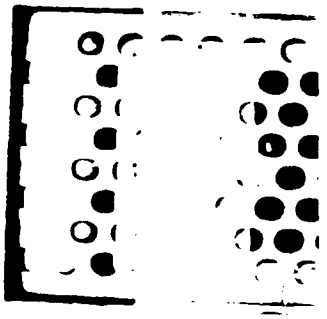

ACKNOWLEDGEMENT

This work was supported by the Office of Naval Research.

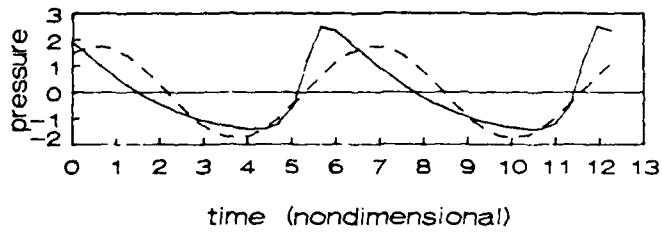

FIG. 1 Waveform on-axis at z = 200 mm, ω = 2.58 MHz, c_0 = 1475 m/s, a = 10.42 mm. ——— nonlinear; – – – linear.

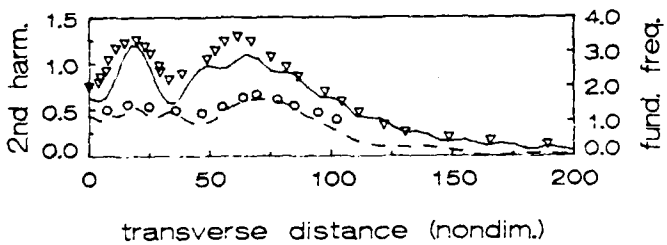

FIG. 2 Transverse amplitude profile at z = 50 mm, ω = 2.58 MHz, c_0 = 1475 m/s, a = 10.42 mm. ——— predicted fundamental; – – – predicted second harmonic; ∇ measured fundamental [11]; o measured second harmonic [11].

REFERENCES

1. D. G. Browning and R. H. Mellen, J. Acoust. Soc. Am. 44, 644-646 (1968).
2. E. Skudrzyk, The Foundations of Acoustics, Springer-Verlag, Berlin (1975).
3. F. Ingenito and A. O. Williams, Jr., J. Acoust. Soc. Am. 49, 319-328 (1971).
4. P. H. Rogers and A. O. Williams, Jr., J. Acoust. Soc. Am. 47, 82(A) (1970).
5. J. C. Lockwood, T. G. Muir, and D. T. Blackstock, J. Acoust. Soc. Am. 53, 1148-1153 (1970).
6. V. P. Kuznetsov, Sov. Phys. Acoust. 16, 467-470 (1971).
7. N. S. Bakhvalov, Ya. M. Zhileiken, E. A. Zabolotskaya, and R. V. Khokhlov, Sov. Phys. Acoust. 22, 272-274 (1976).
8. S. I. Aanonsen, T. Barkve, J. N. Tjøtta, and S. Tjøtta, J. Acoust. Soc. Am. 75, 749-768 (1984).
9. M. A. Foda and J. H. Ginsberg, J. Acoust. Soc. Am. 79, S31-S32 (1986).
10. J. H. Ginsberg, H. C. Miao, and M. A. Foda, J. Acoust. Soc. Am. 81, S25 (1987).
11. R. K. Gould, C. W. Smith, A. O. Williams, Jr., and R. P. Ryan, J. Acoust. Soc. Am. 40, 421-427 (1966).

OBLIQUE REFLECTION AND MODE CONVERSION OF NONLINEAR DILATATIONAL WAVES AT A PLANAR BOUNDARY

Kun-Tien Shu
Jerry H. Ginsberg

School of Mechanical Engineering
Georgia Institute of Technology
Atlanta, Georgia 30332

[Work supported by NSF and ONR]

Presented at 116 th Meeting of ASA

REFERENCES

Buck and Thompson(1966)

- One-dimensional finite amplitude waves reflected from a stress-free boundary
- higher-generated harmonics should decrease due to phase reversal

Van Buren and Breazeale(1968)

- Linear reflection process– No coupling among the harmonics

Qian(1982)

- Finite amplitude plane sound waves upon reflection from a boundary at oblique incidence
- Self-action:
  Secular 2nd order incident wave
  Secular 2nd order reflected wave
- Nonlinear interaction:
  Constant magnitude second harmonic

ASSUMPTIONS

- **ADIABATIC**
- **ISOTROPIC ELASTIC MATERIAL**
  - **Geometrical nonlinearity**
- **NO SHOCK FORMATION ON THE WHOLE PROCESS**
- **PLANE HARMONIC EXCITATION**

BASIC EQUATIONS

Momentum equation:

$$L_{ij,j} = \rho_o u_{i,tt}$$

Constitutive equation:

$$L_{ij} = \rho_o \frac{\partial U}{\partial u_{i,j}}$$

Nonlinear geometrical strain-displacement:

$$\gamma_{ij} = \frac{1}{2}(u_{i,j} + u_{j,i} + u_{k,i}u_{k,j})$$

where

$L_{ij} \equiv$ Lagrangian stress tensor
$U \equiv$ Strain energy density function
$\gamma_{ij} \equiv$ Green's strain tensor

EXPRESSION FOR STRAIN ENERGY FUNCTION

$$\rho_o U = \frac{1}{2} C_{ijkl}\gamma_{ij}\gamma_{kl} + \frac{1}{24} C_{ijklmn}\gamma_{ij}\gamma_{kl}\gamma_{mn} + \text{high-order terms}$$

where

$$C_{ijkl} = \lambda\delta_{ij}\delta_{kl} + \mu(\delta_{ik}\delta_{jl} + \delta_{il}\delta_{jk})$$

$$\begin{aligned} C_{ijklmn} = {} & \alpha\delta_{ij}\delta_{kl}\delta_{mn} + \beta[\delta_{ij}(\delta_{km}\delta_{ln} + \delta_{kn}\delta_{lm}) \\ & + \delta_{kl}(\delta_{im}\delta_{jn} + \delta_{in}\delta_{jm} + \delta_{mn}(\delta_{ik}\delta_{jl} + \delta_{il}\delta_{jk})] \\ & + 3\eta[\delta_{ik}(\delta_{lm}\delta_{nj} + \delta_{ln}\delta_{mj}) + \delta_{il}(\delta_{km}\delta_{nj} + \delta_{kn}\delta_{mj}) \\ & + \delta_{jk}(\delta_{lm}\delta_{ni} + \delta_{ln}\delta_{mi}) + \delta_{jl}(\delta_{km}\delta_{ni} + \delta_{kn}\delta_{mi})] \end{aligned}$$

and

$\lambda, \mu \equiv$ Lamé coefficients

$\alpha, \beta, \eta \equiv$ third-order elastic constants

NONLINEAR EQUATIONS OF MOTION

$$\begin{aligned}\rho_o u_{i,tt} = {} & \rho_o(c_p^2 - c_s^2)u_{m,mi} + \rho_o c_s^2 u_{i,mm} \\ & + (\lambda + \mu + \frac{\beta}{4} + \frac{3}{4}\eta)(u_{n,m}u_{n,im} + u_{i,m}u_{n,mn}) \\ & + (\lambda + \frac{\beta}{4})u_{n,n}u_{i,mm} + \frac{1}{4}(\alpha + \beta)u_{n,n}u_{m,mi} \\ & + (\mu + \frac{3}{4}\eta)(u_{n,i}u_{n,mm} + 2u_{m,n}u_{i,mn} + u_{i,n}u_{n,mm}) \\ & + \frac{1}{4}(\beta + 3\eta)(u_{n,i}u_{m,mn} + u_{m,n}u_{n,im})\end{aligned}$$

STRESS-DISPLACEMENT EQUATIONS

$$\begin{aligned}L_{ij} = {} & \lambda u_{m,m}\delta_{ij} + \mu(u_{i,j} + u_{j,i}) \\ & + (\frac{\lambda}{2}u_{m,n}u_{m,n} + \frac{\alpha}{8}u_{m,m}u_{n,n})\delta_{ij} \\ & + \frac{\beta}{8}(u_{m,n}u_{m,n} + u_{m,n}u_{n,m})\delta_{ij} \\ & + (\mu + \frac{3}{4}\eta)(u_{i,m}u_{j,m} + u_{m,i}u_{m,j} + u_{i,m}u_{m,j}) \\ & + \frac{\beta}{4}u_{m,m}u_{j,i} + \frac{3}{4}\eta u_{j,m}u_{m,i} + (\lambda + \frac{\beta}{4})u_{m,m}u_{i,j}\end{aligned}$$

PERTURBATION EQUATIONS

$$u_i = \epsilon u_i^{(1)} + \epsilon^2 u_i^{(2)} + O(\epsilon^3)$$

$$L_{ij} = \epsilon L_{ij}^{(1)} + \epsilon^2 L_{ij}^{(2)} + O(\epsilon^3)$$

$$\frac{\partial^2 Q_i}{\partial t^2} - (c_p^2 - c_s^2)\frac{\partial^2 Q_m}{\partial x_m \partial x_i} - c_s^2 \frac{\partial^2 Q_i}{\partial x_m \partial x_m} = K_i$$

$$T_{ij} = \lambda \frac{\partial Q_m}{\partial x_m}\delta_{ij} + \mu\left(\frac{\partial Q_i}{\partial x_j} + \frac{\partial Q_j}{\partial x_i}\right) + G_{ij}$$

where

$$K_i, G_{ij} = \begin{cases} 0, & O(\epsilon^1) \\ f(u_i^{(1)}), & O(\epsilon^2) \end{cases}$$

REFLECTION AT A STREE-FREE PLANE BOUNDARY

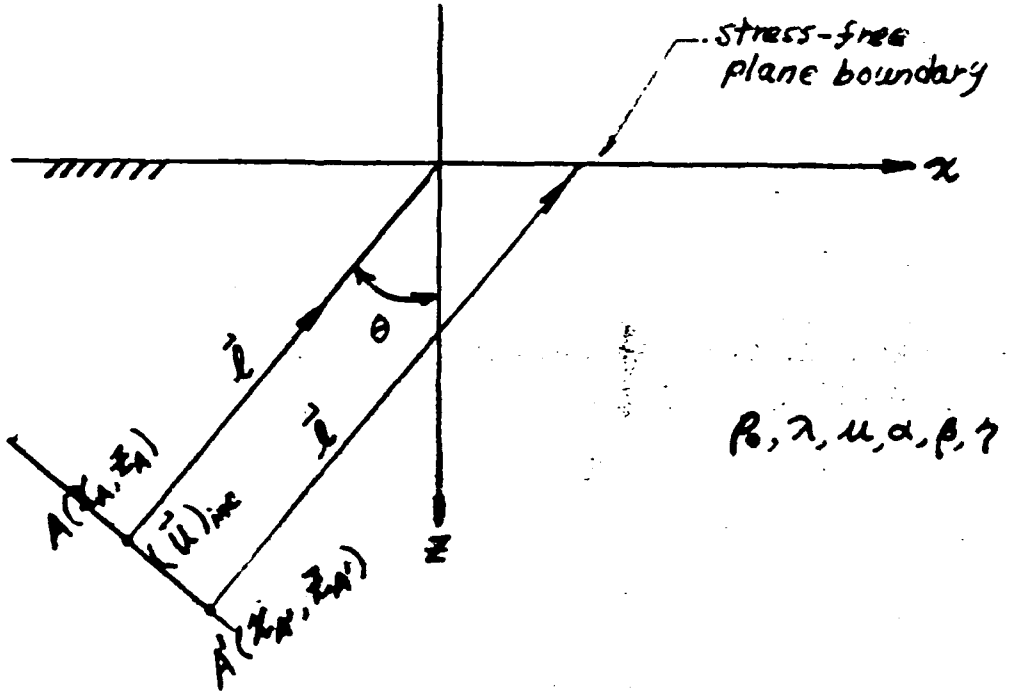

Planar incident P wave:

$$(\vec{u})_{\text{inc}} = \epsilon A_1 \vec{l} \exp[ik_p(\vec{l}\cdot\vec{r} - c_p t)] + \epsilon^2 A_2 \vec{l}(\vec{l}\cdot\vec{r}) \exp[i2k_p(\vec{l}\cdot\vec{r} - c_p t)]$$

where

$$\vec{l} = \sin\theta\vec{e}_x - \cos\theta\vec{e}_z$$

⋆ Plane strain condition

LINEAR REFLECTION

$$O(\epsilon): \qquad u_{i,tt}^{(1)} - (c_p^2 - c_s^2)u_{j,ji}^{(1)} - c_s^2 u_{i,jj}^{(1)} = 0$$

$$L_{ij}^{(1)} = \lambda u_{m,m}^{(1)} \delta_{ij} + \mu(u_{i,j}^{(1)} + u_{j,i}^{(1)})$$
$$= 0 \qquad \text{on} \qquad z = 0$$

First-order Solution

$$(P_1)_{\text{inc}} = A_1 \vec{l} e^{ik_p(x \sin\theta - z\cos\theta - c_p t + \psi)}$$

$$(P_1)_{\text{ref}} = B_1 \vec{n} e^{ik_p(x \sin\theta + z\cos\theta - c_p t + \psi)}$$

$$(SV_1)_{\text{ref}} = C_1(\vec{e}_y \times \vec{n}) e^{ik_s(x \sin\phi + z\cos\phi - c_s t + \psi/\gamma)}$$

where

$$\frac{B_1}{A_1} = \frac{\sin 2\theta \sin 2\phi - \gamma^2 \cos^2 2\phi}{\sin 2\theta \sin 2\phi + \gamma^2 \cos^2 2\phi}$$

$$\frac{C_1}{A_1} = \frac{2\gamma \sin 2\theta \cos 2\phi}{\sin 2\theta \sin 2\phi + \gamma^2 \cos^2 2\phi}$$

and

$$\gamma = \frac{\sin\theta}{\sin\phi} = \frac{k_s}{k_p}$$

$$\psi = -x_A \sin\theta + z_A \cos\theta$$

REFLECTION OF GENERATED HARMONICS

$$u_i^{(2)} = \sum_{\ell=1}^{3} v_{i,\ell}$$

$$\begin{cases} \dfrac{\partial^2 v_{i,1}}{\partial t^2} - (c_p^2 - c_s^2)\dfrac{\partial^2 v_{m,1}}{\partial x_m \partial x_i} - c_s^2 \dfrac{\partial^2 v_{i,1}}{\partial x_m \partial x_m} = K_{i,1} \\ \lambda \dfrac{\partial v_{m,1}}{\partial x_m}\delta_{ij} + \mu\left(\dfrac{\partial v_{i,1}}{\partial x_j} + \dfrac{\partial v_{j,1}}{\partial x_i}\right) = 0 \qquad \text{on} \quad z = 0 \end{cases}$$

$$\begin{cases} \dfrac{\partial^2 v_{i,2}}{\partial t^2} - (c_p^2 - c_s^2)\dfrac{\partial^2 v_{m,2}}{\partial x_m \partial x_i} - c_s^2 \dfrac{\partial^2 v_{i,2}}{\partial x_m \partial x_m} = 0 \\ \lambda \dfrac{\partial v_{m,2}}{\partial x_m}\delta_{ij} + \mu\left(\dfrac{\partial v_{i,2}}{\partial x_j} + \dfrac{\partial v_{j,2}}{\partial x_i}\right) = -G_{ij,2} \quad \text{on} \quad z = 0 \end{cases}$$

where

$$K_i = K_{i,1} + \underbrace{K_{i,2}}_{=0} \qquad \text{and} \qquad G_{ij} = \underbrace{G_{ij,1}}_{=0} + G_{ij,2}$$

SECOND-ORDER NONLINEAR EFFECTS

$O(\epsilon^2)$:

Nonlinear self-action of $(P_1)_{\text{inc}}$:

$$(P_2^N)_{\text{inc}}: \quad A_2\vec{l}(x\sin\theta - z\cos\theta + \psi)e^{i2k_p(x\sin\theta - z\cos\theta - c_p t + \psi)}$$

Nonlinear self-scattering of $(P_1)_{\text{ref}}$:

$$(P_2^N)_{\text{ref}}: \quad B_2\vec{m}(x\sin\theta + z\cos\theta)e^{i2k_p(x\sin\theta + z\cos\theta - c_p t + \psi)}$$

Nonlinear self-scattering of $(SV_1)_{\text{ref}}$:

$$(SS)_{\text{ref}}: \quad \vec{C}_2 e^{i2k_s(x\sin\phi + z\cos\phi - c_s t + \psi/\gamma)}$$

where

$$\frac{A_2}{A_1^2} = \frac{B_2}{B_1^2} = \frac{12\lambda + 24\mu + \alpha + 6\beta + 24\eta}{16\rho_o}\left(\frac{k_p}{c_p}\right)^2$$

$$\sim \frac{\omega^2}{c_p^4}$$

Nonlinear interaction of $(P_1)_{\text{inc}}, (P_1)_{\text{ref}}$:

$$\text{Q-wave:} \quad \vec{D}_2 e^{i2k_p(x\sin\theta - c_p t + \psi)}$$

$$\text{phase speed} = c_p / \sin\theta$$

Nonlinear interaction of $(P_1)_{\text{inc}}, (SV_1)_{\text{ref}}$:

$$\vec{E}_2 e^{i2k_p[x\sin\theta + 1/2 \cdot (\cos\phi/\gamma - \cos\theta)z - c_p t + \psi]}$$

$$\text{phase speed} = \frac{c_p}{\sqrt{(\gamma\sin\phi + \sin\theta)^2 + (\gamma\cos\phi - \cos\theta)^2}}$$

Nonlinear interaction of $(P_1)_{\text{ref}}, (SV_1)_{\text{ref}}$:

$$\vec{F}_2 e^{i2k_p[x\sin\theta + 1/2 + (\cos\phi/\gamma + \cos\theta)z - c_p t + \psi]}$$

$$\text{phase speed} = \frac{c_p}{\sqrt{(\gamma\sin\phi + \sin\theta)^2 + (\gamma\cos\phi + \cos\theta)^2}}$$

PROPAGATING EFFECTS

$(P_2^N)_{inc}$: Accumulative wave – become significant with increasing propagating distance away from source A

$(P_2^N)_{ref}$: Accumulative wave – become significant with increasing propagating distance away from reflected point

$(SS)_{ref}$: Constant magnitude dilatational wave

Q-wave: Non-secular wave – propagates parallel to the boundary surface

$$\tan\varphi' = \frac{r\sin\phi + \sin\theta}{r\cos\phi - \cos\theta}$$

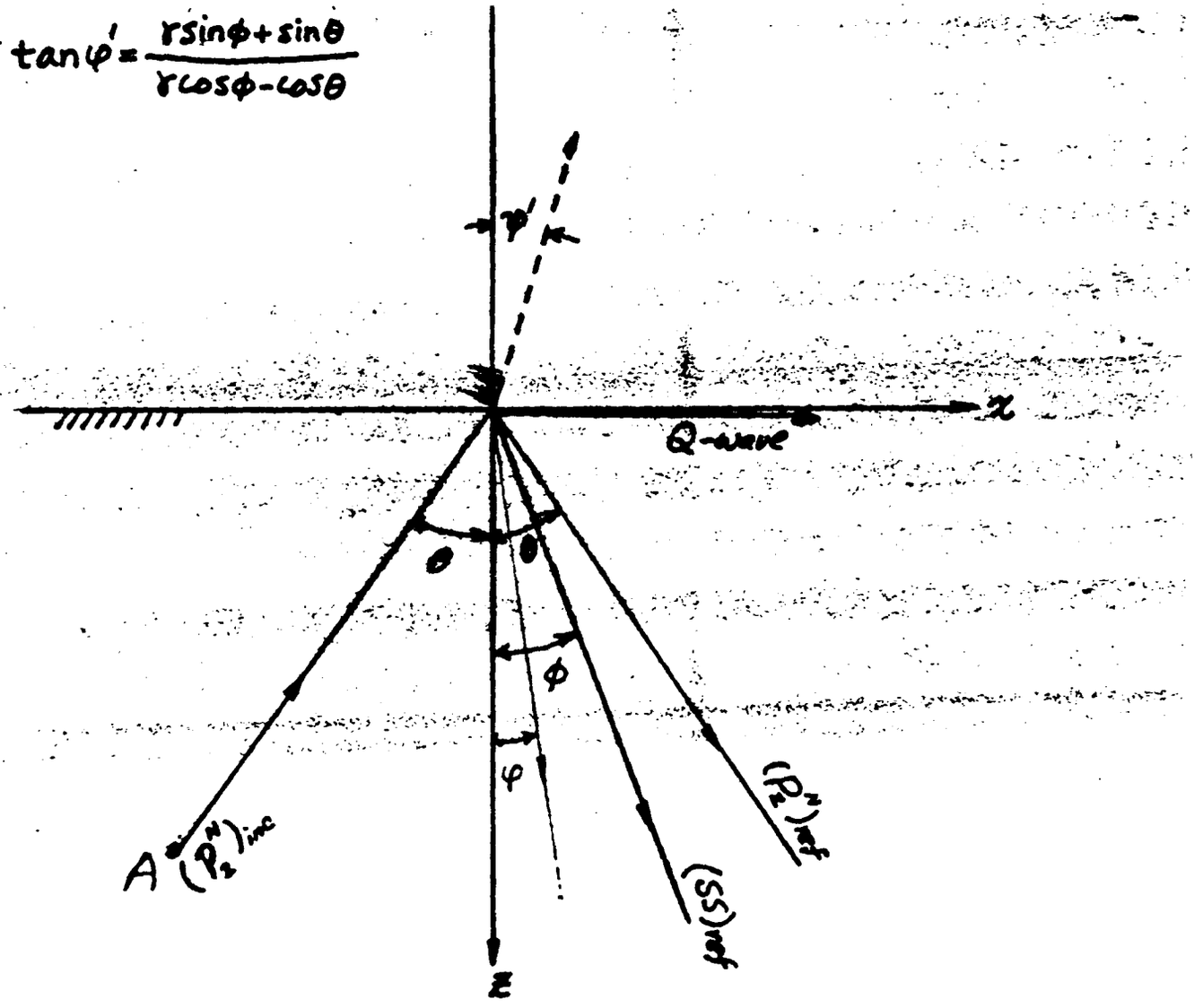

$$\tan\varphi = \frac{r\sin\phi + \sin\theta}{r\cos\phi + \cos\theta}$$

MODE VONVERSION

Boundary effects

$$(P_2)_{\text{inc}} = A_2\vec{\ell}\psi e^{i2k_p(x\sin\theta - z\cos\theta - c_p t+\psi)}$$

$$(P_2^B)_{\text{ref}} = B_3\vec{m}e^{i2k_p(x\sin\theta + z\cos\theta - c_p t+\psi)}$$

$$(SV_2^B)_{\text{ref}} = C_3(\vec{e}_y \times \vec{n})e^{i2k_s(x\sin\phi + z\cos\phi - c_s t+\psi/\gamma)}$$

- **Linear Reflection Theory**
- **Constant Amplitude**

SUMMARY

- Secular terms arise only in the incident and reflected P waves as a continuing process of nonlinear self-action of a P wave on itself

- No secular SV waves arise – Shearing effects will never deviate much from their linear representation

- Q-wave is shown to occur in solids too

- Accumulative effects of reflected P waves are proportional to ω^2

- Mode conversions are governed by linear reflection law

Finite amplitude effects in a dual frequency acoustic beam

M. A. Foda[a] and J. H. Ginsberg
The George W. Woodruff School of Mechanical Engineering, Georgia Institute of Technology, Atlanta, Georgia 30332

(Received 25 November 1986; accepted for publication 14 October 1988)

When an axisymmetric, bifrequency transducer mounted in a rigid baffle is excited at acoustic Mach numbers that are a relatively large fraction, the result is a dual frequency sound beam that exhibits harmonic and intermodulation distortion. The present analysis of this problem develops a perturbation solution based on a wave equation that consistently accounts for nonlinearity and diffraction. The linearized problem is described by a King integral for the sound beam at each primary frequency. Asymptotic analysis using Laplace's method of integration is used to find the second-order potential. The method of renormalization then leads to a uniformly accurate expression for the acoustic pressure. A technique for improvement in computational efficiency is developed by interfacing the King integral predictions to a farfield model for quasispherical waves. Propagation curves for parametric arrays obtained from the model compare favorably with experimental observations.

PACS numbers: 43.25.Lj

LIST OF SYMBOLS

a	circular piston radius
c_0	small signal speed of sound in linear theory
$D_{j_k}(\theta)$	directivity of the spectral component having frequency $j\omega_1 + k\omega_2$ at the spherical transition
$f_j(R)$	amplitude shading functions for the transducer oscillation at each primary frequency
$J_n(x)$	Bessel function of order n
m,n	transverse wavenumber
P_{-R},P_{+R}	outward and inward transverse-axial waves
r	range from the projector
r_0	the range at which spherical divergence begins
$V_j(n)$	Hankel transform of $f_j(R)$
z,R	axisymmetric cylindrical coordinates (dimensional values are z/k, R/k)
$\alpha_j,\beta_j,\xi_j,\eta_j$	strained coordinates for each primary sound beam
β_0	coefficient of nonlinearity
$\epsilon\epsilon_j$	acoustic Mach number in the primary sound beams
μ_n	axial wavenumber
ρ_0	density at ambient conditions
ϕ	velocity potential
ω_0	mean of the primary frequencies (rad/s)
ω_1,ω_2	primary frequencies (dimensional values are $\omega_0\omega_1$, $\omega_0\omega_2$)
$\omega_d = \omega_1 - \omega_2$	difference of nondimensional primary frequencies
$\omega_s = \omega_1 + \omega_2$	sum of the nondimensional primary frequencies
*	denotes complex conjugate

INTRODUCTION

In 1963, Westervelt[1] introduced the concept of a parametric array as a consequence of nonlinear interaction of sound beams at closely spaced primary frequencies. Since Westervelt's work, other theoretical models predicting the difference frequency sound have been proposed. These models have variously employed quasiplanar and quasispherical approximations, and a modified Burgers' equation. The accuracy of each of these models depends on various assumptions concerning the spatial dependence of the primary acoustic fields, the position of the observation point, and the effect of attenuation. For a review of various models, we refer the reader to Fenlon[2] and Bjorno.[3]

The existing models are not able to explain some experimental discrepancies. The primary cause for this lack of agreement seems to be that the hypotheses on which the analyses are based are not always met in practice. For example, in linear theory, diffractive fluctuations in the nearfield of a piston-generated sound beam cannot be approximated by a plane wave, see Zemanek.[4] We shall see that because existing theories have not completely described these complexities in the nearfield of the primary beams, the result is inaccuracy in their description of the nonlinear interaction of primaries.

A different viewpoint of this question arises from recognition that the formation of the second harmonic in a single primary beam is a special case of harmonic generation in the interaction of two primaries. Second-harmonic generation in the acoustic field of a baffled transducer driven sinusoidally at high amplitude has been analyzed by several investigators.

[a] Present address: Department of Mechanical Engineering, EL-Mansoura University, EL-Mansoura, Egypt.

 0001-4966/89/051857-15$00.80

Ingenito and Williams[5] employed a perturbation series for the potential function, in which the leading term was described by the Rayleigh integral. Their solution was not uniformly accurate from the viewpoint of perturbation theory, corresponding to a limitation to the field close to the transducer. In addition, it is valid only for situations where the axial wavelength is very small compared to the transducer radius ($ka > 100$, according to Ref. 5). Lockwood *et al.*[6] neglected nearfield distortion by assuming that the acoustic signal at the beginning of the farfield is a pure sine wave of amplitude proportional to the small signal directivity factor for the piston. This assumption is violated when the source pressure level is sufficient to generate significant distortion within the nearfield. Neglecting nearfield distortion leads to a farfield model based on Lockwood's analysis of nonuniform spherical waves.[7]

One approach for remedying the foregoing limitation is a version of Burgers' equation that has been modified to account for variation transverse to the propagation direction; this model was first derived by Zabolotskaya and Khokhlov[8] for the nondissipative case. The most generally valid solution, which was derived by Aanonsen *et al.*[9] and extended by Hamilton *et al.*[10] has the form of a temporal Fourier series whose coefficients are determined by numerically solving coupled differential equation in the spatial coordinates. A full finite difference solution in space and time apparently was first presented by Bakvalov *et al.*[11] It is not possible in either approach to solve for the signal at isolated locations. Also, the assumptions inherent to the derivation of the Burgers' equation cause concern regarding its suitability for the nearfield.

Ginsberg[12,13] used a perturbation approach to solve a consistent nonlinear wave equation for the velocity potential. The linearized signal was described by the King integral. Uniformly valid expressions for the state variables were derived by employing coordinate transformations that yielded explicit formulas in the form of inversions of Hankel transforms.

The present analysis, which is an outgrowth of Ginsberg's work, treats the interaction of two primary beams at arbitrary frequencies. Prior work on sound beams generated by multiple-frequency inputs have, for the most part, considered parametric array problems, in which the two frequencies are relatively close. The implementation of nonlinear parabolic equations for such problems has been of particular concern to J. N. Tjøtta and S. Tjøtta, who have used the quasilinear approximation to evaluate the difference frequency in parametric arrays.[14] We shall use results for parametic array for comparisons with our analytical predictions, but the parametric array is substantially less general than the problem we treat here.

Situations involving two arbitrary frequencies were addressed in Refs. 15–16. Those investigations, which employed a quasilinear approximation, were limited to the evaluation of the difference and sum frequencies and the second harmonic. In contrast, the goal of the present study is to obtain an overall model that can be used to evaluate waveforms, from which the full spectrum of harmonics may be obtained. We decided that meeting this objective with a numerical model based on Aanonsen's temporal Fourier series formulation would be difficult, due to the computational requirements associated with the need to employ a dual series when the two input frequencies do not correspond to a purely periodic input.

The present investigation employs analytical techniques to account consistently for cumulative growth effects, as well as diffraction. The model is derived from the nonlinear wave equation governing the second-order velocity potential, subject to prescribed boundary conditions on the source and the baffle. It is valid up to the shock formation distance, hence, in both nearfield and farfield regions, subject to the assumption that dissipation is negligible.

The derivation begins by describing each primary beam as a King integral, which is obtained from a Hankel transform in the transverse direction. Asymptotic analysis using Laplace's method of integration leads to the second-order potential, which is subsequently corrected for irregularities in the acoustic pressure through coordinate transformations. Computational difficulties inherent to the result are addressed by interfacing the computed results to the Lockwood model for the farfield of a nonuniform spherical source.

I. EQUATIONS

We formulate the problem in nondimensional cylindrical coordinates (R,z), where $z = 0$ defines the plane occupied by the transducer and baffle and $R = 0$ at the center of the transducer. Let t denote the nondimensional time variable. The corresponding dimensional position coordinates are $(R/k, z/k)$ and dimensional time is t/ω_0, where ω_0 is the mean of the primary frequencies and $k = \omega_0/c_0$ is the wavenumber of a nominal planar wave. Under the assumptions that the fluid is inviscid and that the particle motion is irrotational, we introduce a dimensionless potential function $\phi(R,z,t)$, which is related to the particle velocity components and the acoustic pressure by

$$v_z = c_0 \frac{\partial \phi}{\partial z}, \quad v_R = c_0 \frac{\partial \phi}{\partial R}, \quad p = -\rho_0 c_0^2 \frac{\partial \phi}{\partial t}. \tag{1}$$

Note that there are second-order terms in the last of the foregoing, but their effect is not significant for the present analysis.

We consider the transducer to oscillate axisymmetrically at two distinct frequencies whose dimensional values are $\omega_0\omega_j$. The spatial shading functions $f_j(R)$ are associated with each frequency. The corresponding boundary condition may be written as

$$\left.\frac{\partial \phi}{\partial z}\right|_{z=0} = \frac{\epsilon}{2i}[\epsilon_1 f_1(R)\exp(i\omega_1 t) + \epsilon_2 f_2(R)\exp(i\omega_2 t)] + \text{c.c.}, \tag{2}$$

where c.c. will generally denote the complex conjugate of all preceding terms. It is permissible for the functions $f_j(R)$ to be complex, corresponding to spatial phasing. We require that these functions be bounded such that $R^{1/2} f_j(R)$ is piecewise continuous and absolutely integrable[17] over $R > 0$. The parameters ϵ_j are fractions of the total acoustic Mach number ϵ associated with each primary.

The nonlinear wave equation governing ϕ is obtained by eliminating the pressure and density through path integration of the Navier–Stokes equations and of the equation of state. The result is[18]

$$\nabla^2\phi - \frac{\partial^2\phi}{\partial t^2} = 2(\beta_0 - 1)\frac{\partial\phi}{\partial t}\nabla^2\phi + \frac{\partial}{\partial t}(\nabla\phi\cdot\nabla\phi) + O(\phi^3), \tag{3}$$

where β_0 is the coefficient of nonlinearity,[19] and ∇ denotes the gradient operator in cylindrical coordinates.

In addition to Eq. (2), we must impose the radiation condition. Therefore, we require that the signal should be either an outgoing wave or evanescent at large z, and that it should decay suitably with increasing R. We expand the velocity potential in a perturbation series

$$\phi = \epsilon\phi_1 + \epsilon^2\phi_2 + \cdots. \tag{4}$$

Collecting like powers of ϵ in Eqs. (2) and (3) leads to equations governing ϕ_1 and ϕ_2. The first-order equations are

$$\nabla^2\phi_1 - \frac{\partial^2\phi_1}{\partial t^2} = 0, \tag{5a}$$

$$\left.\frac{\partial\phi_1}{\partial z}\right|_{z=0} = \frac{1}{2i}[\epsilon_1 f_1(R)\exp(i\omega_1 t) + \epsilon_2 f_2(R)\exp(i\omega_2 t)] + \text{c.c.} \tag{5b}$$

Equations (5) are the conventional ones governing linear radiation from a baffled transducer. Nonlinear effects are contained in the second-order, and succeeding, terms. The second-order equation arising from Eq. (3) is

$$\nabla^2\phi_2 - \frac{\partial^2\phi_2}{\partial t^2} = \frac{\partial}{\partial t}\left[(\beta_0 - 1)\left(\frac{\partial\phi_1}{\partial t}\right)^2 + \nabla\phi_1\cdot\nabla\phi_1\right]. \tag{6}$$

Tjøtta and Tjøtta's recent general treatment of second-order nonlinearities[20] showed that second-order terms in boundary conditions do not lead to cumulatively growing terms at that order. That observation agrees with our earlier analysis of the total solution for the second-order potential,[21] where we showed that it is only necessary to construct the particular solution of Eq. (6). The complementary solution, which is determined by the second-order boundary conditions, does not grow with increasing distance from the transducer. Since it represents a uniformly $O(\epsilon^2)$ effect, it is insignificant in comparison to the cumulative growth effects, except in the region very close to the transducer (two to three piston diameters in the cases we considered). Neglecting the complementary solution allows us to ignore the boundary condition at $z = 0$. However, it is necessary that the eventual solution satisfies the Sommerfeld radiation conditions at large distances from the tranducer.

II. LINEARIZED SOLUTION

The King integral, which is essentially an inversion of the Hankel transform, provides a formulation of the linearized problem that is amenable to the task of evaluating ϕ_2. Hence, we let

$$\phi_1(z,R,t) = \int_0^\infty n\Phi_1(z,n,t)J_0(nR)dn + \text{c.c.} \tag{7}$$

This expression satisfies Eq. (5) when

$$\frac{\partial^2\Phi_1}{\partial z^2} - \frac{\partial^2\Phi_1}{\partial t^2} - n^2\Phi_1 = 0, \tag{8a}$$

$$\left.\frac{\partial\Phi_1}{\partial z}\right|_{z=0} = V_1(n)\exp(i\omega_1 t) + V_2(n)\exp(i\omega_2 t), \tag{8b}$$

where the coefficients $V_j(n)$ are the transformations of the spatial shading functions $f_j(R)$:

$$V_j(n) = \frac{\epsilon_j}{2i}\int_0^\infty Rf_j(R)J_0(nR)dR, \quad j = 1,2. \tag{9}$$

The solution of Eqs. (8) is

$$\Phi_1(n,z,t) = -\sum_{j=1}^{j=2}\frac{V_j(n)}{\mu_{nj}}\exp(i\omega_j t - \mu_{nj}z), \tag{10}$$

where

$$\mu_{nj}^2 = n^2 - \omega_j^2. \tag{11a}$$

The radiation condition for $z\to\infty$ requires that ϕ_1 must either vanish, or else represent a wave that propagates in the positive z direction away from the transducer. Hence, we select the branch cut for μ_j such that

$$\mu_{nj} = \begin{cases} i(\omega_j^2 - n^2)^{1/2}, & 0\leqslant n\leqslant\omega_j, \\ (n^2 - \omega_j^2)^{1/2}, & n > \omega_j. \end{cases} \tag{11b}$$

The result of substituting Eq. (10) into Eq. (7) is

$$\phi_1 = -\sum_{j=1}^{j=2}\int_0^\infty \frac{nV_j(n)}{\mu_{nj}}\exp(i\omega_j t - \mu_{nj}z)J_0(nR)dn + \text{c.c.} \tag{12}$$

This expression is the King integral representation corresponding to two primary sound beams. It indicates that the linear signal is a sum of two waves that do not interact.

Before we proceed to formulate the source terms driving the second-order potential, it is convenient to change the integration variable in Eq. (12) by replacing the transform parameter n in each integral by $n\omega_j$. This leads to

$$\phi_1 = -\sum_{j=1}^{j=2}\int_0^\infty \frac{nV_j(n)}{\mu_n}\exp[\omega_j(it - \mu_n z)]J_0(\omega_j nR)dn + \text{c.c.}, \tag{13}$$

where V_j are redefined as

$$V_j(n) = \frac{\epsilon_j}{2i}\int_0^\infty Rf_j(R)J_0(\omega_j nR)d(\omega_j R), \quad j = 1,2 \tag{14}$$

and

$$\mu_n = \begin{cases} (1 - n^2)^{1/2}, & 0 < n < 1, \\ (n^2 - 1)^{1/2}, & n > 1. \end{cases} \tag{15}$$

III. SECOND-ORDER POTENTIAL

We use the first-order solution ϕ_1 in Eq. (13) to formulate the source terms driving ϕ_2 in Eq. (6). Forming quadratic products of the derivatives of ϕ_1 requires that different symbols be used to represent the transverse wavenumber in each term of the product. The resulting equation governing the second-order potential is

$$\nabla^2\phi_2 - \frac{\partial^2\phi_2}{\partial t^2}$$
$$= \int_0^\infty \int_0^\infty 2i\omega_1^3 nm \frac{V_1(n)V_1(m)}{\mu_n\mu_m}\{[-(\beta_0-1)+\mu_n\mu_m]J_0(\omega_1 nR)J_0(\omega_1 mR) + nmJ_1(\omega_1 nR)J_1(\omega_1 mR)\}$$
$$\times\exp[2i\omega_1 t - \omega_1(\mu_n+\mu_m)z]\,dm\,dn + \int_0^\infty\int_0^\infty 2i\omega_2^3 nm\frac{V_2(n)V_2(m)}{\mu_n\mu_m}$$
$$\times\{[-(\beta_0-1)+\mu_n\mu_m]J_0(\omega_2 nR)J_0(\omega_2 mR) + nmJ_1(\omega_2 nR)J_1(\omega_2 mR)\}$$
$$\times\exp[2i\omega_2 t - \omega_2(\mu_n+\mu_m)z]\,dm\,dn + \int_0^\infty\int_0^\infty 2i\omega_1\omega_2\omega_s nm\frac{V_1(n)V_2(m)}{\mu_n\mu_m}$$
$$\times\{[-(\beta_0-1)+\mu_n\mu_m]J_0(\omega_1 nR)J_0(\omega_2 mR) + nmJ_1(\omega_1 nR)J_1(\omega_2 mR)\}$$
$$\times\exp[i\omega_s t - (\omega_1\mu_n+\omega_2\mu_m)z]\,dm\,dn + \int_0^\infty\int_0^\infty 2i\omega_1\omega_2\omega_d nm\frac{V_1(n)V_2^*(m)}{\mu_n\mu_m^*}$$
$$\times\{[(\beta_0-1)+\mu_n\mu_m^*]J_0(\omega_1 nR)J_0(\omega_2 mR) + nmJ_1(\omega_1 nR)J_1(\omega_2 mR)\}$$
$$\times\exp[i\omega_d t - (\omega_1\mu_n+\omega_2\mu_m^*)z]\,dm\,dn + \text{c.c.} \tag{16}$$

The effects appearing on the right side of Eq. (16) are sum and difference frequency interactions of the two primary frequencies. We form the solution for ϕ_2 as a corresponding superposition. Hence, let

$$\phi_2 = \sum_{j=1}^{2}\sum_{l=1}^{2}\phi_2^{(\omega_j\pm\omega_l)}, \tag{17}$$

where

$$\nabla^2\phi_2^{(\omega_j+\omega_l)} - \frac{\partial^2\phi_2^{(\omega_j+\omega_l)}}{\partial t^2}$$
$$= \int_0^\infty\int_0^\infty i\omega_j\omega_l(\omega_j+\omega_l)nm\frac{V_j(n)V_l(m)}{\mu_n\mu_m}$$
$$\times\{[-(\beta_0-1)+\mu_n\mu_m]J_0(\omega_j nR)J_0(\omega_l mR)$$
$$+ nmJ_1(\omega_j nR)J_1(\omega_l mR)\}\exp[i(\omega_j+\omega_l)t$$
$$-(\omega_j\mu_n+\omega_l\mu_m)z]\,dm\,dn + \text{c.c.} \tag{18}$$

and

$$\nabla^2\phi_2^{(\omega_j-\omega_l)} - \frac{\partial^2\phi_2^{(\omega_j-\omega_l)}}{\partial t^2}$$
$$= \int_0^\infty\int_0^\infty i\omega_j\omega_l(\omega_j-\omega_l)nm\frac{V_j(n)V_l^*(m)}{\mu_n\mu_m^*}$$
$$\times\{[(\beta_0-1)+\mu_n\mu_m]J_0(\omega_j nR)J_0(\omega_l mR)$$
$$+ nmJ_1(\omega_j nR)J_1(\omega_l mR)\}\exp[i(\omega_j-\omega_l)t$$
$$-(\omega_j\mu_n+\omega_l\mu_m^*)z]\,dm\,dn + \text{c.c.} \tag{19}$$

We could construct the particular solution of Eqs. (18) and (19) for each i,j pair as the sum of two dual Hankel transforms. The kernel of one transform would be $(\omega_j n)(\omega_l m)J_0(\omega_j nR)J_0(\omega_l mR)$ and the kernel of the second would be $(\omega_j n)(\omega_l m)J_1(\omega_j nR)J_1(\omega_l mR)$. However, we shall utilize a linear combination of the these kernels, because such a representation will ultimately decouple individual terms forming the solution. We begin with the analysis for the terms associated with a sum of the primary frequencies. Let

$$\phi_2^{(\omega_j+\omega_l)} = \int_0^\infty \omega_j n\int_0^\infty \omega_l m\Phi_{21}(z,t,m,n)$$
$$\times[J_0(\omega_j nR)J_0(\omega_l mR)$$
$$-J_1(\omega_j nR)J_1(\omega_l mR)]\,dm\,dn$$
$$+\int_0^\infty\omega_j n\int_0^\infty\omega_l m\Phi_{22}(z,t,m,n)$$
$$\times[J_0(\omega_j nR)J_0(\omega_l mR)$$
$$+J_1(\omega_j nR)J_1(\omega_l mR)]\,dm\,dn. \tag{20}$$

The next step is to substitute Eq. (20) into Eq. (18), and then to employ the recursion relations for Bessel functions and their derivatives. When we match the integrands on either side of the equality, we find

$$\left(\frac{\partial^2\Phi_{21}}{\partial z^2} - \frac{\partial^2\Phi_{21}}{\partial t^2} - (\omega_j n+\omega_l m)^2\Phi_{21}\right)$$
$$\times[J_0(\omega_j nR)J_0(\omega_l mR) - J_1(\omega_j nR)J_1(\omega_l mR)]$$
$$+\left(\frac{\partial^2\Phi_{22}}{\partial z^2} - \frac{\partial^2\Phi_{22}}{\partial t^2} - (\omega_j n-\omega_l m)^2\Phi_{22}\right)$$
$$\times[J_0(\omega_j nR)J_0(\omega_l mR) + J_1(\omega_j nR)J_1(\omega_l mR)]$$
$$-\left(\frac{4}{R^2}J_1(\omega_j nR)J_1(\omega_l mR)\right.$$
$$-\frac{2\omega_j n}{R}J_0(\omega_j nR)J_1(\omega_l mR)$$
$$\left.-\frac{2\omega_l n}{R}J_1(\omega_j nR)J_0(\omega_l mR)\right)(\Phi_{21}-\Phi_{22})$$
$$= -i(\omega_j+\omega_l)\frac{V_j(n)V_l(m)}{\mu_n\mu_m}$$
$$\times[(\beta_0-1-\mu_n\mu_m)J_0(\omega_j nR)J_0(\omega_l mR)$$
$$-nmJ_1(\omega_j nR)J_1(\omega_l mR)]$$
$$\times\exp[i(\omega_j+\omega_l)t-(\omega_j\mu_n+\omega_l\mu_m)z] + \text{c.c.} \tag{21}$$

It would be a considerable simplification if the third term in large parentheses on the left-hand side of the above equation were not present, because like functions of R on either side could then be matched. Since this term has an additional factor $1/R$ not contained in the other terms, it is negligible at large R. This verifies the assumption that the function Φ_{21} and Φ_{22} are independent of R, at least when R is large. Miao[22] demonstrated the validity of this hypothesis for the entire region in the case of a single-frequency beam. He derived independent expansions for the paraxial region (small R) and the off-axis region (large R). He showed that the latter, in the limit $R \ll 1$, is identical to the former, so the off-axis expansion contains the solution in the entire field. We invoke the same argument here. Matching like functions of R, with the $1/R$ terms ignored, then leads to the following pair of differential equations for Φ_{21} and Φ_{22}:

$$\begin{aligned}
&\frac{\partial^2\Phi_{21}}{\partial z^2} - \frac{\partial^2\Phi_{21}}{\partial t^2} - (\omega_j n + \omega_l m)^2\Phi_{21} \\
&\quad = -\frac{i}{2}(\omega_j + \omega_l)\frac{V_j(n)V_l(m)}{\mu_n\mu_m} \\
&\qquad \times (\beta_0 - 1 - \mu_n\mu_m - mn)\exp[i(\omega_j + \omega_l)t \\
&\qquad - (\omega_j\mu_n + \omega_l\mu_m)z] + \text{c.c.}, \\
&\frac{\partial^2\Phi_{22}}{\partial z^2} - \frac{\partial^2\Phi_{22}}{\partial t^2} - (\omega_j n - \omega_l m)^2\Phi_{22} \\
&\quad = -\frac{i}{2}(\omega_j + \omega_l)\frac{V_j(n)V_l(m)}{\mu_n\mu_m} \\
&\qquad \times (\beta_0 - 1 - \mu_n\mu_m - nm)\exp[i(\omega_j + \omega_l)t \\
&\qquad - (\omega_j\mu_n + \omega_l\mu_m)z] + \text{c.c.}
\end{aligned} \tag{22}$$

Because nonlinear distortion, which is associated with generation of harmonics, generally increases with increasing propagation distance z, the particular solution for Φ_{21} and Φ_{22} may be written as follows:

$$\begin{aligned}
\Phi_{21} &= A(z,m,n)\exp[i(\omega_j + \omega_l)t \\
&\qquad - (\omega_j\mu_n + \omega_l m)z] + \text{c.c.}, \\
\Phi_{22} &= B(z,m,n)\exp[i(\omega_j + \omega_l)t \\
&\qquad - (\omega_j\mu_n + \omega_l\mu_m)z] + \text{c.c.}
\end{aligned} \tag{23}$$

Substitution of Eqs. (23) into Eqs. (22) leads to the following pair of uncoupled ordinary differential equations for A and B:

$$\begin{aligned}
&\frac{d^2A}{dz^2} - 2(\omega_j\mu_n + \omega_l\mu_m)\frac{dA}{dz} + [(\omega_j\mu_n + \omega_l\mu_m)^2 \\
&\quad - (\omega_j n + \omega_l m)^2 + (\omega_j + \omega_l)^2]A \\
&\quad = -\frac{i}{2}(\omega_j + \omega_l)\frac{V_j(n)V_l(m)}{\mu_n\mu_m} \\
&\qquad \times (\beta_0 - 1 - \mu_n\mu_m + nm),
\end{aligned} \tag{24a}$$

$$\begin{aligned}
&\frac{d^2B}{dz^2} - 2(\omega_j\mu_n + \omega_l\mu_m)\frac{dB}{dz} + [(\omega_j\mu_n + \omega_l\mu_m)^2 \\
&\quad - (\omega_j n - \omega_l m)^2 + (\omega_j + \omega_l)^2]B \\
&\quad = -\frac{i}{2}(\omega_j + \omega_l)\frac{V_j(n)V_l(m)}{\mu_n\mu_m} \\
&\qquad \times (\beta_0 - 1 - \mu_n\mu_m - nm).
\end{aligned} \tag{24b}$$

Cumulative growth will be manifested by increasing values of the amplitudes A and B. The particular solution for A or B is independent of z if the values of m and n are such that the coefficient of the A or B term in Eqs. (24) do not vanish. In contrast, if either of these coefficients vanishes, the corresponding particular solution for A or B is proportional to z. We find with the aid of Eq. (15) that the coefficient of A vanishes when $m = n$, whereas the coefficient of B vanishes when $m = n = 0$. Inspection of Eqs. (24) reveals that, when $m = n = 0$, the two equations have the same form. Thus the importance of B is restricted to a small region in the transverse wavenumber spectrum, where its behavior is no more singular than that of the coefficient A. Since A has a singularity at every n, we, therefore shall ignore the role of B.

IV. ASYMPTOTIC INTEGRATION

We have shown that the condition where the solution of Eq. (24a) grows with increasing z arises as $m \to n$, whereas regions far from the vicinity of $m = n$ give bounded contributions. The contribution of the region around $m = n$ may be determined by following Laplace's asymptotic integration method.[23] We relate the wavenumber m to the other wavenumber n by a detuning parameter q that is $O(1)$, such that

$$m = n + q\Delta, \tag{25a}$$

where $\Delta \ll 1$ is a positive number indicating the scale of the difference between m and n. When μ_n is not small, i.e., when n is not close to unity, the Taylor series expansion for the μ_m defined in Eq. (15) is found to be

$$\mu_m = \mu_n(1 + nq\Delta/\mu_n^2 - q^2\Delta^2/2\mu_n^4 + \cdots). \tag{25b}$$

Substitution of the above expressions for m and μ_m into Eq. (24a) leads to

$$\begin{aligned}
&\frac{d^2A}{dz^2} - 2\mu_n\left[(\omega_j + \omega_l) + \omega_l\left(\frac{nq\Delta}{\mu_n^2} - \frac{q^2\Delta^2}{2\mu_n^4}\right) + O(\Delta^3)\right]\frac{dA}{dz} \\
&\quad - \left(\omega_j\omega_l\frac{q^2\Delta^2}{\mu_n^2} + O(\Delta^3)\right)A \\
&\quad = -\frac{i}{2}\beta_0(\omega_j + \omega_l)\frac{V_j(n)V_l(n)}{\mu_n^2}.
\end{aligned} \tag{26}$$

When $m = n$, the particular solution of this equation is

$$A|_{m=n} = [i\beta_0 V_j(n)V_l(n)/4\mu_n^3]z. \tag{27}$$

The general solution for A when $m \neq n$ is

$$\begin{aligned}
A &= A_1\exp(\sigma_1 z) + A_2\exp(\sigma_2 z) \\
&\quad + \frac{i}{2}\beta_0\frac{(\omega_j + \omega_l)}{\omega_j\omega_l}\frac{V_j(n)V_l(n)}{q^2\Delta^2},
\end{aligned} \tag{28}$$

where the coefficients σ_1 and σ_2 are the roots of the characteristic equation governing the complementary solution:

$$\begin{aligned}
&\sigma^2 - 2\mu_n\left[(\omega_j + \omega_l) + \omega_l\left(\frac{nq\Delta}{\mu_n^2} - \frac{q^2\Delta^2}{2\mu_n^4}\right)\right]\sigma \\
&\quad - \omega_j\omega_l(q^2\Delta^2/\mu_n^2) = 0.
\end{aligned} \tag{29}$$

Solving this quadratic equation yields

$$\sigma_1 = \frac{1}{2}\frac{\omega_j\omega_l}{(\omega_j+\omega_l)}\frac{q^2\Delta^2}{\mu_n^3} + O(\Delta^3),$$

$$\sigma_2 = 2(\omega_j+\omega_l)\mu_n + O(\Delta). \tag{30}$$

As $q\to 0$ ($m=n$), Eq. (28) must approach Eq. (27). Because σ_2 is $0(1)$, and Eq. (27) has no term that varies exponentially in z, we set $A_2=0$. [It is also necessary that $A_2=0$ in order to satisfy the radiation condition. Otherwise, substitution of Eq. (28) into Eq. (23) would lead to a term that propagates in the negative direction.] Because $\sigma_1\sim q^2\Delta^2$, $\exp(\sigma_1 z)$ may be replaced by the leading terms in the series. Thus equating the limit of Eq. (20) as $m\to n$ to Eq. (27) gives

$$\lim_{q\to 0}\left[A_1\left(1-\frac{\omega_j\omega_l q^2\Delta^2 z}{2(\omega_j+\omega_l)\mu_n^2}\right) + \frac{i}{2}\beta_0\frac{(\omega_j+\omega_l)V_j(n)V_l(n)}{\omega_j\omega_l q^2\Delta^2}\right] = [i\beta_0 V_j(n)V_l(n)/4\mu_n^3]z. \tag{31}$$

The value of A_1 that satisfies the above equation for all values of z is

$$A_1 = (i/2)\beta_0(\omega_j+\omega_l)V_j(n)V_l(n)/(\omega_j\omega_l q^2\Delta^2). \tag{32}$$

In a strict sense, the foregoing represents the limiting behavior of A_1 for $m\approx n$. It is possible that A_1 has a different appearance for arbitrary m and n. However, we can show that such differences are associated with the homogeneous solution for the second-order potential, which we have already discarded.

The general solution for A is obtained by substituting the above expression into Eq. (28). This gives

$$A = \frac{i}{2}\beta_0(\omega_j+\omega_l)\frac{V_j(n)V_l(n)}{\omega_j\omega_l q^2\Delta^2} \times\left[1-\exp\left(-\frac{\omega_j\omega_l q^2\Delta^2}{2(\omega_j+\omega_l)\mu_n^3}\right)\right]. \tag{33}$$

Because the contribution of the function B is negligible, we find from Eqs. (20) and (23) that the total contribution is

$$\phi_2^{(\omega_j+\omega_l)} = \int_0^\infty \omega_j n\int_0^\infty \omega_l m A(z,m,n) \times\exp[i(\omega_j+\omega_l)t-(\omega_j\mu_n+\omega_l\mu_m)z] \times[J_0(\omega_j nR)J_0(\omega_l mR) - J_1(\omega_j nR)J_1(\omega_l mR)]dm\,dn + \text{c.c.} \tag{34}$$

We shall evaluate the inner integral in the above equation asymptotically in the region where z is large. This integration extends over $0<m<\infty$, with n fixed in that range. The major contribution to the integral stems from the vicinity of $m\approx n$ ($q\approx 0$). We isolate this region by selecting a small positive number δ that does not depend on m or n. Denote the integrand in Eq. (34) by $I(n,m,z,R)$. Then for a fixed arbitrary value of the wavenumber n, this equation may be written as

$$\phi_2^{(\omega_j+\omega_l)} = \int_0^\infty \omega_j n\int_0^{n-\delta} I(n,m,z,t)dm\,dn + \int_0^\infty \omega_j n\int_{n+\delta}^\infty I(n,m,z,t)dm\,dn + \int_0^\infty \omega_j n\int_{\delta/\Delta}^{\delta/\Delta} I(n,n+q\Delta,z,t)\Delta dq\,dn. \tag{35}$$

The first and the second integrals above represent the contribution of the regions that are not in the vicinity of $m=n$. The oscillatory nature of the integrand results in boundedness of these integrals, corresponding to destructive interference between source effects associated with disparate values of m and n. This means that the cumulative distortion only originates from the last integral in Eq. (35). Because that is the effect we seek, we shall neglect the first and second integral. (This idea reduces to Stokes method of stationary phase[23] for $n<1$, where μ_n is an imaginary number.) Because δ is defined as a fixed number, the dominant behavior (leading dependence on z) will be obtained if δ/Δ is any value of order one or larger. Because $\Delta\ll 1$, we take δ to be infinite for convenience in evaluating the integral. Furthermore, we may replace m by n the argument of the Bessel functions, and μ_m by μ_n in the exponential term in Eq. (34) without affecting the dominant terms. We obtain the resulting integral from a standard tabulation,[24]

$$\int_0^\infty \frac{1}{q^2}[1-\exp(-\kappa q^2)]dq = \sqrt{\pi\kappa}. \tag{36}$$

Then, we find from Eq. (20) that

$$\phi_2^{(\omega_j+\omega_l)} = \int_0^\infty\left(\frac{1}{2}\omega_j\omega_l(\omega_j+\omega_l)\right)^{1/2}\beta_0 n^2\frac{V_j(n)V_l(n)}{\mu_n\mu_n^*} \times(\pi\mu_n z)^{1/2}\exp[(\omega_j+\omega_l)(it-\mu_n z)] \times[J_0(\omega_j nR)J_0(\omega_l nR) - J_1(\omega_j nR)J_1(\omega_l nR)]dn + \text{SDT} + \text{c.c.}, \tag{37}$$

where SDT stands for subdominant terms, which, in the worst case, increase less rapidly with increasing z than those listed.

We cannot deduce the second-order potential associated with the difference frequency terms $\phi_2^{(\omega_j-\omega_l)}$ directly from Eq. (37). However, the procedure that yielded Eq. (37) is also valid for $\phi_2^{(\omega_j-\omega_l)}$. Such an analysis leads to

$$\phi_2^{(\omega_j-\omega_l)} = -\int_0^\infty h(l-n)\beta_0\left(\frac{1}{2}\omega_j\omega_l\omega_d\right)^{1/2}n^2 \times[V_j(n)V_l^*(n)/\mu_n\mu_n^*](\pi\mu_n^* z)^{1/2} \times\exp[(\omega_j-\omega_l)(it-\mu_n z)] \times[J_0(\omega_j nR)J_0(\omega_l nR) + J_1(\omega_j nR)J_1(\omega_l nR)] + \text{SDT} + \text{c.c.}, \tag{38}$$

where h denotes the Heaviside step function

$$h(1-n) = \begin{cases}1, & n<1,\\ 0, & n>1.\end{cases} \tag{39}$$

When we employ the expressions for $\phi_2^{(\omega_j+\omega_l)}$ and $\phi_2^{(\omega_j-\omega_l)}$ to form the second-order potential according to Eq. (17), and then combine them with the first-order potential in Eq. (13), we obtain

$$\phi = \int_0^\infty \Phi\, dn, \tag{40a}$$

where

$$\Phi = -\epsilon\left(\frac{nV_1(n)}{\mu_n}\exp[\omega_1(it-\mu_n z)]J_0(\omega_1 nR) + \frac{nV_2(n)}{\mu_n}\exp[\omega_2(it-\mu_n z)]J_0(\omega_2 nR)\right)$$

$$+\epsilon^2 i\beta_0(\pi\mu_n z)^{1/2}\left(\omega_1^{3/2}\frac{n^2V_1^2(n)}{\mu_n\mu_n^*}\exp[2\omega_1(it-\mu_n z)][J_0^2(\omega_1 nR)-J_1^2(\omega_1 nR)]\right.$$

$$+\omega_2^{3/2}\frac{n^2V_2^2(n)}{\mu_n\mu_n^*}\exp[2\omega_2(it-\mu_n z)][J_0^2(\omega_2 nR)-J_1^2(\omega_2 nR)] + (2\omega_1\omega_2\omega_s)^{1/2}\frac{n^2V_1(n)V_2(n)}{\mu_n^*\mu_n}$$

$$\times\exp[\omega_s(it-\mu_n z)][J_0(\omega_1 nR)J_0(\omega_2 nR)-J_1(\omega_1 nR)J_1(\omega_2 nR)]$$

$$-ih(1-n)(2\omega_1\omega_2\omega_d)^{1/2}\frac{n^2V_1(n)V_2^*(n)}{\mu_n^*\mu_n}\exp[\omega_d(it-\mu_n z)][J_0(\omega_1 nR)J_0(\omega_2 nR)$$

$$\left.+J_1(\omega_1 nR)J_1(\omega_2 nR)]\right) + \text{c.c.} + \text{SDT}. \tag{40b}$$

Several features are revealed by Eqs. (40). The transducer, which is driven at frequencies ω_1 and ω_2, directly generates two transverse spectra whose magnitude is $O(\epsilon)$, and whose temporal frequencies are ω_1 and ω_2. The $O(\epsilon^2)$ terms represent second harmonics of each wave attributable to self-interaction, and the lowest-order combination frequencies. Both effects are attributable to nonlinear interaction between the primary beams.

The asymptotic integration was carried out under the assumption that μ_n is not small. This is significant because the truncation of the series expansion in Eq. (25), is appropriate only if $q/\mu_n^2 \ll 1$. Only very small values of q satisfy this criterion when $n \to 1$. Therefore, the contribution to the second-order velocity potential from the region around $n = 1$ is not well described asymptotically. One reason for our concern in this regard is that $\mu_n \to 0$ as $n \to 1$. The expression for the acoustic pressure derived from Eqs. (40) has μ_n in denominator of the first-order term and $\mu_n^*\mu_n^{1/2}$ in the denominator of the second-order term. Thus the $O(\epsilon^2)$ term is more singular than the $O(\epsilon)$ term as $n \to 1$. Although both singularities are integrable, the higher degree of singularity in the second term will create difficulties. We shall introduce an appropriate correction later.

V. RENORMALIZATION

We obtain an expression for the acoustic pressure by differentiating Eqs. (40) with respect to time. Let P denote the contribution of a specific wavenumber n to the dimensional acoustic pressure. We then have

$$p = \rho_0 c_0^2 \int_0^\infty P\, dn, \quad P = -\frac{\partial\Phi}{\partial t}. \tag{41}$$

As was true for the potential function in Eqs. (40), the $O(\epsilon^2)$ terms in P grow as $z^{1/2}$ for large z. When $\epsilon z^{1/2}$ is $O(1)$, these terms, which are supposed to be a small correction, become the order of the main term, in violation of the assumption inherent to a perturbation expansion. A perturbation series having this property lacks uniform validity.[25]

In order to determine a uniform expansion, we shall employ the method of renormalization.[26] When nR is large, the asymptotic behavior of P has the appearance of a sum of two interacting waves that propagate in the inward $(+R)$ and in the outward $(-R)$ radial directions, as well as in the axial direction. This is a consequence of the asymptotic expansion of $J_\nu(x)$ for large x, which is

$$J_\nu(x) \sim \tfrac{1}{2}(2/\pi x)^{1/2}\exp[ix-(2\nu+1)\pi/4] + \text{c.c.} \tag{42}$$

Introducing this approximation into Eq. (41) leads to decomposition of the off-axis signal into two waves, given by

$$P = P_{-R} + R_{+R}, \tag{43a}$$

where

$$P_{-R} \sim \epsilon \frac{1}{2}\left(\frac{2}{\pi nR}\right)^{1/2}\left[i\omega_1^{1/2} \frac{nV_1(n)}{\mu_n} \exp\left(\omega_1(it-\mu_n z+inR)-i\frac{\pi}{4}\right)\right.$$
$$+ i\omega_2^{1/2} \frac{nV_2(n)}{\mu_n} \exp\left(\omega_2(it-\mu_n z+inR)-i\frac{\pi}{4}\right)\Big]$$
$$- \epsilon^2\beta_0 \frac{2}{\pi nR} \frac{(\pi\mu_n z)^{1/2}}{\mu_n\mu_n^*}\Big(i\omega_1^{3/2} n^2 V_1^2(n)\exp[2\omega_1(it-\mu_n z+inR)]$$
$$+ i\omega_2^{3/2} n^2 V_2^2(n)\exp[2\omega_2(it-\mu_n z+inR)] + i\frac{\omega_s^{3/2}}{\sqrt{2}} n^2 V_1(n)V_2(n)\exp[\omega_s(it-\mu_n z+inR)]$$
$$\left. - h(1-n)i\frac{\omega_d^{3/2}}{\sqrt{2}} n^2 V_1(n)V_2^*(n)\exp[\omega_d(it-\mu_n z+inR)]\right) + \text{c.c.}, \tag{43b}$$

$$P_{+R} \sim \epsilon \frac{1}{2}\left(\frac{2}{\pi nR}\right)^{1/2}\left[i\omega_1^{1/2} \frac{nV_1(n)}{\mu_n} \exp\left(\omega_1(it-\mu_n z-inR)+i\frac{\pi}{4}\right)\right.$$
$$+ i\omega_2^{1/2} \frac{nV_2(n)}{\mu_n} \exp\left(\omega_2(it-\mu_n z-inR)+i\frac{\pi}{4}\right)\Big]$$
$$+ \epsilon^2\beta_0 \frac{2}{\pi nR} \frac{(\pi\mu_n z)^{1/2}}{\mu_n\mu_n^*}\Big(i\omega_1^{3/2} n^2 V_1^2(n)\exp[2\omega_1(it-\mu_n z-inR)]$$
$$+ i\omega_2^{3/2} n^2 V_2^2(n)\exp[2\omega_2(it-\mu_n z-inR)] + i\frac{\omega_s^{3/2}}{\sqrt{2}} n^2 V_1(n)V_2(n)\exp[\omega_s(it-\mu_n z-inR)]$$
$$\left. - ih(1-n)\frac{\omega_d^{3/2}}{\sqrt{2}} n^2 V_1(n)V_2^*(n)\exp[\omega_d(it-\mu_n z-inR)]\right) + \text{c.c.} \tag{43c}$$

We shall renormalize the expansions given by Eqs. (43b) and (43c) independently for the off-axis region, and then establish the appropriate transformation for the region around the axis. We begin with the term P_{-R}, which we decompose into effects that are associated at the $O(\epsilon^2)$ stage with either the sum or difference frequencies. We group one half of each second harmonic in Eq. (43b) with the sum frequency term, while the other half of each second harmonic is grouped with the difference frequency. For reasons of convenience, we apportion the primary beam at frequency ω_2 equally to the sum and difference frequency. In contrast, for the primary beam at ω_1, we invoke the identity $\exp(-i\pi/4) = (1-i)/\sqrt{2}$. By associating the imaginary part of this identity with the sum frequency group, and the real part with the difference frequency, we phase shift the first primary beam forward and back by $\pi/4$ relative to the second primary. (Since we have restricted $\omega_1 > \omega_2$, there is no reason that the nonlinear expressions should be symmetric in ω_1 and ω_2.) The two groups form the inward wave according to

$$P_{-R} = P^s{}_{-R} + P^d{}_{-R}. \tag{44a}$$

The sum frequency group is

$$P^s{}_{-R} \sim \epsilon \frac{1}{2}\left(\frac{2}{\pi nR}\right)^{1/2}\left[\frac{1}{\sqrt{2}}\omega_1^{1/2} \frac{nV_1(n)}{\mu_n} \exp[\omega_1(it-\mu_n z+inR)]\right.$$
$$+ \frac{i}{2}\omega_2^{1/2} \frac{nV_2(n)}{\mu_n} \exp\left(\omega_2(it-\mu_n z+inR)-i\frac{\pi}{4}\right)\Big]$$
$$- \epsilon^2 i\beta_0 \frac{2}{\pi nR} \frac{(\pi\mu_n z)^{1/2}}{\mu_n\mu_m^*}\Big(\frac{1}{2}\omega_1^{3/2} n^2 V_1^2(n)\exp[2\omega_1(it-\mu_n z+inR)]$$
$$+ \tfrac{1}{2}\omega_2^{3/2} n^2 V_2^2(n)\exp[2\omega_2(it-\mu_n z+inR)]$$
$$\left. + \frac{1}{\sqrt{2}}\omega_s^{3/2} n^2 V_1(n)V_2(n)\exp[\omega_s(it-\mu_n z+inR)]\right) + \text{c.c.} \tag{44b}$$

and the difference frequency group is

$$P^{d}_{-R} = \epsilon \frac{1}{2}\left(\frac{2}{\pi nR}\right)^{1/2}\left[\frac{i}{\sqrt{2}}\omega_1^{1/2}\frac{nV_1(n)}{\mu_n}\exp[\omega_1(it-\mu_n z+inR)]\right.$$
$$+\frac{i}{2}\omega_2^{1/2}\frac{nV_2(n)}{\mu_n}\exp\left(\omega_2(it-\mu_n z+inR)-i\frac{\pi}{4}\right)\Big]$$
$$-\epsilon^2 i\beta_0\frac{2}{\pi nR}\frac{(\pi\mu_n z)^{1/2}}{\mu_n\mu_n^*}\left(\frac{1}{2}\omega_1^{3/2}n^2V_1^2(n)\exp[2\omega_1(it-\mu_n z+inR)]\right.$$
$$+\frac{1}{2}\omega_2^{3/2}n^2V_2^2(n)\exp[2\omega_2(it-\mu_n z+inR)]-h(1-n)\frac{\omega_d^{3/2}}{\sqrt{2}}n^2V_1(n)V_2^*(n)$$
$$\left.\times\exp[\omega_d(it-\mu_n z+inR)]\right)+\text{c.c.} \tag{44c}$$

In order to render the sum frequency term P^{s}_{-R} in Eq. (44b) uniformly valid, we introduce a set of coordinate transformations:

$$\omega_1 z=\alpha_1+\epsilon z^{1/2}[S_{11}(\alpha_1,t,n,P)+S_{12}(\alpha_2,t,n,R)+\text{c.c.}], \tag{45a}$$
$$\omega_2 z=\alpha_2+\epsilon z^{1/2}[S_{22}(\alpha_2,t,n,R)+S_{21}(\alpha_1,t,n,R)+\text{c.c.}]. \tag{45b}$$

The unknown functions S_{jl} must remove the objectionable terms causing nonuniform validity in P^{s}_{-R}. We substitute Eqs. (45) into Eq. (44b), and expand the result in a Taylor series in ascending powers of ϵ. The series expansions are truncated at $O(\epsilon^2)$, with the result that

$$P^{s}_{-R}=\epsilon\frac{1}{2}\left(\frac{2}{\pi nR}\right)^{1/2}\left[\frac{1}{\sqrt{2}}\omega_1^{1/2}\frac{nV_1(n)}{\mu_n}\exp(i\omega_1 t-\mu_n\alpha_1+i\omega_1 nR)\right.$$
$$+\frac{i}{2}\omega_2^{1/2}\frac{nV_2(n)}{\mu_n}\exp\left(i\omega_2 t-\mu_n\alpha_2+i\omega_2 nR-i\frac{\pi}{4}\right)\Big]$$
$$+\epsilon^2\frac{1}{2}\left(\frac{2}{\pi nR}\right)^{1/2}\left[-\frac{1}{\sqrt{2}}\omega_1^{1/2}nV_1(n)z^{1/2}\exp(i\omega_1 t-\mu_n\alpha_1+i\omega_1 nR)(S_{11}+S_{12}+S_{11}^*+S_{12}^*)\right.$$
$$-\frac{i}{2}\omega_2^{1/2}nV_2(n)z^{1/2}\exp\left(i\omega_2 t-\mu_n\alpha_2+i\omega_2 nR-i\frac{\pi}{4}\right)(S_{22}+S_{21}+S_{22}^*+S_{21}^*)$$
$$-2i\beta_0\left(\frac{2}{\pi nR}\right)^{1/2}\frac{(\pi\mu_n z)^{1/2}}{\mu_n\mu_n^*}\left(\frac{1}{2}\omega_1^{1/2}n^2V_1^2(n)\exp(2i\omega_1 t-2\mu_n\alpha_1+2i\omega_1 nR)\right.$$
$$\left.+\frac{1}{2}\omega_2^{3/2}n^2V^2(n)\exp(2i\omega_2 t-2\mu_n\alpha_2+2i\omega_2 nR)+\frac{\omega_1^{3/2}}{\sqrt{2}}n^2V_1V_2\exp(i\omega_1 t-\mu_n\alpha_1-\mu_n\alpha_2+i\omega_1 nR)\right)\Big]+\text{c.c.} \tag{46}$$

The criterion for the selection of straining functions S_{jl} is that they cancel the second-order growth terms in P^{s}_{-R}, which yields

$$\omega_1 z=\alpha_1-\epsilon\left[i\beta_0\left(\frac{2}{\pi nR}\right)^{1/2}\frac{(\pi\mu_n z)^{1/2}}{\mu_n\mu_n^*}\left(\sqrt{2}\omega_1 nV_1(n)\exp(i\omega_1 t-\mu_n\alpha_1+i\omega_1 nR)\right.\right.$$
$$\left.\left.+\frac{\omega_1^{3/2}}{\omega_1^{1/2}}nV_2(n)\exp(i\omega_2 t-\mu_n\alpha_2+i\omega_2 nR)\right)+\text{c.c.}\right], \tag{47a}$$
$$\omega_2 z=\alpha_2-\epsilon\left\{\beta_0\left(\frac{2}{\pi nR}\right)^{1/2}\frac{(\pi\mu_n z)^{1/2}}{\mu_n\mu_n^*}\left[2\omega_2 nV_2(n)\exp\left(i\omega_2 t-\mu_n\alpha_2+i\omega_2 nR+i\frac{\pi}{4}\right)\right.\right.$$
$$\left.\left.-\sqrt{2}\frac{\omega_1^{3/2}}{\omega_2^{1/2}}\left(\frac{\mu_n^*}{\mu_n}\right)^{1/2}nV_1(n)\exp\left(i\omega_1 t-\mu_n\alpha_1+i\omega_1 nR-i\frac{\pi}{4}\right)\right]+\text{c.c.}\right\}. \tag{47b}$$

The corresponding form of $P^s{}_R$ is given by

$$P^s{}_R = \epsilon \frac{1}{2}\left(\frac{2}{\pi nR}\right)^{1/2}\left[\frac{1}{\sqrt{2}}\omega_1^{1/2}\frac{nV_1(n)}{\mu_n}\exp(i\omega_1 t - \mu_n\alpha_1 + i\omega_1 nR)\right.$$
$$\left. + \frac{i}{2}\omega_2\frac{nV_2(n)}{\mu_n}\exp\left(i\omega_2 t - \mu_n\alpha_2 + i\omega_2 nR - i\frac{\pi}{4}\right)\right]$$
$$+ \epsilon^2\frac{i}{2}\beta_0\frac{2}{\pi nR}\frac{(\pi\mu_n^* z)^{1/2}}{\mu_n\mu_n^*}\left[-\omega_1^{3/2}n^2V_1(n)V_1^*(n) + \omega_2^{3/2}n^2V_2(n)V_2^*(n)\right] + \text{c.c.} \tag{47c}$$

These expressions are appropriate to the region where R is large. We obtain forms that are valid for all R by manipulating the asymptotic expansions for the Bessel functions in Eq. (42), which shows that, when the argument x is large,

$$J_0(x) + iJ_1(x) \simeq (2/\pi x)^{1/2}\exp[i(x - \pi/4)],$$
$$J_0(x) - iJ_1(x) \simeq (2/\pi x)^{1/2}\exp[-i(x - \pi/4)]. \tag{48}$$

Therefore, Eqs (47) may be written as follows:

$$P^s{}_R = \epsilon\frac{1}{2}\frac{nV_1(n)}{\sqrt{2}\mu_n}\exp\left(i\omega_1 t - \mu_n\alpha_1 + i\frac{\pi}{4}\right)[J_0(\omega_1 nR) + iJ_1(\omega_1 nR)]$$
$$+ \epsilon\frac{i}{2}\omega_2\frac{nV_2(n)}{\mu_n}\exp(i\omega_2 t - \mu_n\alpha_2)[J_0(\omega_2 nR) + iJ_1(\omega_2 nR)]$$
$$+ \epsilon^2\frac{i}{2}\beta_0\frac{(\pi\mu_n^* z)^{1/2}}{\mu_n\mu_n^*}\{-\omega_1^{5/2}n^2V_1(n)V_1^*(n)[J_0^2(\omega_1 nR) + J_1^2(\omega_1 nR)]$$
$$+ \omega_2^{5/2}n^2V_2(n)V_2^*(n)[J_0^2(\omega_2 nR) + J_1^2(\omega_2 nR)]\} + \text{c.c.}, \tag{49a}$$

where α_1 and α_2 are given by

$$\omega_1 z = \alpha_1 - \epsilon\beta_0\left[i\sqrt{2}\omega_1^{3/2}\frac{nV_1(n)}{\mu_n\mu_n^*}(\pi\mu_n z)^{1/2}\exp\left(i\omega_1 t - \mu_n\alpha_1 + i\frac{\pi}{4}\right)[J_0(\omega_1 nR) + iJ_1(\omega_1 nR)]\right.$$
$$\left. + i\omega_2^{3/2}\left(\frac{\omega_2}{\omega_1}\right)^{1/2}\frac{nV_2(n)}{\mu_n\mu_n^*}(\pi\mu_n z)^{1/2}\exp\left(i\omega_2 t - \mu_n\alpha_2 + i\frac{\pi}{4}\right)[J_0(\omega_2 nR) + iJ_1(\omega_2 nR)] + \text{c.c.}\right]. \tag{49b}$$

$$\omega_2 z = \alpha_2 - \epsilon\beta_0\left[2i\omega_2^{3/2}\frac{nV_2(n)}{\mu_n\mu_n^*}(\pi\mu_n^* z)^{1/2}\exp(i\omega_2 t - \mu_n\alpha_2)[J_0(\omega_2 nR) + iJ_1(\omega_2 nR)]\right.$$
$$\left. - \sqrt{2}\omega_2^{3/2}\left(\frac{\omega_1}{\omega_2}\right)^{1/2}\frac{nV_1(n)}{\mu_n\mu_n^*}(\pi\mu_n^* z)^{1/2}\exp(i\omega_1 t - \mu_n\alpha_1)[J_0(\omega_1 nR) + iJ_1(\omega_1 nR)] + \text{c.c.}\right]. \tag{49c}$$

Analogous operations for the inwardly propagating term associated with the difference of the primary frequencies $P^d{}_R$ lead to

$$P^d{}_R = \epsilon\frac{1}{2}\left[\frac{i}{\sqrt{2}}\omega_1\frac{nV_1(n)}{\mu_n}\exp\left(i\omega_1 t - \mu_n\beta_1 + i\frac{\pi}{4}\right)[J_0(\omega_1 nR) + iJ_1(\omega_1 nR)] + \frac{i}{2}\omega_2\frac{nV_2(n)}{\mu_n}\right]$$
$$\times\exp(i\omega_2 t - \mu_n\beta_2)[J_0(\omega_2 nR) + iJ_1(\omega_2 nR)]$$
$$+ \epsilon\frac{\beta_0}{2}\frac{(\pi\mu_n^* z)^{1/2}}{\mu_n\mu_n^*}\{i\omega_1^{5/2}n^2V_1(n)V_1^*(n)[J_0^2(\omega_1 nR) + J_1^2(\omega_1 nR)]$$
$$+ \omega_2^{5/2}n^2V_2(n)V_2^*(n)[J_0^2(\omega_2 nR) + J_1^2(\omega_2 nR)]\} + \text{c.c.}, \tag{50a}$$

where the coordinate transformations are

$$\omega_1 z = \beta_1 - \epsilon\beta_0\left[\sqrt{2}\omega_1^{3/2}\frac{nV_1(n)}{\mu_n\mu_n^*}(\pi\mu_n z)^{1/2}\exp\left(i\omega_1 t - \mu_n\beta_1 + i\frac{\pi}{4}\right)[J_0(\omega_1 nR) + iJ_1(\omega_1 nR)]\right.$$
$$+ ih(1-n)\omega_2^{3/2}\left(\frac{\omega_2}{\omega_1}\right)^{1/2}\frac{nV_2(n)}{\mu_n\mu_n^*}(\pi\mu_n z)^{1/2}$$
$$\left.\times\exp\left(i\omega_2 t - \mu_n\beta_2 + i\frac{\pi}{4}\right)[J_0(\omega_2 nR) + iJ_1(\omega_2 nR)] + \text{c.c.}\right], \tag{50b}$$

$$\omega_2 z = \beta_2 - \epsilon\beta_0 \left[2i\omega_2^{3/2} \frac{nV_1(n)}{\mu_n\mu_n^*} (\pi\mu_n z)^{1/2} \exp(i\omega_2 t - \mu_n\beta_2)[J_0(\omega_2 nR) + iJ_1(\omega_2 nR)] \right.$$
$$+ \sqrt{2}h(1-n)\omega_d^{3/2}\left(\frac{\omega_1}{\omega_2}\right)^{1/2} \frac{nV_2(n)}{\mu_n\mu_n^*}(\pi\mu_n z)^{1/2}$$
$$\left. \times \exp(i\omega_1 t - \mu_n\beta_1)[J_0(\omega_1 nR) + iJ_1(\omega_1 nR)] + \text{c.c.} \right]. \tag{50c}$$

The same procedures lead to renormalized expressions for the outwardly propagating terms. We find that

$$P_{+R} = P^s_{+R} + P^d_{+R}, \tag{51}$$

where the sum frequency is represented by

$$P^s_{+R} = \epsilon \frac{1}{2}\left[\frac{i}{\sqrt{2}} \omega_1 \frac{nV_1(n)}{\mu_n} \exp\left(i\omega_1 t - \mu_n\zeta_1 - i\frac{\pi}{4}\right)[J_0(\omega_1 nR) - iJ_1(\omega_1 nR)] \right.$$
$$\left. + \frac{i}{2}\omega_2 \frac{nV_2(n)}{\mu_n} \exp(i\omega_2 t - \mu_n\zeta_2)[J_0(\omega_2 nR) - iJ_1(\omega_2 nR)] \right]$$
$$+ \epsilon^2 \frac{1}{2}\beta_0 \frac{(\pi\mu_n^* z)^{1/2}}{\mu_n\mu_n^*}\{i\omega_1^{5/2} n^2 V_1(n) V_1^*(n)[J_0^2(\omega_1 nR) + J_1^2(\omega_1 nR)]$$
$$- \omega_2^{5/2} n^2 V_2(n) V_2^*(n)[J_0^2(\omega_2 nR) + J_1^2(\omega_2 nR)]\} + \text{c.c.} \tag{52a}$$

The corresponding coordinate transformation is

$$\omega_1 z = \zeta_1 + \epsilon\beta_0 \left[\sqrt{2}\omega_1^{3/2} \frac{nV_1(n)}{\mu_n\mu_n^*}(\pi\mu_n z)^{1/2} \exp\left(i\omega_1 t - \mu_n\zeta_1 - i\frac{\pi}{4}\right)[J_0(\omega_1 nR) - iJ_1(\omega_1 nR)] \right.$$
$$+ \omega_2^{3/2}\left(\frac{\omega_2}{\omega_1}\right)^{1/2} \frac{nV_2(n)}{\mu_n\mu_n^*}(\pi\mu_n z)^{1/2}$$
$$\left. \times \exp\left(i\omega_2 t - \mu_n\xi_2 - i\frac{\pi}{4}\right)[J_0(\omega_1 nR) - iJ_1(\omega_1 nR)] + \text{c.c.} \right], \tag{52b}$$

$$\omega_2 z = \zeta_2 - \epsilon\beta_0 \left[2i\omega_2^{3/2} \frac{nV_2(n)}{\mu_n\mu_n^*} (\pi\mu_n z)^{1/2} \exp(i\omega_2 t - \mu_n\zeta_2)[J_0(\omega_2 nR) - iJ_1(\omega_2 nR)] \right.$$
$$\left. - \sqrt{2}\omega_1^{3/2}\left(\frac{\omega_1}{\omega_2}\right)^{1/2} \frac{nV_1(n)}{\mu_n\mu_n^*} (\pi\mu_n^* z)^{1/2} \exp(i\omega_1 t - \mu_n\zeta_1)[J_0(\omega_1 nR) - iJ_1(\omega_1 nR)] + \text{c.c.} \right]. \tag{52c}$$

Finally, we find the difference frequency effect associated with the outwardly propagating waves to be

$$P^d_{-R} = \epsilon \frac{1}{2}\left[-\frac{1}{\sqrt{2}} \frac{\omega_1 nV_1(n)}{\mu_n} \exp\left(i\omega_1 t - \mu_n\eta_1 - i\frac{\pi}{4}\right)[J_0(\omega_1 nR) - iJ_1(\omega_1 nR)] \right.$$
$$\left. + \frac{i}{2}\omega_2 \frac{nV_2(n)}{\mu_n\mu_n^*} \exp(i\omega_2 t - \mu_n\eta_2)[J_0(\omega_2 nR) - iJ_1(\omega_2 nR)] \right]$$
$$+ \epsilon^2 \frac{i}{2}\beta_0 \frac{(\pi\mu_n^* z)^{1/2}}{\mu_n\mu_n^*}\{\omega_1^{5/2} n^2 V_1(n) V_1^*(n)[J_0^2(\omega_1 nR) + J_1^2(\omega_1 nR)]$$
$$+ \omega_2^{5/2} n^2 V_2(n) V_2^*(n)[J_0^2(\omega_2 nR) + J_1^2(\omega_2 nR)]\} + \text{c.c.}, \tag{53a}$$

with

$$\omega_1 z = \eta_1 - \epsilon\beta_0 \left[i\sqrt{2}\omega_1 \frac{nV_1(n)}{\mu_n\mu_n^*} (\pi\mu_n z)^{1/2} \exp\left(i\omega_1 t - \mu_n\eta_1 - i\frac{\pi}{4}\right)[J_0(\omega_1 nR) - iJ_1(\omega_1 nR)] \right.$$
$$\left. - h(1-n)\omega_d^{3/2}\left(\frac{\omega_2}{\omega_1}\right)^{1/2} \frac{nV_2(n)}{\mu_n\mu_n^*} (\pi\mu_n z)^{1/2} \exp\left(i\omega_2 t - \mu_n\eta_2 - i\frac{\pi}{4}\right)[J_0(\omega_2 nR) - iJ_1(\omega_2 nR)] + \text{c.c.} \right], \tag{53b}$$

$$\omega_2 z = \eta_2 - \epsilon\beta_0 \left[2i\omega_2 \frac{nV_2(n)}{\mu_n\mu_n^*} (\pi\mu_n z)^{1/2} \exp(i\omega_2 t - \mu_n\eta_2)[J_0(\omega_2 nR) - iJ_1(\omega_2 nR)] \right.$$
$$\left. + ih(1-n)\sqrt{2}\omega_d^{3/2}\left(\frac{\omega_1}{\omega_2}\right)^{1/2} \frac{nV_1(n)}{\mu_n\mu_n^*} (\pi\mu_n z)^{1/2} \exp(i\omega_1 t - \mu_n\eta_1)[J_0(\omega_1 nR) - iJ_1(\omega_1 nR)] + \text{c.c.} \right]. \tag{53c}$$

The expressions given by Eqs. (43a), (44a), and (49)–(53) yield a uniformly accurate expression for the acoustic pressure. The signal is thereby formed from a superposition of terms that appear far off axis to consist of two trains of waves that propagate in the inward (P_{-R}) and outward (P_{+R}) transverse directions. Each wavetrain is further subdivided into effects associated with the formation of sum and difference frequencies at the first stage of approximation:

$$P = P^{S}_{-R} + P^{d}_{-R} + P^{S}_{+R} + P^{d}_{+R}. \tag{54}$$

We must note at this juncture that the coordinate transformations given by the aforementioned equations describe only one transverse wavenumber n in a continuous spectrum. Inspection of these equations shows that the $O(\epsilon)$ term, which is the term associated with the distortion, contains a factor $\mu_n^{-1/2}$. Thus the $O(\epsilon)$ term tends to be very large as $n \to 1$. If such behavior were to be retained, we would find that the strength of nonlinearity increases as we approach $n = 1$. This violates our physical intuition. Hence, we now recall that the asymptotic development of the second-order potential was obtained by considering μ_n to be substantially larger than zero. Consequently, we may regard the coordinate transformations that have been derived as being the asymptotic representations, for n not close to unity, of alternative functional forms that behave properly as $n \to 1$.

The proper straining functions S_{ij} must feature a dependence on $\mu_n z$ that is proportional to $\mu_n^{1/2}$ in order to cancel the singularity at $n = 1$. A variety of functions, would exhibit suitable behavior. Ginsberg[13] employed the error function, but we shall employ combination of Bessel functions, in accord with Miao's work.[22] When $\mu_n z$ is large, the following representation is valid:

$$\left(\frac{\pi z}{\mu_n}\right)^{1/2} \approx \frac{\pi z^{(l+1)/2}}{(2\sigma)^{1/2}}\left[J_0^2\left(\frac{\mu_n z'}{\sigma}\right) + J_1^2\left(\frac{\mu_n z'}{\sigma}\right)\right]^{1/2} + O\left(\frac{\mu_n z'}{\sigma}\right)^{-3/2}, \tag{55}$$

where σ and l are arbitrary positive parameters that can only be obtained in the context of the present analysis by comparison with experimental data. [We have found $\sigma = (ka)^2/3$ and $l = 3/4$ to give good agreement.] Substitution of Eq. (55) into the coordinate straining transformations eliminates the singularities at $n = 1$.

VI. COMPUTATIONAL ALGORITHM

It is necessary to evaluate the pressure integrals, Eqs. (49a), (50a), (52a), and (53a), numerically. The primary analytical task for the evaluation is the conversion of the integral, as well as the coordinate transformations, to real forms descriptive of the propagating spectrum ($n < 1$), and the evanescent spectrum ($n > 1$). It is important to note that the singularity at $n = 1$ is integrable. We employ the Newton–Raphson technique to solve the coordinate transformations for each of the eight strained coordinates α_j, β_j, ξ_j, and η_j ($j = 1,2$) at a specific transverse wavenumber in the interval $0 < n < 1$ and $n > 1$. We then obtain the contributions of each wavenumber to the pressure integral by a Gauss–Chebychev quadrature. The frequency content of the pressure waveform may be evaluated from a two dimensional Fourier analysis[27] of a dual series in the variables $\tau_1 = \omega_1 t$ and $\tau_2 = \omega_2 t$. The net result is an algorithm that is relatively costly for extensive computation. Nevertheless, it yields a prediction of the acoustic pressure that may be utilized to generate waveforms and propagation curves of the frequency response.

Two alternative algorithms are available for enhancing the computational efficiency. Both approaches are based on interfacing the analytical expressions to the farfield propagation model[7] for spherical waves with directivity. Suppose that the signal at some reference distance r_0 and polar angle θ is known as a two-dimensional Fourier series, which may be written in complex form as

$$p(r_0,\theta,t) = \tfrac{1}{2}\rho_0 c_0^2 \times \sum_{j=-\infty}^{\infty}\sum_{k=-\infty}^{\infty} D_{jk}(\theta)\exp[i(j\omega_1 + k\omega_2)t], \tag{56}$$

$$D_{jk} = D^{*}_{(-j)k} = D^{*}_{j(-k)}. \tag{57}$$

Then, the signal outward from that location is

$$p(r,\theta,t) = \frac{1}{2}\rho_0 c_0^2\left(\frac{r_0}{r}\right) \times \sum_{j=-\infty}^{\infty}\sum_{k=-\infty}^{\infty} D_{jk}(\theta) \times \exp[i(j\omega_1 + k\omega_2)(t - \alpha + r_0)], \tag{58}$$

where α is a strained coordinate that is related to the radial distance by

$$r = \alpha + \beta_0 \ln(r/r_0) rp(r,\theta,t). \tag{59}$$

The only difference between the approaches is the manner in which the complex amplitudes D_{jk} are determined at the interface $r = r_0$.

The first, which we term the nonuniform spherical propagation (NSP) model, uses the nonuniformly valid expression for the acoustic pressure in Eqs. (40). That result predicts the amplitude and phase corresponding to each primary, the second harmonic of each primary, and the sum and difference frequencies. The computation of those responses does not feature coordinate transformations, so it is relatively straightforward. The frequency response is computed in this manner at a spherical spreading distance r_0, which is of the order of magnitude of the Rayleigh distances associated with each primary. The signals at locations beyond r_0 are computed according to the spherical model, Eqs. (57)–(59). This means that only one nonlinear equation, namely Eq. (58) needs to be solved for coordinate straining.

The second algorithm, which we call uniform spherical propagation (USP), employs the nonlinear King integrals. We find the signal at a spherical spreading distance r_0 by carrying out the full evaluation, including the coordinate transformation. Then, we frequency analyze the signal at the interface in order to generate the boundary condition for nonlinear spherical wave.

In either approach, the signal at r_0 provides the boundary condition that drives the directive spherical waves. Clearly, the first algorithm is less difficult than the second.

However, the second algorithm is more accurate than the first, especially if distortion is significant in the nearfield. We shall present the results of the USP model only. The value of r_0 we use is the Rayleigh distance (see Ref. 35), whose nondimensional value is $\frac{1}{2}(ka)^2$.

VII. RESULTS FOR PARAMETRIC ARRAYS

The analytical model that has been derived in this investigation is quite general. However, we are unaware of measurement of the interaction of collinear beams at disparate frequencies. Therefore, we begin with results for parametric arrays, that is, neighboring primary frequencies. The experiments for parametric arrays in water performed by Muir and Willette,[28] Eller,[29] and Bjorno *et al.*,[30] along with the experiment in air reported by Bennett and Blackstock[31] provide useful data for validating the analysis. Other measurements of parametric arrays were not considered for this comparison for a variety of reasons, for example, some considered saturation associated with shock formation, which is an effect not covered by the analytical model. Other experiments used rectangular arrays. The transducer in each of the aforementioned experiments was a circular piston of radius a oscillating with two frequencies ω_1 and ω_2. This corresponds in Eq. (2) to shading functions:

$$f_1(R) = f_2(R) = \begin{cases} 1, & R \leqslant ka, \\ 0, & R > ka, \end{cases} \tag{60}$$

which lead to the following Hankel transform amplitudes:

$$V_j(n) = \epsilon_j (ka/2in) J_1(\omega_j nka), \quad j = 1,2. \tag{61}$$

The comparisons we present are primarily between the measurements and the present analytical model. Also, in each case the rudimentary predictions of the Westervelt model[1] are presented, along with the analytical results, if any, in the cited reference.

In Fig. 1, we compare the predicted theoretical results to the data obtained by Muir and Willette. The measurements describe a 64-kHz difference frequency signal that arose from interaction of 482- and 418-kHz primary signals emitted from a 3.81-cm radius piston operated in fresh water. Each primary was transmitted at a source level of 207.2 dB//1 μPa m. The theoretical and experimental results compare quite favorably.

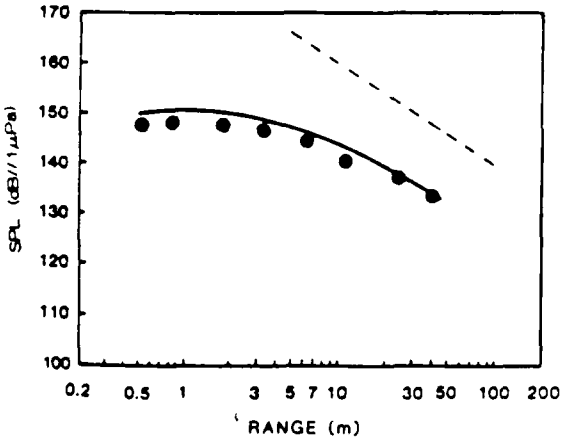

FIG. 1. Axial propagation of the difference frequency $f_1 = 482$ kHz, $f_2 = 418$ kHz, $SL_1 = SL_2 = 207.2$ dB//1 μPa m, $a = 38.1$ mm, fresh water. — present theory; ●: measured[28]; - - - : Westervelt model.[1]

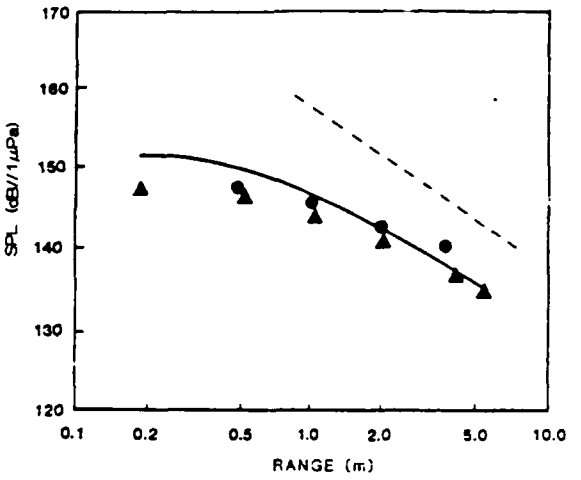

FIG. 2. Axial propagation of the difference frequency $f_1 = 1.46$ MHz, $f_2 = 1.41$ MHz, $SL_1 = SL_2 = 204.0$ dB//1 μPa, $a = 10$ mm, fresh water. —: present theory; ●, Δ: measured in different tanks[29]; - - - : Westervelt model.[1]

The theoretical predictions and Eller's experimental propagation curve for 50-kHz difference frequency component shown in Fig. 2 also are in good agreement. The primary frequencies are 1460 and 1410 kHz, and the source level of each is 204.0 dB//1 μPa m. The piston radius is 1.0 cm and the medium is fresh water.

Figure 3 depicts the theoretical results for a 40-kHz difference frequency signal in measurements made by Bjorno *et al.* The primary frequencies are 910 and 870 kHz emitted from a 1.0-cm radius transducer operated in brackish water. Each primary was transmitted at 208.0 dB//1 μPa m. (We referred to Fenlon and Mackendree[32] to obtain these parameters.)

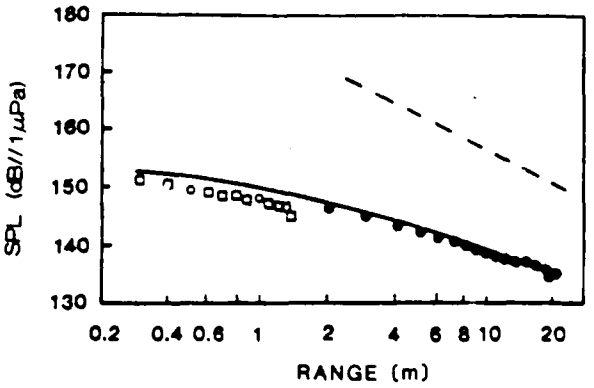

FIG. 3. Axial propagation of the difference frequency $f_1 = 910$ kHz, $f_2 = 870$ kHz, $SL_1 = SL_2 = 208.0$ dB//1 μPa, $a = 10$ mm, brackish water. —: present theory; □: measured in a steel tank[24]; ○: measured in an anechoic tank[24]; ●: measured in a channel[30]; - - - : Westervelt model.[1]

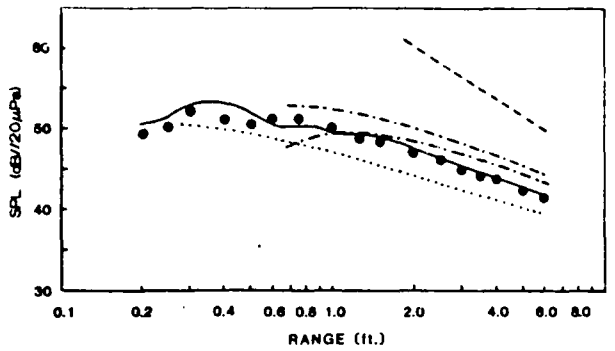

FIG. 4. Axial propagation of the difference frequency $f_1 = 23.6$ kHz, $f_2 = 18.6$ kHz, $SL_1 = 99.7$ dB//20 μPa m, $SL_2 = 104.7$ dB//20 μPa m, $a = 29.2$ mm, air. —: present theory; ●: measured[31]; • • •: numerical integration[31]; – • – • –: perturbation analysis[31]; – – –: Westervelt model.[1]

An example of the agreement between the theoretical predictions and the experimental results for parametric arrays in air is shown in Fig. 4 for Bennett and Blackstock's data. The 5-KHz difference frequency is generated by a 2.921-cm radius piston. The primary frequencies are 23.6 and 18.6 kHz and the source levels are 99.7 dB//20 μPa m and 104.7 dB//20 μPa m. It is particularly noteworthy that our model is in overall agreement with the measured fluctuations in the difference frequency.

Figure 5 displays a waveform at the axial location $z = 18.0$ m for Bennett and Blackstock's data, except the primary frequencies are 25 and 20 kHz. (Choosing ω_1 and ω_2 such that they are integer multiples of $\omega_1 - \omega_2$ reduces the time interval over which the waveform is periodic.) In comparison to the linearized prediction, nonlinearity results in earlier arrival of the maximum compression signals, and retarded arrival of the maximum rarefraction signals. This is consistent with past predictions and observations of monochromatic waves. In addition, Fig. 5 indicates that the distortion of the waveform is largest near the envelope peaks, but the shape near the envelope nodes is nearly unaffected. This supports the suggestion by Moffett and Mellen[33] that the primary waveform should be modeled as a sinusoidal at

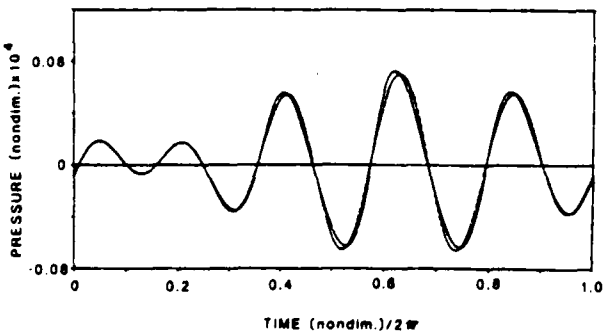

FIG. 5. Waveform on-axis $z = 18$ m, $f_1 = 25$ kHz, $f_2 = 20$ kHz, $SL_1 = 99.7$ dB//20 μPa, $SL_2 = 104.7$ dB//20 μPa m, $a = 29.2$ mm, air. — : present theory; – – – : linear theory.

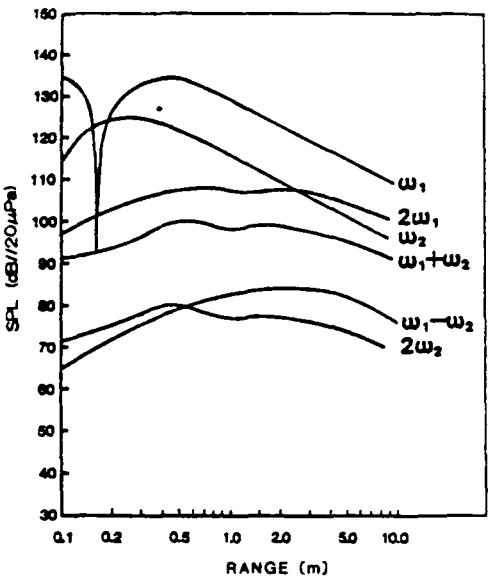

FIG. 6. Axial propagation of the fundamentals and lowest-order harmonics $f_1 = 30.5$ kHz, $f_2 = 20.7$ kHz, $SL_1 = 132.8$ dB//20 μPa m, $SL_2 = 119.5$ dB//20 μPa m, $a = 62.9$ mm, air.

frequency $\frac{1}{2}\omega_d$ near the source that becomes "clipped" near the envelope peaks as the wave progresses.

Theoretical predictions of propagation curves for harmonics and combination frequencies resulting from the nonlinear mixing of two sound beams in which the primary frequencies are not close to each other are shown in Figs. 6 and 7. The primary frequencies are 30.5 and 20.7 kHz, and the corresponding peak source levels are 132.8 dB//20 μPa m and 119.5 dB//20 μPa m. The piston radius is 62.9 mm and is operated in air.

Figure 6 shows the fundamental and the second harmonic of each primary, in addition to the sum and difference frequency signals. The levels of both harmonics (61 and 41.4 kHz) and the levels of sum and difference frequencies (51.2

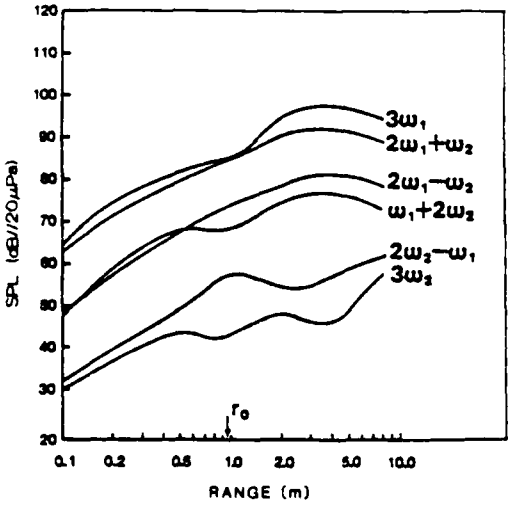

FIG. 7. Axial propagation of the higher-order harmonics for the parameters in Fig. 6.

and 9.8 kHz) increase in the nearfield about 6 dB for a doubling of the distance. In the farfield, the levels of the harmonics and the sum and difference signals decrease at greater distance from the piston. However, these levels decrease slightly less steeply than those of the fundamentals. The oscillations in the nearfield seem to be due to diffraction effects. It should be noted that the level of the sum frequency signal is larger than the difference one because the amplitude of each signal depends on its frequency (both amplitudes depend quadratically on the amplitudes of the primary waves). Figure 7 depicts the curves for the third harmonics and the higher combination frequencies; namely, $3\omega_1$, $3\omega_2$, $|2\omega_1 \pm \omega_2|$, and $|\omega_1 \pm 2\omega_2|$. In the nearfield, the levels of these curves increase approximately 12 dB for doubling of the distance.

It should be remarked that Brinkmann[34] has experimentally obtained comparable behavior for the interaction of two primary waves emitted from a small cylinder suspended at its center of gravity and excited into longitudinal vibration with two frequencies.

VIII. CONCLUSION

Our model for collinear interaction of sound beams is valid from the region quite close to the transducer out to the farfield, provided that the location is closer to the source than the shock formation distance. An account of the primary wave radiation including diffraction effects has been made through the King integral. Numerical results for the difference frequency signal in parametric arrays have been shown to agree well with experimental data for on-axis responses. However, proper validation of the theory developed here requires experimental data for the nonlinear mixing of the collinear sound beams at arbitrary frequencies and strengths.

Note added in proof: Subsequent to the submission of this paper, calculations by Edgerton[35] revealed that, when r_0 is the Rayleigh length, the numerical solution of the coordinate transformations fails to converge for the parameters associated with the experiments of Refs. 28 and 29. We then reexamined our calculations and found in both cases that the present results were obtained for a nondimensional $r_0 = 0.75/\pi(ka)^2$, which is twice the distance suggested by Zemanek[4] as the transition to spherical spreading.

ACKNOWLEDGMENTS

The authors are grateful for the support of this research given by the Office of Naval Research, Code 1125-OA.

[1]P. J. Westervelt, "Parametric acoustic array," J. Acoust. Soc. Am. **35**, 535–537 (1963).
[2]F. H. Fenlon, "Parametric acoustic arrays—A state of the art: Review," Adv. Eng. Sci., NASA, Rep. No. CP-2001, Vol. 3, pp. 917–932 (1976).
[3]L. Bjorno, "Parametric acoustic arrays," in *Aspects of Signal Processing, Part I*, edited by G. Tacconi (Reidel, Dordrecht, The Netherlands, 1977), pp. 33–58.
[4]J. Zemanek, "Beam behavior within the nearfield of a vibrating piston," J. Acoust. Soc. Am. **49**, 181–191 (1971).
[5]F. Ingenito and A. O. Williams, "Calculation of second-harmonic generation in a piston beam," J. Acoust. Soc. Am. **49**, 319–328 (1971).
[6]J. C. Lockwood, T. G. Muir, and D. T. Blackstock, "Directive harmonic generation in the radiation field of a circular piston," J. Acoust. Soc. Am. **53**, 1148–1153 (1973).
[7]J. C. Lockwood, "Two problem in high-intensity sound," Applied Research Laboratory, University of Texas at Austin, Austin, Texas, Rep. No. ARL-TR-71-26 (1971).
[8]E. A. Zabolotskaya and R. V. Khokhlov, "Quasi-plane waves in the nonlinear acoustics of confined beams," Sov. Phys. Acoust. **5**, 35–40 (1969).
[9]S. I. Aanonsen, T. Barkve, J. Naze Tjotta, and S. Tjotta, "Distortion and harmonic generation in the nearfield of a finite amplitude sound beam," J. Acoust. Soc. Am. **75**, 749–768 (1984).
[10]M. F. Hamilton, J. Naze Tjotta, and S. Tjotta, "Nonlinear effects in the farfield of a directive sound source," J. Acoust. Soc. Am. **78**, 202–216 (1985).
[11]N. S. Bakvalov, Ya. M. Zhileikin, E. A. Zabolotskaya, and R. V. Khokhlov, "Nonlinear propagation of a sound beam in a nondissipative medium," Sov. Phys. Acoust. **22**, 272–274 (1976).
[12]J. H. Ginsberg, "Nonlinear King integral for arbitrary axisymmetric sound beams at finite amplitudes. I. Asymptotic evaluation of the velocity potential," J. Acoust. Soc. Am. **76**, 1201–1207 (1984).
[13]J. H. Ginsberg, "Nonlinear King integral for arbitrary axisymmetric sound beams at finite amplitude. II. Derivation of uniformly accurate expressions," J. Acoust. Soc. Am. **76**, 1208–1214 (1984).
[14]J. Naze Tjotta and S. Tjotta, "Nonlinear interaction of two collinear, spherically spreading sound beams," J. Acoust. Soc. Am. **67**, 484–490 (1980).
[15]G. S. Garrett, J. Naze Tjotta, and S. Tjotta, "Nearfield of a large acoustic transducer. Part III: General results," J. Acoust. Soc. Am. **75**, 769–779 (1984).
[16]J. Berntsen, J. Naze Tjotta, and S. Tjotta, "Nearfield of a large acoustic transducer. Part IV: Second harmonic and sum frequency radiation," J. Acoust. Soc. Am. **75** 1383–1391 (1984).
[17]I. N. Sneddon, *The Use of Integral Transforms* (McGraw-Hill, New York, 1972), Chap. 5.
[18]S. Goldstein, *Lectures on Fluid Mechanics, Vol. II* (Wiley–Interscience, New York, 1957), Chap. 4.
[19]A. D. Pierce, *Acoustics, An Introduction to its Physical Principles and Applications* (McGraw-Hill, New York, 1981), Chap. 11.
[20]J. Naze Tjotta and S. Tjotta, "Interaction of sound waves. Part I: Basic equations and plane waves," J. Acoust. Soc. Am. **82**, 1425–1435 (1987).
[21]M. A. Foda and J. H. Ginsberg, "Relationship between near and farfield effects in second harmonic generation in the piston beam," J. Acoust. Soc. Am. Suppl. 1 **79**, S31–S32 (1986).
[22]H. C. Miao, "Analysis of nonsymmetric effects in finite amplitude sound beams," Ph.D. thesis, Georgia Institute of Technology, city, Georgia, 1985.
[23]C. M. Bender and S. A. Orszag, *Advanced Mathematical Methods for Scientists and Engineering* (McGraw-Hill, New York, 1978), Chap. 2.
[24]J. S. Gradshteyn and I. M. Ryzhik, *Table of Integrals, Series and Products* (Academic, New York, 1965), pp. 395 and 446.
[25]D. M. VanDyke, *Perturbation Methods in Fluid Mechanics* (Academic, New York, 1964), Chap. 4.
[26]A. H. Nayfeh and A. Kluwick, "A comparison of three perturbation methods for nonlinear hyperbolic waves," J. Sound Vib. **48**, 293–299 (1976).
[27]C. L. Cuccia, *Harmonics, Sidebands, and Transients in Communication Engineering* (McGraw-Hill, New York, 1952), Chap. 2.
[28]T. G. Muir and J. G. Willette, "Parametric acoustic transmitting arrays," J. Acoust. Soc. Am. **52**, 1481–1486 (1972).
[29]A. I. Eller, "Application of USRD Type E8 as an acoustic parametric source," J. Acoust. Soc. Am. **56**, 1735–1739 (1974).
[30]L. Bjorno, B. Christofferon, and M. P. Schrieber, "Some experimental investigations of the parametric acoustic array," Acustica **35**, 101–106 (1976).
[31]M. B. Bennett and D. T. Blackstock, "Parametric array in air," J. Acoust. Soc. Am. **57**, 562–568 (1975).
[32]F. H. Fenlon and F. S. McKendree, "Axisymmetric parametric radiation—A weak interaction model," J. Acoust. Soc. Am. **66**, 534–547 (1979).
[33]M. B. Moffett and R. H. Mellen, "Model for parametric acoustic sources," J. Acoust. Soc. Am. **61**, 325–337 (1977).
[34]K. Brinkman, "The interaction of two plane sound waves of finite amplitude and coincident direction of propagation," Acustica **20**, 92–100 (1968).
[35]J. B. Edgerton, Jr., "Finite amplitude acoustic waves generated by a baffled, multiharmonic transducer," Ph. D. thesis, Georgia Institute of Technology, Atlanta, GA (1988).

Ray theory solution for finite amplitude effects in a two-dimensional hard-walled waveguide

Kun-Tien Shu and Jerry H. Ginsberg
The George W. Woodruff School of Mechanical Engineering, Georgia Institute of Technology, Atlanta, Georgia 30332

(Received 6 October 1988; accepted for publication 18 April 1989)

Ray theory and perturbation analysis are combined to analyze the cumulative growth of nonlinear effects resulting from excitation of a single nonplanar mode in a two-dimensional waveguide whose walls are rigid. The first-order (linear) signal is decomposed into a pair of obliquely propagating planar waves. The signal associated with each ray is required to satisfy the inhomogeneous second-order wave equation. A single ray emanating from its source is followed to its first incidence at one wall, and the reflection of such a ray is determined by requiring that incident and reflected rays combine to satisfy the hard-wall boundary condition. The method of images then leads to a generalization of the result to the case of a ray that undergoes multiple reflections. Nonuniform validity of the ray signal determined in this manner is corrected by the method of renormalization, which leads to the conclusion that a ray behaves like a simple nonlinear planar wave, except that the propagation distance is measured by tracing the ray back to its source. The overall signal at a specified field point is determined by superposing the signals associated with the two rays that intersect at that location. The result is shown to be in complete agreement with earlier modal analyses of the same problem, provided that the frequency is sufficiently low to inhibit resonant energy transfer between nearly parallel rays. Although the analysis is less direct than that used previously, it yields physical insight into the distortion process not previously available.

PACS numbers: 43.25. – x, 43.20.Dk, 43.20.Mv

INTRODUCTION

In linear theory, a two-dimensional mode in a hard-walled waveguide at a frequency exceeding cutoff may be decomposed into a pair of obliquely propagating planar waves. Nonlinearity associated with finite amplitude effects leads to two types of harmonic generation. Each planar wave generates a planar second harmonic that propagates jointly with the fundamental. This leads to a resonant self-action process, in which energy is continuously transferred from the fundamental to higher harmonics of that planar wave. This is the cumulative distortion effect commonly encountered in simple waves. In contrast, the interaction between different oblique planar waves is a dispersive process, in which the interchange between fundamental and second harmonic is not resonant. Cumulatively growing distortion in this case only arises at frequencies substantially above cutoff.

Most analyses of nonlinear effects in a waveguide have been founded on perturbation techniques. Nayfeh and Tsai used the method of multiple scales to study waveguides having rectangular[1] and circular[2] cross sections, in the case where the walls are acoustically treated. The wave propagation phenomena in the linearized version of such systems are dispersive, which inhibits the type of resonant interactions that leads to cumulatively growing distortion. Consideration of resonant interactions was also avoided in the analysis by Keller and Millman[3] of propagation in a rigid-walled waveguide whose cross section is not rectangular. Their perturbation technique was the method of strained parameters based on an expansion of the wavenumber. The method of multiple scales was used by Vaidya and Wang[4] to investigate nonlinear interaction effects in a rigid-walled waveguide that is subjected to a multiharmonic excitation. The walls in the system they studied were rigid, corresponding in linear theory to nondispersive waves. Resonant self-action was predicted by their analysis, but the complications associated with the method of multiple scales and the multitude of interactions prevented analytical solution of the partial differential equations governing the amplitudes of the modes.

Finite amplitude propagation phenomena arising from multimode excitation of a rigid-walled waveguide were also studied by Ginsberg.[5] He employed the method of renormalization to examine nonlinear self-action effects within groups of nondispersive waves. The overall response was shown to be a superposition of the various nondispersive groups, each of whose distortion is governed by the signal associated with that group. Hamilton and TenCate[6] incorporated the effects of thermoviscous attenuation into their analysis of interactions for a low-frequency excitation of a waveguide mode. That investigation evaluated the pressure by solving numerically the differential equations governing the amplitudes of a Fourier series expansion.

The latter two studies both avoided consideration of the high-frequency regime, in which the pair of oblique planar waves is nearly parallel to the axis of the waveguide. In that situation, the transverse wavelength of a mode is much greater than the axial wavelength, so the mode has a nearly planar appearance. Significant coupling with the truly planar mode then arises, even though the planar mode is not directly excited. Ginsberg and Miao[7] developed an analytical procedure for treating high-frequency modes by using

 0001-4966/89/080771-06$00.80

the method of renormalization. They considered the case of excitation of the (2,0) mode as a prototypical example.

An important aspect of the aforementioned investigations is that they all employed separation of variables concepts in order to develop solutions of the perturbation partial differential equations. One may consider them to be modal formulations, in contrast to our solution, which is based on evaluation of the propagation of signals along rays that reflect off the rigid walls. Our solution is suggested by studies performed by Feng[8,9] and Qian[10] of the reflection of a distorted plane wave obliquely incident on the boundary of an infinite half-space. However, those works only addressed the mechanisms by which second harmonics are generated, whereas the present study fully explores the distortion process.

It is the intent of this presentation to develop the ray approach, and to use the solution to gain additional insight into physical phenomena. Since the earlier modal formulations adequately describe the response throughout the frequency spectrum, we shall avoid the complications of dissipation and quasiplanar coupling phenomena by limiting the analysis to the moderate frequency regime. Also, for the sake of simplicity, we consider only the case of a monochromatic excitation that excites a single mode according to linear theory.

The treatment begins by decomposing the first-order (i.e., linear) velocity potential into the pair of oblique waves, from which the nonlinear source terms generating the second-order signal are derived. A specific ray is then followed from its source through its first reflection at one of the rigid walls. The result is extended to the case of a ray that has undergone many reflections by applying the method of images. The overall signal in the waveguide is then synthesized by tracing the rays arriving at a specified field point back to their respective sources.

The ray solution explains an apparent paradox in the earlier modal analyses. Specifically, although the signal may be decribed in terms of a pair of oblique planar waves that propagate in both the axial and transverse directions, the scale of the distortion process is independent of the transverse position. Conversely, the earlier modal solutions provide validation for the present analysis, which indicates that the solution is a superposition of the signal associated with each ray. One corollary of the analysis is to prove that the laws for linear reflection from a rigid planar surface also apply to the nonlinear ray.

I. EVALUATION OF THE FIRST- AND SECOND-ORDER RAYS

We consider a two-dimensional waveguide whose rigid walls occupy the planes $x = 0$ and $x = L$, with z measuring axial distance. Perturbational equations for the velocity potential ϕ in the absence of dissipation and shocks, correct to second order, are

$$\phi = \epsilon\phi_1 + \epsilon^2\phi_2 + \cdots, \tag{1}$$

$$c_0^2\nabla^2\phi_1 - \frac{\partial^2\phi_1}{\partial t^2} = 0, \tag{2}$$

$$c_0^2\nabla^2\phi_2 - \frac{\partial^2\phi_2}{\partial t^2} = \frac{\partial}{\partial t}(\nabla\phi_1\cdot\nabla\phi_1) + 2(\beta_0 - 1)\frac{\partial\phi_1}{\partial t}\nabla^2\phi_1, \tag{3}$$

where ϵ is the acoustic Mach number of the excitation, $\epsilon \ll 1$, c_0 is the speed of sound in linear theory, and β_0 is the coefficient of nonlinearity for the fluid. The particle velocity and pressure may be obtained from

$$\mathbf{v} = \nabla\phi, \quad p = -\rho_0\frac{\partial\phi}{\partial t} + O(\phi^2). \tag{4}$$

We postulate the existence of a velocity distribution along $z = 0$ that excites only nonplanar mode $(m, 0)$. The corresponding boundary condition is

$$\left.\frac{\partial\phi}{\partial z}\right|_{z=0} = \epsilon c_0 \sin(\omega t)\cos(k_x x), \quad k_x = \frac{m\pi}{L}. \tag{5}$$

The rigid wall conditions are

$$\left.\frac{\partial\phi}{\partial x}\right|_{x=0} = \left.\frac{\partial\phi}{\partial x}\right|_{x=L} = 0. \tag{6}$$

The cutoff frequency, below which the solution for ϕ_1 evanesces, is c_0k_x. We are concerned here only with the propagating case, which leads to

$$\phi_1 = (c_0/k_z)\cos(k_z z - \omega t)\cos(k_x x), \tag{7}$$

where

$$k = \omega/c_0, \quad k_z = (k^2 - k_x^2)^{1/2}, \quad k > k_x. \tag{8}$$

The first-order potential may equivalently be described as two trains of planar waves. As depicted in Fig. 1, for the case $m = 2$, the respective rays are parallel to the directions $\mathbf{n}_{\mathrm{I}}$ and $\mathbf{n}_{\mathrm{II}}$, both of which are oriented at angle θ from the axial direction, where the propagation angle is given by

$$k\sin\theta = k_x, \quad k\cos\theta = k_z. \tag{9}$$

The specific expression obtained from Eq. (7) is

$$\phi_1 = F_1[\cos(kz_{\mathrm{I}} - \omega t) + \cos(kz_{\mathrm{II}} - \omega t)], \quad F_1 = c_0/2k\cos\theta, \tag{10}$$

where the distances z_{I} and z_{II} are the projections in the directions of propagation of the position $\mathbf{x}$ relative to the origin. Specifically,

$$z_{\mathrm{I}} = \mathbf{n}_{\mathrm{I}}\cdot\mathbf{x} = x\sin\theta + z\cos\theta, \quad z_{\mathrm{II}} = \mathbf{n}_{\mathrm{II}}\cdot\mathbf{x} = -x\sin\theta + z\cos\theta. \tag{11}$$

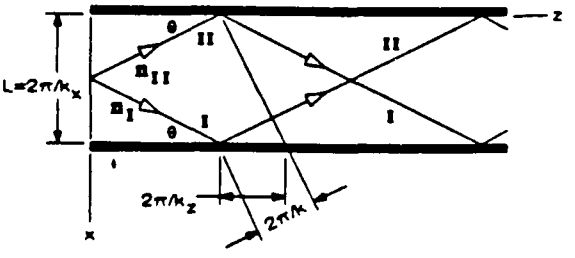

FIG. 1. Geometry of the pair of oblique planar waves.

Substitution of Eq. (10) into Eq. (3) leads to

$$c_0^2\nabla^2\phi_2 - \frac{\partial^2\phi_2}{\partial t^2} = -\omega k^2 F_1^2\{\beta_0[\sin(2kz_{\rm I} - 2\omega t) + \sin(2kz_{\rm II} - 2\omega t)] + 2\beta'\sin(2k_z z - 2\omega t)\}. \quad (12)$$

In the foregoing, the last term arises from the dot product of the $\mathbf{n}_{\rm I}$ and $\mathbf{n}_{\rm II}$ terms in $\nabla\phi_1$. Correspondingly, the coefficient $\beta' = \beta_0 - 2\sin^2\theta$ is the coefficient of nonlinearity for interaction of two noncollinear planar waves.[11,12] This is contrasted by the terms in Eq. (12) associated with β_0, which represent self-action of the respective rays. They arise from dot products involving solely an $\mathbf{n}_{\rm I}$ or $\mathbf{n}_{\rm II}$ term.

The source terms in Eq. (12) corresponding to self-action are solutions of the homogeneous wave equation, whereas the term arising from interaction of the intersecting planar waves is not. As we shall see, the effect of self-action is to produce terms in ϕ_2 that grow in magnitude with increasing z, corresponding to the familiar cumulative distortion process. The interaction term leads to a solution for ϕ_2 whose overall amplitude is independent of z, although it has the appearance of spatial beats.[7,12] The amplitude of these beats is singular in the high-frequency limit, for which $k_z \to k$ and $\theta \to 0$. Our purpose here is to gain additional understanding of the distortion due to self-action. For that reason, we shall not address this limiting case. Correspondingly, we denote as $O(\epsilon^2)$, without further analysis, all second-order terms, including ray interaction, whose magnitude does not grow with increasing z.

Rather than using modal procedures to evaluate the self-action effect, the present approach will synthesize the appropriate solution from an analysis of the reflection process of a ray obliquely incident at one of the walls. Since the terms that are uniformly $O(\epsilon^2)$ are to be ignored, the general solution for ϕ_2 is associated with the first two source terms in Eq. (12). The form of the solution is

$$\phi_2 = F_2[(z_{\rm I} + C_{\rm I})\cos(2kz_{\rm I} - 2\omega t) + (z_{\rm II} + C_{\rm II})\cos(2kz_{\rm II} - 2\omega t)] + O(\epsilon^2). \quad (13)$$

In order that Eq. (13) satisfy Eq. (12), it must be that

$$F_2 = \beta_0\omega k F_1^2/4c_0^2 \equiv \beta_0 c_0/16\cos^2\theta. \quad (14)$$

The constants $C_{\rm I}$ and $C_{\rm II}$ arise from the complementary solution. In order to determine them, consider a region near the origin, such that a ray undergoes only one reflection at $x = 0$. Such a situation appears in Fig. 2, where ray II emanating from source point A is incident at point B, resulting in the reflected ray I. Since boundary condition (5) is satisfied by ϕ_1, it must be that $\partial\phi_2/\partial z = 0$ at $z = 0$. Applying this condition to the secular portion of ray II in Eq. (13) leads to $z_{\rm II} + C_{\rm II} = 0$ at $z = 0$, $x = x_{\rm A}$, so that

$$C_{\rm II} = x_{\rm A}\sin\theta. \quad (15)$$

This result is consistent with the notion that the nonlinear effect grows with increasing distance from the source, since it leads to $\phi_2 = 0$ at $z = 0$.

We find from the foregoing that the incident ray is

$$(\phi_2)_{\rm inc} = F_2(z_{\rm II} + x_{\rm A}\sin\theta)\cos(2kz_{\rm II} - 2\omega t). \quad (16)$$

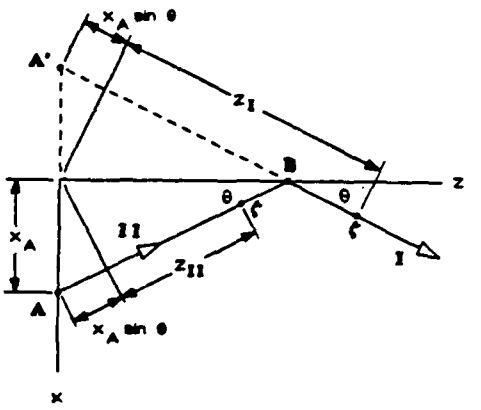

FIG. 2. Reflection of a ray at a rigid wall.

Since $\partial z_{\rm I}/\partial x = -\partial z_{\rm II}/\partial x$, the sum $(\phi_2)_{\rm inc} + (\phi_2)_{\rm ref}$ given by Eq. (13) satisfies the rigid wall condition at $x = 0$, if $C_{\rm I} = C_{\rm II}$. Hence, the reflected ray departing from point B is

$$(\phi_2)_{\rm ref} = F_2(z_{\rm I} + x_{\rm A}\sin\theta)\cos(2kz_{\rm I} - 2\omega t). \quad (17)$$

The significance of these expressions lies in our ability to generalize them. We observe in Fig. 2 that $z_{\rm I}$ and $z_{\rm II}$ are the distances in the respective directions $\mathbf{n}_{\rm I}$ and $\mathbf{n}_{\rm II}$ measured from the origin, while $x_{\rm A}\sin\theta$ is the distance between source point A and the origin measured along $\mathbf{n}_{\rm II}$. However, $x_{\rm A}\sin\theta$ is also the distance between image point A' and the origin measured along $\mathbf{n}_{\rm I}$. Furthermore, note that $z_{\rm I} = z_{\rm II}$ at point B. If $\boldsymbol{\zeta}$ denotes the position of a generic point on either ray, and A, A', and B denote the position of the respective points, then Eqs. (16) and (17) may be rewritten as

$$\begin{aligned}(\phi_2)_{\rm inc} &= F_2\mathbf{n}_{\rm II}\cdot(\boldsymbol{\zeta} - \mathbf{A})\cos(2k\mathbf{n}_{\rm II}\cdot\boldsymbol{\zeta} - 2\omega t),\\ (\phi_2)_{\rm ref} &= F_2\mathbf{n}_{\rm I}\cdot(\boldsymbol{\zeta} - \mathbf{A}')\cos(2k\mathbf{n}_{\rm I}\cdot\boldsymbol{\zeta} - 2\omega t)\\ &= F_2[\mathbf{n}_{\rm II}\cdot(\mathbf{B} - \mathbf{A}) + \mathbf{n}_{\rm I}\cdot(\boldsymbol{\zeta} - \mathbf{B})]\\ &\quad\times\cos\{2k[\mathbf{n}_{\rm II}\cdot\mathbf{B} + \mathbf{n}_{\rm I}\cdot(\boldsymbol{\zeta} - \mathbf{B})] - 2\omega t\}.\end{aligned} \quad (18)$$

The two forms for the reflected ray lead to alternative interpretations of the reflection process. In the first, the ray appears to emanate from the image point A', where it is undistorted, while the second form corresponds to a ray emanating from the reflection point B. In the latter viewpoint, the expression for $(\phi_2)_{\rm inc}$ shows the second-order signal in the reflected ray at point B to be equal to the signal in the ray incident at that point. The second interpretation leads us through mathematical induction to recognize that the characterization is quite general—it does not rely on the fact that the reflection in Fig. 2 is from the wall at $x = 0$. All that is required to apply Eqs. (18) to reflection from the wall at $x = L$ is to interchange the subscripts I and II. Equally important, it follows that the results are valid even if the incident ray itself arises from a prior reflection.

We see from the foregoing that the reflection of the second-order ray associated with the self-distortion process is the same as the familar reflection law for a ray in linear acoustics. This is precisely the conclusion reached earlier by Feng[8,9] and Qian.[10] Although the second expression for $(\phi_2)_{\rm ref}$ in Eqs. (18) is more useful for qualitative under-

standing of reflection, the first expression, which uses the image point, will lead us in the next section to a construction of the particle velocity and pressure at a specified location.

II. UNIFORMLY VALID FIELD SOLUTION

In Fig. 3, we have selected a specific field point at position x. The source points A and C are for the I and II rays intersecting this point, and A′ and C′ are the corresponding image points. The distances s_I and s_{II} are the respective distances from the image points to the field point. (The fact that $s_I = s_{II} = z/\cos\theta$ will be important later.) Combining the term for either ray obtained from Eq. (10) with the first expression for a reflected ray in Eqs. (18) yields the potential function associated with self-action of the rays:

$$\phi_I = \epsilon F_1 \cos(kz_I - \omega t) + \epsilon^2 F_2 s_I \cos(2kz_I - 2\omega t),$$
$$\phi_{II} = \epsilon F_1 \cos(kz_{II} - \omega t) + \epsilon^2 F_2 s_{II} \cos(2kz_{II} - 2\omega t). \tag{19}$$

Since $s_I - z_I$ and $s_{II} - z_{II}$ are constants along the respective rays, the particle velocity associated with each ray is

$$\mathbf{v}_I = \frac{\partial \phi_I}{\partial z_I}\mathbf{n}_I = -\epsilon k \mathbf{n}_I (F_1 \sin\psi_I + 2\epsilon F_2 s_I \sin 2\psi_I) + O(\epsilon^2),$$
$$\mathbf{v}_{II} = \frac{\partial \phi_{II}}{\partial z_{II}}\mathbf{n}_{II} = -\epsilon k \mathbf{n}_{II} (F_1 \sin\psi_{II} + 2\epsilon F_2 s_{II} \sin 2\psi_{II}) + O(\epsilon^2), \tag{20}$$

where the phase variables are

$$\psi_I = kz_I - \omega t, \quad \psi_{II} = kz_{II} - \omega t. \tag{21}$$

The corresponding pressures are

$$p_I = -\rho_0 \frac{\partial \phi_I}{\partial t} + O(\phi^2) = \rho_0 c_0 \mathbf{v}_I \cdot \mathbf{n}_I,$$
$$p_{II} = -\rho_0 \frac{\partial \phi_{II}}{\partial t} + O(\phi^2) = \rho_0 c_0 \mathbf{v}_{II} \cdot \mathbf{n}_{II}. \tag{22}$$

Equations (20) contain ϵ^2 terms that grow with increasing distance, so they are not uniformly valid. We correct this behavior by invoking the method of renormalization, which introduces a near-identity transformation between the linear phase variables ψ_I, ψ_{II} and nonlinear phases χ_I, χ_{II}. The details of the renormalization may be found in the Appendix. The result is that

$$\mathbf{v}_I = -\epsilon k F_1 \mathbf{n}_I \sin\chi_I, \quad \mathbf{v}_{II} = -\epsilon k F_1 \mathbf{n}_{II} \sin\chi_{II}, \tag{23}$$

where the transformations have implicit functional forms given by

$$\psi_I = \chi_I + \beta_0 k s_I \mathbf{v}_I \cdot \mathbf{n}_I / c_0,$$
$$\psi_{II} = \chi_{II} + \beta_0 k s_{II} \mathbf{v}_{II} \cdot \mathbf{n}_{II} / c_0. \tag{24}$$

The nonlinear phase variable corresponding to a specified value of a linear variable may be found by numerical solution of Eqs. (24), after substitution of Eqs. (23). The velocity components v_x and v_z, and the pressure p associated with the cumulative nonlinear distortion process, may then be determined by superposition of the results for the two rays. This leads to

$$v_x = (\mathbf{v}_I \cdot \mathbf{n}_I - \mathbf{v}_{II} \cdot \mathbf{n}_{II}) \sin\theta = -\epsilon k F_1 \sin\theta (\sin\chi_I - \sin\chi_{II}),$$
$$v_z = (\mathbf{v}_I \cdot \mathbf{n}_I + \mathbf{v}_{II} \cdot \mathbf{n}_{II}) \cos\theta = -\epsilon k F_1 \cos\theta (\sin\chi_I + \sin\chi_{II}),$$
$$p = \rho_0 c_0 (\mathbf{v}_I \cdot \mathbf{n}_I + \mathbf{v}_{II} \cdot \mathbf{n}_{II}) = -\epsilon \rho_0 c_0 k F_1 (\sin\chi_I + \sin\chi_{II}). \tag{25}$$

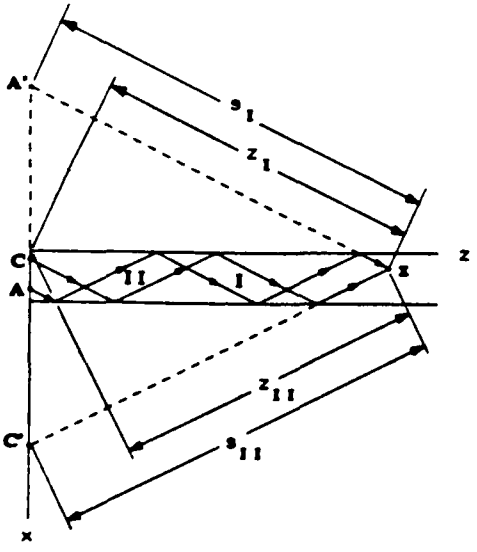

FIG. 3. Source and image points for the rays intersecting at a selected field point.

III. VALIDATION

It is not difficult to prove that the combination of Eqs. (23) and (24) for either ray is identical to the Earnshaw solution[13] for the finite amplitude planar wave generated by a low Mach number harmonic excitation. Specifically, if the particle velocity v at position $s = 0$ is $\epsilon c_0 \sin(\omega t - \delta)$, the Earnshaw solution for small ϵ is

$$v = -\epsilon c_0 \sin[\omega(s/c - t) + \delta], \quad c = c_0 + \beta_0 v. \tag{26}$$

The linear and nonlinear phase variables for the planar wave are

$$\psi = ks - \omega t + \delta \tag{27}$$

and

$$\chi = k\left(\frac{c_0}{c}\right)s - \omega t + \delta = \psi - \frac{\beta_0 k s v}{c_0} + O\left(\frac{s v^2}{c_0^2}\right), \tag{28}$$

respectively.

The second equation, which relates χ and ψ, is comparable to that indicated by Eqs. (24) for either ray. In order to ascertain the phase lag associated with each ray, we rewrite Eqs. (21) as

$$\psi_I = ks_I - \omega t - k(s_I - z_I),$$
$$\psi_{II} = ks_{II} - \omega t - k(s_{II} - z_{II}). \tag{29}$$

Inspection of Fig. 3 shows that the distances $s_I - z_I$ and $s_{II} - z_{II}$ may be expressed in terms of the locations of the respective image points $x_{A'}$ and $x_{C'}$. As a consequence, the phase lags are

$$\delta_I = -k(s_I - z_I) \equiv kx_{A'} \sin\theta = k_x x_{A'},$$
$$\delta_{II} = -k(s_{II} - z_{II}) \equiv -kx_{C'} \sin\theta = -k_x x_{C'}. \tag{30}$$

Geometrical analysis reveals that $x_{A',C'} = \pm x_{A,C} \pm 2jL$, where the integer j and the choice of sign depend solely on the number of reflections the ray undergoes prior to its arrival at the field point. Since $k_x L = m\pi$, the phase lags may be equivalently written as

$$\delta_I = \pm k_x x_A, \quad \delta_{II} = \pm k_x x_C. \tag{31}$$

Clearly, the phase delay in each ray stems from its origination from a point that is not at the x,z origin.

We have seen that the signal along each ray behaves like a simple planar wave, whose distortion depends on the propagation distance measured obliquely along each ray. This seems to conflict with the results of the modal analyses, which found that the distortion process is dependent only on the axial position. There actually is no inconsistency. In order to demonstrate this, let us convert Eqs. (23)–(25) to variables associated with the x,z spatial coordinates. First, we apply the trigonometric identities for the sum and difference of two sines to Eqs. (25), and define new nonlinear independent variables η and ξ, such that

$$k\eta \sin\theta = \tfrac{1}{2}(\chi_I - \chi_{II}), \quad k\xi \cos\theta = \tfrac{1}{2}(\chi_I + \chi_{II}) + \omega t. \tag{32}$$

This converts Eqs. (25) to

$$v_x = -2\epsilon k F_1 \sin\theta \sin(k\eta \sin\theta) \cos(k\xi \cos\theta - \omega t), \tag{33}$$
$$p = \rho_0 c_0 v_x / \cos\theta$$
$$= -2\epsilon\rho_0 c_0 k F_1 \cos(k\eta \sin\theta) \sin(k\xi \cos\theta - \omega t).$$

Elimination of θ and F_1 from these expressions, by substitution of Eqs. (9) and (10), shows these expressions to be the same as Eqs. (43) and (44b) in the paper by Ginsberg and Miao,[7] which are the approximations for moderate frequencies of the general expressions for the signal.

We obtain relations for η and ξ by subtracting and adding Eqs. (24). Since $s_I = s_{II} = z/\cos\theta$, this step yields

$$\tfrac{1}{2}(\psi_I - \psi_{II}) = k\eta \sin\theta + (\beta_0 kz/2c_0 \cos\theta) \times (\mathbf{v}_I \cdot \mathbf{n}_I - \mathbf{v}_{II} \cdot \mathbf{n}_{II}),$$
$$\tfrac{1}{2}(\psi_I + \psi_{II}) = k\xi \cos\theta - \omega t + (\beta_0 kz/2c_0 \cos\theta) \times (\mathbf{v}_I \cdot \mathbf{n}_I + \mathbf{v}_{II} \cdot \mathbf{n}_{II}). \tag{34}$$

The left side of each relation may be simplified by the introduction of Eqs. (9), (11), and (21), while Eqs. (25) simplify the right side. The result is

$$x = \eta + [\beta_0 z/(2\sin^2\theta \cos\theta)](v_x/c_0),$$
$$z = \xi + [\beta_0 z/(2\cos^3\theta)](v_x/c_0). \tag{35}$$

When Eqs. (9) are used to eliminate θ from the foregoing, the result is identical to Ginsberg and Maio's Eq. (45).

It is obvious that the magnitudes of the differences $\eta - x$ and $\xi - z$, which represent the degree to which the phases of v_x, v_z, and p differ from their linear analogs, are proportional to z. This result is obtained, even though each ray depends on both x and z, because the propagation distance of intersecting rays is identical and depends only on z; see Fig. 3. Hence, when z is held fixed, the pair of rays intersecting at different x have all propagated through the same distance, even though they originate from different sources on $z = 0$. The location of the source point for each of these rays only affects the phase lag of its signal, as shown in Eqs. (31). It is for this reason that the only apparent effect of transverse position in Eqs. (33) is the sinusoidal phase factor mirroring the excitation.

IV. DISCUSSION

We have demonstrated that finite amplitude propagation phenomena in a waveguide may be described in terms of rays. Although the formulation is less straightforward than the comparable analysis[5] using modal techniques, the result provides physical insight not available from the earlier solutions. It was shown here that two rays emanate from each source point at the boundary where the excitation is applied. The signal along each ray distorts in the same manner as a conventional planar wave, with the propagation distance measured along each ray. Reflection of a ray at a hard wall obeys the linear rule for oblique reflection at a rigid surface: angle of incidence equals angle of reflection, no loss in signal strength, and no change of phase.

If the frequency of excitation is not too high, interaction between crossing rays is insignificant in comparison to the self-action distortion phenomena for each ray. However, at high frequencies the near parallelism of crossing rays enhances their interaction. This phenomenon, which was treated by Ginsberg and Miao,[7] was not considered in the present analysis. (It seems reasonable to expect that nearly parallel rays for proximate modes in a case of multimodal excitation will couple in the same manner.)

When interaction between rays is omitted, the signal may be obtained by superposing the signal associated with each ray. This explains the observation in an earlier analysis by Ginsberg[14] that shocks form along the wave fronts for either ray. The ray picture also emphasizes the increasing role of dissipation, which was not included in the present work, when the frequency is allowed to approach cutoff. In that case, the decrease in the wavenumber k is accompanied by an increase in the angle θ between the rays and the axis of the waveguide. If one considers a fixed position, the propagation distance for the rays intersecting at that position increases in proportion to $\sec\theta$. This leads to an increase in the dissipation loss factor.

ACKNOWLEDGMENTS

The authors wish to thank the National Science Foundation and the Office of Naval Research for their support of this research.

APPENDIX

The method of renormalization, described by Nayfeh,[15] is based on the notion that a weakly nonlinear process is comparable to the linear process, except that the independent variables correspond to a distortion of the space-time grid that increases with increasing distance from the source. Consider the nonuniformly valid description of ray I, as given by the first of Eqs. (20). Since the second-order term is proportional to s_I, the nonlinear phase variable χ_I should equal the linear variable ψ_I at $s_I = 0$, and the difference $\chi_I - \psi_I$ should increase in proportion to ϵs_I. Hence, we seek a near identity transformation in the form

$$\psi_I = \chi_I + \epsilon s_I G_I(\chi_I), \tag{A1}$$

where the unspecified function $G_I(\chi_I)$ must be selected to cancel the nonuniformly valid term.

In order to determine G_I, we substitute Eq. (A1) into the first of Eqs. (20), and expand the result in a Taylor series in powers of ϵ. This gives

$$\begin{aligned} \mathbf{v}_I &= -\epsilon k \mathbf{n}_I [F_1 \sin(\chi_I + \epsilon s_I G_I) \\ &\quad + 2\epsilon F_2 s_I \sin(2\chi_I + 2\epsilon s_I F_I)] \\ &= -\epsilon k \mathbf{n}_I [F_1 \sin\chi_I + \epsilon s_I \cos\chi_I \\ &\quad \times (F_1 G_I + 4F_2 \sin\chi_I)] + O(\epsilon^2). \end{aligned} \tag{A2}$$

Setting the factor containing G_I to zero leads to

$$\begin{aligned} \mathbf{v}_I &= -\epsilon k \mathbf{n}_I F_1 \sin\chi_I, \\ \psi_I &= \chi_I - 4\epsilon s_I (F_2/F_1) \sin\chi_I = \chi_I + \beta_0 k s_I \mathbf{v}_I \cdot \mathbf{n}_I / c_0. \end{aligned} \tag{A3}$$

The relations for the second ray may be obtained by changing the subscripts in Eqs. (A3) from I to II.

[1] A. H. Nayfeh and M. S. Tsai, "Nonlinear acoustic propagation in two-dimensional ducts," J. Acoust. Soc. Am. 55, 1166–1172 (1974).
[2] A. H. Nayfeh and M. S. Tsai, "Nonlinear wave propagation in acoustically lined circular ducts," J. Sound Vib. 35, 77–89 (1974).
[3] J. B. Keller and M. H. Millman, "Finite-amplitude sound-wave propagation in a waveguide," J. Acoust. Soc. Am. 49, 329–333 (1971).
[4] P. G. Vaidya and K. S. Wang, "Non-linear propagation of complex sound fields in rectangular ducts, Part I: The self-excitation phenomenon," J. Sound Vib. 50, 29–42 (1977).
[5] J. H. Ginsberg, "Finite-amplitude two-dimensional waves in a rectangular duct induced by arbitrary periodic excitation," J. Acoust. Soc. Am. 65, 1127–1133 (1979).
[6] M. F. Hamilton and J. A. TenCate, "Finite amplitude sound near cutoff in higher-order modes of a rectangular duct," J. Acoust. Soc. Am. 84, 327–334 (1988).
[7] J. H. Ginsberg and H. C. Miao, "Finite amplitude distortion and dispersion of a nonplanar mode in a waveguide," J. Acoust. Soc. Am. 80, 911–920 (1986).
[8] S. S. Feng, "Reflection of finite amplitude waves," Sov. Phys. Acoust. 6, 488–490 (1961).
[9] S. S. Feng, "The reflection and refraction of finite amplitude plane sound wave in two dimensions," Chin. J. Acoust. 2, 293–302 (1983).
[10] Z. Qian, "Reflection of finite-amplitude sound waves on a plane boundary of half-space," Sci. Sin. 25, 492–501 (1982).
[11] M. F. Hamilton and D. T. Blackstock, "On the coefficient of nonlinearity β in nonlinear acoustics," J. Acoust. Soc. Am. 83, 74–77 (1988).
[12] J. N. Tjøtta and S. Tjøtta, "Interaction of sound waves. I: Basic equations and plane waves," J. Acoust. Soc. Am. 82, 1425–1428 (1987).
[13] J. W. S. Rayleigh, *The Theory of Sound* (Dover, New York, 1945), Vol. II, pp. 37–38.
[14] J. H. Ginsberg, "A re-examination of the nonlinear interaction between an acoustic fluid and a flat plate undergoing harmonic excitation," J. Sound Vib. 60, 449–458 (1978).
[15] A. H. Nayfeh, *Perturbation Methods* (Wiley-Interscience, New York, 1973), pp. 95–98.

REFRACTION AND REFLECTION OF AN OBLIQUELY INCIDENT FINITE AMPLITUDE PLANE P WAVE AT A PLANE [redacted] INTERFACE

Kun-Tien Shu
Jerry H. Ginsberg

School of Mechanical Engineering
Georgia Institute of Technology
Atlanta, Georgia 30332

[Work supported by NSF and ONR]

26 May 1989

Presented at 117th Meeting of ASA
Syracuse, NY

$$- \sqrt{2}\,\frac{\omega_1^{3/2}}{\omega_2^{1/2}}\left(\frac{\mu_n^*}{\mu_n}\right)^{1/2} nV_1(n)\exp\left(i\omega_1 t - \mu_n\alpha_1 + i\omega_1 nR - i\,\frac{\pi}{4}\right)\Big] + \text{c.c.}\Big\}. \tag{47b}$$

NONLINEAR WAVE EQUATION

Fluid case for simplicity:

$$c_0^2\nabla^2\phi - \frac{\partial^2\phi}{\partial t^2} = \frac{\partial}{\partial t}\Big[\frac{1}{c_0^2}(\beta_0 - 1)\Big(\frac{\partial\phi}{\partial t}\Big)^2 + \nabla\phi\cdot\nabla\phi\Big] + O(\phi^3)$$

$$p = -\rho_0\frac{\partial\phi}{\partial t} - \mathcal{L} + O(\phi^3)$$

$$\mathbf{v} = \nabla\phi$$

where

$$\beta_0 = 1 + \frac{B}{2A} \qquad \text{fluids}$$

$$= \frac{\gamma+1}{2} \qquad \text{gases}$$

$$\mathcal{L} = \frac{\rho_0}{2}\Big[\nabla\phi\cdot\nabla\phi - \frac{1}{c_0^2}\Big(\frac{\partial\phi}{\partial t}\Big)^2\Big]$$

PERTURBATION EXPANSION

$$\phi(x,z,t) = \epsilon\phi_1(x,z,t) + \epsilon^2\phi_2(x,z,t) + \cdots$$

where

$$\epsilon \equiv \text{Acoustic Mach Number} = \frac{v}{c_0}$$

$O(\epsilon)$:

$$c_0^2\nabla^2\phi_1 - \frac{\partial^2\phi_1}{\partial t^2} = 0$$

$$p_1 = -\rho_0\frac{\partial\phi_1}{\partial t}$$

$O(\epsilon^2)$:

$$c_0^2\nabla^2\phi_2 - \frac{\partial^2\phi_2}{\partial t^2} = \frac{\partial}{\partial t}(\nabla\phi_1\cdot\nabla\phi_1) + 2(\beta_0 - 1)\frac{\partial\phi_1}{\partial t}\nabla^2\phi_1$$

$$p_2 = -\rho_0\frac{\partial\phi_2}{\partial t} - \mathcal{L}_1$$

PERTURBATION ANALYSIS

DIFFICULTY FOR STRAIGHTFORWARD PERTURBATION APPROACH:

Should **not** satisfy first-order boundary conditions with first-order solution because this leads to a situation where the second-order boundary conditions **cannot** be satisfied

MODIFIED APPROACH:

Consider the incident, reflected, and transmitted waves at first order to be **separate** entities: phase variables ψ_i, ψ_r, ψ_t

$$\phi_1 = \sin \omega\psi_i + \mathrm{R} \sin \omega\psi_r + \mathrm{T} \sin \omega\psi_t$$

Boundary conditions will be satisfied by **total** solution

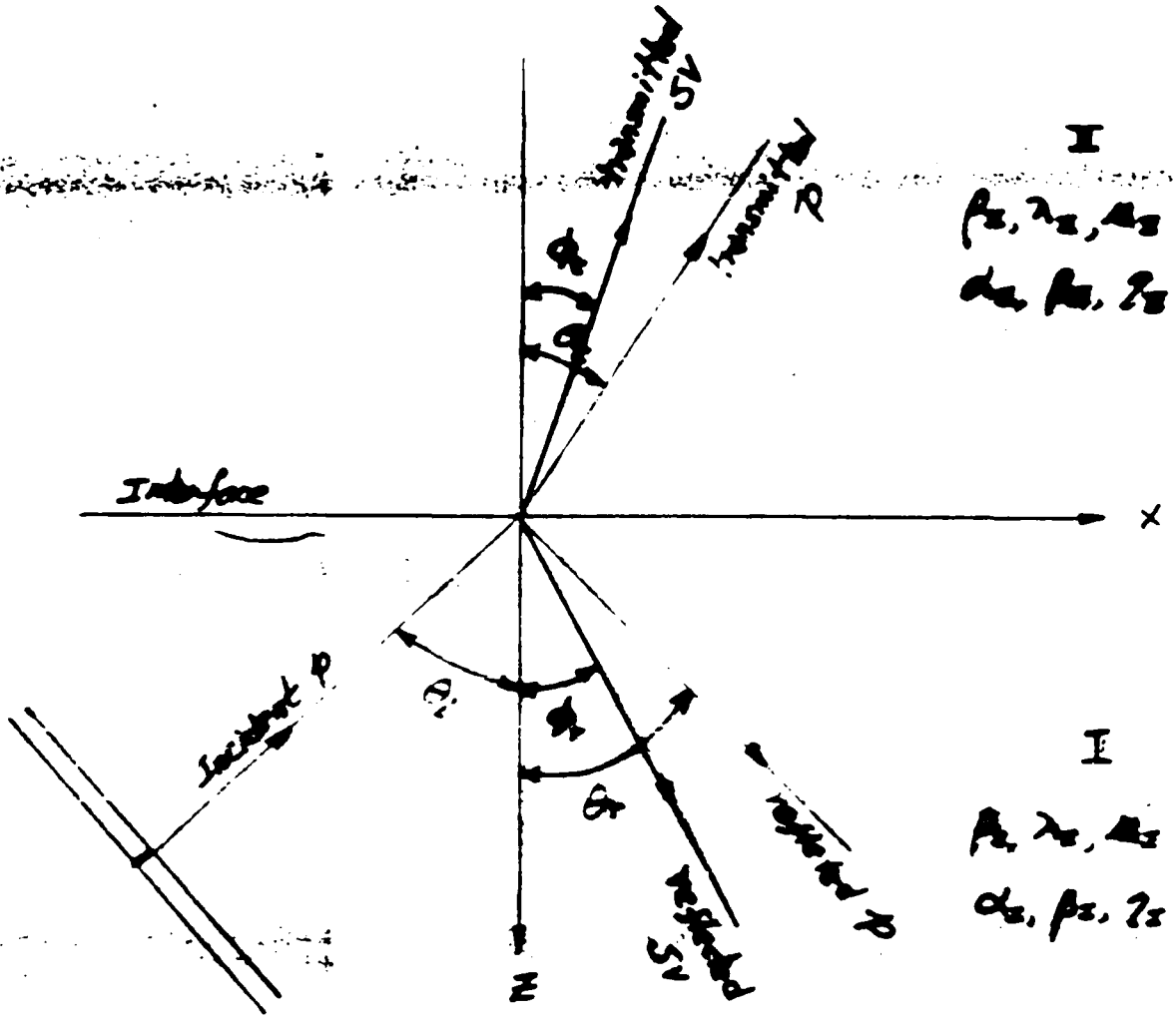

$$\theta_r = \theta_i$$

$$\frac{\sin\theta_i}{C_p^I} = \frac{\sin\phi_r}{C_s^I} = \frac{\sin\theta_t}{C_p^{II}} = \frac{\sin\phi_t}{C_s^I}$$

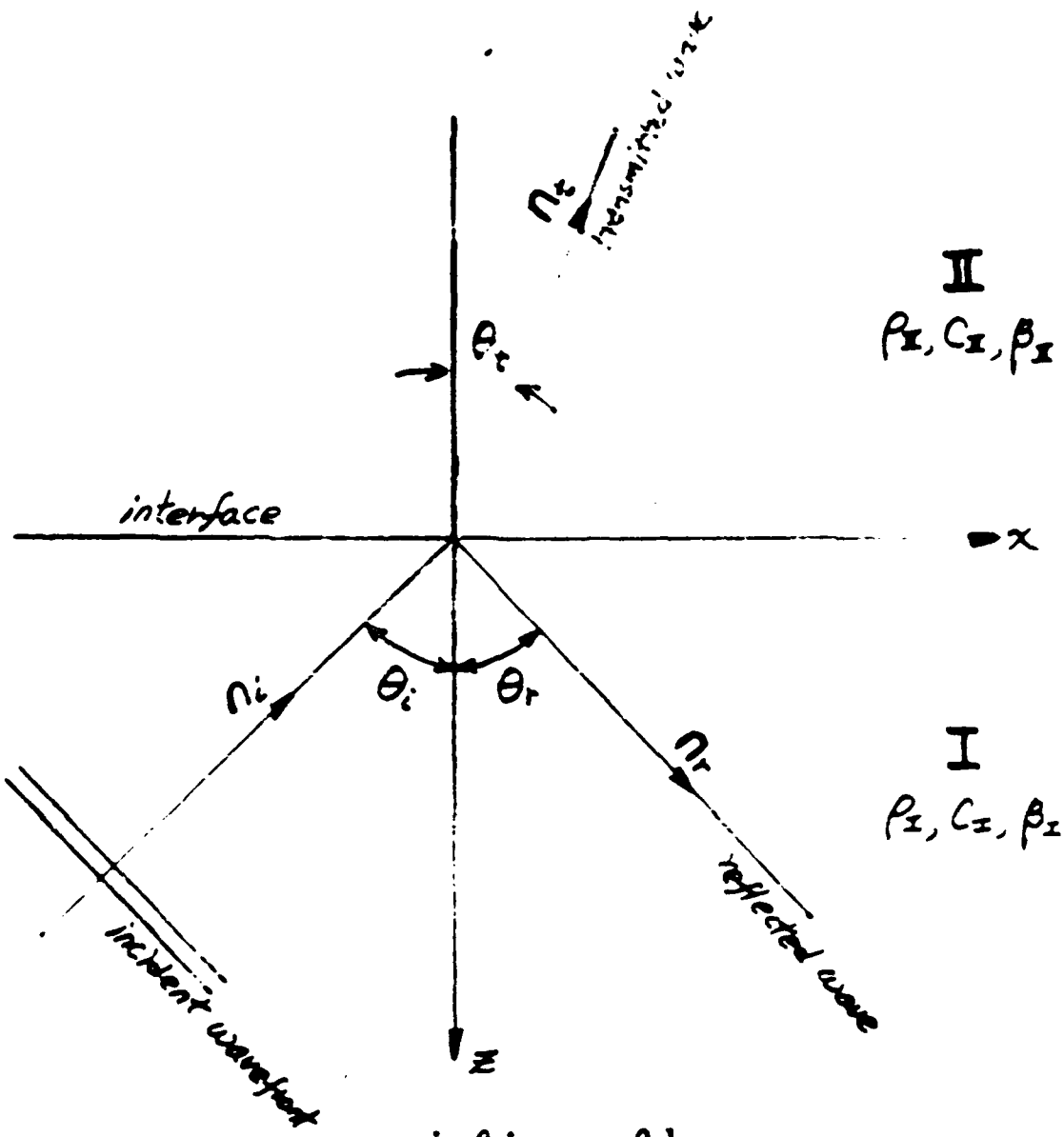

$$\mathbf{n}_i = \sin\theta_i \mathbf{i} - \cos\theta_i \mathbf{k}$$

$$\mathbf{n}_r = \sin\theta_r \mathbf{i} + \cos\theta_r \mathbf{k}$$

$$\mathbf{n}_t = \sin\theta_t \mathbf{i} - \cos\theta_t \mathbf{k}$$

SECOND-ORDER SOLUTION

Nonlinear Self-action: Secular effect

$$(\phi_2)_i = F_1 z_1 \cos(2\omega\psi_i)$$

$$(\phi_2)_r = F_1 \mathrm{R}^2 z_2 \cos(2\omega\psi_r), \quad F_1 = -\frac{\beta_{\mathrm{I}} k_{\mathrm{I}}^3}{4\omega}$$

$$(\phi_2)_t = F_2 \mathrm{T}^2 z_3 \cos(2\omega\psi_t), \quad F_2 = -\frac{\beta_{\mathrm{II}} k_{\mathrm{II}}^3}{4\omega}$$

Nonlinear Interaction: Nonsecular effect

$$\mathrm{NSW} \sim \sin\omega(\psi_i + \psi_r)$$

where

$$\psi_i = t - \frac{z_1}{c_{\mathrm{I}}}, \qquad z_1 = x\sin\theta_i - z\cos\theta_i$$

$$\psi_r = t - \frac{z_2}{c_{\mathrm{I}}}, \qquad z_2 = x\sin\theta_r - z\cos\theta_r$$

$$\psi_t = t - \frac{z_3}{c_{\mathrm{II}}}, \qquad z_3 = x\sin\theta_t - z\cos\theta_t$$

RENORMALIZATION PROCESS – REMOVE SECULAR TERMS

Add First- and **secular** second- order signals to form velocity potential for each wave

Evaluate **physical** response variables

$$\mathbf{v} = \nabla\phi, \quad p = -\rho_0 \frac{\partial\phi}{\partial t} + O(\epsilon^2)$$

Employ a set of **strained** coordinates transformation along the **direction of propagation** of each individual wave

$$z_i = \xi_i + \epsilon Z_i(\xi_i, t)$$

Choose straining functions Z_i to Cancel out the secualr terms

Result is an **Earnshaw–type** solution for incident, reflected, and transmitted waves:

$$\mathbf{v}_i = v_0 \mathbf{n}_i \sin \omega \Psi_i$$

$$\mathbf{v}_r = \mathrm{R} v_0 \mathbf{n}_r \sin \omega \Psi_r$$

$$\mathbf{v}_t = \mathrm{T} v_0 \mathbf{n}_t \sin \omega \Psi_t$$

where

$$\Psi_i = t - \frac{z_1 + L_i}{c_\mathrm{I} + \beta_\mathrm{I} v_i}$$

$$\Psi_r = t - \frac{z_2 + L_r}{c_\mathrm{I} + \beta_\mathrm{I} v_r}$$

$$\Psi_t = t - \frac{z_3 + L_t}{c_\mathrm{II} + \beta_\mathrm{II} v_t}$$

$L_i \equiv$ distance between initial incident wavefront and place of origination (known)

$L_r, L_t \equiv$ phase lags of reflected and transmitted waves (unknown)

$R, T \equiv$ reflected and transmitted coefficients (unknown)

BOUNDARY CONDICTIONS

Continuity of **normal particle velocity** and acoustic pressure across the interface $z = 0$

$$v_z^{\mathrm{I}} = v_z^{\mathrm{II}}, \quad p^{\mathrm{I}} = p^{\mathrm{II}} \qquad \text{at} \quad z = 0$$

Fundamental harmonic excitation at the source

$$v_z = v_0 \sin \omega t \qquad \text{at} \quad z_1 = -L_1$$

First-order terms on boundary conditions determine **secular** effects

Second-order terms may be satisfied with second-order **homogeneous** solution, which are nonsecular - **NEGLECT !**

FINITE AMPLITUDE EFFECTS

Match Phase Variables on $z = 0$ yields

a. Finite amplitude form of Snell's law

$$\frac{\sin\theta_i}{c_I + \beta_I v_i|_{z=0}} = \frac{\sin\theta_r}{c_I + \beta_I v_r|_{z=0}} = \frac{\sin\theta_t}{c_{II} + \beta_{II} v_t|_{z=0}}$$

b. Phase lags

$$\frac{L_i}{c_I + \beta_I v_i|_{z=0}} = \frac{L_r}{c_I + \beta_I v_r|_{z=0}} = \frac{L_t}{c_{II} + \beta_{II} v_t|_{z=0}}$$

Algebraic equality gives

$$R = \frac{m\cos\theta_r - n\cos\theta_t}{m\cos\theta_r + n\cos\theta_t}$$

$$T = \frac{n(\cos\theta_i + \cos\theta_r)}{m\cos\theta_r + n\cos\theta_t}$$

where

$$m = \frac{\rho_{II}}{\rho_I}, n = \frac{c_I}{c_{II}}$$

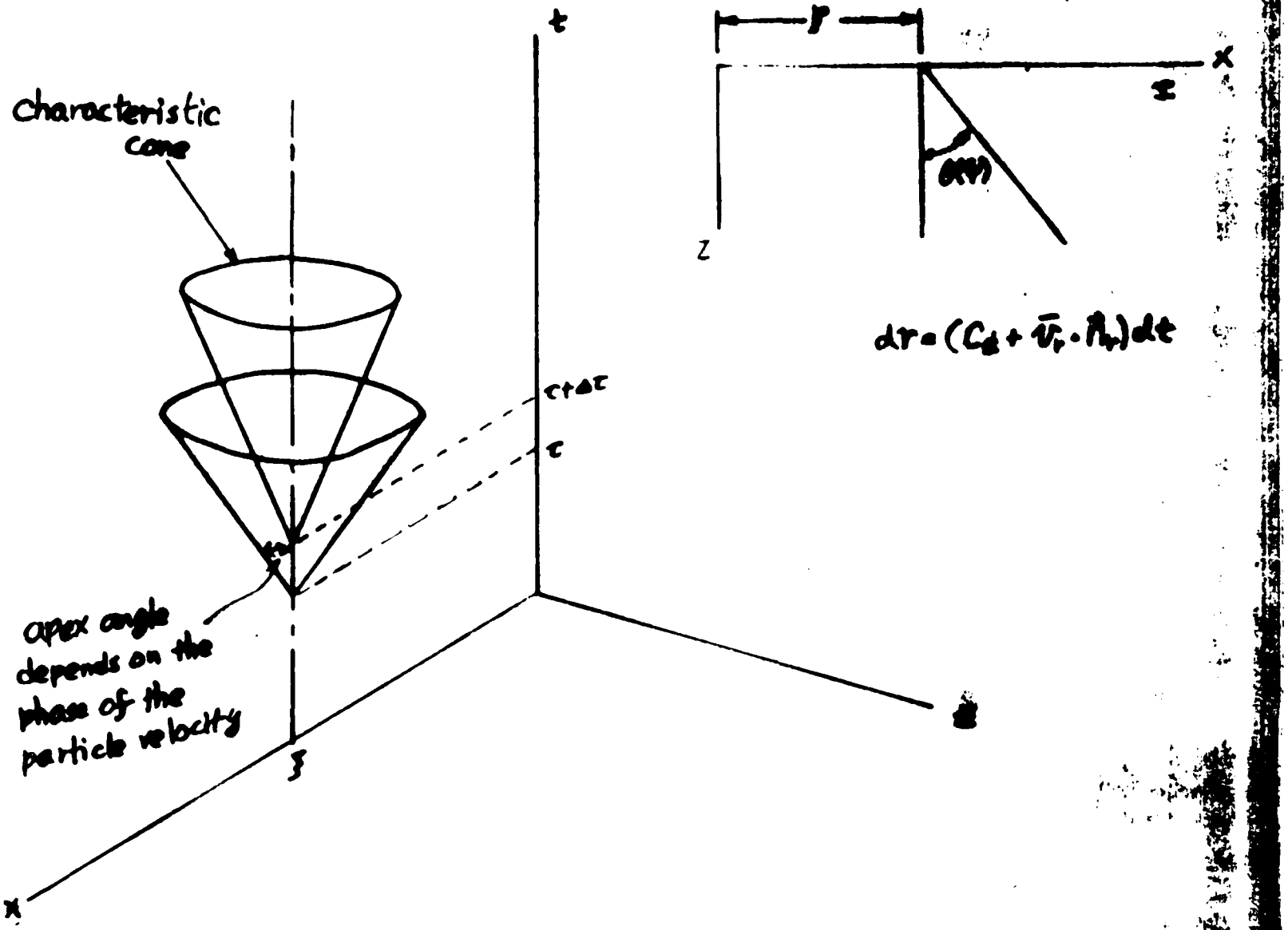
characteristic cone
t
x
y
z
c(t+Δt)
ct
apex angle depends on the phase of the particle velocity
r
x
z
dr = (C_s + v_p · n_r) dt

NUMERICAL EVALUATION

at $T = 20°c$

Fluid I = water, $B/A = 5.0 \Rightarrow \underline{\beta_1 = 3.5}$

Fluid II = acetone, $B/A = 9.2 \Rightarrow \underline{\beta_{11} = 5.1}$

$$c_1 = 1480 \quad m/s, \qquad c_{11} = 1150 \quad m/s$$

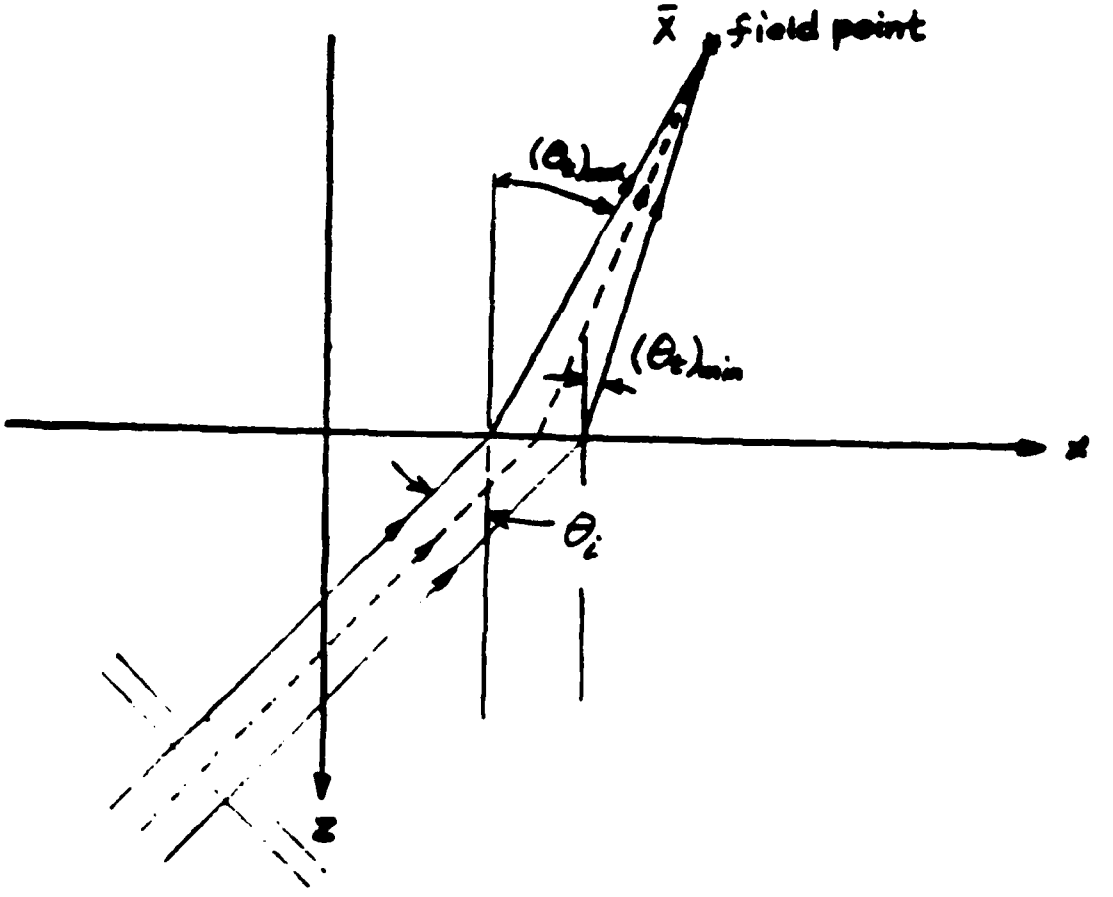

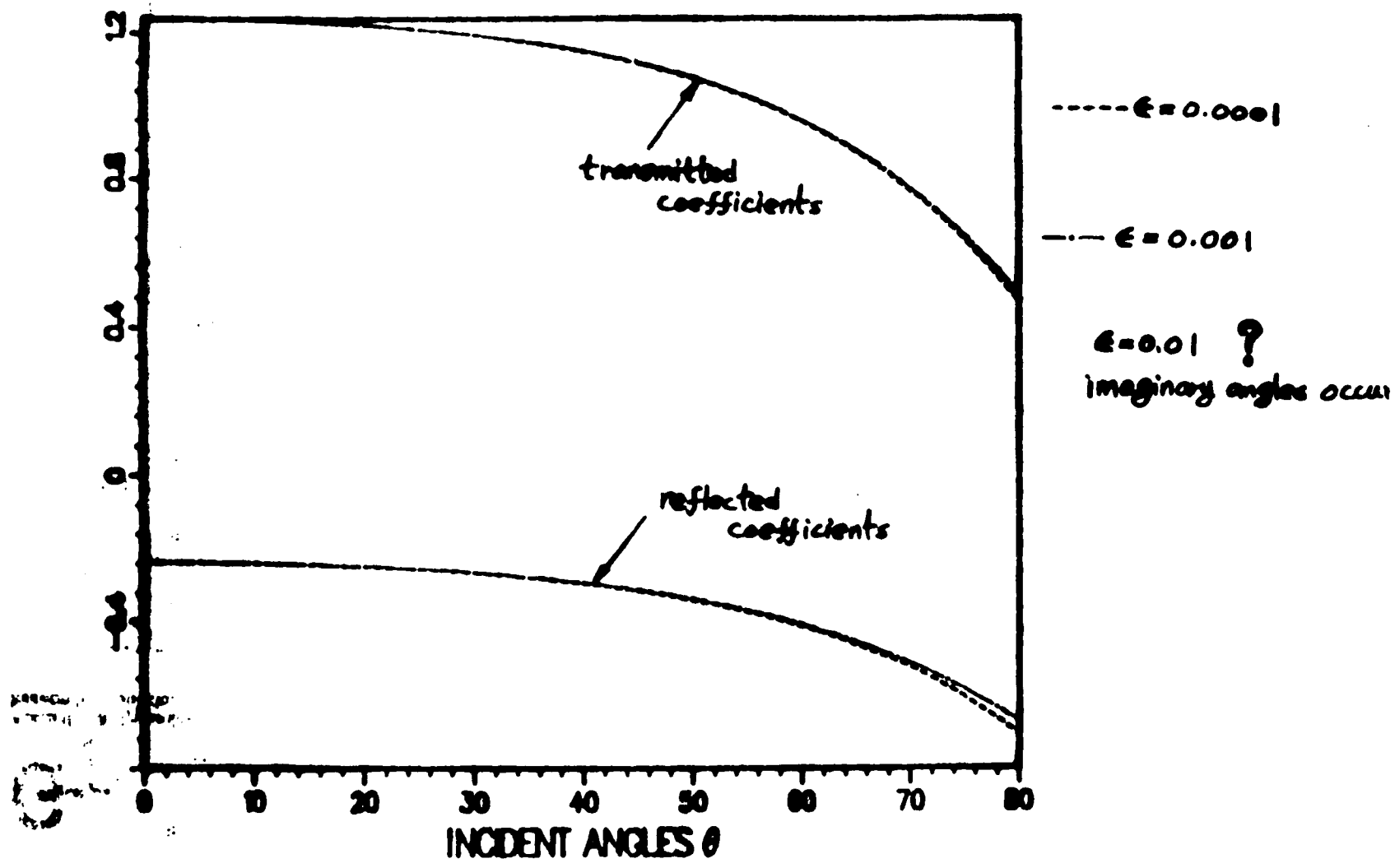
transmitted coefficients
reflected coefficients
0
10
20
30
40
50
60
70
80
INCIDENT ANGLES θ
-----ε=0.0001
-·-·- ε=0.001
ε=0.01 ?
imaginary angles occur

$\epsilon = 0.001$

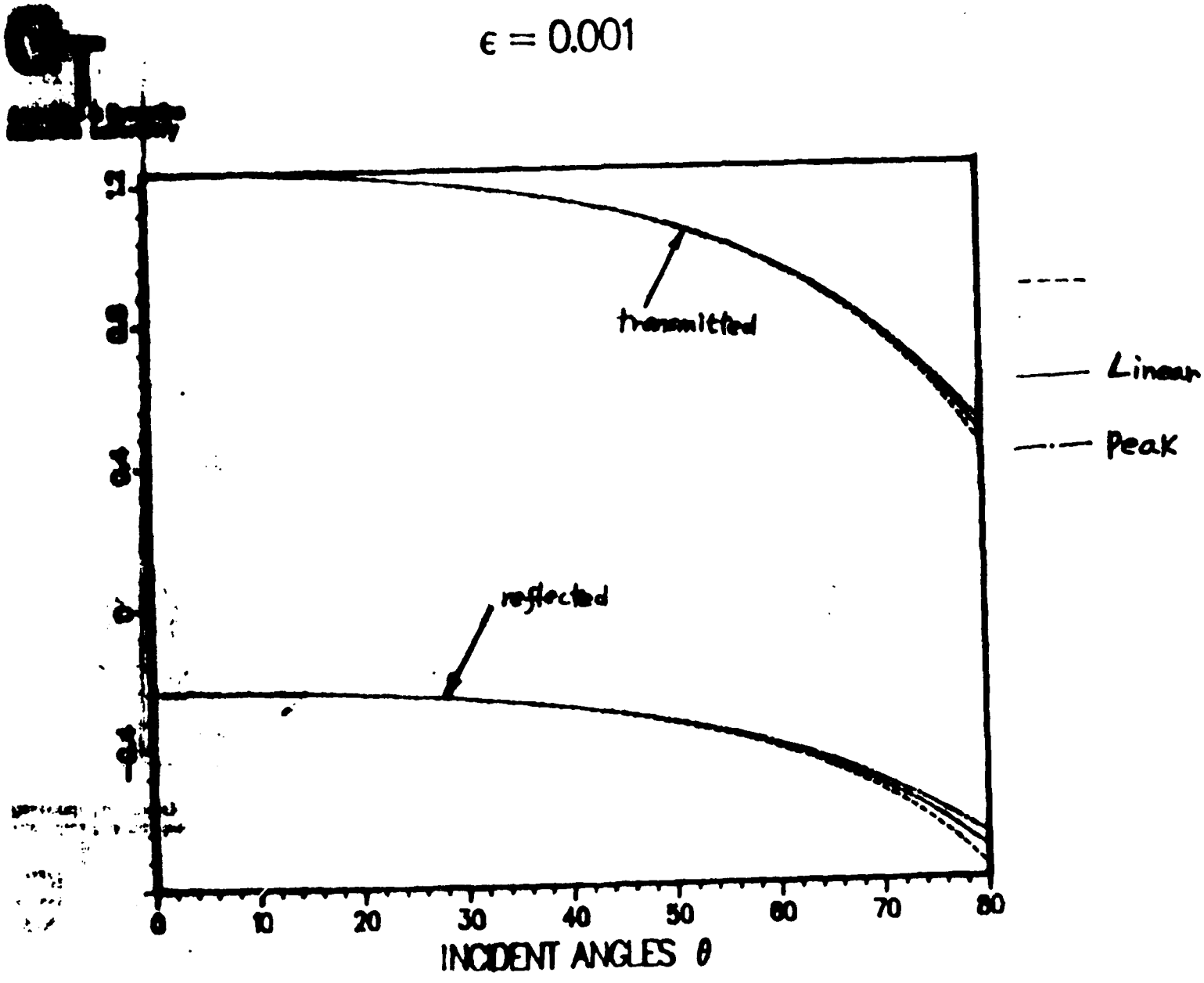

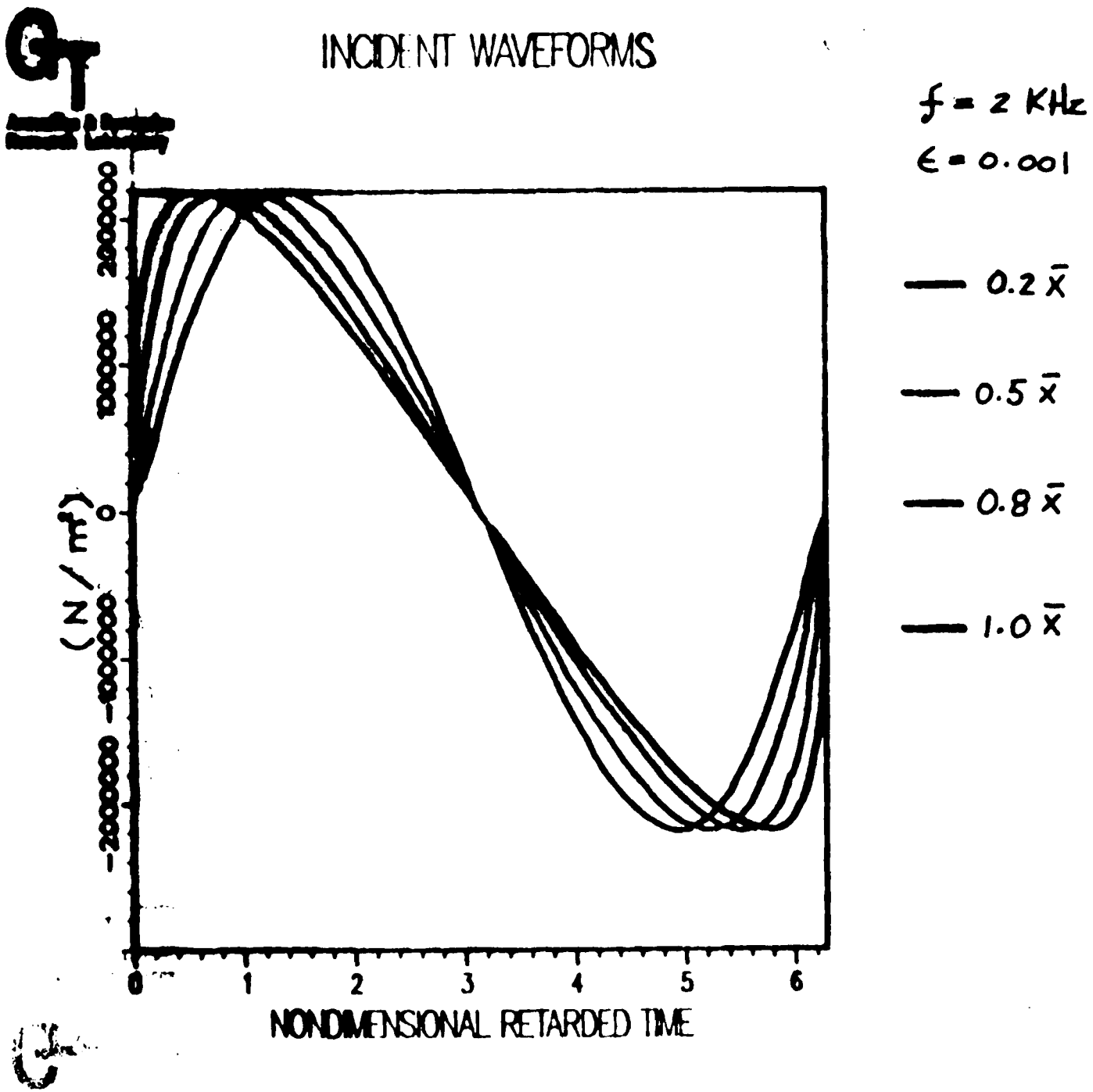
INCIDENT WAVEFORMS
f = 2 KHz
ε = 0.001
— 0.2 x̄
— 0.5 x̄
— 0.8 x̄
— 1.0 x̄
2000000
1000000
0
-1000000
-2000000
(N/m²)
0
1
2
3
4
5
6
NONDIMENSIONAL RETARDED TIME

REFLECTED WAVEFORMS

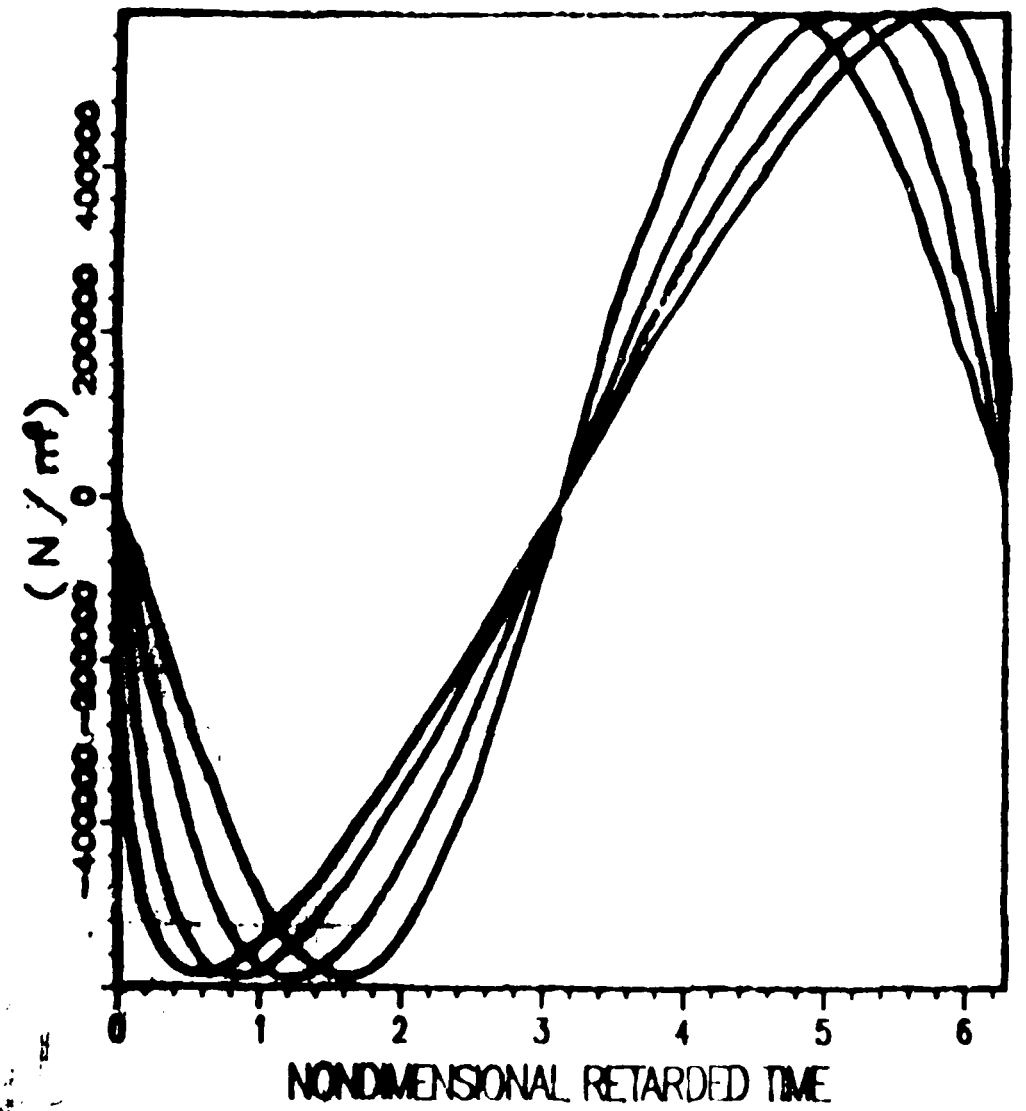

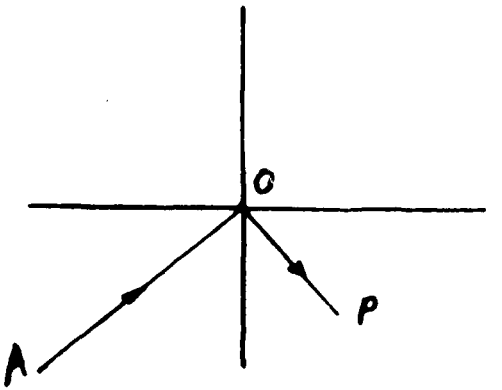

$A\text{-}O\text{-}P \sim \bar{x}$

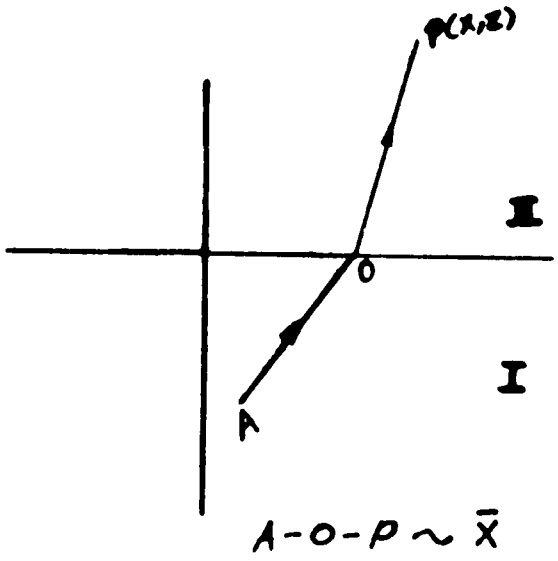

A-O-P ~ $\bar{X}$

TRANSMITTED WAVEFORMS

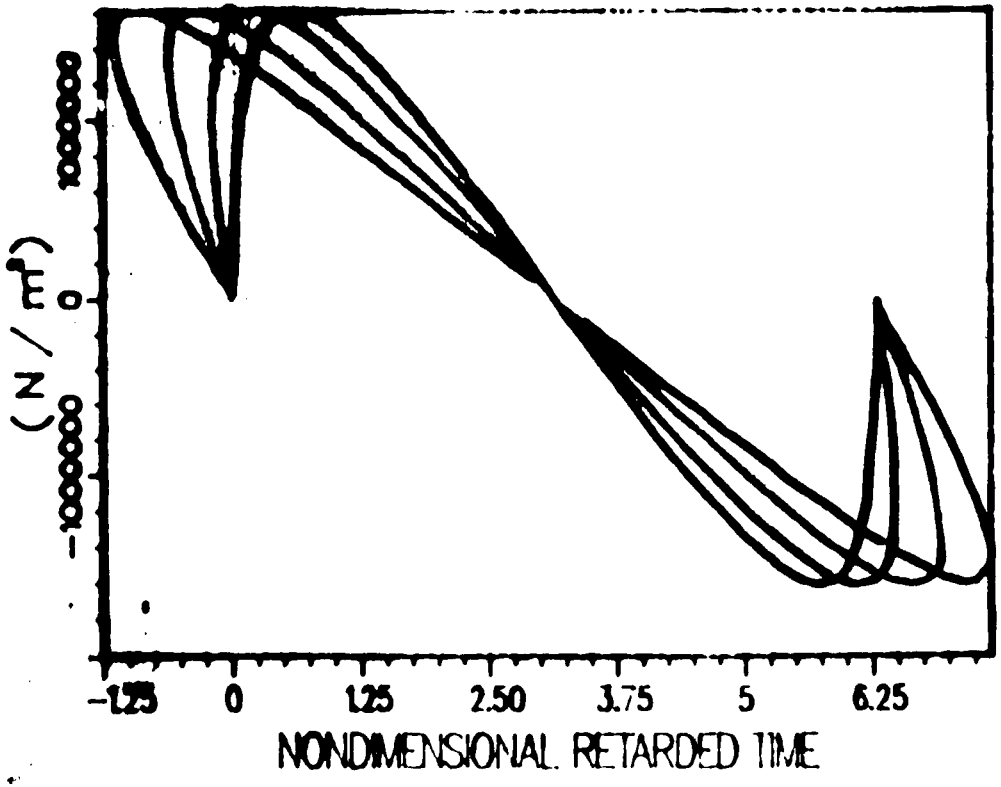

CONCLUSIONS AND RECOMMENDATIONS

NONLINEAR INTERACTION CAN BE NEGLECTED WHEN THE INCIDENT SIGNAL IS WEAK

NONLINEAR EFFECTS ON REFLECTION AND TRANSMISSION ARE VERY SMALL FOR SMALL INCIDENT ANGLES

DIFFERENT WAVELETS REFLECT AND TRANSMIT AT DIFFERENT ANGLES WHICH HAVE PERIODIC FLUCTUATION ABOUT LINEAR MEAN

CRITICAL INCIDENCE MAY BE TREATED BY COMPLEX FORM OF SOLUTION

THE METHOD MAY BE EXTENDED TO ELASTIC WAVES IN SOLIDS WHERE TRANSVERSE SHEAR WAVES EXIST

ACOUSTICAL SOCIETY OF AMERICA

116th MEETING
ST. LOUIS, MISSOURI
ADAM'S MARK HOTEL
27 NOVEMBER-1 DECEMBER 1988
JAMES D. MILLER, CHAIRMAN

JANET M. WEISENBERGER
TECHNICAL PROGRAM CHAIRMAN
CENTRAL INSTITUTE FOR THE DEAF
818 S. EUCLID
ST. LOUIS, MISSOURI 63110
(314) 652-3200

September 1989

TO: Jerry H. Ginsberg

RE: On supercritical incidence of a finite amplitude plane dilatational wave in an elastic solid

Your submitted abstract has been accepted for presentation in St. Louis on 30 November 1989 in Session PP which begins at 3:00 A.M./P.M. You have been allocated 15 minutes and the presentation is lecture style. If your paper has coauthors, please forward this information to them since this notification is being sent only to you.

Authors are requested to adhere to the scheduled time limits and to allow at least two minutes for audience response. The enclosed "Guidelines for Oral Presentations" should help make your lecture more interesting and informative. Also 35-mm and overhead projectors will be available in a preview room at the meeting so speakers can preview their slides before their presentation.

Please contact your Session Chairman at least 15 minutes before the beginning of the session to let him or her know you are present, to review your slides or transparencies with the projectionist, and to receive any last-minute instructions.

If for any reason you are unable to present your paper at its assigned time, try to find a suitable replacement to present the paper (perhaps your Session Chairman) or, failing that, assure that your Session Chairman is informed ahead of time that the paper will not be presented. It is important that you send written notice of your absence to Acoustical Society headquarters. If your notification of absence will not arrive before the meeting, telephone or send a message to the Acoustical Society registration desk at the meeting hotel.

A paper copying service will be available at the meeting for those who wish to obtain reprints. Please leave a reproducible copy of your text and projection material at the copy center desk when you register, or as soon as as possible during the meeting.

Yours truly,

Janet M. Weisenberger

Janet M. Weisenberger
Technical Program Chairman

Enclosure

On supercritical incidence of a finite amplitude plane dilatational wave in an elastic solid. Kun-Tien Shu and Jerry H. Ginsberg (School of Mechanical Engineering, Georgia Institute of Technology, Atlanta, GA 30332)

An earlier analysis [K. T. Shu and J. H. Ginsberg, J. Acoust. Soc. Am. Suppl. 1, 85, EEE1 (1989)] described nonlinear reflection and refraction phenomena of a finite amplitude dilatational wave at subcritical incidence on a plane interface between two bonded solids. The present work extends the earlier description to cases where the angle of incidence exceeds the critical value. The incoming wave is assumed to originate from the slower medium, so two critical angles exist, associated with evanescence of either the transmitted dilatational or shear wave. The finite amplitude version of Snell's law indicates that the dependence of the phase speed of the incident wave on its instantaneous amplitude induces, in the case of evanescent waves, fluctuations in the phase velocity parallel to the interface and in the decay rate normal to the boundary. This effect mirrors the fluctuations in the transmission and reflection angles of propagative waves. A numerical algorithm is developed to evaluate reflected or transmitted waveforms at a specified field point. In the special case of incidence close to a linear critical angle, the finite amplitude Snell's law indicates that the corresponding wave fluctuates between propagative and evanescent properties within a single period. [Work supported by NSF.]

Technical Committee: Physical Acoustics

PACS Subject Classification number(s): 43.25.Dc, 43,25.Jh

Telephone number: (404)894-3265 (J. H. Ginsberg)

Send acceptance or rejection notice to J. H. Ginsberg

ON SUPERCRITICAL INCIDENCE OF A FINITE-AMPLITUDE PLANE DILATATIONAL WAVE IN ELASTIC SOLIDS

Kun-Tien Shu

Jerry H. Ginsberg

The George W. Woodruff School of Mechanical Engineering
Georgia Institute of Technology
Atlanta, Georgia 30332

[Work supported by NSF and ONR]

1. The role of nonlinearity on the supercritical incidence
2. Uniformly valid expression for evanescent waves
3. Field solution (waveform)

FORMULATIONS OF PROBLEM

Solid I:

$$\frac{\partial^2 u_i}{\partial t^2} - (c_d^2 - c_s^2)\frac{\partial^2 u_m}{\partial a_m \partial a_i} - c_s^2 \frac{\partial^2 u_i}{\partial a_m \partial a_m} = \frac{K_i}{\rho_0}$$

$$T_{ij} = \lambda \frac{\partial u_m}{\partial a_m}\delta_{ij} + \mu\left(\frac{\partial u_i}{\partial a_j} + \frac{\partial u_j}{\partial a_i}\right) + \frac{G_{ij}}{\rho_0}$$

Solid II:

$$\frac{\partial^2 u_i'}{\partial t^2} - (c_d'^2 - c_s'^2)\frac{\partial^2 u_m'}{\partial a_m \partial a_i} - c_s'^2 \frac{\partial^2 u_i'}{\partial a_m \partial a_m} = \frac{K_i'}{\rho_0'}$$

$$T_{ij}' = \lambda' \frac{\partial u_m'}{\partial a_m}\delta_{ij} + \mu'\left(\frac{\partial u_i'}{\partial a_j} + \frac{\partial u_j'}{\partial a_i}\right) + \frac{G_{ij}'}{\rho_0'}$$

where

$$c_d = \sqrt{\frac{\lambda + 2\mu}{\rho_0}} \quad ; \quad c_s = \sqrt{\frac{\mu}{\rho_0}}$$

$$c_d' = \sqrt{\frac{\lambda' + 2\mu'}{\rho_0'}} \quad ; \quad c_s' = \sqrt{\frac{\mu'}{\rho_0'}}$$

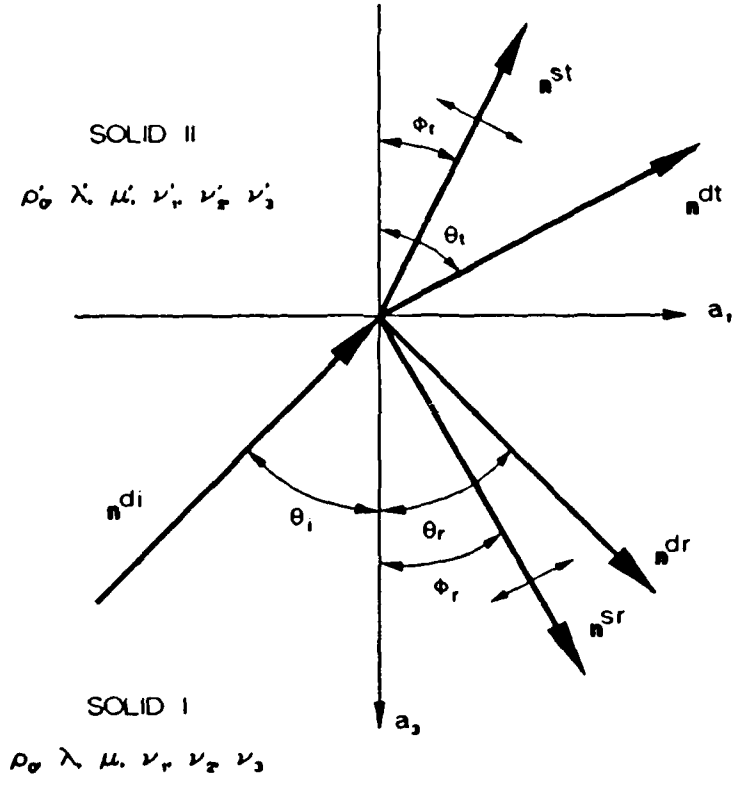
SOLID II
ρ_0' λ', μ', ν_1', ν_2', ν_3'
n^{st}
Φ_t
n^{dt}
θ_t
a_1
n^{di}
θ_i
θ_r
n^{dr}
Φ_r
n^{sr}
a_3
SOLID I
ρ_0 λ, μ, ν_1, ν_2, ν_3

PERTURBATION SERIES SOLUTIONS

- Ray description of the reflection and refraction processes
- Due to nonlinear self-action, Secularity occurs in the $O(\epsilon^2)$ incident, reflected and refracted P waves, but not in the $O(\epsilon^2)$ reflected and refracted SV waves (Ref. Lardner, 1985)
- Nonlinear interactions between individual wave trains (dilatation and shear) are not important (exception: near grazing incidence)
- Boundary effects create secular waves that depend on distance perpendicular to the direction of wave propagation

UNIFORMLY VALID PARTICLE VELOCITY

1. Figure out the linear reflection and refraction patterns
2. Form particle velocities by the method of characteristics

$$\mathbf{v} = -\frac{i}{2}\epsilon\mathbf{A}\exp\left[i\omega\left(t - \frac{\mathbf{n}\cdot\mathbf{r} + L}{\alpha}\right)\right] + c.c.$$

where

$$\alpha \equiv c_d + \beta_d(\mathbf{v}\cdot\mathbf{n}) \quad \text{dilatational wave}$$
$$\equiv c_s \quad \text{shear wave}$$

3. Match nonlinear trace velocities along the interface to yield finite amplitude forms of Snell's law
4. Obtain a system of equations to solve the unknowns
5. Apply the algorithm that we have developed earlier to obtain stress waveforms at a specific field point for the regular reflection and transmission patterns

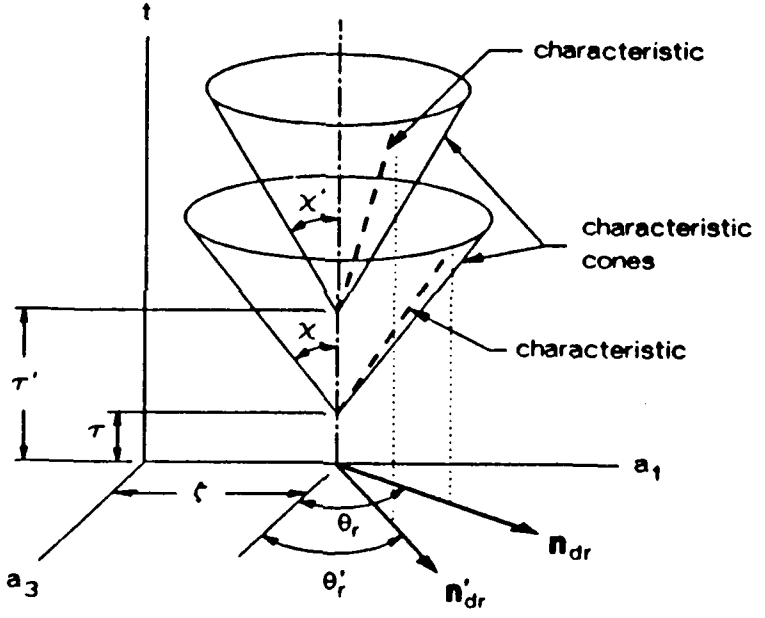
t
characteristic
characteristic
cones
characteristic
χ'
χ
τ'
τ
a1
ζ
θr
θ'r
a3
ndr
n'dr

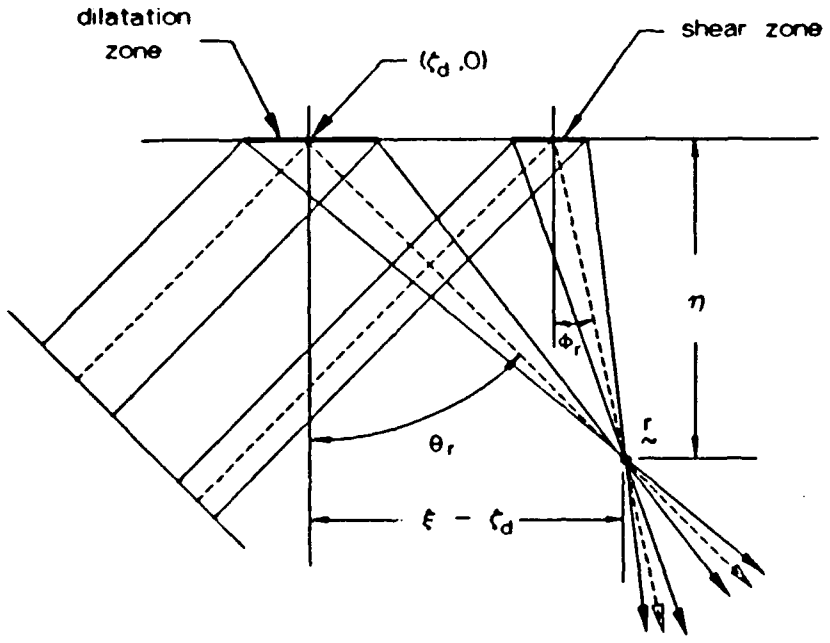
dilatation
zone
$(\zeta_d, 0)$
shear zone
η
Φ_r
θ_r
$\underset{\sim}{r}$
$\xi - \zeta_d$

CRITICAL ANGLES FOR PLANE WAVES SCATTERING AT A PLANE SOLID–SOLID INTERFACE

Dilatational wave (P) incidence

$c_d > c'_d > c'_s$	0
$c'_d > c_d > c'_s$	1
→ $c'_d > c'_s > c_d$	2

Shear wave (SV) incidence

$c_s > c'_d > c'_s$	1
$c'_d > c_s > c'_s$	2
$c'_d > c'_s > c_s$	3

INCIDENT P WAVE

$$[A]\{X\} = \{C\}$$

where

$$[A] = \begin{bmatrix} -\sin\theta_r & -\cos\phi_r & \sin\theta_t & -\cos\phi_t \\ \cos\theta_r & -\sin\phi_r & \cos\theta_t & \sin\phi_t \\ -(\gamma^2 - 2\sin^2\theta_r) & \gamma\sin 2\phi_r & mn(\gamma'^2 - 2\sin^2\theta_t) & mn\gamma'^2\sin 2\phi_t \\ \sin 2\theta_r & \gamma\cos 2\phi_r & mn\sin 2\theta_t & -mn\gamma'^2\cos 2\phi_t \end{bmatrix}$$

$$\{X\} = \begin{Bmatrix} A_{dr}/A_{di} \\ A_{sr}/A_{di} \\ A_{dt}/A_{di} \\ A_{st}/A_{di} \end{Bmatrix}, \qquad \{C\} = \begin{Bmatrix} \sin\theta_i \\ \cos\theta_i \\ \gamma^2 - 2\sin^2\theta_i \\ \sin 2\theta_i \end{Bmatrix}$$

$$\gamma \equiv \frac{c_d}{c_s} = \sqrt{\frac{\lambda + 2\mu}{\mu}}, \qquad \gamma' \equiv \frac{c'_d}{c'_s} = \sqrt{\frac{\lambda' + 2\mu'}{\mu'}}$$

$$\frac{c_d}{c'_d} = n, \qquad \frac{\mu'}{\mu} = m$$

1. $0 \leq \theta_i \leq \theta_{dc}$: Regular reflection and transmission case, where both refracted P and SV waves in solid II are propagating away from the interface.

2. $\theta_{dc} < \theta_i \leq \theta_{sc}$: The evanescent refracted P wave occurs

3. $\theta_{sc} < \theta_i < \frac{\pi}{2}$: Both refracted P and SV waves are evanescent

$$\sin\theta_{dc} \simeq n[1 + (\beta_d - \beta'_d n T^{\circ}_{dd})\frac{v_{di}}{c_d}]$$

$$\sin\theta_{sc} = n\gamma'(1 + \beta_d \frac{v_{di}}{c_d})$$

- $\theta_{dc} < \theta_i \leq \theta_{ec}$: $\quad (\Rightarrow \sin\theta_t > 1)$

  set

$$\cos\theta_t = -i(\sin^2\theta_t - 1)^{1/2}$$
$$\equiv -i\left(\frac{N_1^2}{n^2}\sin^2\theta_i - 1\right)^{1/2}$$

  where

$$N_1 = \frac{1+\beta_d' T_{dd}^{\circ} n v_{di}/c_d}{1+\beta_d v_{di}/c_d}$$

- $\theta_{ec} < \theta_i < \frac{\pi}{2}$: $\quad (\Rightarrow \sin\theta_t > 1 \text{ and } \sin\phi_t > 1)$

  set

$$\cos\phi_t = -i(\sin^2\phi_t - 1)^{1/2}$$
$$\equiv -i\left(\frac{N_1^2}{\gamma'^2 n^2}\sin^2\theta_i - 1\right)^{1/2}$$

  where

$$N_2 = \frac{1}{1+\beta_d v_{di}/c_d}$$

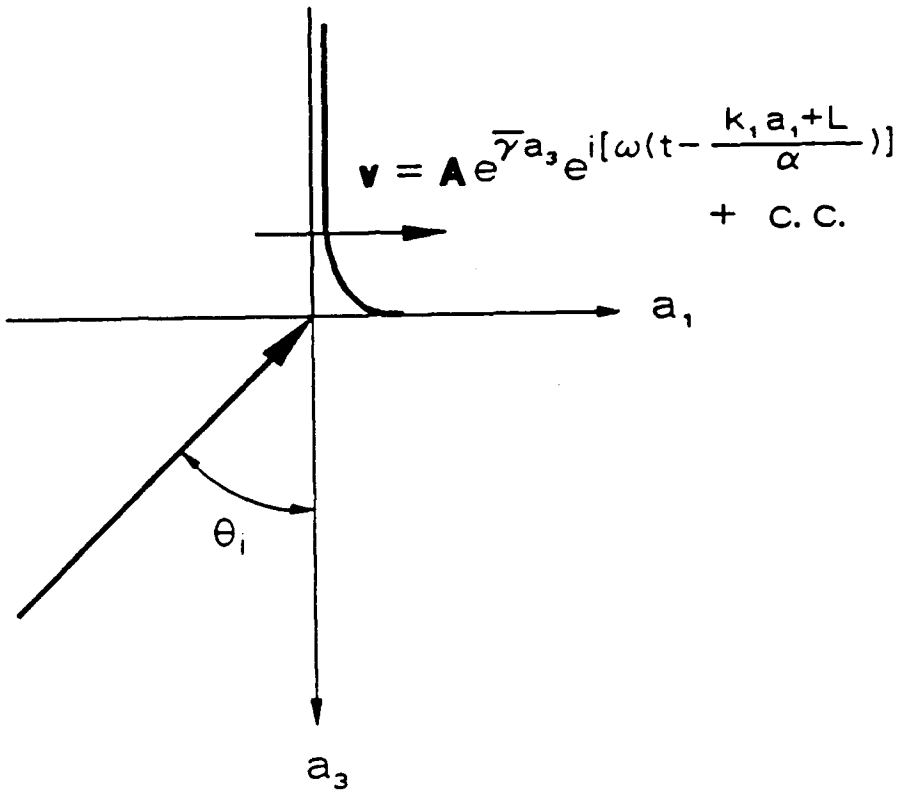

- All locations at constant a_1 have same phase
- Trace velocity matches that of the nonlinear incident wave
- Decay rate depends on the phase of the incident wave

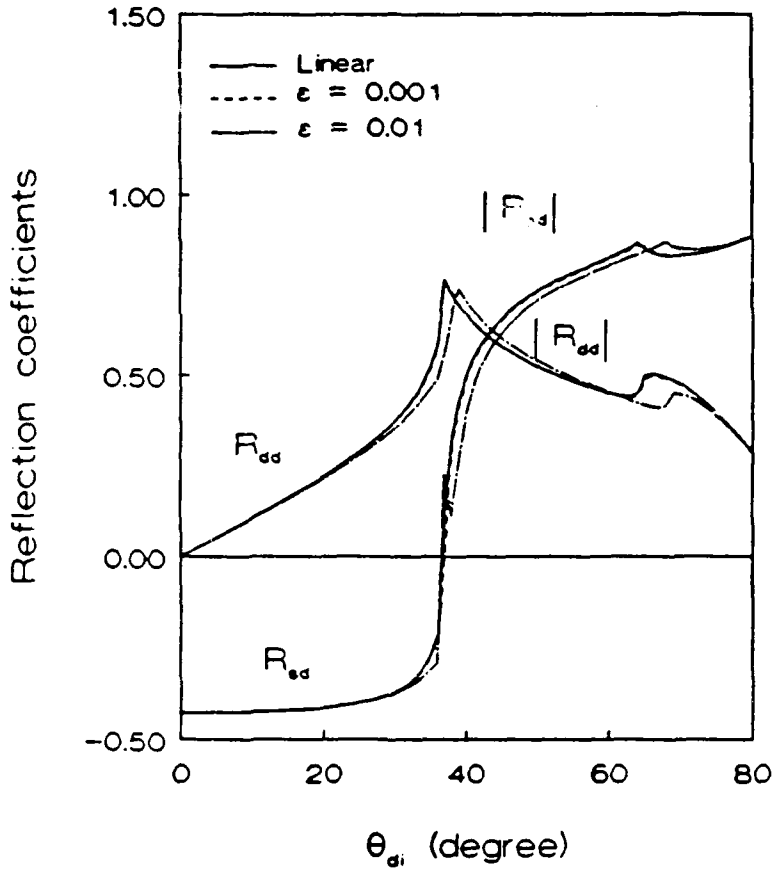
1.50
1.00
0.50
0.00
−0.50
0
20
40
60
80
Linear
ε = 0.001
ε = 0.01
|R_sd|
|R_dd|
R_dd
R_sd
Reflection coefficients
θ_di (degree)

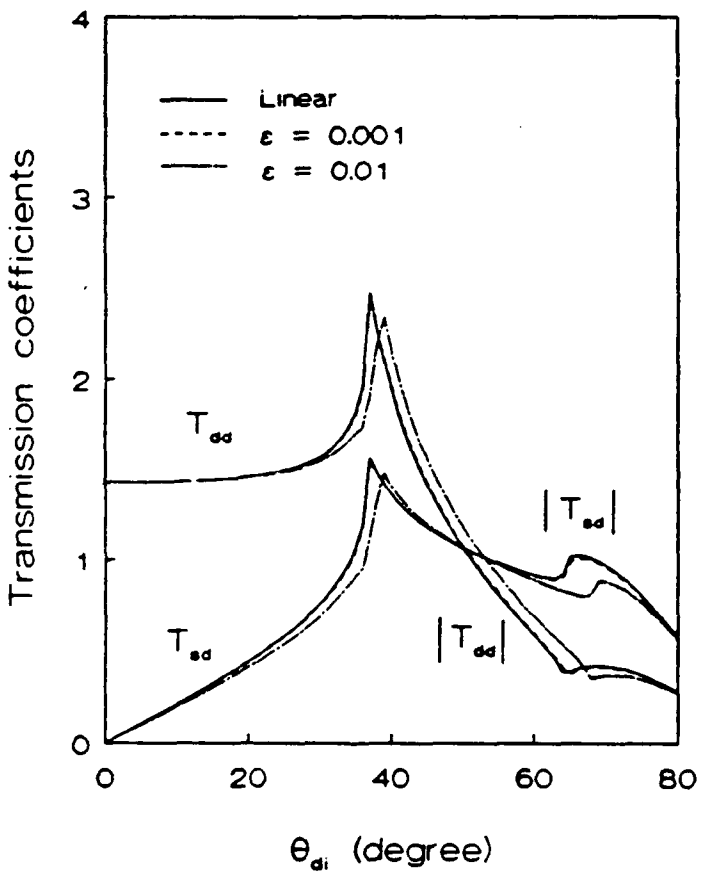
Linear
ε = 0.001
ε = 0.01
Transmission coefficients
T_{dd}
$|T_{sd}|$
T_{sd}
$|T_{dd}|$
0
1
2
3
4
0
20
40
60
80
θ_{di} (degree)

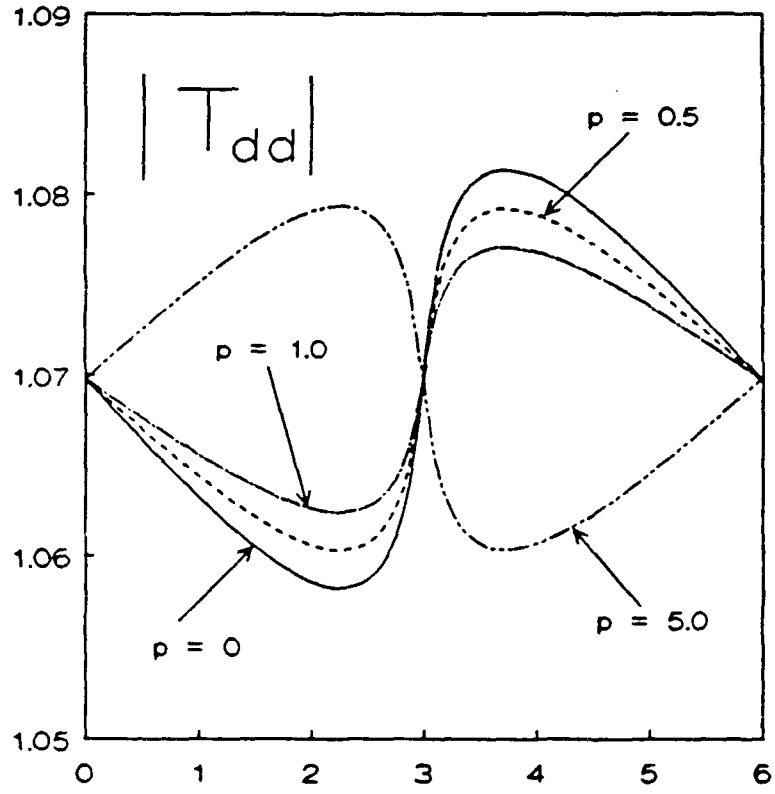
1.09
1.08
1.07
1.06
1.05
0
1
2
3
4
5
6
| Tdd |
p = 0.5
p = 1.0
p = 0
p = 5.0

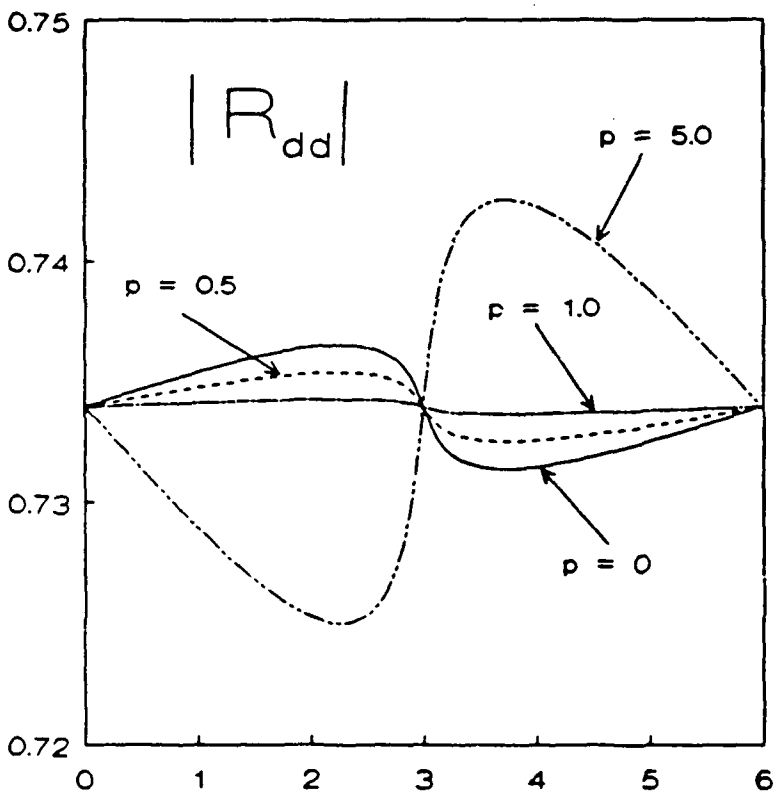

f = 2Mz, ϵ = 0.001, LDI = 0.8,
γ' = 1.5, n = 0.6, m = 1.0

CONCLUSIONS

1. Nonlinearity is to cause reflected and refracted waves to propagate in variable directions
2. Evanescent waves propagate along the interface & decay rates depend on the incident wave
3. For supercritical incidence, shocks occurs in transmitted field when it occurs on boundary in the incident wave
4. For ~~super~~ near-critical incidence, the finite amplitude Snell's law indicates that the corresponding wave fluctuates between propagative and evanescent properties within a single period
5. In reality, the response to an incident finite amplitude wave will be near the response for the linear counterpart

Modification of the NPE Computer Code to Describe the Propagation of Axisymmetric Sound Beams in Infinite Media

Gee-Pinn James Too
Jerry H. Ginsberg

Georgia Institute of Technology

presented at 118th Meeting of ASA

work sponsored by ONR

Modification of the NPE computer code to describe the propagation of axisymmetric sound beams in infinite media. Gee-Pinn James Too and Jerry H. Ginsberg (School of Mechanical Engineering, Georgia Institute of Technology, Atlanta, GA 30332)

NPE is a nonlinear progressive wave equation computer code developed by McDonald and Kuperman [Comp. & Math. w. Appl. 11, 843-851 (1985)] to evaluate transient propagation in acoustic waveguides. It is suitable for two-dimensional phenomena, as well as for radial propagation of azimuthally symmetric waves. The present study describes the modifications required to employ NPE for the evaluation of axially propagation axisymmetric waves, particularly those associated with sound beams radiated by a baffled piston. In addition to implementing a formulation in which the propagation is essentially parallel to the axis of a set of cylindrical coordinates, it is necessary to account for the transverse spreading of the beam into an infinite medium. Another issue is the manner in which the initial waveform input to NPE is obtained. The predictions of NPE for a linear sound beam when the input is obtained from the King integral, which is an exact solution in quadrature form, is compared to the results obtained for a simple input based on assumption of planar wave behavior in the vicinity of the transducer. The results in both cases are also compared to the analytical solution for the far-field radiation pattern.

Technical Committee: Physical Acoustics or Underwater Acoustics
Subject classification number: 43.20.Fn, 43.30.Bp
Telephone: (404) 894-3265 (J. H. Ginsberg)
Send notice to J. H. Ginsberg

Computer Code Application

(McDonald & Kuperman, Comp. & Math. w. Appl. 1985)

Case 1 Two dimensional waveguide (x, y)

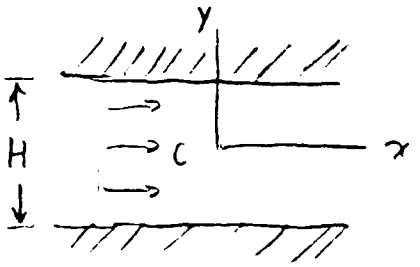

$$D_t R = -\frac{\partial}{\partial x}\left(c_1 R + \frac{1}{2}\beta c_0 R^2\right) - \frac{c_0}{2}\frac{\partial^2}{\partial y^2}\int_{x_0}^{x} R\, dx$$

Case 2 Azimuthally symmetric waveguide (r, z)

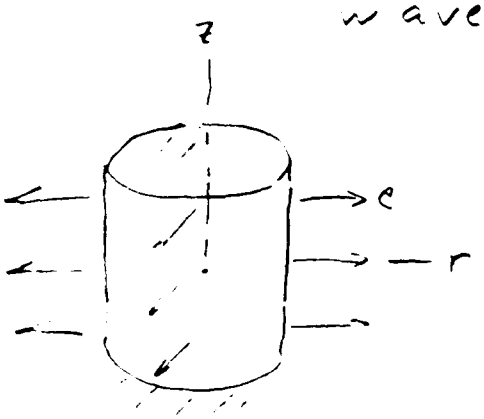

refraction

$$D_t R = -\frac{\partial}{\partial r}\left(c_1 R + \frac{1}{2}\beta R^2\right)$$

nonlinear steepening

$$-\frac{c_0 R}{\partial r} - \frac{c_0}{2}\frac{\partial^2}{\partial z^2}\int_{r_0}^{r} R\, dr$$

radial spreading

diffraction

Initialization of Window for Linear Theory

1. Calculate density perturbation using linear sound beam theory (Rayleigh or King integral)
   (a) select $\bar{\sigma}_{max} > 3a$ - needs to be increased with increasing x and decreasing ka
   (b) Select $L > 5$ wavelengths ($L > 10\pi/k$) needed to establish steady-state

2. Use planar wave approximation.
   If $p = \rho_0 c_0 v_n(t)$ on $x = 0$, then

$$R(x,t,\bar{\sigma}) = \begin{cases} \frac{1}{c_0} v_n(t - x/c_0); & \sigma < a \\ 0 : \sigma > a \end{cases}$$

   Still need $L > 10\pi/k$

Implementation

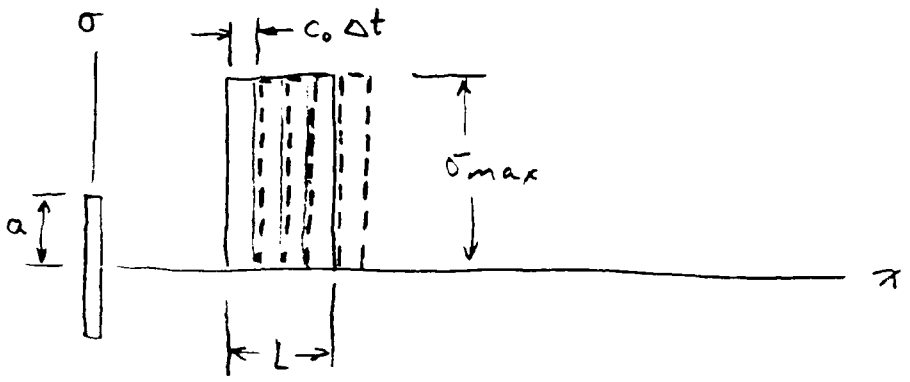

Axisymmetry $\Rightarrow \frac{\partial \rho}{\partial \sigma} = 0$ at $\sigma = 0$

Moving window:

$R \neq 0$ in $c_0 t < x < c_0 t + L$ & $0 < \sigma < \sigma_{max}$

Open domain; $R \equiv 0$ for $\sigma > \sigma_{max}$

Subdivide window into N parts.

Case 3 Sound beams - axial propagation with azimuthal symmetry (σ, x)

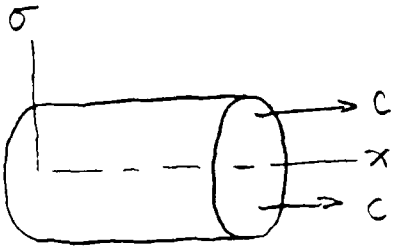

$$D_t R = -\frac{\partial}{\partial x}\left(c_1 R + \frac{1}{2}\beta c_0 R^2\right) - \frac{c_0}{2}\left(\frac{\partial^2}{\partial \sigma^2} + \frac{1}{\sigma}\frac{\partial}{\partial \sigma}\right)\int_{x_0}^{x} R\,dx$$

* Like 2-D waveguide except for change in Laplacian for diffraction

* Open domain

Special cases

Homogeneous medium: $c_1 = 0$

Linear theory: $\beta = 0$

Derivation of NPE Equation

Combine momentum & mass conservation;
(Lighthill formulation), density $= \rho_0 + \rho$

$$\frac{\partial^2 \rho}{\partial t^2} = \nabla^2 p + \partial_i \partial_j (\rho V_i V_j) \qquad (A)$$

Adiabatic state equation:

$$p = c^2 \rho + \frac{1}{2} \rho^2 \frac{\partial^2 p}{\partial \rho^2} + O(\rho^3) \qquad (B)$$

For V_j, take first order result for a plane wave at small angle θ relative to X direction;

$$V_j = c \frac{\rho}{\rho_0} \delta_{j,x} + O(\rho^3, \rho^2 \theta^2) \qquad (C)$$

Eliminate p & V_j from (A-C):

$$\frac{\partial^2 R}{\partial t^2} = \nabla^2 \left[c^2 (R + \beta R^2) \right] + \text{higher order}$$

where $R = \rho / \rho_0$

Heterogeneous medium:

$$c = c_0 + c_1(\underset{\sim}{r})$$

Introduce a moving reference frame translating in the X direction at speed c_0:

$$X = x + c_0 t \Rightarrow \frac{\partial}{\partial t} = D_t - c_0 \frac{\partial}{\partial x} \qquad (E)$$

The nonlinear wave equation becomes:

$$\left(D_t - c_0 \frac{\partial}{\partial x}\right)^2 R = \left(\frac{\partial^2}{\partial x^2} + \frac{\partial^2}{\partial y^2} + \frac{\partial^2}{\partial z^2}\right)(c_0 + c_1)^2 (R + \beta R^2) \qquad (F)$$

(a) (b) (c) (d) (e)

Terms (a-e) are small compared to others - drop products of small terms.

Integrate in x direction:

$$D_t R = -\frac{\partial}{\partial x}\left(c_1 R + \beta c_0 R^2\right) - \frac{c_0}{2}\left(\frac{\partial^2}{\partial y^2} + \frac{\partial^2}{\partial z^2}\right)\int_{x_0}^{x} R\, dx$$

THREE-DIMENSIONAL NPE

Output

1. Select time step $\Delta t = c_0 \Delta x$. Then a subdivision of the window will be at a selected field point at each instant.
2. Construct a temporal waveform
3. Fourier analyze to obtain amplitude.

GT
Acoustics & Dynamics
Research Laboratory

1st harmonic comparison starts at r=0.2m

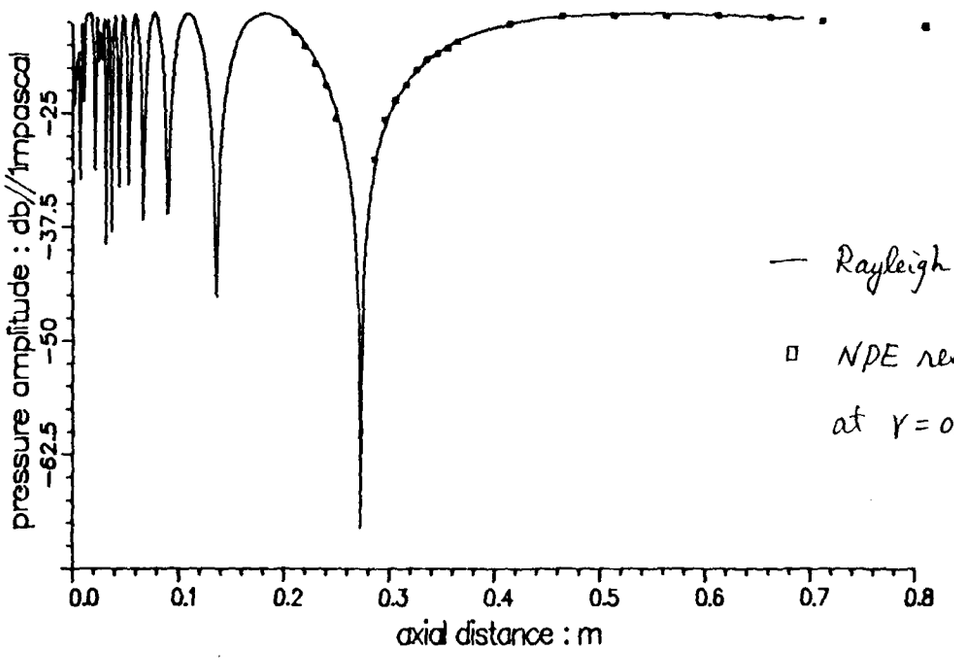

— Rayleigh integral on axis

□ NPE result with input at r=0.2m by King integral

GT
Acoustics & Dynamics
Research Laboratory

1st harmonic comparison starts at r=0.1m

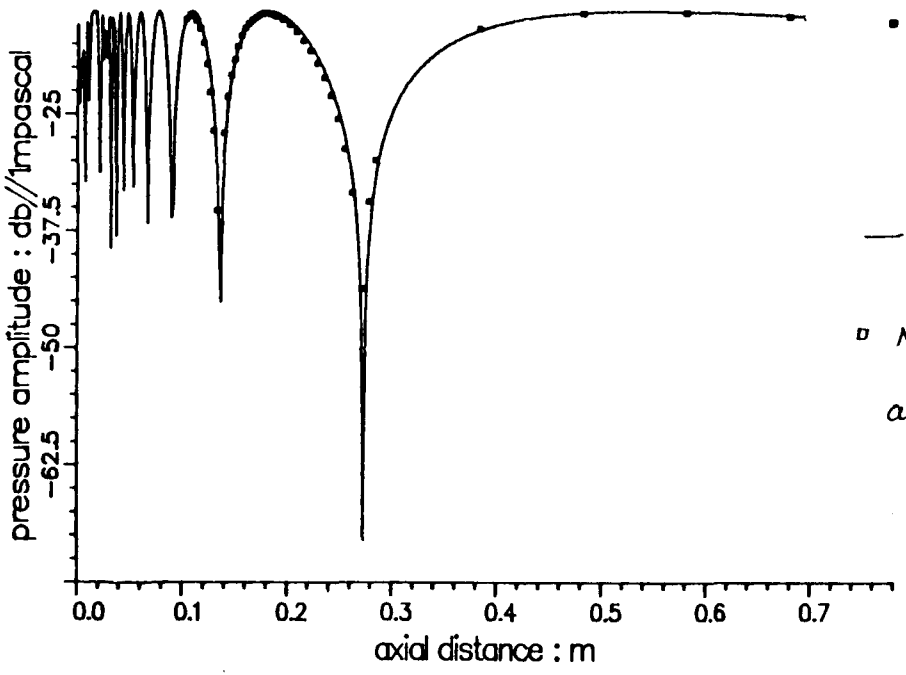

— Rayleigh integral

▫ NPE result with input at r=0.1 m by King integral

P12

GT
Acoustics & Dynamics
Research Laboratory

1st harmonic comparison starts at r=0.05m

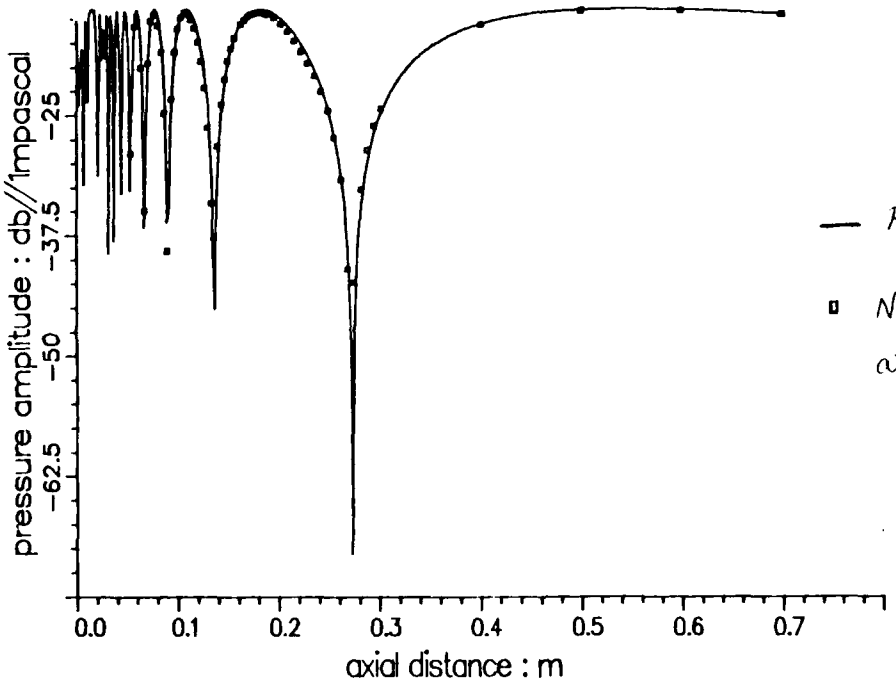

— Rayleigh integral on axis

▫ NPE result with input at r=0.05 m by King integral

GT
Acoustics & Dynamics
Research Laboratory

1ST HARMONIC COMPARISON ON AXIS

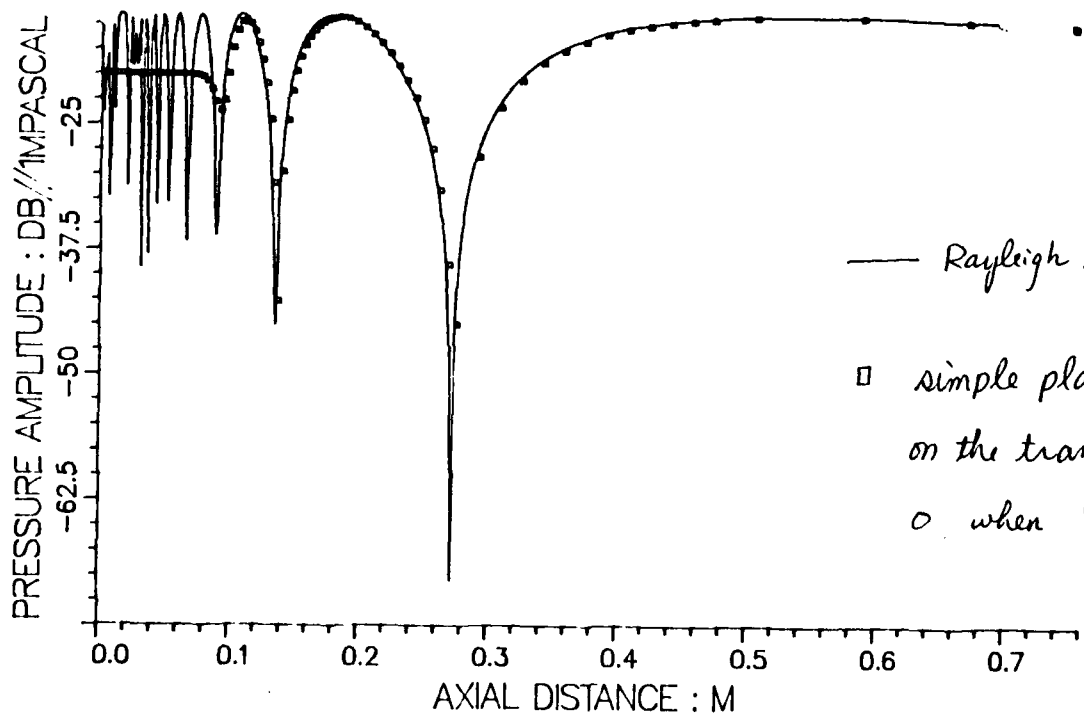

— Rayleigh integral on axis

□ simple plane wave input on the transducer and

○ when σ > radius

GT
Acoustics & Dynamics
Research Laboratory

1st harmonic comparison on axis

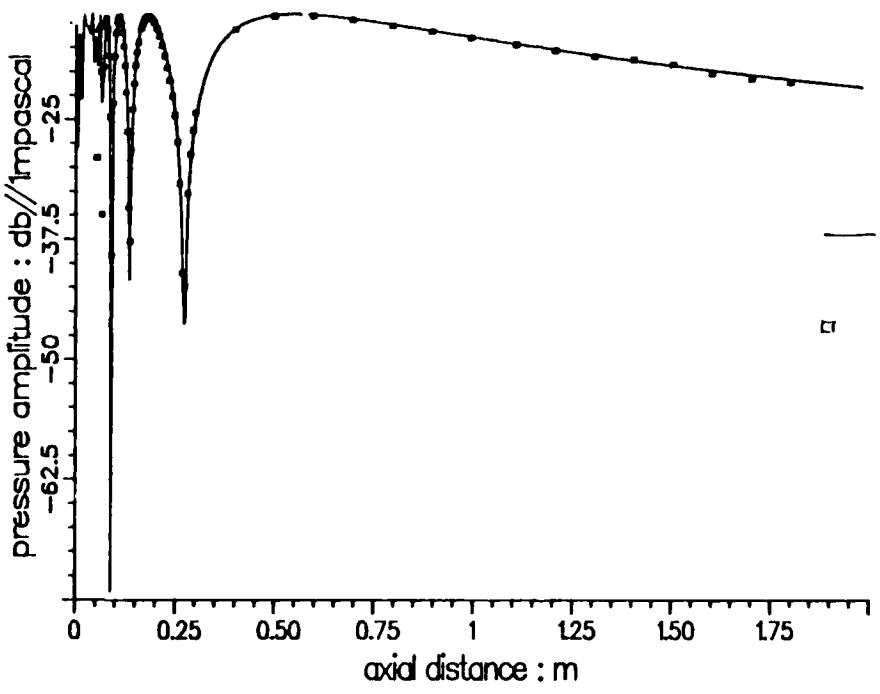

— Rayleigh integral

□ NPE results

GT
Acoustics & Dynamics
Research Laboratory

1st harmonic comparison at z=500 mm

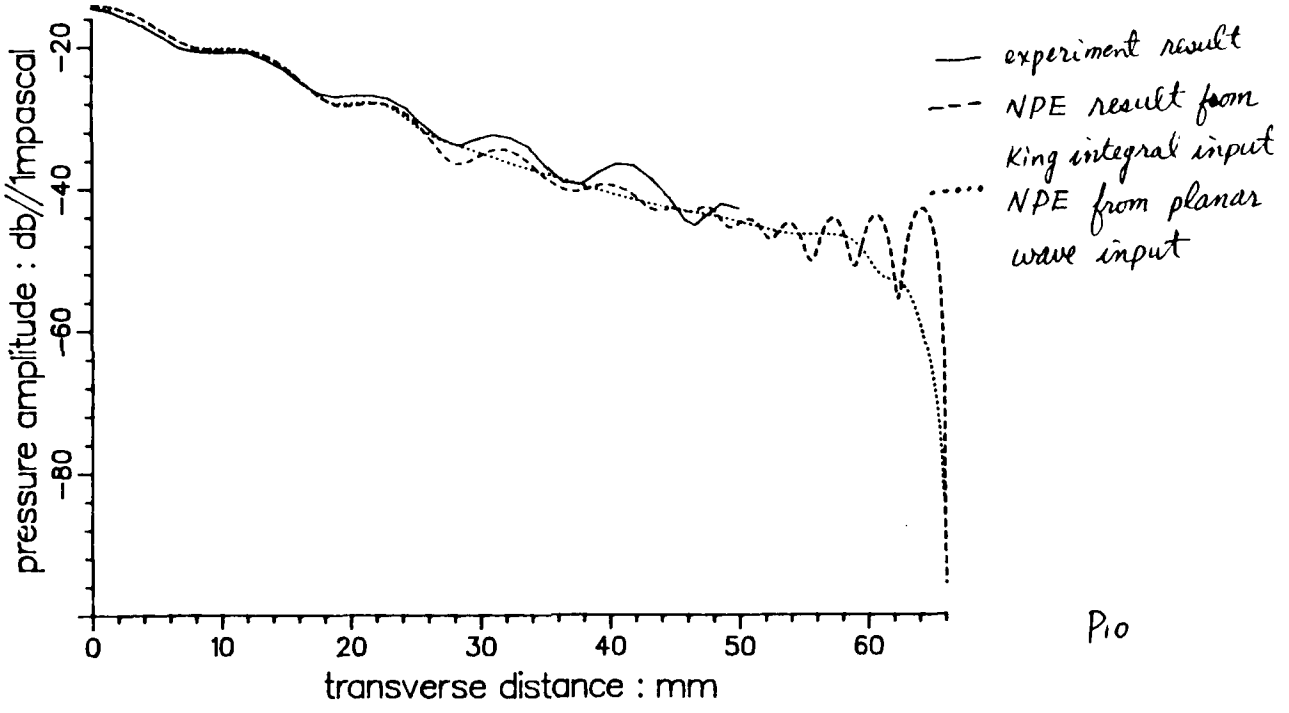

P10

GT
Acoustics & Dynamics
Research Laboratory

1ST HARMONIC AMPLITUDE AT Z = 275 MM

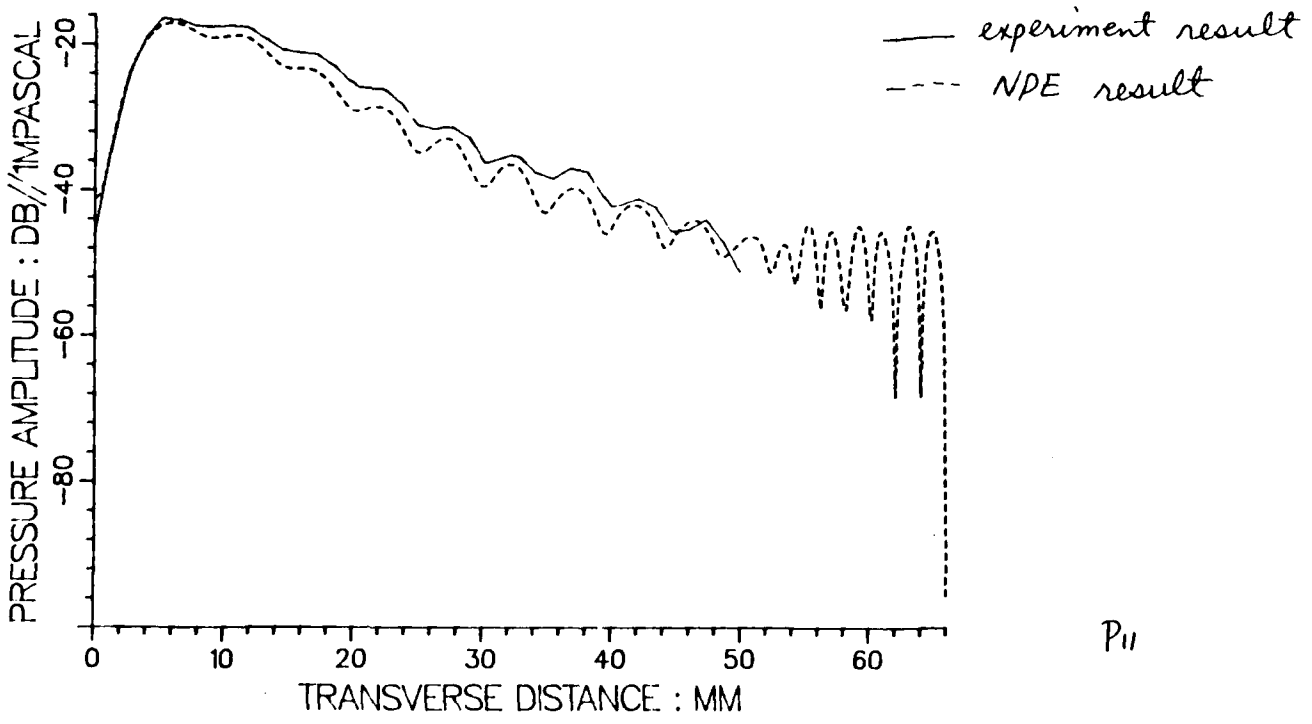

GT
Acoustics & Dynamics
Research Laboratory

BEAM PATTERN COMPARISON AT Z=3.529 M

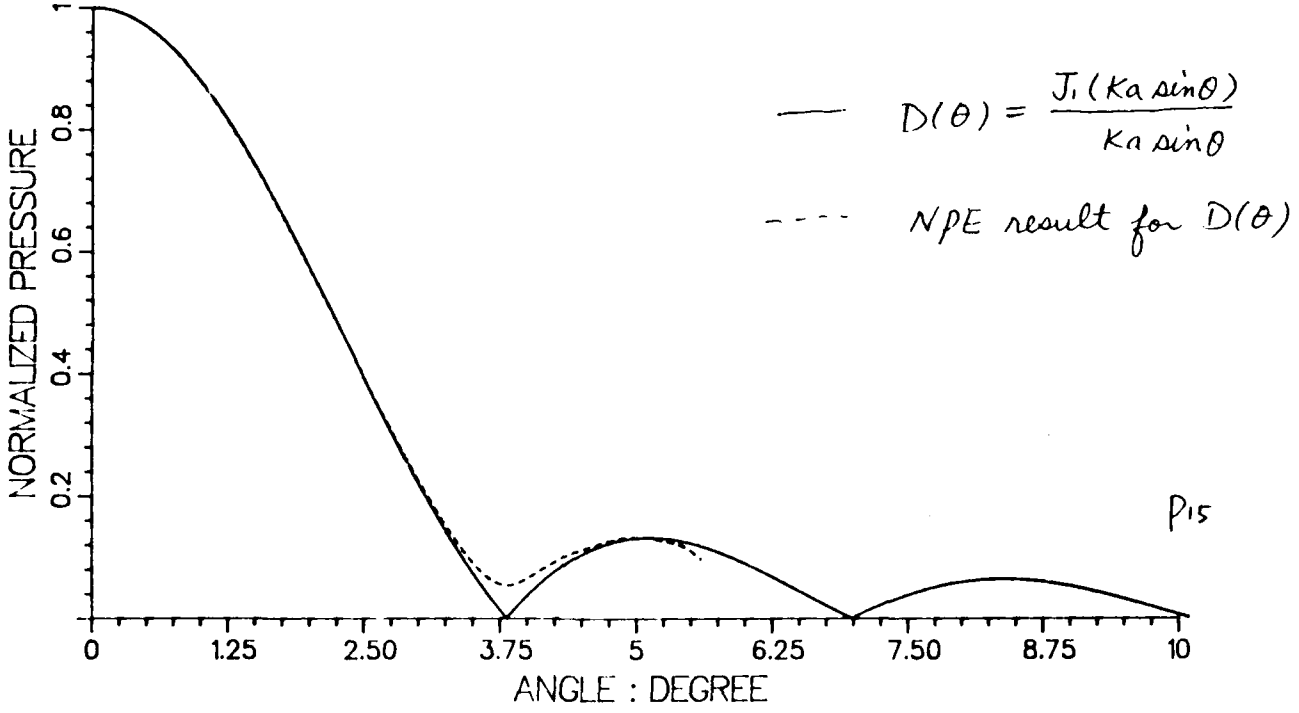

P15

Conclusions

1. NPE, which is a time domain formulation, can be used to study CW signals.

2. NPE is accurate for linear sound beams, even near the projector.

3. Accuracy in the near field requires initialization of the moving time window using linear sound beam theory.

4. Piston approximation gives good results only at sufficiently large distances from the source

5. QUESTION

   What theory should one use to initialize the moving window when nonlinear effects are important?

OBLIQUE REFLECTION OF A NONLINEAR P WAVE FROM THE BOUNDARY OF AN ELASTIC HALF-SPACE

K. T. Shu

System analyst

Jerry H. Ginsberg

George W. Woodruff Chair in Mechanical Systems, Fellow ASME

School of Mechanical Engineering

Georgia Institute of Technology

Atlanta, GA 30332

May, 1990

38 pages + 8 figures

ABSTRACT

This paper describes mode conversion effects and subsequent waveform distortion arising when a finite amplitude dilatational (P) wave that has already experienced nonlinear distortion is obliquely incident on a stress-free boundary of an isotropic elastic half-space. A two-term perturbation expansion is first employed to identify the dominant nonlinear effects. The understanding of wave interactions obtained from the perturbation analysis is then exploited to derive a successful solution using the method of characteristics for two-dimensional wave. It is shown that the incident and reflected P waves undergo nonlinear amplitude dispersion along their ray paths. The orientation of the rays for the reflected waves are time-dependent, being governed by a modified form of Snell's law, in which the phase speed incorporates the nonlinear correction for the associated particle velocity. The reflection coefficients are shown to resemble those of linear theory, except for the dependence on the variable angles of reflection. The nonlinear propagation and reflection laws are employed to determine temporal waveforms for the reflected P and SV waves. This requires an iterative procedure in order to trace rays arriving at a specified field point at an arbitrary instant back to their source.

INTRODUCTION

It is well-understood that nonlinearity has a much greater distortional effect for dilatational waves in a homogeneous medium than for shear waves. Such behavior cannot be assumed when one introduces a boundary, such as a free surface. Because of the phenomenon of mode conversion, a dilatational (P) wave that has already undergone significant distortion prior to its incidence at the boundary must impart its distortion to both the reflected P and the vertically polarized shear (SV) waves that are generated in the reflection process. The present work is an analysis of the mechanisms governing nonlinear effects in the mode conversion process, propagative distortion, and interaction of the incident and reflected waves. The incident P wave is considered to be generated by a harmonic planar source of sufficiently broad extent and high frequency to consider the amplitude to be constant across planar wavefronts. This wave is assumed to have undergone significant nonlinear distortion, limited only by the restriction that a shock has not formed prior to its arrival at the boundary. To a certain extent, the analysis is similar to our earlier development of a nonlinear ray description for waves in a hard-walled waveguide[1]. However, the present solution is more general due to its reliance on the method of characteristics for two-dimensional waves. Indeed, the basic principles derived here may readily be extended to treat sources having arbitrary time dependence.

With the exception of a few studies of oblique reflection of shock waves, investigation of nonlinear elastic waves reflection phenomena prior to this work had been limited to situations in which the wave is one-dimensional, such that the planar signal has constant phase along a wavefront. The method of characteristics was employed by Blackstock[2] to study a finite amplitude wave propagating in a lossless, perfect gas upon normal reflection from a rigid wall. He found that the effect of the wall is to double the variational sound speed in comparison with the free space case. It was shown experimentally by Breazeale and Lester[3] that the phase of each generated harmonic of a finite amplitude plane harmonic wave could be changed upon normal reflection from various types of reflectors. The results led to some interesting phenomena. When a distorted, but unshocked, wave is normally incident on a resilient surface, the distortion of the reflected waveform continued to increase with increasing propagation distance. In contrast, a wave reflected from a pressure-release surface is distorted in the "wrong direction" as it travels back toward the transducer, resulting in delayed shock formation. Analogous results were obtained by Buck and Thompson[4] by studying the problem of one-dimensional finite amplitude elastic waves at normal incidence to a stress-free boundary, based on a one-dimensional equation of motion for the Lagrangian displacement. Their analysis indicated that the amplitudes of the higher harmonics in the reflected wave should decrease due to phase reversal in the reflection process, with the eventual result that they would vanish when the wave returns to its originating source.

Studies of the reflection of obliquely incident finite amplitude waves have been limited for the most part to acoustic waves in fluids. Van Buren and Breazeale[5] treated the reflection of finite amplitude waves by assuming there was no coupling among the harmonics. A corollary of such assumption is that the reflection of a distorted wave is equivalent to the independent reflection of its harmonic components. Feng[6] considered finite amplitude sound waves upon oblique reflection from a rigid wall in the special case where the angle of incidence is 45°. Much later, Qian[7] extended Feng's work to arbitrary angle of incidence. He found that nonlinear interaction of the incident and reflected waves generates a constant magnitude second harmonic wave that propagates parallel to the surface, which he named the Q-wave. A two-term perturbation expansion method was employed by both Feng and Qian in their papers. Since both works only addressed the mechanisms by which second harmonics are generated, they did not fully explore the distortion process.

Recently, Cotaras[8] also employed a two-term perturbation expansion method to analyze the reflection and refraction of finite amplitude waves at a plane interface between two lossless fluids. Although the nonlinear interactions between incident and reflected fields and local nonlinear effect due to the movement of the boundary were treated in detail, the resulting second-order solutions are not uniformly valid in the range of the independent variables under consideration. Specifically, the second-order solutions contain secular terms, which

make the ratio of second-order solutions to first-order solutions unbounded as the independent variables tend to infinity. Cotaras also hypothesized a finite amplitude form of Snell's law for the wave refraction in a fluid-fluid interface, according to which the trace velocities that are matched along the boundary are formed from the nonlinear phase velocities. One corollary of the finite amplitude form of Snell's law is the observation that a specific phase in the waveform of an incident wave refracts at an angle that depends on the particle velocity associated with that phase.

Reid[9] and Wright[10] investigated the oblique reflection of a finite amplitude plane dilatational shock wave from the boundary of an elastic half-space. Although there are differences in detail, both found that the primary effect of nonlinearity on the oblique reflection process is to modify the reflection angles and amplitudes to account for the nonlinear phase speed of the incident and reflected shock waves. Such results are consistent with the finite amplitude version of Snell's law.

The aim of the present study is to develop a uniformly valid picture of the manner in which nonlinearity affects the process of reflection in lossless, isotropic elastic media. In the following section, we shall first formulate the problem in the Lagrangian coordinates for the displacement components. The dominant nonlinear effects are identified in Sec. II by using a second-order perturbation expansion method. The results are shown to lack uniform validity. Rather than performing cumbersome manipulations to correct this situation, an

alternative approach based on the method of characteristics for two-dimensional waves is developed in Sec. III and IV. It describes the propagative distortion for each waves, and enables one to identify the manner in which the incident and reflected rays are related at the boundary. One outcome of the analysis is to prove that Cotaras' hypothesis regarding the finite amplitude form of Snell's law is valid for the present problem. In Sec. V, we describe a numerical algorithm to determine the reflected waveforms for the stress components of P and SV waves at a specific field point, and apply it to a quantitative example.

I. EQUATIONS OF MOTION AND BOUNDARY CONDITIONS

In the absence of body forces, the Lagrangian equations of motion for adiabatic dynamic deformation of a compressible, elastic solid are[11]

$$\text{momentum:} \quad \frac{\partial T_{ij}}{\partial a_j} = \rho_0 \frac{\partial^2 u_i}{\partial t^2}, \tag{1}$$

$$\text{constitutive:} \quad T_{ij} = \rho_0 \frac{\partial W}{\partial (\partial u_i / \partial a_j)}, \tag{2}$$

$$\text{strain-displacement:} \quad E_{ij} = \frac{1}{2} \left(\frac{\partial u_i}{\partial a_j} + \frac{\partial u_j}{\partial a_i} + \frac{\partial u_k}{\partial a_i} \frac{\partial u_k}{\partial a_j} \right), \tag{3}$$

where T_{ij} is the Piola-Kirchhoff stress tensor, E_{ij} is the Green strain tensor, u_i is the particle displacement vector referred to the original coordinates a_i, ρ_0 is the mass density at the undeformed state, and W is

the strain energy density function. In these equations, a repeated subscript implies a summation. For isotropic materials, the strain energy density is an invariant function of the Green strain tensor, and can therefore be expanded in a Taylor series of the three invariants I_1, I_2, and I_3 of E_{ij}. Thus $W(I_1,I_2,I_3)$ may then be written, correct to third order in E_{ij}, as

$$\rho_0 W = \frac{1}{2}\lambda I_1^2 + \mu I_2 + \frac{1}{24}\alpha I_1^3 + \frac{1}{4}\beta I_1 I_2 + \gamma I_3 + O(I_1^4), \tag{4}$$

where

$$\begin{aligned} I_1 &= E_{ii} \\ I_2 &= E_{ij}E_{ij} \\ I_3 &= E_{ij}E_{jk}E_{ki} \end{aligned} \tag{5}$$

In these expression, λ and μ are the Lamé coefficients, while α, β, and γ are the third-order elastic constants. (Our definition of the third-order elastic constants differs from Bruger's, see Ref. 12.)

We first obtain an expression for the strain energy density in terms of displacement by substituting Eq. (3) into Eq. (4) and discarding terms higher than third-order in the displacement gradient. Next, we use this truncated strain energy to form T_{ij} by applying Eq. (2), and then substitute the result into the momentum equation, Eq. (1). The result is a set of nonlinear displacement equations of motion having the following form:

$$\frac{\partial^2 u_i}{\partial t^2} - (c_d^2 - c_s^2)\frac{\partial^2 u_m}{\partial a_m \partial a_i} - c_s^2 \frac{\partial^2 u_i}{\partial a_m \partial a_m} = K_i/\rho_o, \tag{6}$$

which are accompanied by a set of stress-displacement equations

$$T_{ij} = \lambda \frac{\partial u_m}{\partial a_m} \delta_{ij} + \mu\left(\frac{\partial u_i}{\partial a_j} + \frac{\partial u_j}{\partial a_i} \right) + G_{ij}/\rho_0 . \tag{7}$$

In the foregoing

$$c_d^2 = \frac{\lambda + 2\mu}{\rho_0} \qquad \text{and} \qquad c_s^2 = \frac{\mu}{\rho_0}, \tag{8}$$

are the velocities of planar dilatational and shear waves, respectively, and δ_{ij} is the Kronecker delta function. The terms K_i and G_{ij}, which represent the effects of geometric and material nonlinearities, are given by

$$\begin{aligned} K_i = {} & (\lambda + \mu + \frac{\beta}{4} + \frac{3}{4}\gamma)(u_{n,m}u_{n,im} + u_{i,m}u_{n,nm}) + (\lambda + \frac{\beta}{4})u_{n,n}u_{i,mm} \\ & + \frac{1}{4}(\alpha + \beta)u_{n,n}u_{m,mi} + \frac{1}{4}(\beta + 3\gamma)(u_{m,n}u_{n,im} + u_{n,i}u_{m,mn}) \\ & + (\mu + \frac{3}{4}\gamma)(u_{n,i}u_{n,mm} + 2u_{m,n}u_{i,mn} + u_{i,n}u_{n,mm}), \end{aligned} \tag{9}$$

$$\begin{aligned} G_{ij} = {} & (\frac{\lambda}{2} u_{m,n}u_{m,n} + \frac{\alpha}{8} u_{m,m}u_{n,n})\delta_{ij} + \frac{\beta}{4} u_{m,m}u_{j,i} + \frac{3}{4}\gamma\, u_{j,m}u_{m,i} \\ & + \frac{\beta}{8}(u_{m,n}u_{m,n} + u_{m,n}u_{n,m})\delta_{ij} + (\lambda + \frac{\beta}{4})u_{m,m}u_{i,j} \\ & + (\mu + \frac{3}{4}\gamma)(u_{i,m}u_{j,m} + u_{m,i}u_{m,j} + u_{i,m}u_{m,j}). \end{aligned} \tag{10}$$

Consistent with truncation of W at third-order terms, K_i and G_{ij} are homogeneous quadratic functions of displacement gradients.

We now consider a finite amplitude planar P wave propagating in the a_1-a_3 plane, obliquely incident on the boundary of an elastic half-space defined by $a_3 \geq 0$, as shown in Fig. 1. The propagation direction of this incoming wave is defined as

$$\underset{\sim}{n}_{di} = \underset{\sim}{e}_1 \sin \theta_i - \underset{\sim}{e}_3 \cos \theta_i, \tag{11}$$

where θ_i is the angle of incidence measured from the a_3-axis. This planar wave is assumed to be generated by a harmonically oscillating planar source whose width is much greater than the wavelength. Correspondingly, the particle velocity at the source is given by

$$\underset{\sim}{v}_{di} = -\frac{i}{2} \epsilon c_d \underset{\sim}{n}_{di} \exp(-i\omega t) + \text{c.c.} \quad \text{at} \quad \underset{\sim}{n}_{di} \cdot \underset{\sim}{r} = -L_{di}, \tag{12}$$

where L_{di} is the distance between the source and origin and $\underset{\sim}{n}_{di} \cdot \underset{\sim}{r} = -L_{di}$ defines the plane of the source. In addition, ϵ is the acoustic Mach number of the excitation, ω is its angular frequency, and c.c. is the complex conjugate of the preceding terms.

The stress-free condition at the boundary requires that the corresponding surface tractions should be equal to zero. Since we are following a Lagrangian formulation, in which the surface tractions are referred to the undeformed state of the boundary, the surface tractions will vanish if the Piola-Kirchhoff stress components satisfy

$$T_{13} = T_{33} = 0 \quad \text{on} \quad a_3 = 0. \tag{13}$$

II. IDENTIFICATION OF SIGNIFICANT NONLINEAR EFFECTS

Our objective in this section is to examine the manner in which nonlinearity introduces distortion into the incident and reflected waves an causes them to interact. For this portion of the analysis, we employ a straightforward perturbation series expansion of the displacements u_i and stresses T_{ij}. Thus we write

$$u_i = \epsilon u_i^{(1)} + \epsilon^2 u_i^{(2)} + \cdots, \tag{14}$$

$$T_{ij} = \epsilon T_{ij}^{(1)} + \epsilon^2 T_{ij}^{(2)} + \cdots. \tag{15}$$

Substitution of Eqs. (14) and (15) into Eqs. (6) and (7), followed by matching of like powers of ϵ, converts the equations of motion and stress-displacement relations to the following form.

$$\frac{\partial^2 u_i^{(k)}}{\partial t^2} - (c_d^2 - c_s^2) \frac{\partial^2 u_m^{(k)}}{\partial a_m \partial a_i} - c_s^2 \frac{\partial^2 u_i^{(k)}}{\partial a_m \partial a_m} = K_i^{(k)}/\rho_0 \quad (k = 1,2), \tag{16}$$

$$T_{ij}^{(k)} = \lambda \frac{\partial u_m^{(k)}}{\partial a_m} \delta_{ij} + \mu \left(\frac{\partial u_i^{(k)}}{\partial a_j} + \frac{\partial u_j^{(k)}}{\partial a_i} \right) + G_{ij}^{(k)}/\rho_0 \quad (k = 1,2), \tag{17}$$

where the inhomogeneities $K_i^{(k)}$, $G_{ij}^{(k)}$ are zero for the first-order case. $k = 1$, while the second-order terms, $k = 2$, are given by Eqs. (9) and (10) with the displacement components represented as $u_i^{(1)}$.

The first-order (linearized) system is governed by Eqs. (16) and (17) for k = 1. Satisfying the boundary conditions at $a_3 = 0$ requires the existence of both types of reflected waves, which is the phenomenon of mode conversion[13]. Hence, the general solution of the $O(\epsilon)$ wave equations consists of a sum of the incident P, and reflected P and SV waves, according to

$$\underset{\sim}{u}^{(1)} = \frac{1}{2}\{A_{di}^{(1)}\underset{\sim}{n}_{di}\exp(i\omega\psi_{di}) + A_{dr}^{(1)}\underset{\sim}{n}_{dr}\exp(i\omega\psi_{dr}) + A_{sr}^{(1)}(\underset{\sim}{e}_2 \times \underset{\sim}{n}_{sr})\exp(i\omega\psi_{sr})\} + c.c., \tag{18}$$

where $A_{di}^{(1)}$, $A_{dr}^{(1)}$, and $A_{sr}^{(1)}$ are the amplitudes of the first-order incident P and reflected P and SV waves, respectively. The phase variables ψ_{di}, ψ_{dr}, and ψ_{sr} are defined as

$$\psi_{di} = \frac{1}{c_d}(\underset{\sim}{n}_{di} \cdot \underset{\sim}{r} + L_{di}) - t, \tag{19}$$

$$\psi_{dr} = \frac{1}{c_d}(\underset{\sim}{n}_{dr} \cdot \underset{\sim}{r} + L_{dr}) - t, \tag{20}$$

$$\psi_{sr} = \frac{1}{c_s}(\underset{\sim}{n}_{sr} \cdot \underset{\sim}{r} + L_{sr}) - t, \tag{21}$$

where

$$\underset{\sim}{n}_{dr} = \underset{\sim}{e}_1 \sin\theta_r + \underset{\sim}{e}_3 \cos\theta_r \quad ; \quad \underset{\sim}{n}_{sr} = \underset{\sim}{e}_1 \sin\phi_r + \underset{\sim}{e}_3 \cos\phi_r. \tag{22}$$

In the above, θ_r and ϕ_r are the angles between the a_3-axis and the wave normals $\underset{\sim}{n}_{dr}$ and $\underset{\sim}{n}_{sr}$ of the reflected P and SV waves, respectively, and

L_{dr}/c_d and L_{sr}/c_s are the phase lags of the reflected P and SV waves, respectively. Note that the phase lag L_{di}/c_d for the incident P wave is selected to satisfy the source condition, Eq. (12).

Snell's law, which equates trace velocities along the surface, is obtained by substituting Eq. (18) into the boundary condition, Eq. (13), and matching the phase dependence of each term on a_1. This yields

$$\theta_r = \theta_i, \tag{23}$$

$$\frac{\sin \theta_i}{\sin \phi_r} = \frac{c_d}{c_s} = \left(\frac{\lambda+2\mu}{\mu}\right)^{1/2} = \delta. \tag{24}$$

Similarly, matching the phase lags of each term at the boundary leads to

$$L_{dr} = L_{di} \quad ; \quad L_{sr} = L_{di}/\delta. \tag{25}$$

After the phases are matched, the reflection coefficients of the (linear) reflected P and SV waves, $\Gamma_{dd}^{(1)}$, $\Gamma_{sd}^{(1)}$ may be obtained by solving the remaining algebraic equations:

$$\Gamma_{dd}^{(1)} = \frac{A_{dr}^{(1)}}{A_{di}^{(1)}} = \frac{\sin 2\theta_i \sin 2\phi_r - \delta^2 \cos^2 2\phi_r}{\sin 2\theta_i \sin 2\phi_r + \delta^2 \cos^2 2\phi_r}, \tag{26}$$

$$\Gamma_{sd}^{(1)} = \frac{A_{sr}^{(1)}}{A_{di}^{(1)}} = \frac{2\delta \sin 2\theta_i \cos 2\phi_r}{\sin 2\theta_i \sin 2\phi_r + \delta^2 \cos^2 2\phi_r}. \tag{27}$$

The foregoing fully define the $O(\epsilon)$ solution, so we next proceed to an evaluation of the second-order displacements. We use Eq. (18) to form the inhomogeneous terms $K_i^{(2)}$ and $G_{ij}^{(2)}$ in Eqs. (16) and (17). Using the latter to formulate the boundary condition, Eq. (13), leads to the analytical task of solving a pair of inhomogeneous differential equations for $\underset{\sim}{u}^{(2)}$ subject to inhomogeneous boundary conditions. We simplify this task by considering each inhomogeneity individually through the decomposition,

$$u_i^{(2)} = u_{i,1}^{(2)} + u_{i,2}^{(2)}. \tag{28}$$

The first term consists of the homogeneous solution of the differential equations subject to inhomogeneous boundary conditions,

$$\frac{\partial^2 u_{i,1}^{(2)}}{\partial t^2} - (c_d^2 - c_s^2)\frac{\partial^2 u_{m,1}^{(2)}}{\partial a_m \partial a_i} - c_s^2 \frac{\partial^2 u_{i,1}^{(2)}}{\partial a_m \partial a_m} = 0,$$

$$\lambda \frac{\partial u_{m,1}^{(2)}}{\partial a_m}\delta_{ij} + \mu\left(\frac{\partial u_{i,1}^{(2)}}{\partial a_j} + \frac{\partial u_{j,1}^{(2)}}{\partial a_i}\right) = -G_{ij}(\underset{\sim}{u}^{(1)})/\rho_0 \quad \text{on} \quad a_3 = 0, \tag{29}$$

while the last term in Eq. (28) is the particular solution of the differential equations subject to homogeneous boundary conditions,

$$\frac{\partial^2 u_{i,2}^{(2)}}{\partial t^2} - (c_d^2 - c_s^2)\frac{\partial^2 u_{m,2}^{(2)}}{\partial a_m \partial a_i} - c_s^2 \frac{\partial^2 u_{i,2}^{(2)}}{\partial a_m \partial a_m} = K_i(\underset{\sim}{u}^{(1)})/\rho_0, \tag{30}$$

$$\lambda \frac{\partial u^{(2)}_{m,2}}{\partial a_m} \delta_{ij} + \mu\left(\frac{\partial u^{(2)}_{i,2}}{\partial a_j} + \frac{\partial u^{(2)}_{j,2}}{\partial a_i}\right) = 0 \quad \text{on} \quad a_3 = 0.$$

Note that the solutions of the first set of equations are equivalent to linear free waves, whose magnitude remain constant. Although such solutions might represent new types of wave, their effects remains $O(\epsilon^2)$ at all locations, and hence are negligible compared to the $O(\epsilon)$ solutions. In contrast, the source terms $K_i(\underset{\sim}{u}^{(1)})$ will be seen to resonantly excite waves in a manner that cannot be ignored. Accordingly, we consider $u^{(2)}_{i,1} = 0$ and $u^{(2)}_{i,2} = u^{(2)}_i$.

When we substitute the $O(\epsilon)$ solution, Eq. (18), into Eqs. (30), in order to form the source terms K_i, the resulting coupled equations governing $u^{(2)}_1$ and $u^{(2)}_3$ are found to be

$$\begin{aligned}
&\frac{\partial^2 u^{(2)}_1}{\partial t^2} - (c_d^2 - c_s^2)\left(\frac{\partial^2 u^{(2)}_1}{\partial a_1^2} + \frac{\partial^2 u^{(2)}_3}{\partial a_1 \partial a_3}\right) - c_s^2\left(\frac{\partial^2 u^{(2)}_1}{\partial a_1^2} + \frac{\partial^2 u^{(2)}_1}{\partial a_3^2}\right) \\
&\quad = -\frac{i}{4\rho_0} M_3 k_d^3 \left[A^{(1)}_{di}\right]^2 \sin\theta_i \left[\exp(i2\omega\psi_{di}) + \Gamma^{(1)2}_{dd} \exp(i2\omega\psi_{dr})\right] \\
&\quad\quad - \frac{i}{4\rho_0} M_3' k_s^3 \left[A^{(1)}_{sr}\right]^2 \sin\phi_r \exp(i2\omega\psi_{sr}) \\
&\quad\quad + B_1\left\{\exp[i\omega(\psi_{di} + \psi_{dr})] + \exp[i\omega(\psi_{di} - \psi_{dr})]\right\} \\
&\quad\quad + C_1\left\{\exp[i\omega(\psi_{di} + \psi_{sr})] + \exp[i\omega(\psi_{di} - \psi_{sr})]\right\} \\
&\quad\quad + D_1\left\{\exp[i\omega(\psi_{dr} + \psi_{sr})] + \exp[i\omega(\psi_{dr} - \psi_{sr})]\right\} + \text{c.c.},
\end{aligned} \tag{31}$$

$$\begin{aligned}
&\frac{\partial^2 u^{(2)}_3}{\partial t^2} - (c_d^2 - c_s^2)\left(\frac{\partial^2 u^{(2)}_3}{\partial a_3^2} + \frac{\partial^2 u^{(2)}_1}{\partial a_1 \partial a_3}\right) - c_s^2\left(\frac{\partial^2 u^{(2)}_3}{\partial a_1^2} + \frac{\partial^2 u^{(2)}_3}{\partial a_3^2}\right) \\
&\quad = -\frac{i}{4\rho_0} M_3 k_d^3 \left[A^{(1)}_{di}\right]^2 \cos\theta_i \left[\exp(i2\omega\psi_{di}) - \Gamma^{(1)2}_{dd} \exp(i2\omega\psi_{dr})\right]
\end{aligned}$$

$$
\begin{aligned}
&- \frac{i}{4\rho_0} M_3' k_s^3 \left[A_{sr}^{(1)}\right]^2 \cos\phi_r \exp(i2\omega\psi_{sr}) \\
&+ B_3 \left\{\exp[i\omega(\psi_{di} + \psi_{dr})] + \exp[i\omega(\psi_{di} - \psi_{dr})]\right\} \\
&+ C_3 \left\{\exp[i\omega(\psi_{di} + \psi_{sr})] + \exp[i\omega(\psi_{di} - \psi_{sr})]\right\} \\
&+ D_3 \left\{\exp[i\omega(\psi_{dr} + \psi_{sr})] + \exp[i\omega(\psi_{dr} - \psi_{sr})]\right\} + \text{c.c.}, \qquad (32)
\end{aligned}
$$

where

$$M_3 = 3\lambda + 6\mu + \frac{1}{4}\alpha + \frac{3}{2}\beta + 6\gamma, \qquad (33)$$

$$M_3' = \lambda + 2\mu + \frac{1}{4}\beta + \frac{3}{2}\gamma, \qquad (34)$$

and B_1, B_3, ..., D_1, D_3 are function of θ_i that will be seen to be unimportant. Note that Eqs. (31) and (32) are obtained by using the first-order reflection coefficient, Eq. (26).

Each source term appearing in Eqs. (31) and (32) leads to a corresponding particular solution that is temporally a second harmonic. The phase speeds of the terms whose phases are $(\psi_{di} \pm \psi_{dr})$, $(\psi_{di} \pm \psi_{sr})$, and $(\psi_{dr} \pm \psi_{sr})$ do not match the phases of homogeneous solutions of the equations, which represent freely propagating linear waves. Hence, the corresponding particular solutions are nonsecular waves of constant amplitude. Moreover, the particular solution for the source term whose phase is $2\psi_{sr}$ can also be shown to be nonsecular. (This observation is consistent with a previous analysis of a finite amplitude shear wave[14], which showed that secular growth of harmonics in a shear wave occurs at the third order in a perturbation series.) These conditions are contrasted by the source terms with phases $2\psi_{di}$ and $2\psi_{dr}$, whose phase

speeds match that of homogeneous second harmonic dilatational waves. The method of variation of parameters reveals that the corresponding particular solutions are secular, with amplitudes that grow linearly with propagation distance. The particular solution for the second-order displacements is thereby found to be

$$\underset{\sim}{u}_P^{(2)} = \frac{1}{2} A_{di}^{(2)} (\underset{\sim}{n}_{di} \cdot \underset{\sim}{r}) \underset{\sim}{n}_{di} \exp(i2\omega\psi_{di}) + \frac{1}{2} \left[\Gamma_{dd}^{(1)}\right]^2 A_{di}^{(2)} (\underset{\sim}{n}_{dr} \cdot \underset{\sim}{r}) \underset{\sim}{n}_{dr} \exp(i2\omega\psi_{dr}) + \text{NST} + \text{c.c.}; \quad (35)$$

where

$$A_{di}^{(2)} = \frac{M_3 k_d^2}{4M_2} \left[A_{di}^{(1)}\right]^2, \quad (36)$$

$$M_2 = \lambda + 2\mu, \quad (37)$$

and NST denotes the nonsecular solutions.

Since this particular solution has no free parameters, satisfaction of the $O(\epsilon^2)$ stress-free boundary conditions requires the addition of the complementary solution of Eqs. (31) and (32). This leads us to a paradoxical situation. First, we note that evaluating derivatives of $\underset{\sim}{u}_P^{(2)}$ on $a_3 = 0$ results in terms whose dependence matches the phase dependence of the incident and reflected P waves parallel to the boundary, both of which are $2k_d \sin\theta_i a_1 - 2k_d L_{di} - 2\omega t$, since $\theta_r = \theta_i$. Furthermore, because of the secular condition, the amplitude of these terms grows linearly with distance along the boundary. Now consider the corresponding homogeneous solution. Its terms must have the same phase dependence,

which suggests that the homogeneous solution should consist of free waves that propagate in the direction $\underset{\sim}{n}_{dr}$, and possibly $\underset{\sim}{n}_{sr}$. However, since the homogeneous solutions have constant amplitude, they cannot match the growing amplitude dependence created by $\underset{\sim}{u}_p^{(2)}$ on the boundary.

A Helmholtz resolution of the second-order homogeneous solution,

$$\underset{\sim}{u}_H^{(2)} = \underset{\sim}{\nabla}\Phi^{(2)} + \underset{\sim}{\nabla}\times\underset{\sim}{H}^{(2)}; \quad \underset{\sim}{\nabla}\cdot\underset{\sim}{H}^{(2)} = 0, \tag{38}$$

leads to the observation that a P wave propagating in a direction $\underset{\sim}{n}_{dr}$ that depends linearly on distance measured transversely to $\underset{\sim}{n}_{dr}$ is a homogeneous solution. A comparable statement applies for an SV wave. Hence, it is possible to construct a homogeneous solution suitable for satisfying the boundary conditions, according to

$$\begin{aligned}\underset{\sim}{u}_H^{(2)} = {} & C_1(\underset{\sim}{n}_{dr}\times \underset{\sim}{r}\cdot\underset{\sim}{e}_2)\underset{\sim}{n}_{dr}\exp(i2\omega\psi_{dr}) \\ & + C_2(\underset{\sim}{n}_{sr}\times \underset{\sim}{r}\cdot\underset{\sim}{e}_2)(\underset{\sim}{e}_2\times \underset{\sim}{n}_{sr})\exp(i2\omega\psi_{sr}) + c.c.,\end{aligned} \tag{39}$$

where C_1 and C_2 are coefficients to be determined.

We shall not proceed further with such an analysis, because the qualitative insight provided by the forms of $\underset{\sim}{u}_p^{(2)}$ and $\underset{\sim}{u}_H^{(2)}$ lead us to a drastically simplified solution process. The key observations are:

1. Nonlinear interactions between incident and reflected waves are negligible, because they do not lead to secular terms.

2. P and SV waves are reflected at both the first and second orders.
3. Secularity occurs in the second-order P waves, but not in the second-order SV wave.
4. The fact that the second-order reflected waves contain terms that depend on distance perpendicular to the direction of propagation suggests that the direction in which such waves propagate deviates by an $O(\epsilon)$ amount from the directions θ_r and ϕ_r.

III. GENERAL SOLUTIONS BY THE METHOD OF CHARACTERISTICS

The analysis in the preceding section indicates that the reflection process generates reflected P and SV waves to accompany the incident P wave, with each wave uncoupled from the others. This leads to an appreciable simplification as the incident P, reflected P and SV waves can be treated independently. We first consider the incident P wave. This wave propagates at a constant angle of incidence θ_i, but its phase speed depends on the local wave amplitude resulting in a cumulative distortion of the wave profile. In view of the source boundary condition, Eq. (12), the particle velocity in this incoming P wave may be written as[15]

$$\underset{\sim}{v}_{di} = -\frac{i}{2}\epsilon A_{di}\underset{\sim}{n}_{di}\exp(i\omega\Psi_{di}) + O(\epsilon^2) + c.c., \tag{40}$$

where

$$\Psi_{di} = \frac{\underset{\sim}{n}_{di}\cdot\underset{\sim}{r} + L_{di}}{c_d + \beta_d(\underset{\sim}{v}_{di}\cdot\underset{\sim}{n}_{di})} - t. \tag{41}$$

where $\beta_d = -M_3/2M_2$ is the coefficient of nonlinearity for a plane progressive dilatational wave and $O(\epsilon^2)$ represents constant magnitude terms. Note that this wave exhibits amplitude dispersion, because its phase speed is $c_d + \beta_d(\underset{\sim}{v}_{di} \cdot \underset{\sim}{n}_{di})$.

Since the reflected P wave does not interact with the other waves, it also must propagate nonlinearly. If $\underset{\sim}{v}_{dr}$ is the particle velocity in this wave, then the appropriate phase speed is $c_d + \beta_d(\underset{\sim}{v}_{dr} \cdot \underset{\sim}{n}_{dr})$. However, it is not necessary that $\underset{\sim}{n}_{dr}$ match the direction predicted by linear theory. Furthermore, it is not even necessary that $\underset{\sim}{n}_{dr}$ be invariant.

In order to understand this feature, let us view the propagation of a dilatational signal in the characteristic space whose coordinates are a_1, a_3, and t. Let $\underset{\sim}{v}_{dr}$ be the particle velocity of the signal emanating from a point on the boundary $a_3 = 0$ at distance $a_1 = \zeta$ at time $t = \tau$. In order for this to be a dilatational motion, the particle velocity is assumed to be parallel to the propagation direction, i.e. $\underset{\sim}{v}_{dr} = |\underset{\sim}{v}_{dr}|\underset{\sim}{n}_{dr}$.

The characteristic for this signal is a straight line emanating from the boundary point $(\zeta,0,\tau)$ in the characteristic space. As shown in Fig. 2, the tangent of the angle χ between this line and the line through $(\zeta,0,\tau)$ parallel to the t-axis must be the propagation speed, so

$$\chi = \tan^{-1}[c_d + \beta_d(\underset{\sim}{v}_{dr} \cdot \underset{\sim}{n}_{dr})] \tag{42}$$

In other words, the characteristic line is a generator of a characteristic cone having apex angle 2χ.

The significant aspect of the foregoing lies in the fact that any line on the characteristic cone represents a solution that satisfies the equation of motion.[16,17] The corresponding propagation direction $\underset{\sim}{n}_{dr}$ for the signal appears in the characteristic space as the projection of the characteristic line onto the a_1-a_3 plane. Consider the signal radiating from $a_1 = \zeta$, $a_3 = 0$ at a different instant $t = \tau'$, also shown in Fig. 2. The particle velocity in this case is $\underset{\sim}{v}'_{dr}$ in the direction $\underset{\sim}{n}'_{dr}$. The apex angle of the characteristic cone will be $2\chi'$, where χ' is obtained from Eq. (42), and the projection of the corresponding characteristic line onto the a_1-a_3 plane will be $\underset{\sim}{n}'_{dr}$. Note that $\underset{\sim}{n}'_{dr}$ need not be the same as $\underset{\sim}{n}_{dr}$, although they are identical for propagation of a planar wave through a one-dimensional medium and for cases of normal incidence.

Since the incident P wave in Eq. (40) varies harmonically, we assume that the reflected P wave has a comparable dependence, so we take the following as its general solution,

$$\underset{\sim}{v}_{dr} = -\frac{i}{2}\,\epsilon A_{dr}\,\underset{\sim}{n}_{dr}\exp(i\omega\Psi_{dr}) + O(\epsilon^2) + \text{c.c.}, \tag{43}$$

where ψ_{dr} is a phase variable given by

$$\Psi_{dr} = \frac{\underset{\sim}{n}_{dr}\cdot\underset{\sim}{r} + L_{dr}}{c_d + \beta_d(\underset{\sim}{v}_{dr}\cdot\underset{\sim}{n}_{dr})} - t. \tag{44}$$

Consistent with the discussion of the characteristic space, we see that $\underset{\sim}{n}_{dr}$ may be a function of Ψ_{dr} without altering the constancy of $\underset{\sim}{v}_{dr}$ along a characteristic line.

Aside from a few details, the situation for the reflected SV wave is very much like that for dilatation. First, we recall that the influence of nonlinearity on the phase speed of shear waves is a third-order effect. Hence, in our analysis this speed is constant at c_s, from which it follows that the apex angle for the characteristic cone of the reflected SV wave is $\chi = \tan^{-1}(c_s)$. Moreover, since this is a vertically polarized shear wave, its particle velocity $\underset{\sim}{v}_{sr}$ lies in the a_1-a_3 plane, perpendicular to the propagation direction $\underset{\sim}{n}_{sr}$. By analogy with Eqs. (40) and (43), we therefore express the general solution for the reflected SV wave as

$$\underset{\sim}{v}_{sr} = -\frac{i}{2}\,\epsilon A_{sr}(\underset{\sim}{e}_2 \times \underset{\sim}{n}_{sr})\exp(i\omega\Psi_{sr}) + O(\epsilon^2) + \text{c.c.}, \tag{45}$$

where the phase variable for this wave is

$$\Psi_{sr} = \frac{\underset{\sim}{n}_{sr}\cdot\underset{\sim}{r} + L_{sr}}{c_s} - t. \tag{46}$$

As was true for $\underset{\sim}{n}_{dr}$, the foregoing is a general solution of the equations of motion, even if $\underset{\sim}{n}_{sr}$ depends on Ψ_{sr}.

IV. SATISFACTION OF THE BOUNDARY CONDITIONS

The expressions derived in the previous section describe the various waves in terms of their particle velocity. These must be converted to stress components relative to the a_1-a_3 plane before the boundary conditions can be addressed. Consider first a planar dilatational signal propagating in direction x. Ignoring constant magnitude second-order effects, the strain-displacement relations yield

$$E_{xx} = \frac{\partial u_x}{\partial x} + \frac{1}{2}\left(\frac{\partial u_x}{\partial x}\right)^2 = \frac{\partial u_x}{\partial \psi}\frac{\partial \psi}{\partial x} + \frac{1}{2}\left(\frac{\partial u_x}{\partial \psi}\frac{\partial \psi}{\partial x}\right)^2, \tag{47}$$

where ψ is the phase variable for the wave, while the particle velocity is

$$v_x = \frac{\partial u_x}{\partial t} = \frac{\partial u_x}{\partial \psi}\frac{\partial \psi}{\partial t}. \tag{48}$$

Since $\psi = (x+c_d)/(c_d+\beta_d v_x) - t$ for a finite amplitude dilatational wave and $u_x = O(\epsilon)$, we find that

$$E_{xx} = -\frac{v_x}{c_d+\beta_d v_x} + O(\epsilon^2) = -\frac{v_x}{c_d} + O(\epsilon^2). \tag{49}$$

A similar analysis for a shear wave polarized in direction z and propagating in direction x yields the shear strain

$$E_{xz} = \frac{1}{2}\frac{\partial u_z}{\partial x} = -\frac{1}{2}\frac{v_z}{c_s}. \tag{50}$$

We employ Eq. (49) to describe both incident and reflected P waves, while Eq. (50) applies to the reflected SV wave. Each of these strain may be transformed to components relative to the a_1, a_3 coordinate system. The direction of x in each case is the corresponding propagation direction of that wave. Once the strains are described, we derive expressions for the stress components T_{ij} from the constitutive equation, Eq. (2), the strain-displacement equation, Eq. (3), and the strain energy density, Eq. (4). Note that all nonlinear terms arising in these relations are products of spatial derivatives of displacement, so they are negligible $O(\epsilon^2)$ effects. The results of these operation are

$$\begin{aligned}&[(T_{11})_{di}\ (T_{33})_{di}\ (T_{13})_{di}]\\ &\quad = [-(\lambda+2\mu\sin^2\theta_i)\quad -(\lambda+2\mu\cos^2\theta_i)\quad \mu\sin 2\theta_i]\ \underset{\sim}{v}_{di}\cdot\underset{\sim}{n}_{di}/c_d,\end{aligned} \tag{51}$$

$$\begin{aligned}&[(T_{11})_{dr}\ (T_{33})_{dr}\ (T_{13})_{dr}]\\ &\quad = [-(\lambda+2\mu\sin^2\theta_r)\quad -(\lambda+2\mu\sin^2\theta_i)\quad -\mu\sin 2\theta\ ]\ \underset{\sim}{v}_{dr}\cdot\underset{\sim}{n}_{dr}/c_d,\end{aligned} \tag{52}$$

$$\begin{aligned}&[(T_{11})_{sr}\ (T_{33})_{sr}\ (T_{13})_{sr}]\\ &\quad = [-\mu\sin 2\phi_r\quad \mu\sin 2\phi_r\quad -\mu\cos 2\phi_r]\ \underset{\sim}{v}_{sr}\cdot(\underset{\sim}{e}_2\times\underset{\sim}{n}_{sr})/c_s.\end{aligned} \tag{53}$$

The subscripts di, dr, and sr for the stress components denote the stresses induced by the incident P and reflected P and SV waves, respectively.

The boundary conditions require that the resultant normal and shear stress components vanish on $a_3 = 0$, so we set

$$T_{33} = (T_{33})_{di} + (T_{33})_{dr} + (T_{33})_{sr} = 0 \quad \text{on} \quad a_3 = 0, \tag{54}$$

$$T_{13} = (T_{13})_{di} + (T_{13})_{dr} + (T_{13})_{sr} = 0 \quad \text{on} \quad a_3 = 0. \tag{55}$$

We substitute the expressions for particle velocities, Eqs. (40), (43), and (45) into Eqs. (51)-(53) to form stress components, which we then use to form boundary condition equations (54) and (55). This yields two equations in which the unknowns are A_{dr}, A_{sr}, L_{dr}, L_{sr}, θ_r, and ϕ_r. In order that the equations be satisfied for all a_1 and t, the phase of each term must be identical. Matching the a_1-dependent terms yields the finite amplitude form of Snell's law:

$$\frac{\sin \theta_i}{c_d + \beta_d(\underset{\sim}{v}_{di} \cdot \underset{\sim}{n}_{di})\big|_{a_3=0}} = \frac{\sin \theta_r}{c_d + \beta_d(\underset{\sim}{v}_{dr} \cdot \underset{\sim}{n}_{dr})\big|_{a_3=0}} = \frac{\sin \phi_r}{c_s}. \tag{56}$$

The phase lags of the reflected waves relative to the incident wave can be obtained by equating the a_1-independent terms,

$$\frac{L_{di}}{c_d + \beta_d(\underset{\sim}{v}_{di} \cdot \underset{\sim}{n}_{di})\big|_{a_3=0}} = \frac{L_{dr}}{c_d + \beta_d(\underset{\sim}{v}_{dr} \cdot \underset{\sim}{n}_{dr})\big|_{a_3=0}} = \frac{L_{sr}}{c_s}. \tag{57}$$

When the above are satisfied, the boundary conditions reduce to two simultaneous, algebraic equations. Solving these for the amplitude of each reflected wave in terms of A_{di} yields the following expressions for

the reflection coefficients Γ_{dd} and Γ_{sd} of the P and SV waves, respectively,

$$\Gamma_{dd} = \frac{A_{dr}}{A_{di}} = \frac{\sin 2\theta_i \sin 2\phi_r - (\delta^2 - 2\sin^2\theta_i)\cos 2\phi_r}{\sin 2\theta_r \sin 2\phi_r + (\delta^2 - 2\sin^2\theta_r)\cos 2\phi_r}, \tag{58}$$

$$\Gamma_{sd} = \frac{A_{sr}}{A_{di}} = \frac{\sin 2\theta_i(\delta^2 - 2\sin^2\theta_r) + \sin 2\theta_r(\delta^2 - 2\sin^2\theta_r)}{\delta[\sin 2\theta_r \sin 2\phi_r + (\delta^2 - 2\sin^2\theta_r)\cos 2\phi_r]}. \tag{59}$$

Note that these coefficients reduce to the linear forms, Eqs. (26) and (27), when Snell's law in Eq. (56) is linearized by ignoring the particle velocity terms, as well as when $\beta_d = 0$, which means the material is a linearly elastic solid up to second order[18].

Equations (56)-(59) fully define the reflection process. Equation (56), which governs the directions of propagation of the reflected P and SV waves, indicates that at a specific boundary point, the reflection angle of each reflected wave fluctuates because of the temporal variation of the incident particle velocity. Furthermore, since $\underset{\sim}{v}_{di} \cdot \underset{\sim}{n}_{di}$ is periodic, the angles for the reflected P and SV waves exhibit periodic fluctuations about the constant values predicted by linear theory. Each ray determined in this manner represents the locus of points at which the particle velocity departing from the boundary at a specific instant will be observed with increasing time.

V. QUANTITATIVE EVALUATIONS

The preceding discussion leads to the realization that the rays for the instantaneous signal at a specific field point $\underset{\sim}{r}(\xi,\eta)$ are situated within a wedge of influence. A typical situation is depicted in Fig. 3. According to Eq. (56), the orientation of any ray within this wedge depends on the reflected particle velocities. However, the latter quantities depend on the reflection coefficients, which in turn depend on the reflection angles. Evaluating the particle velocity at $\underset{\sim}{r}$ in these circumstances is obviously not a trivial task.

Although it involves an approximation, the algorithm we have developed greatly simplifies the computations. It is assumed in the following that the properties of the incident wave, as defined by ϵ, A_{di}, θ_i, and L_{di}, are specified constants. We begin by addressing the evaluation procedure for the dilatational waveform at $\underset{\sim}{r}$.

1. Starting from zero, select a value of Ψ_{dr} in the range $0 \leq \Psi_{dr} \leq 2\pi/\omega$.
2. Use the linear reflection coefficients $\Gamma_{dd}^{(1)}$, $\Gamma_{sd}^{(1)}$ to form an initial estimate of the particle velocities on the boundary. (This is a reasonable approximation, since the $O(\epsilon)$ deviation of the reflection angles from their linear counterparts produces an $O(\epsilon)$ error in Γ_{dd}, which feeds back into Snell's law through $\underset{\sim}{v}_{dr}$ as an $O(\epsilon^2)$ effect.) Since all rays intersecting a boundary

point are associated with the same phase, the particle speeds at the boundary are therefore approximated by

$$\begin{aligned}
\underset{\sim}{v}_{di}\cdot\underset{\sim}{n}_{di}\Big|_{a_3=0} &= -\frac{i}{2}\,\epsilon A_{di}\exp(i\omega\Psi_{dr}) + c.c.,\\
\underset{\sim}{v}_{dr}\cdot\underset{\sim}{n}_{dr}\Big|_{a_3=0} &= -\frac{i}{2}\,\epsilon\Gamma^{(1)}_{dd}A_{di}\exp(i\omega\Psi_{dr}) + c.c.,\\
\underset{\sim}{v}_{sr}\cdot(\underset{\sim}{e}_2\times\underset{\sim}{n}_{sr})\Big|_{a_3=0} &= -\frac{i}{2}\,\epsilon\Gamma^{(1)}_{sd}A_{di}\exp(i\omega\Psi_{dr}) + c.c..
\end{aligned} \tag{60}$$

3. Use Eqs. (60) to evaluate θ_r and ϕ_r from Eqs. (56), as well as L_{dr} from the first of Eqs. (57).
4. The angles θ_r and ϕ_r found in the preceding step yield corrected values of the reflection coefficients Γ_{dd} and Γ_{sd} according to Eq. (58) and (59).
5. Replace the linear reflection coefficients in step 2 by the values found above and use the new estimates of particle velocities to redo steps 3 and 4. Repeat this process until θ_r and ϕ_r converge.
6. The results of the previous steps lead through Eqs. (60) and (52) to values of the $(\underset{\sim}{v}_{dr}\cdot\underset{\sim}{n}_{dr})$ and the stress components $(T_{11})_{dr}$, $(T_{33})_{dr}$ and $(T_{13})_{dr}$. The corresponding value of t is computed from Eq. (44) with Ψ_{dr} equated to the assumed value.
7. If it is desired to identify the boundary position $(\zeta_d,0)$ from which the dilatational ray emanated, use Fig. 3 to find

$$\xi - \zeta_d = \eta\,\tan\theta_r \tag{61}$$

8. Increment the value of Ψ_{dr} and return to step 2.

This algorithm yields values of the particle velocity and stress components of a discrete number of time instants. Note that because Ψ_{dr} depends on $\underset{\sim}{v}_{dr}$, $\underset{\sim}{n}_{dr}$, the time increments for this discretization are not constant. A comparable procedure based on incrementing Ψ_{sr} yields the time waveforms for particle speed and stress components in the reflected SV wave.

The material that we choose for numerical evaluation is steel (Hecla 37 carbon steel), which has "quasi-isotropic" elastic properties. The material properties are[19]: $\rho_0 = 7.823 \times 10^3$ kg/m^3, $\lambda = 11.1 \times 10^{10}$ N/m^2, $\mu = 8.21 \times 10^{10}$ N/m^2, $\alpha = -143.2 \times 10^{10}$ N/m^2, $\beta = -112.8 \times 10^{10}$ N/m^2, $\gamma = -23.6 \times 10^{10}$ N/m^2, so the coefficient of nonlinearity is $\beta_d \approx 3.1$. The reflection coefficients for the instant when the incident P wave is in its maximum phase, which represents the maximum deviation from linear theory, are shown in Fig. 4. Since β_d is a small value, the nonlinear phenomena are not appreciable for realistic values of ϵ. In order to magnify the nonlinear effects, we consider here $\epsilon = 0.01$ and 0.1. It is apparent that the nonlinear effect is very small unless ϵ is large. It also can be seen that the nonlinear effect increase with increasing angle of incidence.

Figures 5 and 6 show the time waveforms of stress components of the reflected P and SV signals generated by a 2-MHz dilatational source. The wavelength of the incident P wave is about 3 mm. The angle of incidence

of the incoming P wave is 60° and the acoustic Mach number ϵ is 0.01. For this calculation, the field point (ξ,η) = (6.6 mm, 3.8 mm) was selected such that, measured along the linear dilatational rays ($\theta_r = \theta_i$), the distance from the field point to the origin equals the distance L_{di} from the origin to the source. Further, L_{di} is taken to be one half of the shock formation distance for a planar P wave, $L_{di} = c_d/(2\epsilon\beta_d\omega)$. Hence, if the incident wave were to propagate along the ray path without undergoing a decrease in amplitude and change of phase due to the reflection process, it would first form a shock at the field point.

The zones of influence on the boundary for dilatation and shear reflection of this particular case were found to be $-1.20 \text{ mm} \leq (a_1)_d \leq 0.81 \text{ mm}$ and $4.48 \text{ mm} \leq (a_1)_s \leq 4.64 \text{ mm}$, respectively. These "spot sizes" are smaller than either wavelength. It is interesting to note that the SV wave at the field point shows more distortion than the P wave, even though the SV wave propagates without amplitude dispersion. This phenomenon arises from a combination of factors. The primary cause is the phase reversal of the P wave upon reflection, which cause the waveform to become like a backward sawtooth. This is similar to the effect noted by Breazeale and Lester[2] for reflection at a pressure release boundary. In addition, the incident P wave that generates the SV wave travels through a greater distance to the boundary, and therefore undergoes more distortion than its counterpart that generates the reflected P wave. A third factor influencing the level of distortion is associated with the mode conversion process, which lowers the overall amplitude of the P wave. In other words, the distance from the boundary

to the field point, which was selected to be half the shock formation distance for the incident P wave, is much less than half the distance for shock formation for the reflected P wave. We may conclude from this that mode conversion in reflection extends the distance along the ray path of a P wave at which a shock first forms.

A comparison between the finite amplitude forms of Snell's law and linear forms of Snell's law is also depicted at Figs. 5 and 6. The latter, which includes the nonlinear self-action effects of the waves, but considers the reflection angles to be constant, is equivalent to the approach that was developed by Van Buren and Breazeale. It is found that the nonconstancy of the reflected angles tends to alter the mean values of the fluctuations and makes the waveforms unsymmetrical, but the wave profiles obtained from both theories are almost identical. Also note that the effect of nonconstancy of the angle for the reflected P wave is much more significant than that for the reflected SV wave, because the reflected P waves have larger angles of reflection, resulting in a larger zone of influence.

Propagation curves for the fundamental through third harmonic components of the reflected P waveform, $(T_{33})_{dr}$, are depicted in Fig. 7, where $\bar{r}$ is the shock formation distance of a simple planar P wave with $\epsilon = 0.01$, and r is the distance measured from the boundary along the linear dilatational ray path. As mentioned, the phase reversal of the P wave upon reflection causes a reversal in the distortion of the reflected P waveform. Hence, the signal levels of the second and third

harmonics decrease with increasing distance away from the reflecting surface. However, unlike the curves obtained from the linear form of Snell's law, the amplitudes of the second and third harmonics obtained from the finite amplitude form of Snell's law does not fully vanish at $\sigma \approx 3$ because of the effect of rays arriving from the different spots on the boundary. Figure 8 shows the propagation curves for the fundamental through third harmonic components of the reflected SV waveform, $(T_{33})_{sr}$. Since the reflected SV wave propagates without amplitude dispersion, the curves obtained by both linear and finite amplitude forms of Snell's law are almost identical.

VI. CONCLUSIONS

Our analysis has shown that if a P wave undergoes significant distortion prior to incidence at a free surface, the distortion is transferred to the reflected P and SV waves. The angles of reflected rays were proven to be governed by simple modifications of Snell's law that account for the particle velocity dependence of phase speed when the trace velocities are formed. These corrections carry over into corrections of the linearized relations governing the amplitude and phase lag of the instantaneous signal associated with a ray. The primary significance of the nonlinear Snell's law is that the orientation of reflected rays fluctuates due to the oscillatory nature of the particle velocity in the incident wave.

The mechanism by which a reflected P wave distorts is the same as that for the incident wave, but the effect is smaller because of the reduction of amplitude level due to mode conversion. Interestingly, the reflected SV wave was shown to pick up substantial distortion, since its phase dependence at the boundary must match that of the incident wave. However, unlike the P wave, the SV wave propagates without additional distortion. A primary result derived from the perturbation analysis, which was performed as a preliminary to the method of characteristics, is the observation that the free-field interaction between each type of wave is insignificant.

The task of constructing the waveform at a specified field point is complicated by the fact that reflected rays arrive from zones on the boundary. These zones of influence correspond to the extrema in the fluctuations of the reflection angles. An iterative numerical algorithm for evaluating waveforms was employed to study harmonic generation in the reflected signals. An earlier analysis indicated that phase reversal initially causes the amplitude of the higher harmonics in the P wave to decrease with increasing propagation distance. This was confirmed, but the associated prediction that there is a location where all higher harmonics vanish was shown to be incorrect due to the fluctuations in the angle of reflection.

Finally, we note that the portion of the analysis using the method of characteristics in two dimensions is quite general. Its extension to transient signals seems to be rather straightforward, since the main

elements of the analysis did not rely on any properties specific to the sinusoidal dependence associated with the assumed excitation.

ACKNOWLEDGEMENTS

The authors wish to thank the National Science Foundation, grant no. MSM-8512818, and the Office of Naval Research, code 1125-UA, for their support of this research.

REFERENCES

1. K. T. Shu and J. H. Ginsberg, "Ray theory solution for finite amplitude effects in a two-dimensional hard-walled waveguide," J. Acoust. Soc. Am. 86, 771-776 (1989).

2. D. T. Blackstock, "Normal reflection of finite ampltude plane waves from a rigid wall," Proc. 3rd Intern. Cong. Acoust., Stuttgart, Ed. L. Cremer, Vol. I, 309-311 (1959).

3. M. A. Breazeale and W. W. Lester, "Demonstration of the "east stable waveform" of finite amplitude waves," J. Acoust. Soc. Am. 33, 1803 (1961).

4. O. Buck and D. O. Thompson, "Relation of finite amplitude waves to third order elastic constants," Mater. Sci. Eng. 1, 117-140 (1966).

5. A. L. Van Buren and M. A. Breazeale, "Reflection of finite-amplitude ultrasonic waves. I. Phase shift," J. Acoust. Soc. Am. 44, 1014-1020 (1968).

6. S. S. Feng, "Reflection of finite amplitude waves," Sov. Phys. Acoust. 6, 488-490 (1961).

7. Z. Qian, "Reflection of finite-amplitude sound wave on a plane boundary of half space," Sci. Sin. 25, 492-501 (1982).

8. F. D. Cotaras, "Reflection and refraction of finite amplitude acoustic waves at a fluid-fluid Interfaces," Tech. Report ARL-TR-89-1, Applied Research Laboratories, The University of Texas at Austin (1989).

9. S. R. Reid, "The influence of non-linearity upon the reflection of finite amplitude shock waves in elastodynamics," Quart. J. Mech. Appl. Math. 25, 185-206 (1972).

10. T. W. Wright, "Critical angles and grazing incidence: the breakdown of regular shock reflection in solids," J. Elast. 11, 81-107 (1981).

11. D. R. Bland, Nonlinear Dynamic Elasticity, (Blaisdell, Waltham, Mass., 1969), pp. 19.

12. K. Brugger, "Thermodynamic Definition of Higher Order Elastic Coefficients," Phys. Rev. 133, A1611-A1612 (1964).

13. L. M. Brekhovskikh, Waves in Layered Media, 2nd Ed., (Academic Press, New York, 1980), pp. 33-38.

14. R. W. Lardner, "Nonlinear Effects on Transverse Shear Waves in an Elastic Medium," J. Elast. 15, 53-57 (1985).

15. R. N. Thurston and M. J. Shapiro, "Interpretation of Ultrasonic Experiments on Finite-Amplitude Waves," J. Acoust. Soc. Am. 41, 1112-1125 (1967).

16. A. Kluwick, "On the Non-linear Distortion of Waves Generated by Flat Plates Under Harmonic Excitations," J. Sound Vib. 73, 601-605 (1980).

17. A. Jeffrey and T. Taniuti, Non-linear Wave Propagation, (Academic Press, New York, 1964).

18. M. A. Breazeale and J. Ford, "Ultrasonic Studies of the Nonlinear Behavior of Solids," J. Appl. Phys. 36, 3486-3490 (1965).

19. R. T. Smith, R. Stern, and R. W. B. Stephens, "Third-Order Elastic Moduli of Polycrystalline Metals from Ultrasonic Velocity Measurements," J. Acoust. Soc. Am. 40, 1002-1008 (1966).

LIST OF CAPTIONS

Figure 1. Incident and reflected wave systems for an incident P wave.

Figure 2. An illustration of two characteristic cones in the characteristic space.

Figure 3. Schematic diagram showing the wedges of influence for the rays arriving at a field point.

Figure 4. Reflection coefficients for the instant when the incident P wave is in its maximum phase. (---) linear, (---) $\epsilon = 0.01$, (-·-) $\epsilon = 0.1$.

Figure 5. Time waveforms of stress component in the reflected P wave generated by a 2-MHz dilatational source at a selected field point (6.6 mm, 3.8 mm): $\theta_i = 60^\circ$, $\epsilon = 0.01$, $\beta_d \approx 3.1$, $L_{di} = 7.64$ mm.

Figure 6. Time waveforms of stress component in the reflected SV wave generated by a 2-MHz dilatational source at a selected field point (6.6 mm, 3.8 mm): $\theta_i = 60^\circ$, $\epsilon = 0.01$, $\beta_d \approx 3.1$, $L_{di} = 7.64$ mm.

Figure 7. Amplitudes of the first three harmonics of the reflected P waveform $(T_{33})_{dr}$ generated by a 2-MHz dilatational source at

a selected field point (6.6 mm, 3.8 mm): $\theta_i = 60^\circ$, $\epsilon = 0.01$, $\beta_d \approx 3.1$, $L_{di} = 7.64$ mm.

Figure 8. Amplitudes of the first three harmonics of the reflected SV waveform $(T_{33})_{sr}$ generated by a 2-MHz dilatational source at a selected field point (6.6 mm, 3.8 mm): $\theta_i = 60^\circ$, $\epsilon = 0.01$, $\beta_d \approx 3.1$, $L_{di} = 7.64$ mm.

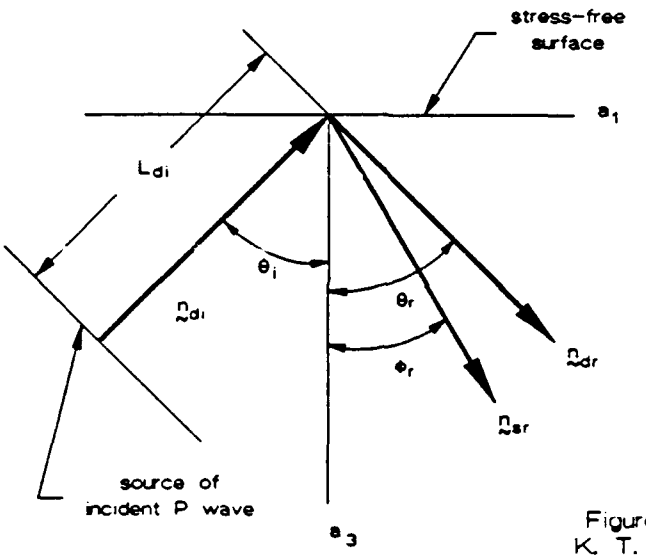

Figure 1
K. T. SHU

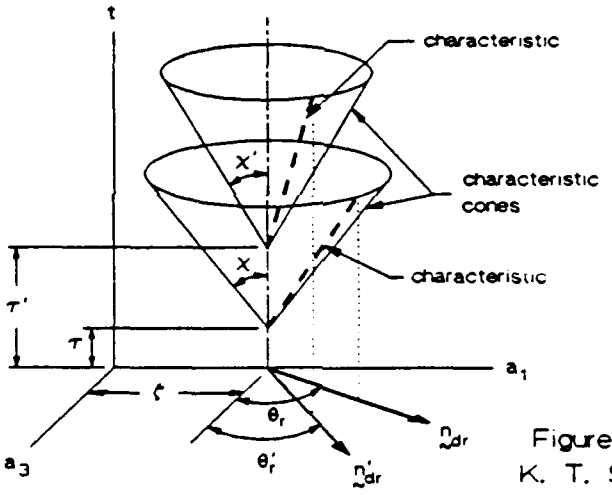

Figure 2
K. T. SHU

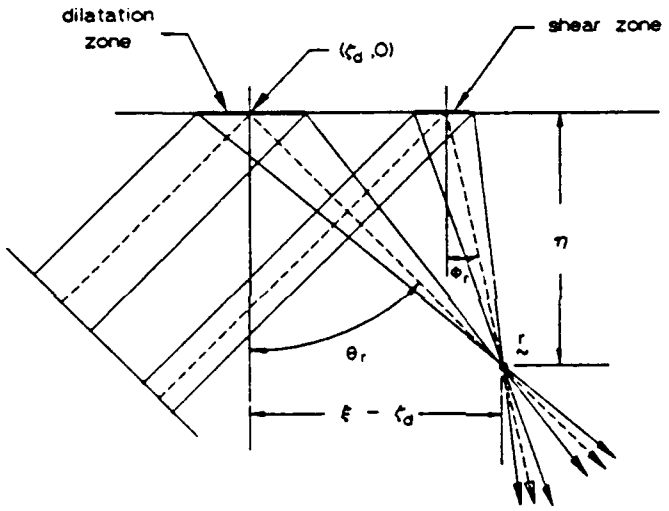

Figure 3
K. T. SHU

FIGURE 4

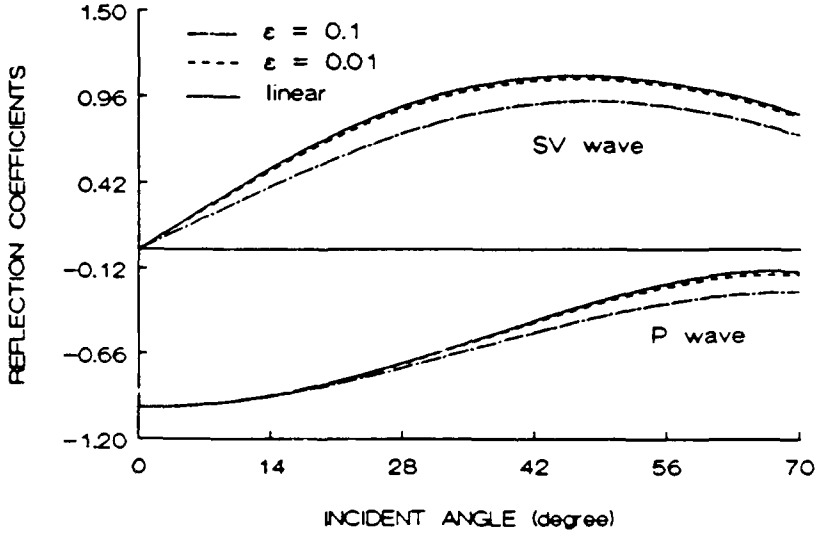
1.50
0.96
0.42
−0.12
−0.66
−1.20
REFLECTION COEFFICIENTS
ε = 0.1
ε = 0.01
linear
SV wave
P wave
0
14
28
42
56
70
INCIDENT ANGLE (degree)

FIGURE 5

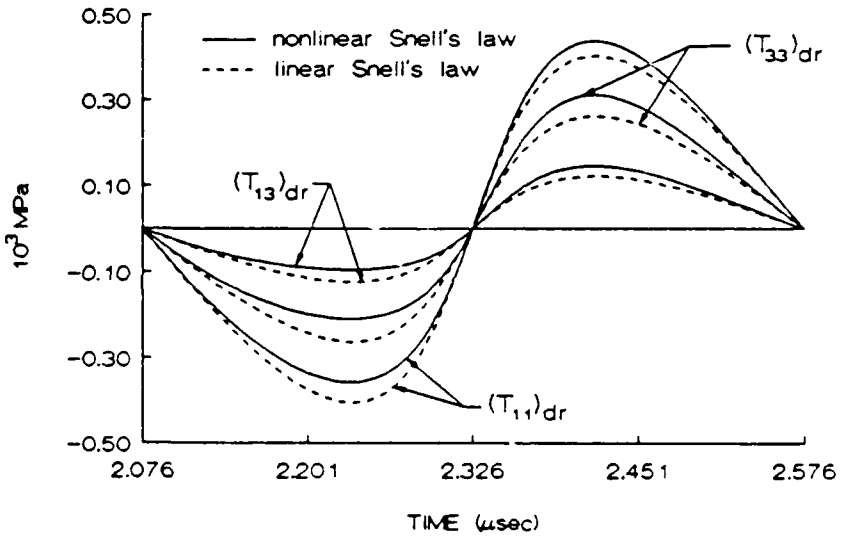
0.50
0.30
0.10
−0.10
−0.30
−0.50
10^3 MPa
nonlinear Snell's law
linear Snell's law
$(T_{33})_{dr}$
$(T_{13})_{dr}$
$(T_{11})_{dr}$
2.076
2.201
2.326
2.451
2.576
TIME (μsec)

FIGURE 6

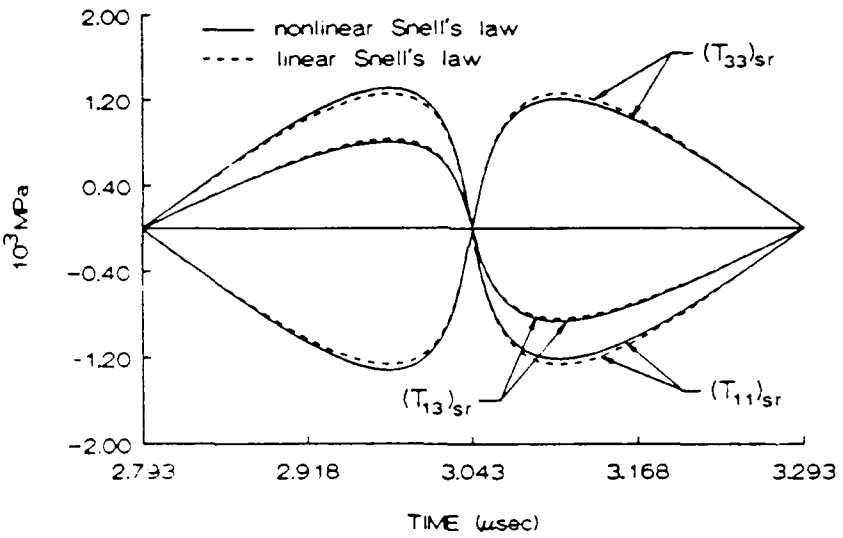
2.00
1.20
0.40
-0.40
-1.20
-2.00
10^{-3}MPa
nonlinear Snell's law
linear Snell's law
$(T_{33})_{sr}$
$(T_{13})_{sr}$
$(T_{11})_{sr}$
2.793
2.918
3.043
3.168
3.293
TIME (μsec)

FIGURE 7

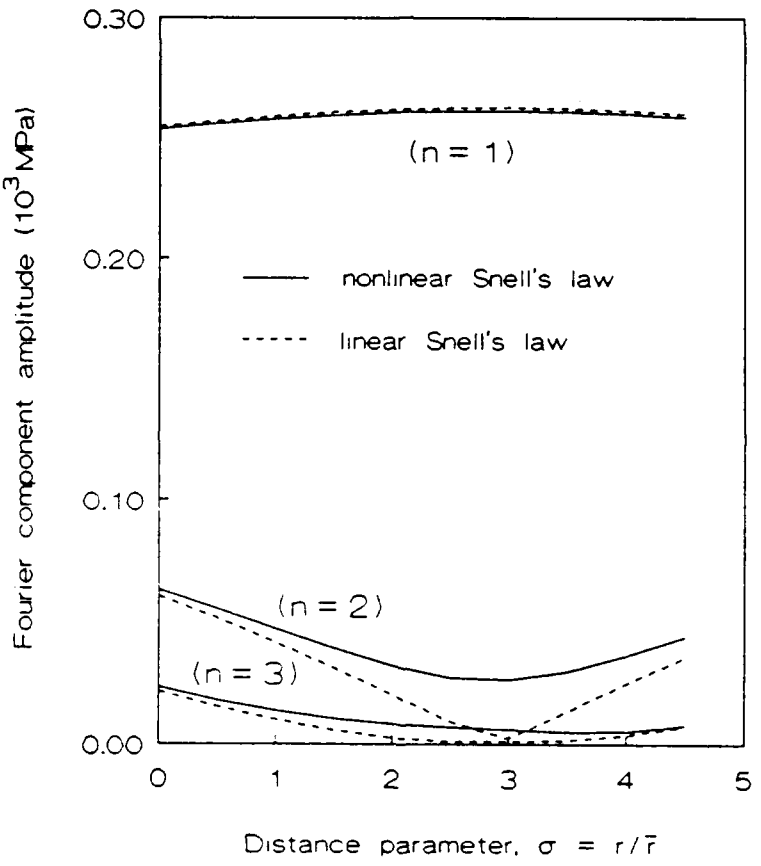
0.30
0.20
0.10
0.00
0
1
2
3
4
5
(n = 1)
nonlinear Snell's law
linear Snell's law
(n = 2)
(n = 3)
Fourier component amplitude (10^3MPa)
Distance parameter, $\sigma = r/\bar{r}$

FIGURE 8

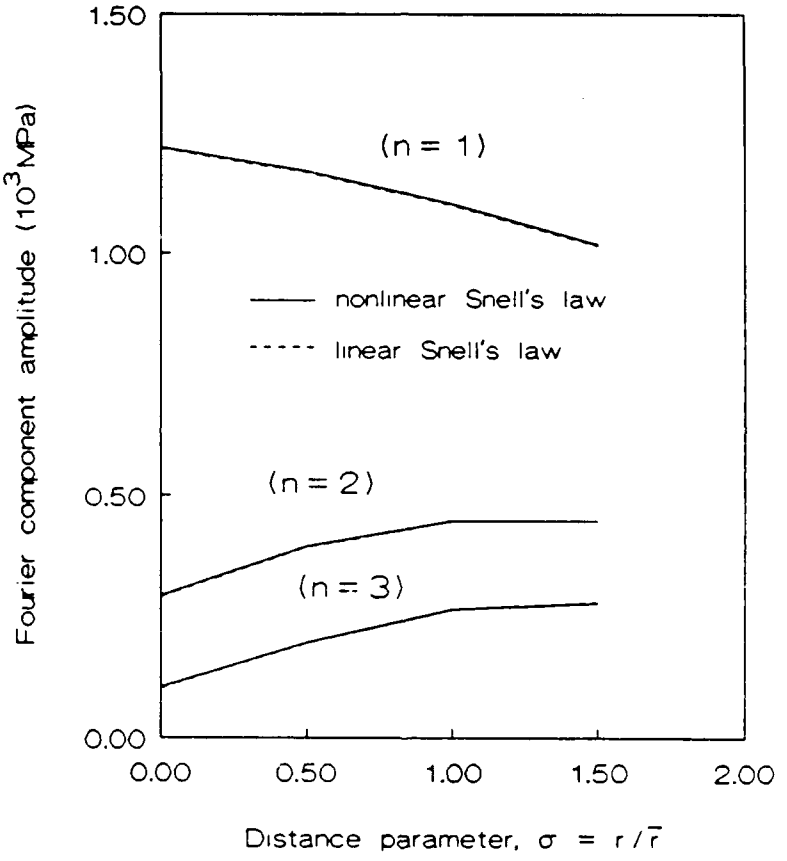
1.50
1.00
0.50
0.00
0.00
0.50
1.00
1.50
2.00
Fourier component amplitude (10^3MPa)
(n = 1)
nonlinear Snell's law
linear Snell's law
(n = 2)
(n = 3)
Distance parameter, σ = r / r̄

Session FD: Invited Session on Topics in Physical Acoustics

Wednesday, January 24, 1990; 2:00 p.m.–4:20 p.m.

Grand Salon B

Presiding: ROGER HANSON, Department of Physics, University of Northern Iowa, Cedar Falls, IA 50614

FD1 2:00 Classical Acoustics Solves Quantum Mechanical Puzzles*

J.D. MAYNARD, The Pennsylvania State University, University Park, PA 16802

In physics it is usually recognized that effects that arise from quantum mechanics, while crucial to the understanding of physical nature, may be subtle, difficult to comprehend, and outside the realm of everyday experience. However, current frontiers in physics involve the effects of geometry and statistics on the wave mechanical properties of quantum systems, and these effects are the same whether applied to quantum mechanical waves or classical waves. Indeed, the Schrödinger wave equation for states of constant energy in quantum mechanics is mathematically identical to the wave equation for sound waves. As a consequence, macroscopic acoustic systems may be fabricated that simulate the salient features of a quantum mechanical system, and which may be used to make much more direct observations and measurements. Contemporary problems in quantum mechanics that have been solved in this manner include the behavior of electrons in disordered metals and the properties of a new state of matter called quasi-crystalline.

*Work supported by NSF DMR 8701682 and the Office of Naval Research.

FD2 2:35 Reflection and Refraction of Nonlinear Dilatational and Shear Waves at a Planar Interface*

JERRY H. GINSBERG+ AND K.T. SHU,♦ George W. Woodruff School of Mechanical Engineering, Georgia Institute of Technology, Atlanta, GA 30332-0405

According to the linear theory of elasticity, oblique incidence of either a dilatational (P) wave or vertically polarized shear (SV) wave at a planar interface between two media results in reflection and transmission of both types of waves in constant directions that are determined by Snell's law. When nonlinear effects in the incident wave are considered, the phase speed is dependent on the amplitude of that phase, which undermines the matching of trace velocities on which Snell's law is based. The first step in the solution of this problem is to analyze the case of reflection of a finite amplitude P wave at the stress-free boundary of an elastic half-space. A straightforward perturbation analysis is used to identify the dominant nonlinear effects. Although such an approach ultimately encounters difficulty in consistently satisfying the boundary conditions, the understanding of wave interactions obtained from it is exploited to derive a successful solution using the method of characteristics for two-dimensional waves. The rays of the reflected P and SV waves are found to be straight lines, but the direction of each ray is shown to be governed by the nonlinear version of Snell's law, in which the trace velocities are formed from the nonlinear (amplitude-dependent) phase speeds. The relations for the reflection coefficients are found to resemble the predictions of linear theory, except that they are formed from the variable directions of the reflected rays. One consequence of these phenomena is that the waveforms of the reflected and P and SV waves received at a specified field depend on signals that arrive from zones on the boundary. The physical and mathematical insight gained from the analysis leads directly to a generalized solution for the case of an interface between arbitrary elastic and/or fluid media.

*This work was supported by NSF and ONR.

+George W. Woodruff Chair in Mechanical Systems.

♦Graduate Research Assistant.

FD3 3:10 The Laser as a Powerful Research Tool in Acoustics*

YVES H. BERTHELOT, School of Mechanical Engineering, Georgia Institute of Technology, Atlanta, GA 30332-0405

Laser beams can be used to either generate or detect sound waves without having any bulky transducer perturbing the medium under investigation. This type of noninvasive transduction is very attractive in many different research areas of physics and engineering. For instance, the laser generation and detection of ultrasound in solids has proven to be a very valuable tool in assessing the structural properties of a sample (Nondestructive Testing), especially when the sample is in an environment unfriendly to conventional techniques, e.g., very hot (welding industry), radioactive (nuclear industry), or simply inaccessible (aircraft industry). Another growing field in which laser beams are used to generate and detect sound waves is that of underwater acoustics (Sonar engineering). High-power lasers can be used to generate acoustic waves in the ocean from an airborne platform. These types of sources, known as thermoacoustics arrays, are

REFLECTION AND REFRACTION OF NONLINEAR DILATATIONAL AND SHEAR WAVES AT A PLANAR INTERFACE

Jerry H. Ginsberg
Kun-Tien Shu

School of Mechanical Engineering
Georgia Institute of Technology
Atlanta, Georgia 30332

[Work supported by NSF and ONR]

STRESS WAVES IN SOLIDS

SNELL'S LAW (LINEAR)

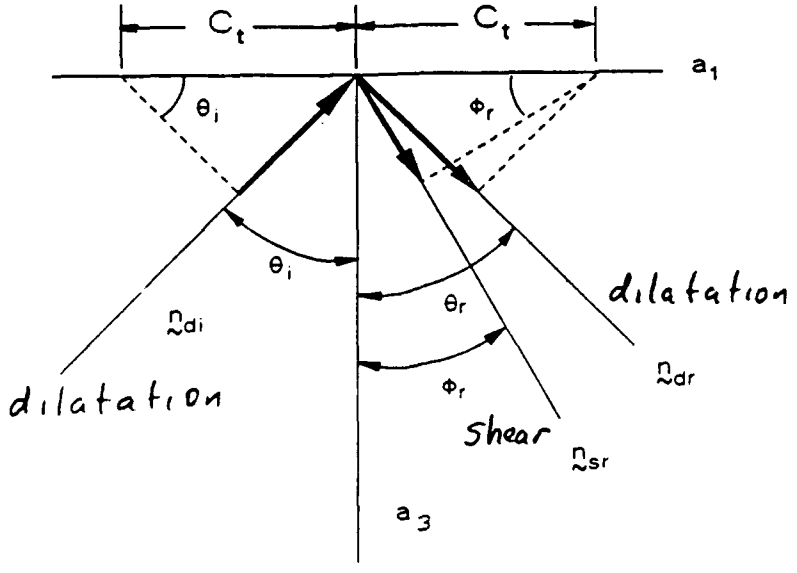

- Matching trace velocities along the boundary

$$\theta_i = \theta_r = \theta \quad \text{and} \quad \frac{\sin\theta}{c_d} = \frac{\sin\phi}{c_s}$$

- Reflection coefficients – mode conversion

$$\Gamma_{dd} = \frac{A_{dr}}{A_{di}} = \frac{\sin 2\theta \sin 2\phi - (c_d/c_s)^2 \cos^2 2\phi}{\sin 2\theta \sin 2\phi + (c_d/c_s)^2 \cos^2 2\phi}$$

$$\Gamma_{sd} = \frac{A_{sr}}{A_{di}} = \frac{2(c_d/c_s)\sin 2\theta \cos 2\phi}{\sin 2\theta \sin 2\phi + (c_d/c_s)^2 \cos^2 2\phi}$$

PREVIOUS RESEARCH

Buck and Thompson (1966)

- One-dimensional finite amplitude waves reflected from a stress-free boundary
- Higher order harmonics should decrease due to phase reversal

Van Buren and Breazeale (1968)

- Linear reflection and refraction process: No coupling among the harmonics

Qian (1982)

- Finite amplitude plane waves upon oblique reflection in fluids
- Self-action:
  - Secular second order incident wave
  - Secular second order reflected wave
- Nonlinear interaction:
  - Constant magnitude second harmonic

Feng (1983)

- Two-dimensional reflection and refraction at a planar fluid-fluid interface
- Straightforward perturbation analysis

Cotaras (1989)

- Straightforward perturbation analysis
- Nonlinear interaction between the incident and reflected waves and the local nonlinear boundary effects were investigated
- Finite amplitude form of Snell's law — matching nonlinear trace velocities along the interface

BASIC EQUATIONS

Momentum equation:

$$\frac{\partial T_{ij}}{\partial a_j} = \rho_0 \frac{\partial^2 u_i}{\partial t^2}$$

Constitutive equation:

$$T_{ij} = \rho_o \frac{\partial W}{\partial(\partial u_i / \partial a_j)}$$

Nonlinear geometrical strain-displacement:

$$E_{ij} = \frac{1}{2}\left(\frac{\partial u_i}{\partial a_j} + \frac{\partial u_j}{\partial a_i} + \frac{\partial u_k}{\partial a_i}\frac{\partial u_k}{\partial a_j} \right)$$

where

$u_i \equiv$ displacement components

$a_i \equiv$ Lagrangian coordinates

$T_{ij} \equiv$ Piola-Kirchhoff stress tensor

$E_{ij} \equiv$ Green's strain tensor

$W \equiv$ Strain energy density function

STRAIN ENERGY DENSITY FUNCTION

Assumptions of materials:

1. Adiabatic
2. Homogeneous and Isotropic

Taylor series expansion:

$$\rho_0 W = \frac{1}{2}\lambda I_1^2 + \mu I_2 + \frac{1}{24}\nu_1 I_1^3 + \frac{1}{4}\nu_2 I_1 I_2 + \nu_3 I_3 + O(I_3^{4/3})$$

$$I_1 = E_{ii}, \quad I_2 = E_{ij} E_{ij}, \quad I_3 = E_{ij} E_{jk} E_{ki}$$

where

$\lambda, \mu \equiv$ Lamé coefficients

$\nu_1, \nu_2, \nu_3 \equiv$ third-order elastic constants

PERTURBATION EQUATIONS

$$u_i = \epsilon u_i^{(1)} + \epsilon^2 u_i^{(2)} + \cdots$$

$$T_{ij} = \epsilon T_{ij}^{(1)} + \epsilon^2 T_{ij}^{(2)} + \cdots$$

$$\frac{\partial^2 u_i^{(k)}}{\partial t^2} - (c_d^2 - c_s^2)\frac{\partial^2 u_m^{(k)}}{\partial a_m \partial a_i} - c_s^2 \frac{\partial^2 u_i^{(k)}}{\partial a_m \partial a_m} = \frac{K_i^{(k)}}{\rho_0}$$

$$T_{ij}^{(k)} = \lambda \frac{\partial u_m^{(k)}}{\partial a_m}\delta_{ij} + \mu\left(\frac{\partial u_i^{(k)}}{\partial a_j} + \frac{\partial u_j^{(k)}}{\partial a_i}\right) + \frac{G_{ij}^{(k)}}{\rho_0}$$

where

$$K_i^{(k)}, G_{ij}^{(k)} = \begin{cases} 0, & k = 1 \\ K_i(u_i^{(1)}), G_{ij}(u_i^{(1)}), & k = 2 \end{cases}$$

REFLECTION OF GENERATED HARMONICS

- Superposition of two solutions: $u_i^{(2)} = w_i^{I} + w_i^{II}$

(I) Particular solution for $K_i \neq 0$

$$\frac{\partial^2 w_i^{I}}{\partial t^2} - (c_d^2 - c_s^2)\frac{\partial^2 w_m^{I}}{\partial a_m \partial a_i} - c_s^2 \frac{\partial^2 w_i^{I}}{\partial a_m \partial a_m} = K_i$$

$$\lambda \frac{\partial w_m^{I}}{\partial a_m}\delta_{i3} + \mu\left(\frac{\partial w_i^{I}}{\partial a_3} + \frac{\partial w_3^{I}}{\partial a_i}\right) = 0 \quad \text{on} \quad a_3 = 0$$

(II) Complementary solution satisfying time dependent boundary conditions ($G_{i3} \neq 0$)

$$\frac{\partial^2 w_i^{II}}{\partial t^2} - (c_d^2 - c_s^2)\frac{\partial^2 w_m^{II}}{\partial a_m \partial a_i} - c_s^2 \frac{\partial^2 w_i^{II}}{\partial a_m \partial a_m} = 0$$

$$\lambda \frac{\partial w_m^{II}}{\partial a_m}\delta_{i3} + \mu\left(\frac{\partial w_i^{II}}{\partial a_3} + \frac{\partial w_3^{II}}{\partial a_i}\right) = -G_{i3} \quad \text{on} \quad a_3 = 0$$

(I) leads to cumulative solutions–become **significant** with increasing propagation distance

(II) produces nonsecular solutions (i.e. bounded everywhere) — **NEGLECT!**

SECOND ORDER NONLINEAR EFFECTS

$$\mathcal{L}\begin{pmatrix} w_1^{\mathrm{I}} \\ w_3^{\mathrm{i}} \end{pmatrix} = \begin{cases} \exp(2i\psi_{d_1}) \\ \exp(2i\psi_{d_2}) \\ \exp(2i\psi_{s_2}) \\ \exp[i(\psi_{d_1} \pm \psi_{d_2})] \\ \exp[i(\psi_{d_1} \pm \psi_{s_2})] \\ \exp[i(\psi_{d_2} \pm \psi_{s_2})] \end{cases}$$

- Secular terms consist of second order harmonics of incident and reflected dilatational waves
- No secularity in vertically polarized shear wave
- Noncollinear interaction terms are not solution of the homogeneous wave equation $\Rightarrow$ not secular
- Generating additional complementary solutions to satisfy d.e. & b.c. is complicated

- **Hypothesis** stated by Cotaras (1989): refraction in fluids

— Finite amplitude form of Snell's law: Variation of reflected and transmitted angles

- Key observation from perturbation analysis:

1. Nonlinear interactions between waves are negligible
2. Inhomogeneous boundary conditions are not important
3. P and SV waves are reflected at both the first and second orders
4. Secularity occurs in the second order incident and reflected P waves, but not in the second-order reflected SV wave

ALTERNATIVE ANALYSIS – THE METHOD OF CHARACTERISTICS

One-Dimensional Outgoing Planar Wave

v = **constant**, along each characteristic

$$\frac{dx}{dt} = c_0 + \beta v; \qquad \beta = \frac{\gamma + 1}{2}$$

$$v = v(t - \frac{x}{c_0 + \beta v}) \quad ; \quad p = \rho_0 c_0 v + O(\epsilon^2)$$

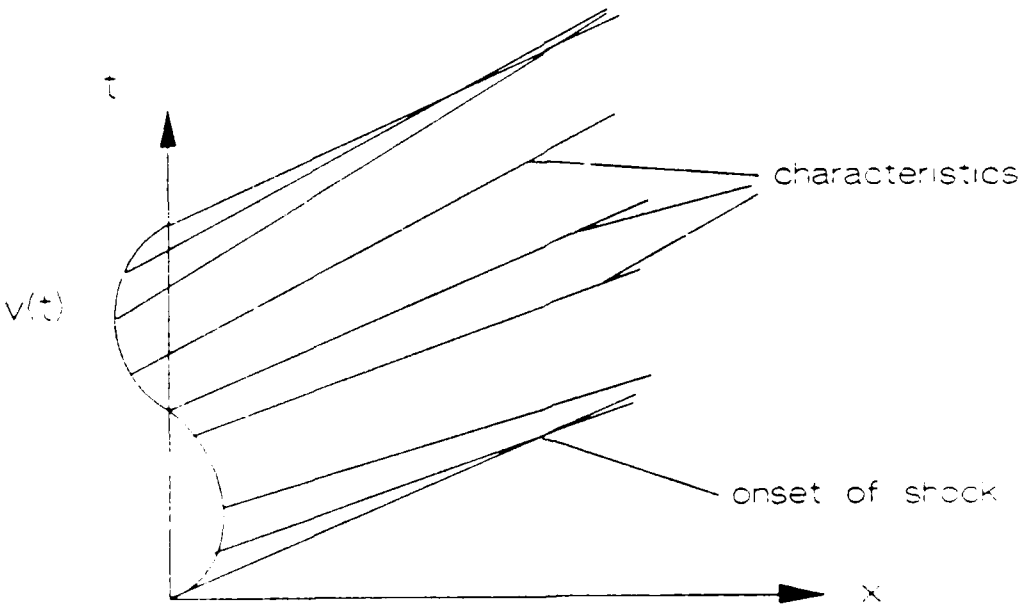

CHARACTERISTIC CONES

$$\chi = \tan^{-1}(c_d + \beta_d v_d)$$

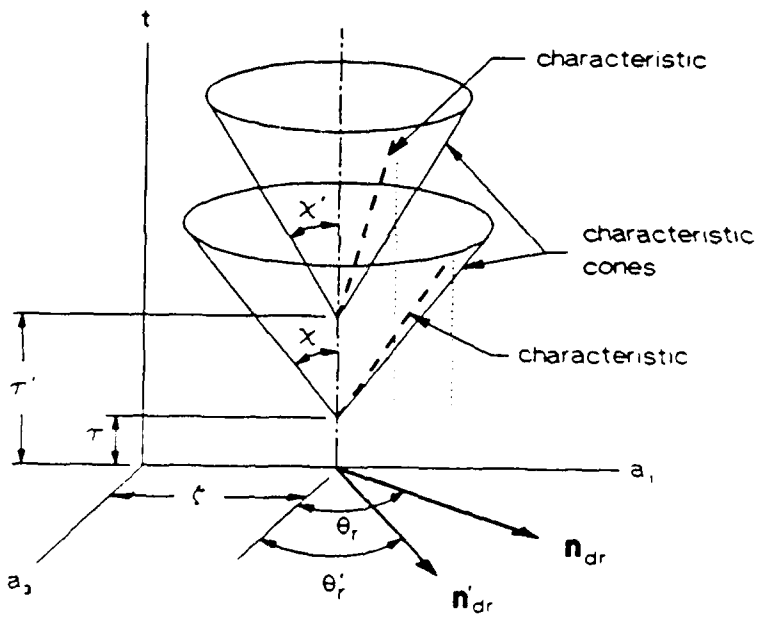

NONLINEAR PARTICLE VELOCITY

Individual waves:

$$\mathbf{v}_{d,i} = -\frac{i}{2}\epsilon A_{d,i}\,\mathbf{n}_{d,i}\,\exp(i\omega\Psi_{d,i}) + O(\epsilon^2) + c.c.$$

$$\mathbf{v}_{d,r} = -\frac{i}{2}\epsilon A_{d,r}\,\mathbf{n}_{d,r}\,\exp(i\omega\Psi_{d,r}) + O(\epsilon^2) + c.c.$$

$$\mathbf{v}_{s,r} = -\frac{i}{2}\epsilon A_{s,r}\,(\mathbf{e}_2 \times \mathbf{n}_{s,r})\exp(i\omega\Psi_{s,r}) + O(\epsilon^2) + c.c.$$

Projection of characteristics at a fixed time

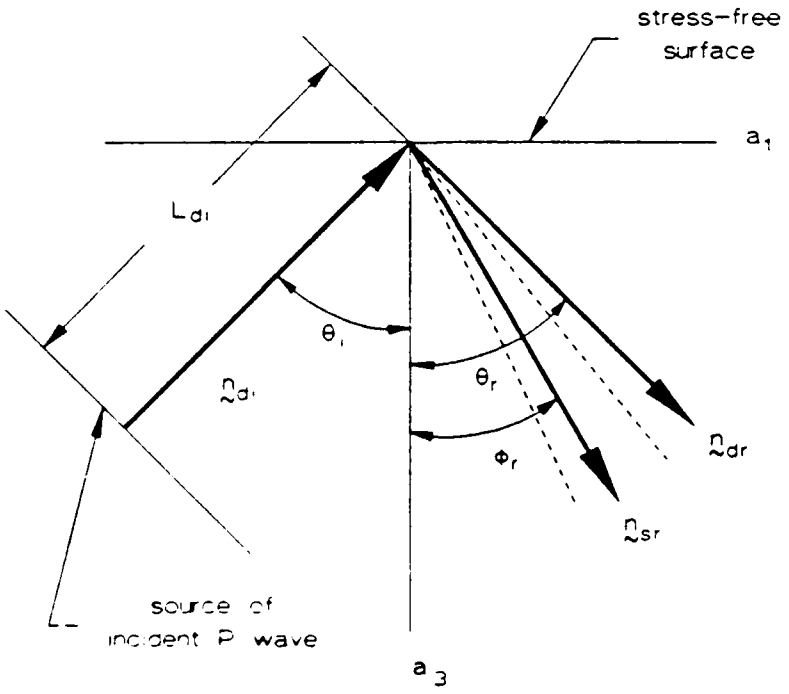

NONLINEAR PHASE VARIABLES

$$\Psi_{di} = \frac{\mathbf{n}_{di} \cdot \mathbf{r} + L_{di}}{c_d + \beta_d (\mathbf{v}_{di} \cdot \mathbf{n}_{di})} - t$$

$$\Psi_{dr} = \frac{\mathbf{n}_{dr} \cdot \mathbf{r} + L_{dr}}{c_d + \beta_d (\mathbf{v}_{dr} \cdot \mathbf{n}_{dr})} - t$$

$$\Psi_{sr} = \frac{\mathbf{n}_{sr} \cdot \mathbf{r} + L_{sr}}{c_s} - t$$

- Thurston & Shapiro (1967):

$\beta_d = -\dfrac{M_3}{2M_2} \equiv$ coefficient of nonlinearity for solids

$M_2 = \lambda + 2\mu$:Geometrical nonlinearity

$M_3 = 3M_2 + \dfrac{\nu_1}{4} + \dfrac{2}{3}\nu_2 + 6\nu_3$

L_{i1}: distance between initial incident wavefront and origin

L_{di}, L_{sr}: Phase lags of reflected dilatational and shear waves

SATISFACTION OF THE BOUNDARY CONDITIONS

1. Form stress components for each wave
   Plane dilatational wave:

$$E_{xx} = -\frac{v_x}{c_d + \beta_d v_x} + O(\epsilon^2) = -\frac{v_x}{c_d} + O(\epsilon^2)$$

   Plane shear wave:

$$E_{xz} = \frac{1}{2}\frac{\partial u_z}{\partial x} = -\frac{1}{2}\frac{v_z}{c_s}$$

2. Apply Mohr's circle resolution into a_1-a_3 plane

3. Require resultant stress components vanish on $a_3 = 0$

4. Matching phase variables on $a_3 = 0$ yields:

a. Finite amplitude form of Snell's law

$$\frac{\sin\theta_{d_i}}{c_d + \beta_d v_{d_i}|a_3 = 0} = \frac{\sin\theta_{d_r}}{c_d + \beta_d v_{d_r}|_{a_3=0}} = \frac{\sin\theta_{s_r}}{c_s}$$

b. Phase lags of reflected waves relative to the incident wave

$$\frac{L_{d_i}}{c_d + \beta_d v_{d_i}|a_3 = 0} = \frac{L_{d_r}}{c_d + \beta_d v_{d_r}|_{a_3=0}} = \frac{L_{s_r}}{c_s}$$

5. Nonlinear reflection coefficients

$$\frac{A_{dr}}{A_{di}} = \frac{\sin 2\theta_i \sin 2\phi_r - (\gamma^2 - 2\sin^2 \theta_i)\cos 2\phi_r}{\sin 2\theta_r \sin 2\phi_r + (\gamma^2 - 2\sin^2 \theta_r)\cos 2\phi_r}$$

$$\frac{A_{sr}}{A_{di}} = \frac{\sin 2\theta_i (\gamma^2 - 2\sin^2 \theta_r) + \sin 2\theta_r (\gamma^2 - 2\sin^2 \theta_i)}{\gamma[\sin 2\theta_r \sin 2\phi_r + (\gamma^2 - 2\sin^2 \theta_r)\cos 2\phi_r]}$$

6. $\theta_r \approx \theta + O(\epsilon)$ & $\phi_r \approx \phi + O(\epsilon)$

- Nonlinear reflection coefficients $\approx$ linear reflection coefficients $+ O(\epsilon)$
- Deviation from linear angles is oscillatory

CONSTRUCTION OF A FIELD SOLUTION

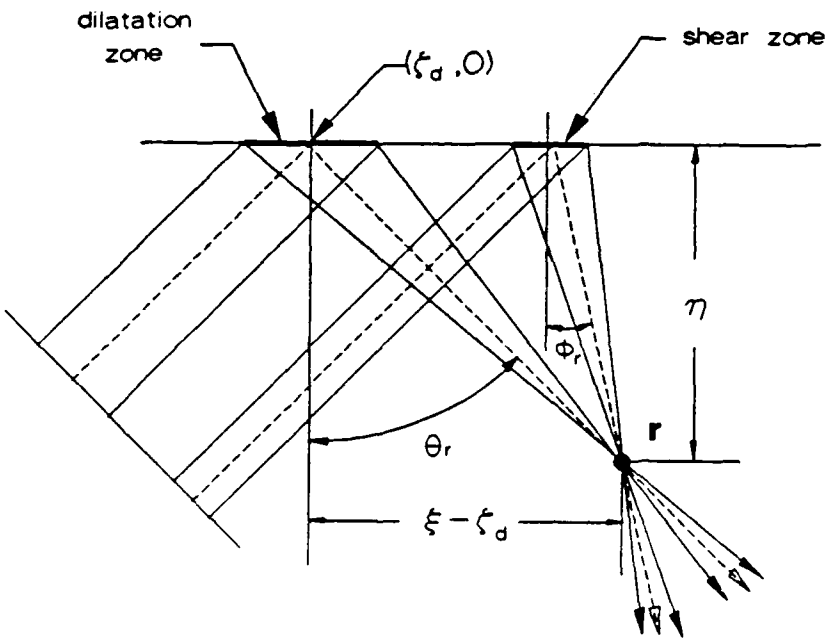

GENERAL RULE

1. Solve the linear problem

a. Incident ray: dilatation or shear

b. Reflected rays: dilatation and shear

c. Transmitted rays (two media in contact): dilatation and shear

d. Special case: ideal fluids $\Rightarrow$ omit shear waves

2. For each wave, let

$$\mathbf{v} = -\frac{i}{2}\epsilon\mathbf{A}\,\exp\left[i\omega\left(\frac{\mathbf{n}\cdot\mathbf{r}+L}{\alpha}-t\right)\right]+c.c.$$

$$\begin{aligned}\alpha &\equiv c_d+\beta_d(\mathbf{v}\cdot\mathbf{n}) && \text{dilatational wave,}\\ &\equiv c_s && \text{shear wave}\end{aligned}$$

3. Use Snell's law with c replaced by α to obtain reflected and refracted angles

4. Use linear relation with nonlinear angles from Snell's law to obtain reflection and transmission coefficients

CLOSURE

- For engineering materials, nonlinear parameters are small, so the response to an incident nonlinear wave will be near the response for the linear counterpart.

- Nonlinearity causes reflected and refracted waves to propagate in variable directions, as though surface was rotating in an oscillatory manner.

- Phase shifting in higher harmonics of a waveform and signal arrival from a specific spot might lead to useful NDT application.

MULTIDIMENSIONAL REFLECTION AND REFRACTION OF FINITE AMPLITUDE STRESS WAVES IN ELASTIC SOLIDS

A Thesis

Presented to

The Academic Faculty

By

Kun-Tien Shu

In Partial Fulfillment

of the Requirements for the Degree

Doctor of Philosophy

in the School of Mechanical Engineering

Gerogia Institute of Technology

March, 1990

TABLE OF CONTENTS

SUMMARY

In small-signal (linear) theory, oblique incidence of either a plane dilatational (P) wave or vertically polarized shear (SV) wave at a plane interface between two elastic media results in reflection and transmission of both types of waves. The direction of propagation of each wave is constant and is governed by Snell's law. If the incident wave arrives at the boundary in a distorted manner as a result of nonlinearity, the reflection and transmission pattern becomes intricate due to coupling effects between dilatational and shear waves.

The first study of this problem addresses a special case—the reflection of an initially sinusoidal, finite amplitude plane P wave from a plane stress-free boundary of an elastic half-space. A second-order perturbation expansion successfully discloses the most significant nonlinear effects, but it ultimately encounters difficulty for making the results uniformly valid. This shortcoming is corrected by an analysis using the method of characteristics for two-dimensional waves. Allowing the incident and reflected waves to undergo nonlinear distortion along ray paths having variable propagation direction leads to finite amplitude forms of Snell's law and the reflection coefficients of the outgoing P and SV waves at each instant. A numerical algorithm is developed to calculate the waveforms of the reflected P and SV wave received at a specified point. The physical and mathematical insight provided from the analysis leads directly to a generalized solution for the case of an interface between arbitrary elastic and/or fluid media, in which critical angles may exist.

EVALUATION OF TRANSIENT RESPONSES GENERATED BY SOUND BEAMS USING A MODIFIED VERSION OF THE NPE

G. James Too and Jerry H. Ginsberg

presented at 119th meeting of ASA

work sponsored by ONR

NPE -- Derivation & Assumption

- mass and momentum equation

$$\frac{\partial^2 \rho}{\partial t^2} = \nabla^2 P + \partial_i \partial_j (\rho V_i V_j) \qquad (1)$$

- adiabatic state equation,

$$P = c^2 \rho' + \frac{1}{2} \rho'^2 \frac{\partial^2 P}{\partial \rho'^2} + O(\rho'^3) \qquad (2)$$

- particle velocity $\approx$ in x direction

$$V_i = c\, \rho'/\rho_0\, \delta_{i,x} + O(\rho'^2, \rho'\theta), \qquad (3)$$

From equations(1-3), one obtains

$$\frac{\partial^2 R}{\partial t^2} = \nabla^2 c^2 (R + \beta R^2) + \text{higher order terms}, \qquad (4)$$

where R is dimensionless density : $R = \rho'/\rho_0$

Reference frame translating at c_0 in x direction.

The time derivative in the moving frame is :

$$D_t = \frac{\partial}{\partial t} + c_0 \frac{\partial}{\partial x}. \qquad (5)$$

Substituting eq(5) into eq(4) leads to

$$\underset{\text{a.}}{\left(D_t - c_0 \partial_x\right)^2} R = \left(\partial_x^2 + \underset{\text{b.}}{\partial_y^2} + \underset{\text{c.}}{\partial_z^2}\right) \left(c_0 + \underset{\text{d.}}{c_1}\right)^2 \left(R + \underset{\text{e.}}{\beta} R^2\right) \quad (6)$$

Consider a,b,c,d,e terms are small

$$D_t R = -\partial_x\left[c_1 R + \tfrac{1}{2}\beta c_0 R^2\right] - \tfrac{1}{2} c_0 \left(\partial_y^2 + \partial_z^2\right) \int_{x_f}^{x} R \, dx. \quad (7)$$

APPLICATION FOR NPE

Three different formulations of NPE:

CASE 1: Two dimensional waveguide

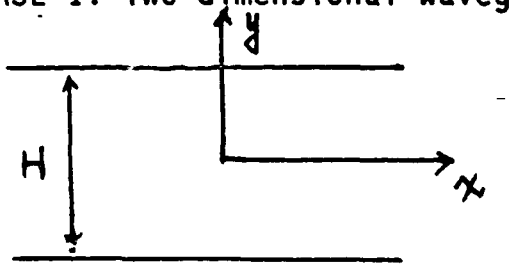

(x , y)

$$D_t R = - \partial_x \left(c_1 R + \tfrac{1}{2}\beta c_0 R^2 \right) - \tfrac{1}{2} c_0 \int_{x_f}^{x} \partial_z^2 R \, dx. \qquad (8)$$

CASE 2: Azimuthal symmetry -- in radial propagation

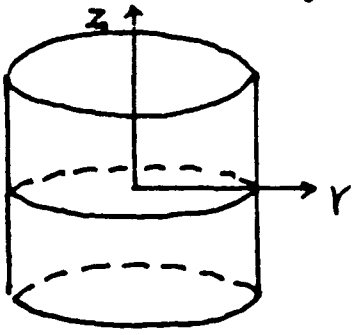

(r , z)

propagate in r direction

$$D_t R = - \partial_r \left(c_1 R + \tfrac{1}{2}\beta c_0 R^2 \right) - \frac{c_0 R}{2 r} - \tfrac{1}{2} c_0 \int_{r_f}^{r} \partial_z^2 R \, dr. \qquad (9)$$

MODIFIED VERSION OF NPE

CASE 3: Our problem ,

Azimuthal sysmmetry -- in axial direction

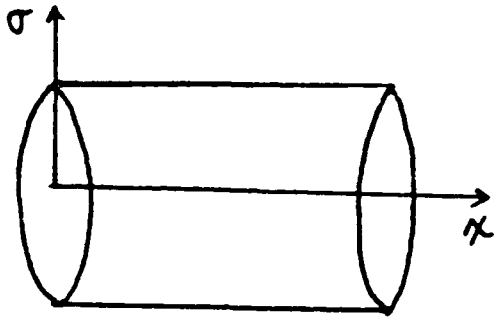

(σ , x)

propagate in x direction

$$D_t R = -\partial_x\left[c_1 R + \frac{1}{2}\beta c_0 R^2\right] - \frac{1}{2}c_0\left(\frac{1}{\sigma}\frac{\partial}{\partial\sigma} + \frac{\partial^2}{\partial\sigma^2}\right)\int_{x_f}^{x} R\, dx. \quad (10)$$

Present study

- Homogeneous: $c_1 = 0$
- Linear : $\beta = 0$

$$D_t R = -\frac{1}{2}c_0\left(\frac{1}{\sigma}\frac{\partial}{\partial\sigma} + \frac{\partial^2}{\partial\sigma^2}\right)\int_{x_f}^{x} R\, dx. \quad (11)$$

INITIALIZATION OF NPE

1. King integral for steady state cases

2. Rayleigh integral for steady state and transient cases

3. Planar wave assumption:

   if r < radius , p = f(t - x/c)

   if r > radius , p = 0.

GT
Acoustics & Dynamics Research Laboratory

Previous result for steady state
ref: Abstract at previous meeting

1st harmonic comparison starts at r=0.05 m

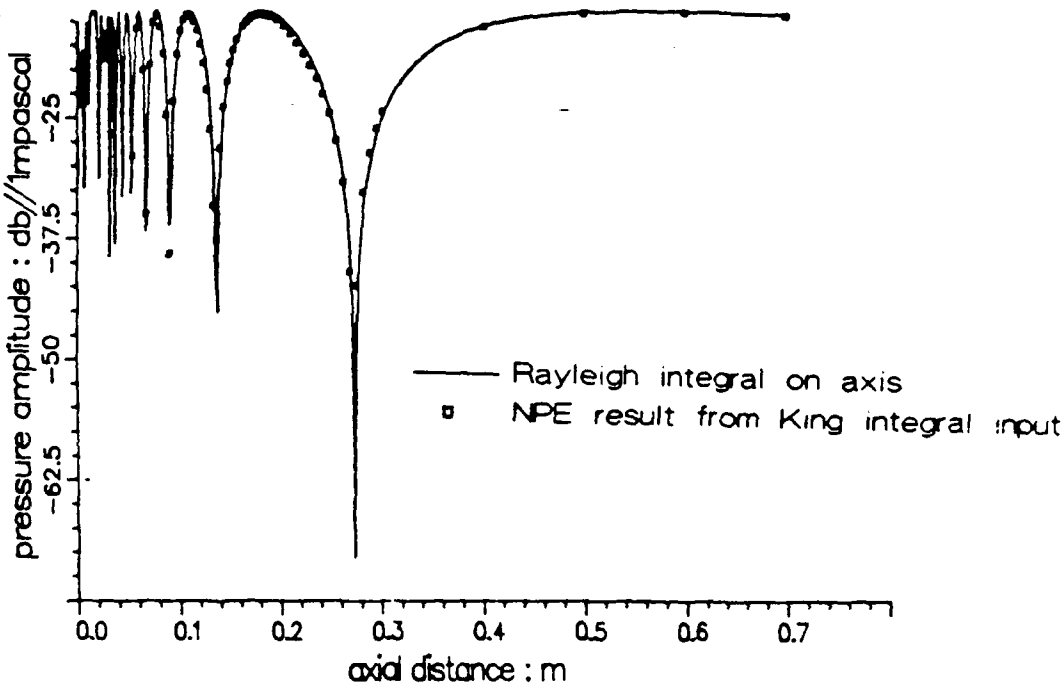

GT
Acoustics & Dynamics
Research Laboratory

Previous result for steady state
ref: Abstract at previous meeting

1st harmonic comparison at z=500 mm

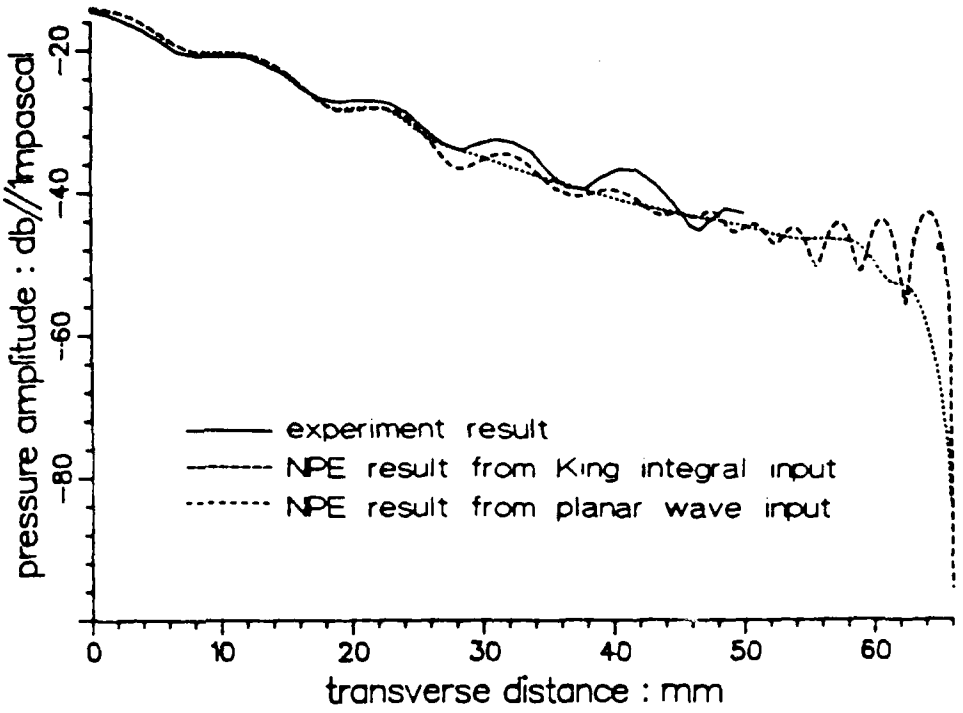

PREVIOUS CONCLUSION

1. NPE , which is a time domain formula, can be used to study steady state signal.

2. NPE is quite accurate for linear propagation, even in the vicinity of the projector.

3. Simple, yet accurate, initialization of moving window for NPE may be obtained by using a linear field theory close to the projector.

QUESTION?

How accurate is the modified version of NPE for transient pulse(s) propagation generated by a circular piston?

TRANSIENT RESPONSE FOR A SINE LOBE PULSE GENERATED BY A CIRCULAR PISTON

PROCEDURE:

1. Initialize sound field -- $0 < x < 0.6\ \lambda$

   -- $0 < \sigma < 3\ a$

   using Rayleigh integral

$$P = \rho c\ H(a - \sigma)\ V_n\left(t - \frac{x}{c}\right)$$

$$- \frac{\rho c}{\pi} \int_{-\pi/2}^{\pi/2} \frac{a(a + \sigma \sin(\psi))}{\sigma^2 + a^2 + 2\sigma a \sin(\psi)} V_n\left(t - \frac{R}{c}\right)\ d\psi$$

where R is $(\sigma^2 + a^2 + 2\sigma a \sin(\psi))^{1/2}$

2. Propagate the sound field to a specific distance.

3. Compare to evaluation of Rayleigh integral

Note: Singularity in Rayleigh integral

at the location: $\sigma = a$ & $\sin(\psi) = -1$.

Asymptotic evaluation of contribution

of singularity using

$\sigma = a\,(\,1 + \epsilon\,)$,

$\psi = -\frac{\pi}{2} + \Delta$

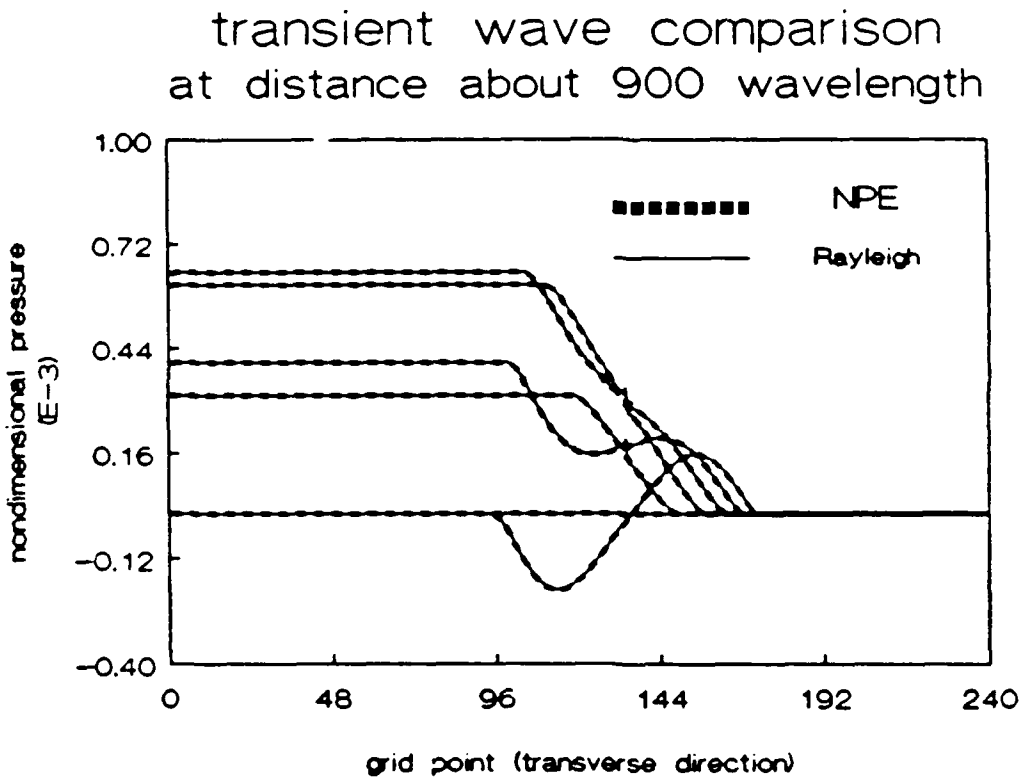
transient wave comparison
at distance about 900 wavelength
1.00
0.72
0.44
0.16
−0.12
−0.40
nondimensional pressure
(E−3)
NPE
Rayleigh
0
48
96
144
192
240
grid point (transverse direction)

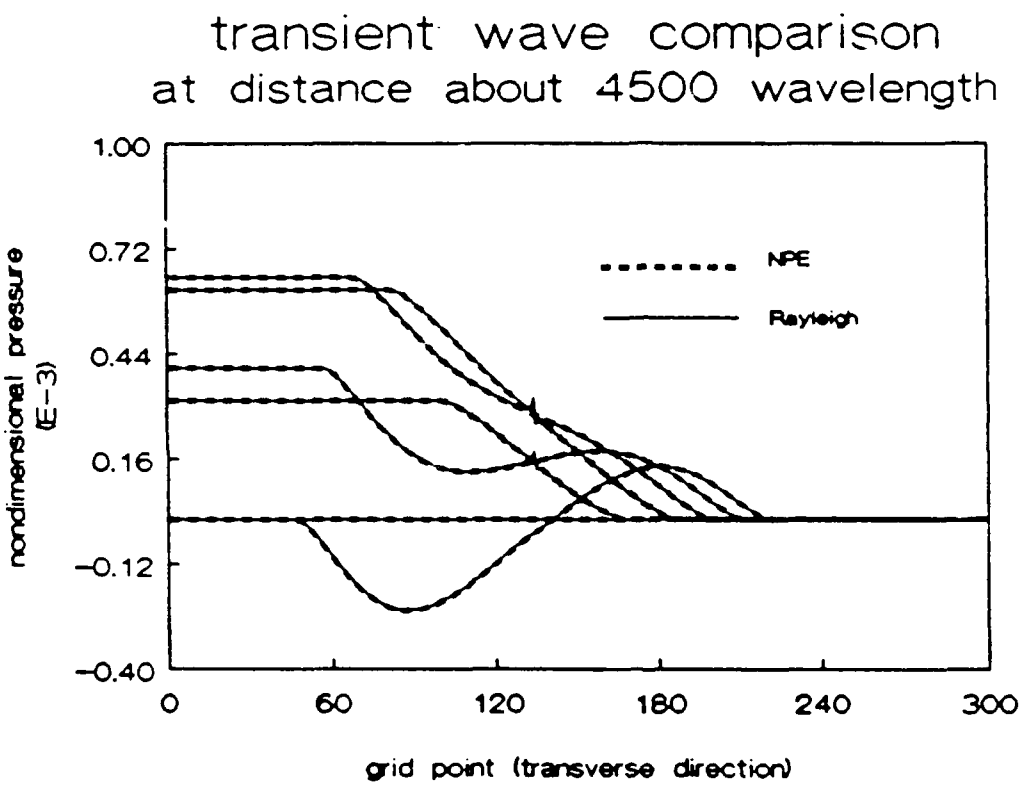
transient wave comparison
at distance about 4500 wavelength
1.00
0.72
0.44
0.16
−0.12
−0.40
nondimensional pressure
(E−3)
NPE
Rayleigh
0
60
120
180
240
300
grid point (transverse direction)

CONCLUSION

1. NPE is quite accurate to describe linear transient signal generated by a circular piston.

2. From previous study, NPE can be used to describe linear steady-state signal generated by a circular piston.

3. Application of NPE for sound beams in presence of nonlinear effects (finite amplitudes) needs to be explored.

Evaluation of a finite amplitude sound beam in the time domain using a modified version of the NPE computer code

Gee-Pinn James Too and Jerry H. Ginsberg
School of Mechanical Engineering,
Georgia Institute of Technology, Atlanta, GA 30332, USA

ABSTRACT

The NPE computer code [1] generates a time domain solution of a parabolic equation that is derived by assuming that, to a first order, the particle velocity is in the direction in which the signal propagates. The present work extends an earlier study [2], which modified NPE to evaluate the linear signal generated by a piston in an infinite baffle. The present problem, which is concerned with the effects of nonlinearity, addresses three alternative descriptions of the input field: (1) The waveform very close to the transducer and extending to several piston radii transversely is calculated from the King integral for the linear problem. (2) Inside a cylinder extending outward from the piston, the input signal is represented as a linear planar wave, while outside that cylinder the input field is considered to be zero. (3) Nonlinear waveforms in a region beyond the farthest anti-node for the fundamental is obtained from the nonlinear King integral [3]. Temporal waveforms are computed at nearfield and farfield locations, and then frequency analyzed for content at the lowest three harmonics. The results are compared to experimental data [4][7]. [Work supported by ONR.]

INTRODUCTION

The nonlinear progressive wave equation (NPE) developed by McDonald and Kuperman [1] was used to evaluate a time domain solution in a waveguide and to study the behavior of weak shock at a caustic. In a previous work [2], a modified version of the NPE computer code was obtained to evaluate the linear signal generated by a baffled piston. The purpose of the present study is to explore the ability of the modified NPE to describe the propagation of a finite amplitude sound beams. In the past year, numerical solutions [5][6] for a finite amplitude sound beam have been obtained in a frequency domain approach. In contrast, the present study uses a time domain approach, for which an appropriate sound field in the nearfield is

input and then propagated to the farfield. In order to demonstrate this application, three alternative descriptions of the input field shall be addressed. The results are discussed in detail, and compared to experiment data in the nearfield[4] and farfield[7].

GOVERNING EQUATIONS

In the previous derivation by McDonald and Kuperman [8], the combined mass and momentum equation, which is

$$\frac{\partial^2 \rho}{\partial t^2} = \nabla^2 P + \partial_i \partial_j (\rho V_i V_j), \tag{1}$$

and the adiabatic state equation,

$$P = c^2 \rho' + \frac{1}{2} \rho'^2 \frac{\partial^2 P}{\partial \rho'^2} + O(\rho'^3), \tag{2}$$

are used as the basic equations. It is assumed in the derivation that, to a first order, the particle velocity is in the direction in which the signal propagates.

$$V_i = c \, \rho'/\rho_0 \, \delta_{i,x} + O(\rho'^2, \rho'\theta), \tag{3}$$

where $\delta_{i,x}$ is the Kronecker delta.

From equations(1-3), one obtains

$$\frac{\partial^2 R}{\partial t^2} = \nabla^2 c^2 (R + \beta R^2) + \text{higher order terms}, \tag{4}$$

where R is defined as a dimensionless density perturbation: $R = \rho'/\rho_0$
A reference frame moving in the propagation direction with a constant speed c_0 was introduced. The time derivative in the moving frame is :

$$D_t = \frac{\partial}{\partial t} + c_0 \frac{\partial}{\partial x}. \tag{5}$$

Substituting equation(5) into equation(4) leads to

$$\underset{\text{a.}}{(D_t} - c_0 \partial_x)^2 R = \underset{\text{b.}}{(\partial_x^2} + \underset{\text{c.}}{\partial_y^2} + \partial_z^2) \underset{\text{d.}}{(c_0 +} c_1)^2 \underset{\text{e.}}{(R + \beta R^2)}. \tag{6}$$

It is assumed that terms marked a,b,c,d and e are small compared to the dominant terms. The products of these small terms in equation(6) are

negligible. Then, equation(6) is integrated with respect to x, which gives the NPE in three dimensions.

$$D_t R = -\partial_x\left(c_1 R + \frac{1}{2}\beta c_0 R^2\right) - \frac{1}{2}c_0(\partial_y^2 + \partial_z^2)\int_{x_f}^{x} R\, dx. \tag{7}$$

APPLICATION FOR NPE

There are two different formulations of NPE in its original development [8], depending on the type of coordinate system to be used. One, described by equation(8), is suitable for two-dimensional waveguide problems in Cartesian coordinate, while the other, described by equation(9), is suitable for problems having azimuthal symmetry with signal propagation in radial direction r.

$$D_t R = -\partial_x\left(c_1 R + \frac{1}{2}\beta c_0 R^2\right) - \frac{1}{2}\, c_0\int_{x_f}^{x} \partial_z R\, dx. \tag{8}$$

$$D_t R = -\partial_r\left(c_1 R + \frac{1}{2}\beta c_0 R^2\right) - \frac{c_0 R}{2\, r} - \frac{1}{2}c_0\int_{r_f}^{r} \partial_z\, R\, dr. \tag{9}$$

The present study employs a modification of NPE suitable for the evaluation of axially propagating axisymmetric waves. The modification is obtained by changing equation(6) to cylindrical coordinates in which the axial coordinate x is in the propagation direction, and then, dropping products of small terms. By integrating over x, one obtains a modified version of NPE which can be used for finite amplitude sound beams problems,

$$D_t R = -\partial_x\left(c_1 R + \frac{1}{2}\beta c_0 R^2\right) - \frac{1}{2}c_0\left(\frac{1}{\sigma}\frac{\partial}{\partial\sigma} + \frac{\partial^2}{\partial\sigma^2}\right)\int_{x_f}^{x} R\, dx. \tag{10}$$

In addition, the axisymmetry condition requires that $\partial R/\partial\sigma = 0$ on the axis. The moving frame used for the present study was taken to extend five wavelengths in the axial direction and three radii in the transverse direction. Three alternative descriptions of the input field are used .

(1) The waveform very close to the transducer and extending to three piston radii transversely is calculated from the King integral for the linear problem,

$$p/\rho_0 c_0 = \frac{1}{2}\,\epsilon\int_0^{\infty} G_n \exp(it - \mu_n z)\, J_0(nR)\, dn + c.c., \tag{11}$$

where c.c. represents complex conjugate of the previous term.

(2) Inside a cylinder extending outward from the piston, the input signal is represented as a linear planar wave, based on the assumption that $p = \rho_0 c_0 v_x$ on the face of the piston, while outside that cylinder the input field is considered to be zero.

(3) Nonlinear waveforms in a region beyond the farthest anti-node for the fundamental are obtained from the nonlinear King integral[3].

Temporal waveforms at nearfield and farfield locations are computed from NPE by matching the time increment to the spatial resolution in the axial direction. The last step is to perform a frequency analysis of the waveforms for the amplitude and phase at the lowest three harmonics.

NUMERICAL RESULTS

In this section, numerical results for harmonic generation obtained from the modified NPE computer code for the three alternative inputs shall be compared to experimental data in the nearfield and farfield. Figures 1-6 concern nearfield situations, for which the third of the aforementioned input schemes is not applicable. The parameters for the example are ka = 180.75, an average pressure amplitude on the piston face = 100 kPa, fundamental frequency = 2.25 MHz, speed of sound = 1486. m/sec and piston radius = 19 mm. These parameters are the same as those in previous experiments [4]. Figures 1-3 describe the amplitude variation along the axis of the sound beam, while, Figures 4-6 show the transverse variation at the axial distance z = 275 mm. It can be seen that the planar wave input and the linear King integral input both give good results, except in the region very close to the piston. Although not shown, it was found that increasing the distance from the transducer at which either input field is generated increases the discrepancy with experiment, especially for higher harmonics.

Figures 7 and 8 display farfield results obtained from the second and third input schemes. The parameters for these examples are fundamental frequency = 450 kHz, piston radius = 51 mm, SPL(r.m.s)= 212.7 db//1 μPa-m and speed of sound = 1418 m/sec. These parameters are the same as those in previous experiments [7]. For the region around the axis, the results of each are in close agreement with experiment. It should be noted that the lower measured level of the second harmonic at longer ranges is consistent with the estimate for dissipation in reference [7]

figures 1-8 y-axis represent pressure amplitude : db re. 1Mpascal

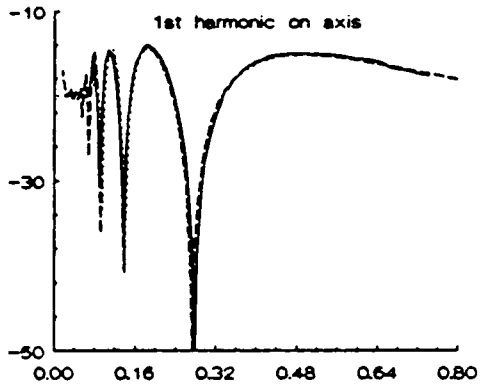

figure 1. axial distance: m

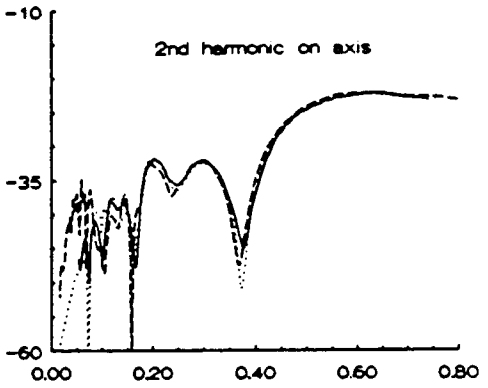

figure 2. axial distance : m

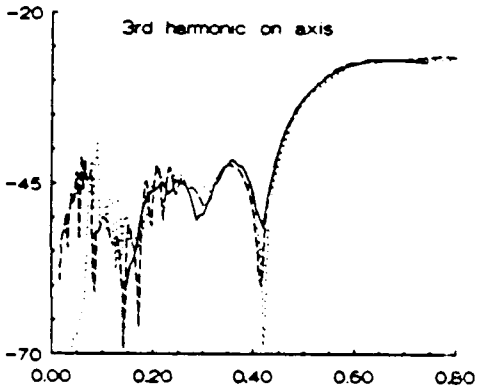

figure 3. axial distance : m

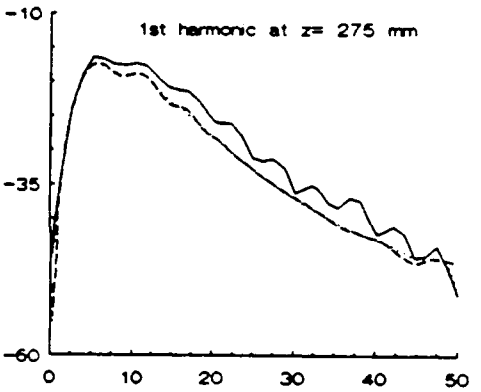

figure 4. transverse distance: mm

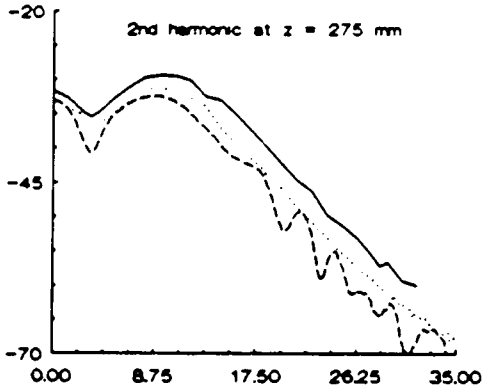

figure 5. transverse distance: mm

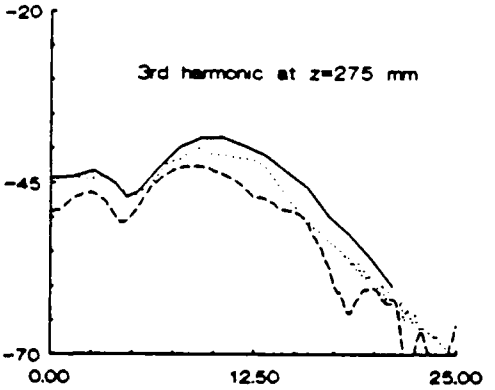

figure 6. transverse distance: mm

——————— experimental data

..... planar wave input on the face of piston

- - - - - - - - - - - linear King integral input at z = 0.02 m

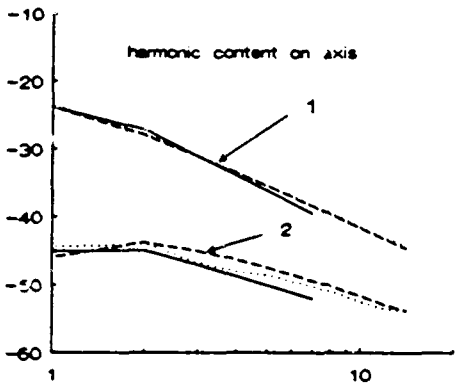

figure 7. axial distance : m

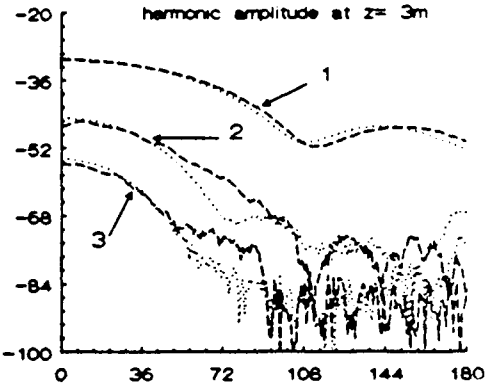

figure 8. transverse axis : mm

——————— experimental data
..... planar wave input on the face of piston
- - - - - - - - - - - - nonlinear King integral input at z = 1.0 m

CONCLUSION

Based on the evaluations, it is reasonable to conclude that NPE, which is a time domain formulation, can be used to study CW signal generation. This requires a proper initialization of the window. Due to the planar wave assumption, which ignores diffractive effects, initialization of the window based on this approximation causes some errors for nearfield locations. However, the planar wave assumption is certainly the most efficient manner in which the input field can be generated, and it is reasonably accurate outside the region close to the piston.

REFERENCE

1. B. E. McDonald and W. A. Kuperman, Comp. & Math. w. Appl. 11, 843-851 (1985)
2. G. P. Too and J. H. Ginsberg, J. Acoust. Soc. Am. Suppl. 1, 86, S63 (1989)
3. J. H. Ginsberg, J. Acoust. Soc. Am., 76, 1208-1214 (1986)
4. A. C. Baker ,K. Anastasiadis,Victor F. Humphrey. J. Acoust. Soc. Am., 84, 1483-1487 (1988)
5. S.I.Aanonsen, T.Barkve, J.Naze Tjotta, and S. Tjotta, J. Acoust. Soc. Am. 75, 749-768(1984).
6. M.F.Hamilton,J.Naze Tjotta, and S. Tjotta, J. Acoust. Soc. Am. 78, 202-216(1985).
7. Mark B. Moffett, J. Acoust. Soc. Am. 65(2), 318-323(1979).
8. B. E. McDonald and W. A. Kuperman, Naval Ocean Research and Developement Activity Report 215(1987).